INSTITUTE OF AGROPHYSICS
POLISH ACADEMY OF SCIENCES

Vadym Chibrikov

MODELING OF MECHANICAL PROPERTIES OF HEMICELLULOSE-CELLULOSE NETWORKS IN PLANT CELL WALL ANALOGUES

Ph.D. Thesis

Doctoral Thesis was prepared under the supervision of
Prof. D.Sc. Artur Zdunek, Corresponding Member of PAS

Lublin 2024

Declaration of a Supervisor

I hereby declare that the Ph.D. Thesis presented herein has been prepared under my supervision, and I affirm that it meets the requirements for submission in the proceedings for the conferral of an academic degree.

08.04.2024
date

signature

Declaration of an Author

Being aware of legal responsibility, I declare that this Ph.D. Thesis has been written by myself and does not contain any content obtained in violation of any regulations applicable. I also declare that the presented Thesis has not been previously subjected to procedures related to obtaining an academic degree at any other education institution. Furthermore, I declare that this Ph.D. Thesis is identical to an electronic version.

08.04.2024
date

signature

Many thanks to my Mom, Dad and the whole family
for your kind support and belief in me.

I would like to express my heartfelt gratitude to my Supervisor
Prof. D.Sc. Artur Zdunek for support on which I could always rely.

I also extend my gratitude to
D.Sc. Eng. Piotr Mariusz Pieczywek, for sharing the intricacies
of laboratory techniques and for constantly inspiring me
to creatively approach the pursuit of scientific problem-solving
and supporting by project 2019/35/D/NZ9/00555.

I thank to all people of Ukraine,
who made possible to prepare the following study.

Research was funded by the National Science Centre, Poland Centre in the project "*Modeling of mechanical properties of hemicellulose-cellulose networks in plant cell wall analogues*", 2019/35/D/NZ9/00555

Author was a scholarship holder in the project of the National Science Centre "*Modeling of mechanical properties of hemicellulose-cellulose networks in plant cell wall analogues*" (2019/35/D/NZ9/00555) within years 2020-2023

Author was a scholarship holder in the project of the National Science Centre "*Cellulose-pectin hydrogels cross-linked with divalent metal ions for immobilization of antagonistic microorganisms*" (2020/37/B/NZ9/03159) within years 2023-2024

Abstract (Polish)

Ściana komórkowa roślin jest wysoce uporządkowaną i wyspecjalizowaną siecią, utworzoną głównie z polisacharydów, glikoproteinów, związków fenolowych, minerałów i enzymów. Główne funkcje ściany komórkowej roślin są stosunkowo dobrze znane - kontrola morfogenezy roślin, jej architektury, zarządzanie reakcjami mechanicznymi, wytrzymałością, elastycznością, odpornością, wzrostem, komunikacją międzykomórkową itp. Pomimo niespójności relacji między strukturą a właściwościami ściany komórkowej roślin, która jest tematyką dyskusyjną od końca lat 60-tych XX wieku, rola interakcji celuloza-hemiceluloza w odniesieniu do mechanobiologii ściany komórkowej roślin nie jest kwestionowana. Celuloza jest głównym składnikiem ściany komórkowej roślin przenoszącym obciążenia, a właściwości mechaniczne ściany komórkowej roślin są zależne od interakcji pomiędzy włóknami celulozy, w których pośredniczą hemicelulozę.

Pomimo znaczącego w ostatnich latach postępu z badaniach ściany komórkowej, wciąż pozostaje wiele pytań dotyczących właściwości fizykochemicznych polisacharydów ścian komórkowych roślin i ich właściwości mechanicznych. Istnieje kilka podejść metodycznych w tej kwestii. Ściana komórkowa roślin może być badana bezpośrednio poprzez dekompozycję jej składników w ścianie komórkowej (*in muro)*, hamowanie biosyntezy, rozpuszczenie *in vitro* lub modyfikację chemiczną. Jednak ocena właściwości mechanicznych ściany komórkowej roślin jest poważnie ograniczona przez stosowane techniki eksperymentalne, co sprawia, że wyniki są zmienne i uzależnione od kontekstu badań. Manipulowanie materiałem ściany komórkowej roślin jest również wyzwaniem, gdy chodzi o badania pojedynczych komórek, gdyż wyniki są uzależnione od lokalizacji materiału badawczego w ścianie komórkowej roślin. Opracowanie analogów ściany komórkowej roślin w postaci celulozy bakteryjnej i hemiceluloz ściany komórkowej roślin może służyć jako narzędzie do uzyskania uproszczonych reprezentacji ściany komórkowej roślin w makroskali, które mają jednorodną strukturę i są powtarzalne. Dotychczas, podobne podejście umożliwiło skatalogowanie wpływu głównych polisacharydów ściany komórkowej roślin na strukturę i właściwości mechaniczne analogów ściany komórkowej roślin, oraz zdefiniowanie mechanizmów interakcji polisacharydów z celulozą. Jednak, konwencjonalne techniki laboratoryjne sprawiają trudności z określeniem sił adhezji pomiędzy włóknami celulozy, co jest kluczowe dla mechanobiologii ściany komórkowej roślin. Modelowanie numeryczne *in silico* pozwala na przybliżenie struktury i właściwości mechanicznych ściany komórkowej roślin w odniesieniu do składu, parametrów przestrzenno-czasowych i właściwości fizykochemicznych polisacharydów ściany komórkowej roślin. Pozwala to również na uzyskanie wglądu w strukturę i mechanikę sieci w odniesieniu do specyfiki jej tworzenia, gęstości, lokalizacji i siły połączeń pomiędzy celulozą a hemicelulozami oraz roli innych polisacharydów ściany komórkowej roślin.

W niniejszej rozprawie doktorskiej dokonano przeglądu wiedzy dotyczącej właściwości mechanicznych celulozy bakteryjnej, hemiceluloz (ksylanu, arabinoksylanu, ksyloglukanu i glukomananu), dwuskładnikowych (celuloza bakteryjna-hemicelulozy) i trójskładnikowych (celuloza bakteryjna-hemicelulozy-pektyn) analogów ściany komórkowej roślin oraz przedyskutowano je z uwzględnieniem określonych polisacharydów, ich pochodzenia, metod produkcji, stosowanej obróbki oraz różnych podejść metodologicznych do syntezy celulozy bakteryjnej.

W dalszej części rozprawy doktorskiej skupiono się na analizie podstaw teoretycznych istniejących modeli numerycznych ściany komórkowej roślin w odniesieniu do struktury sieci włókien, jej właściwości supramolekularnych i powinowactwa wiązania polisacharydów. W tym celu przeprowadzono przegląd istniejących koncepcji struktury ściany komórkowej roślin, co pozwoliło na włączenie pewnych fizycznych i biomechanicznych aspektów architektury ściany komórkowej roślin do zrozumienia mechanizmów, które pozwalają kontrolować mechaniczne odpowiedzi ściany komórkowej roślin.

W kolejnym etapie pracy zbadano właściwości mechaniczne i molekularne celulozowo-hemicelulozowych analogów ściany komórkowej roślin w celu określenia wpływu właściwości fizykochemicznych różnych hemiceluloz (ksylan, arabinoksylan, ksyloglukan i glukomannan) na ogólną wydajność mechaniczną celulozowo-hemicelulozowych analogów ściany komórkowej roślin pod względem deformacji sprężystej i plastycznej. Przeprowadzone badania potwierdziły, że właściwości mechaniczne celulozowo-hemicelulozowych analogów ściany komórkowej roślin determinowane są głównie przez odkształcenie włókien celulozy, w łączeniu których pośredniczą hemicelulozy. Podczas gdy odkształcenie sprężyste celulozowo-hemicelulozowych analogów ściany komórkowej roślin jest uwarunkowane drganiami rozciągającymi wiązań strukturalnych celulozy i hemicelulozy, odkształcenie plastyczne jest związane ze zmianami na poziomie supramolekularnym zachodzącym w strukturze celulozowo-hemicelulozowych analogów ściany komórkowej roślin.

W dalszej części rozprawy doktorskiej skupiono się na opracowaniu modelu numerycznego celulozowo-hemicelulozowych analogów ścian komórkowych roślin. Opracowano model numeryczny z użyciem metody gruboziarnistej dynamiki molekularnej, gdzie włókna polisacharydów modelowano przy użyciu kulek i sprężyn. Aby zweryfikować model i wyjaśnić strukturalną i mechaniczną rolę hemiceluloz, celulozę bakteryjną syntetyzowano w obecności różnych stężeń ksylanu, arabinoksylanu, ksyloglukanu lub glukomannanu i poddano analizom strukturalnym i mechanicznym w nano i makroskali. Uzyskane dane wykorzystano do interpretacji wpływu każdego rodzaju hemicelulozy na właściwości mechaniczne celulozowo-hemicelulozowych analogów ściany komórkowej roślin w oparciu o czułość modelu. Uzyskano zgodność strukturalną pomiędzy modelem a zsyntetyzowanymi analogami ściany komórkowej roślin. Zaobserwowano, że właściwości mechaniczne celulozowo-hemicelulozowych analogów ściany komórkowej roślin nie są determinowane przez odkształcenie samej hemicelulozy, ale głównie przez odkształcenie włókien celulozowych, w którym pośredniczą hemicelulozy. Takie mediatory, koncepcyjnie podobne do biomechanicznych hotspotów występujących *in muro*, zmieniają siłę oddziaływania między włóknami, będąc głównym czynnikiem wpływającym na właściwości mechaniczne celulozowo-hemicelulozowych analogów ściany komórkowej roślin. Ponadto na siłę oddziaływania między włóknami wpływ mają także cechy morfologiczne celulozowo-hemicelulozowych analogów ściany komórkowej roślin, takie jak szerokość/długość/moduł włókna. Wykazano również, że uzyskane eksperymentalnie właściwości mechaniczne celulozowo-hemicelulozowych analogów ściany komórkowej roślinnej odpowiadają właściwościom symulowanych sieci, co potwierdza przydatność opracowanych modeli do badania mechanobiologii sieci włókien celulozowych.

W ramach badań uzupełniających przeprowadzono badania wpływu specyficznych enzymów degradujących hemicelulozy na strukturę i właściwości mechaniczne celulozowo-hemicelulozowych analogów ściany komórkowej roślin. Badania wykazały, że hemicelulozy zawarte w sieci włókien celulozy bakteryjnej istnieją jako dostępne i niedostępne dla enzymów. W konsekwencji oceniono, że hemicelulozy niedostępne dla enzymów są kluczowe dla trendów zmiany właściwości mechanicznych analogów, podczas gdy hemiceluloz dostępne dla enzymów powodują fluktuację danych.

Słowa kluczowe: celuloza bakteryjna, hemicelulozy, analogi ściany komórkowej roślin, właściwości mechaniczne, symulację dynamiką molekularną.

Abstract (English)

The plant cell wall is a highly ordered and specialized network, formed mainly of polysaccharides, glycoproteins, phenolic compounds, minerals and enzymes. Being the most widespread and probably the most complex structural network in Nature, the main functions of plant cell wall are relatively clear - determination of plant morphogenesis, architecture, management of mechanical responses, strength, flexibility, growth management, defense responses, intercellular communication etc. Despite the inconsistency of the relationships between structure and properties of plant cell wall, which has been debated since the late 1960^s, the role of cellulose-hemicellulose interactions with respect to mechanobiology of plant cell wall is undisputed. Modern theory supports the notion that cellulose is the main load-bearing component of plant cell wall, while the key component of plant cell wall mechanical properties - interfiber adhesion - is determined by the hemicellulose-mediated interactions.

Despite recent progresses, there is still much to consider on physicochemical properties of plant cell wall polysaccharides and the mechanical properties of plant cell wall. But how can the respected results be achieved? Plant cell wall may be studied directly by either decomposition of its constituents in plant cell wall (*in muro)*, inhibition of biosynthesis, *in vitro* solubilization or chemical modification. However, evaluation of the mechanical properties of plant cell wall is severely limited by the experimental techniques used, making the results variable and context-dependent. Sample processing is also challenging in single-cell studies, and even when processed, results are mainly site-dependent. The development of plant cell wall analogues of interconnected bacterial cellulose and plant cell wall hemicelluloses can serve as a tool to achieve a simplified macroscale representations of plant cell wall that have a homogeneous structure and are repeatable. Such an approach has already made possible to catalogue the effects of the main plant cell wall polysaccharides on the structure and mechanical properties of the plant cell wall analogues and to define the mechanisms of polysaccharide interaction with cellulose. However, conventional laboratory techniques are struggling to allow the determination of the interfiber adhesive forces, which is undisputedly crucial for the mechanobiology of plant cell wall. *In silico* numerical modelling allows to approximate the structure and mechanical properties of plant cell wall with respect to introduced composition, spatio-temporal parameters, and physicochemical properties of plant cell wall polysaccharides introduced. It also allows to reach promising insights on network structure and mechanics with regard to its formation, density, location and strength of cellulose-hemicellulose junctions as well as the nature of the role of other plant cell wall polysaccharides.

In current Ph.D. Thesis, all the crucial theoretical background regarding mechanical properties of bacterial cellulose, hemicelluloses (xylan, arabinoxylan, xyloglucan, and glucomannan), their binary (bacterial cellulose-hemicellulose) and ternary (bacterial cellulose-hemicellulose-pectin) composites has been gathered, and discussed with respect to the type of specific polysaccharides, their origin, production methods, applied treatment, as well as various methodological approaches to the biosynthesis of bacterial cellulose.

In the following part of current Ph.D. Thesis, theoretical explorations have been focused on the exploration of an existing numerical models of plant cell wall regarding the network fine structures, its supramolecular properties and polysaccharide binding affinities. For this purpose, extensive revision of an existing concepts of plant cell wall structure has been also conducted, allowing to incorporate certain physical and biomechanical aspects of cell wall architecture to the understanding of the mechanisms, which allow to control cell wall mechanical responses.

In the next stage of the following research, mechanical and molecular properties of bacterial cellulose-hemicellulose plant cell wall analogues were investigated to determine the effect of physicochemical properties of various hemicellulose polysaccharides (xylan, arabinoxylan, xyloglucan and glucomannan) on overall performance of bacterial cellulose-hemicellulose plant cell wall analogues in terms of elastic and plastic responses. Current research supported an idea that mechanical properties of bacterial cellulose-hemicellulose plant cell wall analogues are determined predominantly by the deformation of cellulose fibers, mediated by hemicelluloses. While elastic deformation of bacterial cellulose-hemicellulose plant cell wall analogues is determined by stretching vibrations of the structural bonds of cellulose and hemicelluloses, plastic deformation is defined by the supramolecular changes occurring within the structure of bacterial cellulose-hemicellulose plant cell wall analogues.

The following part of current Ph.D. Thesis was focused on establishing of the numerical model of bacterial cellulose-hemicellulose plant cell wall analogues following the principles of coarse-grained molecular dynamics, with fibers modelled using the bead-spring approach. To validate the model and explain the structural and mechanical role of hemicelluloses, bacterial cellulose was synthesized in the presence of different concentrations of xylan, arabinoxylan, xyloglucan, or glucomannan and subjected to nano- and macroscale structural and mechanical characterization. The data obtained were used to interpret the effects of each hemicellulose on the mechanical properties of bacterial cellulose-hemicellulose plant cell wall analogues based on the sensitivity of the model. Current part of the work showed an agreement between simulated networks and synthesized plant cell wall analogues. It was observed that mechanical properties of bacterial cellulose–hemicellulose plant cell wall analogues are not determined by the deformation of hemicelluloses itself, but mainly by the deformation of cellulose fibers, mediated by hemicelluloses. Such a mediates, conceptually similar to biomechanical hotspots occurring *in muro*, change the force of interfiber interaction, being the main factor affecting the mechanical properties of bacterial cellulose–hemicellulose plant cell wall analogues. In addition, force of interfiber interaction is also defined by the morphological features of bacterial cellulose–hemicellulose plant cell wall analogues, such as fiber width/length/modulus. It was also shown that mechanical properties of bacterial cellulose–hemicellulose plant cell wall analogues correspond to those of simulated networks, confirming applicability of the latter for the exploration of the mechanobiology of cellulose–based fiber networks.

As a supplementary research, exploration of the effect of hemicellulose–specific enzymes on the structure and mechanical performance of bacterial cellulose–hemicellulose plant cell wall analogues was conducted. Current research supported showed that hemicelluloses, incorporated in bacterial cellulose fiber network exist as both enzyme–accessible and enzyme–inaccessible. It results in enzyme–inaccessible hemicelluloses are defining trends on data change of the mechanical properties of the respected plant cell wall analogues, while enzyme–accessible hemicelluloses are defining data fluctuation.

Keywords: bacterial cellulose, hemicellulose, plant cell wall analogues, mechanical properties, molecular dynamics simulation.

Content

List of symbols

Symbol	Description
AX	Arabinoxylan
BC	Bacterial cellulose
CESA	Cellulose synthase proteins
CG	Coarse-grained
DP	Degree of polymerization
DS	Degree of substitution
DS_{Ac}	Degree of acetylation
GGM	Galactoglucomannan
KGM	Konjac glucomannan
GGMO	Galactoglucomannan oligosaccharides
MD	Molecular dynamics
MM	Molecular modeling
PCW	Primary plant cell wall
SEM	Scanning electron microscopy
XGY	Xyloglucan
XEGH	Xyloglucan endotransglycosylase/hydrolase
XYL	Xylan

The list of publications forming Ph.D. Thesis

Current Ph.D. Thesis is based on a series of four peer-reviewed publications focusing on the following topic:

Modeling of mechanical properties of hemicellulose-cellulose networks in plant cell wall analogues:

P1: Chibrikov, V., Pieczywek, P. M., Zdunek, A., 2023. Tailor–Made Biosystems–Bacterial Cellulose–Based Films with Plant Cell Wall Polysaccharides. *Polymer Reviews*, 63(1), 40-66. DOI: 0.1080/15583724.2022.2067869

Impact Factor$_{2022}$: **13.1**;
Points (according to Ministry of Science and Education of Poland): **140**.

P2: Pieczywek, P. M., Chibrikov, V., Zdunek, A., 2023. *In silico* studies of plant primary cell walls–structure and mechanics. *Biological Reviews*, 98(3), 887-899. DOI: 10.1111/brv.12935

Impact Factor$_{2022}$: **10.0**;
Points (according to Ministry of Science and Education of Poland): **200**.

P3: Chibrikov, V., Pieczywek, P. M., Cybulska, J., Zdunek, A., 2023. Evaluation of elasto–plastic properties of bacterial cellulose–hemicellulose composite films. *Industrial Crops and Products*, 205, 117578. DOI: 10.1016/j.indcrop.2023.117578

Impact Factor$_{2022}$: **5.9**;
Points (according to Ministry of Science and Education of Poland): **200**.

P4.: Chibrikov, V., Pieczywek, P. M., Cybulska, J., Zdunek, A., 2024. Coarse-grained molecular dynamics model to evaluate the mechanical properties of bacterial cellulose–hemicellulose composites. *Carbohydrate Polymers*, 121827. DOI: 10.1016/j.carbpol.2024.121827

Impact Factor$_{2022}$: **11.2**;
Points (according to Ministry of Science and Education of Poland): **140**.

The above published results have been complemented by studies not published yet, presenting the effect of hemicellulose–specific enzymes on the structure and mechanical performance of bacterial cellulose–hemicellulose plant cell wall analogues. This additional material has been submitted on May 9, 2024 to *Scientific Reports* journal and is presented in this dissertation as a Supplementary research P5 entitled: Chibrikov, V., Pieczywek, P. M., Cybulska, J., Zdunek, A. The effect of hemicellulose–specific enzymes on the structure and mechanical performance of cellulose–hemicellulose hydrogels.

1. Introduction

1.1. Exploration of plant cell wall in terms of its structure and composition

The primary plant cell wall (PCW) is still discussed as an independent dynamic organelle, but it is assumed to be a highly ordered and specialized network. According to the methods of chemical treatment, PCW is a material that remains insoluble after extraction with buffers and organic solvents (Brillouet et al., 1988). Being the most widespread and probably the most complex structural network in nature, the main functions of PCW are relatively clear – determination of plant morphogenesis, architecture, control of mechanical reactions, strength, flexibility, growth control, defense reactions, intercellular communication, etc. (B. Zhang et al., 2021).

In terms of modern agriculture, exploration of PCW functionality is one of unapparent cornerstones. As PCW ensures sufficient structure and impact response of plant tissue, leading to its uniform shape and texture, it results in PCW exploration in terms of agricultural safety of humankind (Sarkar et al., 2009; Tenhaken, 2015). It includes exploration of PCW composition and structure as a matter of plant genotype (Allison et al., 2011; Cone & Engels, 1993), maturity (Goto et al., 1991; Wallsten & Hatfield, 2016), cultivation conditions (Hori et al., 2020; Houston et al., 2016), etc. Another point of PCW study in terms of agriculture and horticulture is an exploration of cost-effective biorefinery in connection to PCW composition and ultrastructure (Himmel, 2008). It includes both techniques of genomic modification of PCW (Bhatia et al., 2017; Carpita & McCann, 2020), as well as various treatment techniques (Bichot et al., 2018; C. O. G. Silva et al., 2018). In addition, PCW adaptation/resistance mechanisms to abiotic stresses makes exploration of PCW morphology of the high priority to define morphological, physiological and biochemical mechanisms of plant survival in changing climate (Le Gall et al., 2015).

Such important functionality of PCW in plants and a broad potential in green-industry development is ensured by its relatively simple chemical composition. The main component of PCW is water, which accounts for up to 65% of its volume (D. S. Thompson, 2005). The dry matter of PCW consists mainly of polysaccharides (up to 90% of the dry matter), while the other components are glycoproteins, phenolic compounds, minerals and enzymes (up to 10% of the dry matter). According to the structural composition, PCW polysaccharides are divided into cellulose, hemicelluloses (xyloglucan, mannan, xylan, etc.) and pectin (homogalacturonan, rhamnogalacturonan) (Rose, 2003). According to its mass distribution, PCW generally consists of 15–40% cellulose, 30–50% pectin and 20–30% hemicelluloses (Cosgrove & Jarvis, 2012). Regarding the proportion of hemicelluloses and pectin in PCW, three general types of PCW are defined – Type I (containing predominantly pectin, xyloglucan and/or galactoglucomannan), Type II (rich in arabinoxylan and pectin) and Type III (rich in mannan, low in pectin) (Carpita, 1996; Carpita & Gibeaut, 1993; G. B. Silva et al., 2011).

Cellulose, which is a paracrystalline array of (1→4)–β–D–glucans, is the main building block for the formation of PCW (Carpita, 2011). It consists of approximately 7000–15000 D–glucose units oscillating at an angle of 180° and exhibiting a twofold helical conformation (Berglund, 2018; Gibson, 2012). Equatorial (1→4)–β linkages and surface hydroxyl groups force the cellulose chain to form an inter– and intramolecular cellulose–cellulose hydrogen bond network (Fig.1), which organizes the microfibres into a ribbon–like structure (Martinez-Sanz, Pettolino, et al., 2017; Matthews et al., 2006).

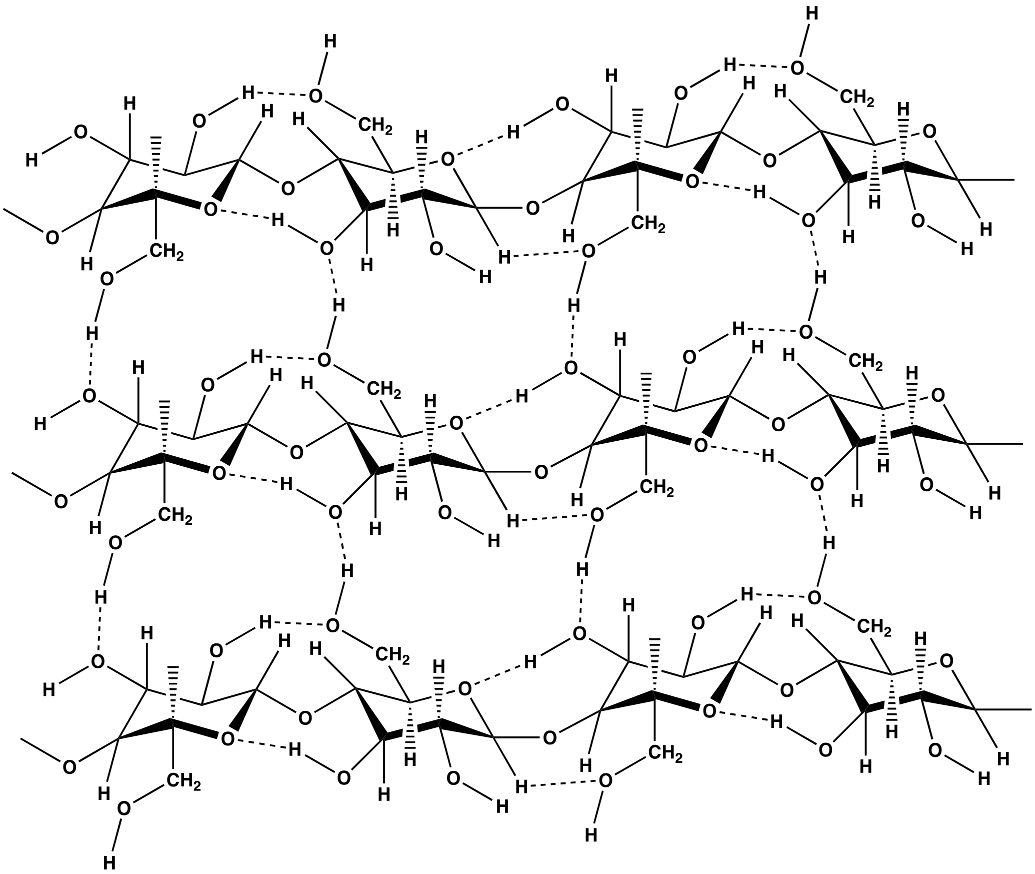

Fig.1. Molecular network of cellulose polysaccharide chains. Redrawn after (Douglass, 2010).

In plant cell wall (*in muro)*, cellulose biosynthesis takes place in terminal complexes and is led by a cellulose synthase protein (CESA). About 36 proteins are already known in the CESA group that catalyze the elongation of the (1→4)–β–D–glucan polymer chains with their further random tedding and crystallization (Braidwood et al., 2014; Endler & Persson, 2011; Fernandes et al., 2011; Pauly et al., 2013). The deposition of fibers *in muro* is a consequence of the movement of CESA proteins movement along the plasma membrane (McFarlane et al., 2014). Cellulose in the fibers does not consist of a single chain, but is rather an assembly of parallel organized chains. Individual units (18 according to modern computational models, 24 and 36 in previous references) may coordinate to form microfibers with a diameter of 3–4 nm, which may form crystalline, paracrystalline, and non–crystalline domains (Martinez-Sanz, Pettolino, et al., 2017). According to the structural pattern, cellulose fibers *in planta* may range from 2–5 nm up to 40 nm in diameter (Newman et al., 2013; Thomas et al., 2013).

In muro, cellulose fibers are structurally heterogeneous with two main crystalline forms – Iα and Iβ. Since all the hydroxyl groups in cellulose are equatorial, the sides of the cellulose chain are polar and may form regular crystalline packing via interchain hydrogen bonding and hydrophobic sides interrelations. Such packing may lead to the formation of a phase with a triclinic system with one chain per unit cell (Iα cellulose) and a more stable monoclinic system with two chains per unit cell (Iβ cellulose). Such heterogeneity in the arrangement and structure of the cellulose packing could represent a match between stiffness and flexibility of the PCW skeleton (Matthews et al., 2006). There are several other possible options of PCW architecture related to cellulose chain length and crystallinity, but the fundamentals are similar in different plants (Burton et al., 2010).

Hemicelluloses are a group of neutral or acidic polysaccharides with predominantly glucose, mannose and xylose (1→4)–β–linked backbones. The sidechains are also decorated with some neutral/acidic saccharide sidechains, such as arabinose, fucose, xylose, glucuronic acid, ferulic acid, etc. (Scheller & Ulvskov, 2010). It is assumed that its biosynthesis takes place in the Golgi through polymerization of activated nucleotide monosaccharides (Pauly et al., 2013).

Xyloglucan is the most widely distributed hemicellulose among the dicotyledons (Park & Cosgrove, 2015). It is a (1→4)–β–D–glucan chain of glucose, galactose, and xylose with an average degree of polymerisation (DP) of 300–3000, as well as other, minor substituents – L–arabinopyranose, L–arabinofuranose, D–galacturonic acid, L–fucose, etc. (Nishinari et al., 2007; Park & Cosgrove, 2015; Tuomivaara et al., 2015; K. Uhlin, 1990; York et al., 1990). The relative molecular weight of xyloglucan varies from 9 kDa (extracted from Golgi) to >1000 kDa, with an average of 100–300 kDa (Lima et al., 2004). Xylosyl residues can be substituted with other glucosyl and non–glucosyl constituents depending on the plant family, tissue specification and germination state of the cell (Nishinari et al., 2007; Pauly & Keegstra, 2016). According to the systematic approach of xyloglucan structure definition, an unsubstituted glucosyl residue (Fig.2, G) and a glucosyl residue with xylosyl substitution at the O6 position (Fig.2, X) are defined as the basic structural patterns of xyloglucan. Pattern X has 17 other identified backbone structures, which are also encoded with single–letter abbreviations (Fig.2) (Tuomivaara et al., 2015). According to the aforementioned naming convention, the most common xyloglucan oligosaccharides are XXXG, XXFG, XXLG, XLXG, XLFG, XLLG, XXGG, XXGGG (Park & Cosgrove, 2015; York et al., 1993). The biosynthesis of xyloglucan is localised in the Golgi and is thought to be related to the CESA–like C protein family (McDougall & Fry, 1989; Schultink et al., 2014). Patterns of sidechain substitutions have been found to be driven by different glycosyltransferases depending on the site of substitution (Schultink et al., 2014). Many of the genes related to xyloglucan biosynthesis have already been identified and characterised, while some are still under exploration (Tuomivaara et al., 2015).

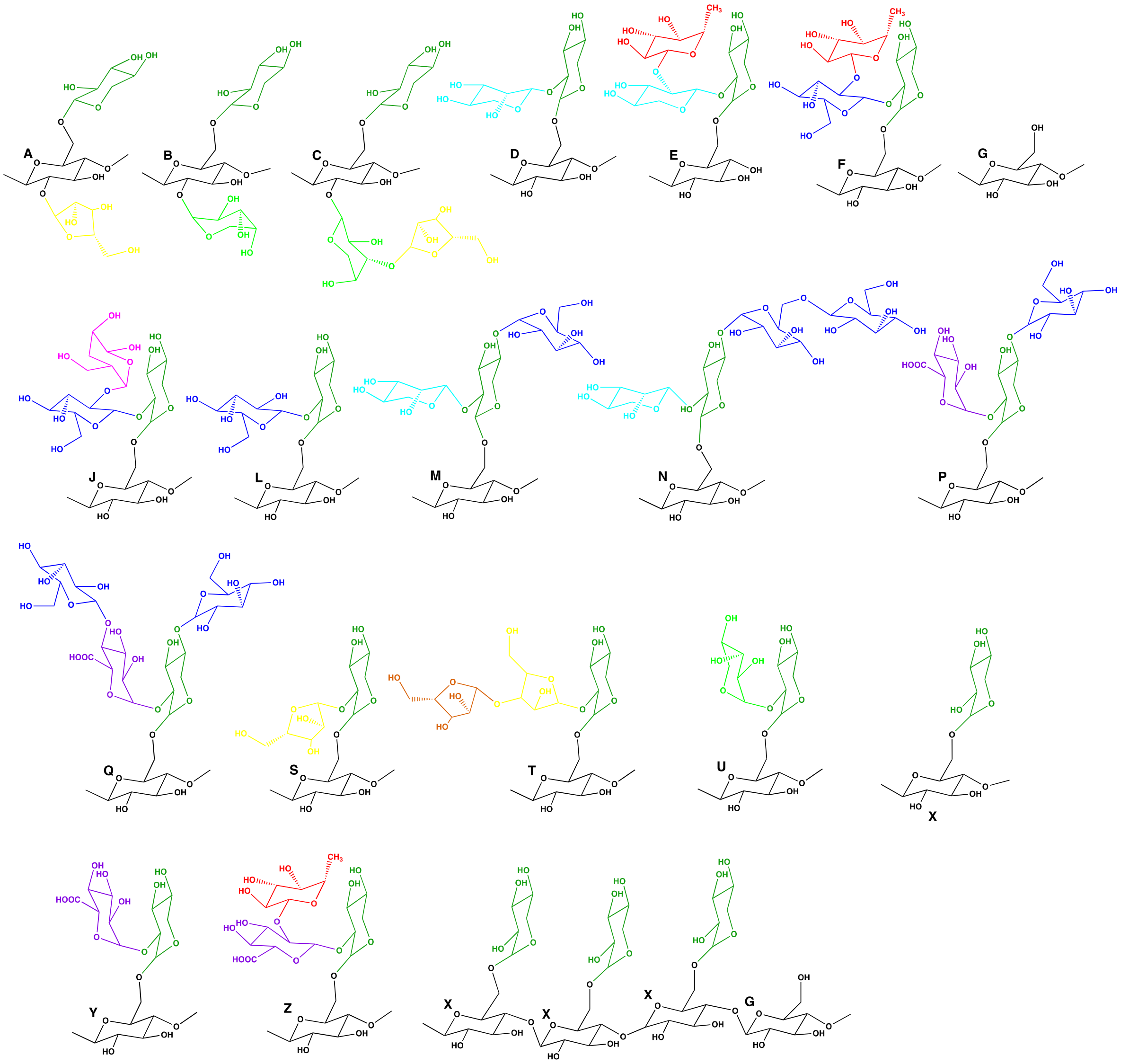

Fig. 2. Chemical structure of xyloglucan oligosaccharides: structures of naturally occurring xyloglucan oligosaccharides encoded with one–letter abbreviations, and structure of the XXXG oligosaccharide. Monosaccharide substitutes are marked with specific colours. Redrawn after (Park & Cosgrove, 2015; Tuomivaara et al., 2015).

Mannans are the second common group of hemicelluloses, consisting of linear **mannan**, **galactomannan, glucomannan and galactoglucomannan** (GGM) (Fig.3). Linear mannan are homopolysaccharides of (1→4)–β–D–mannopyranose with a low amount of galactose substitutes (Mestechkina et al., 2000). Galactomannan consists of polymeric (1→4)–β–D–mannopyranose with >5% mass of (1→6)–β–galactopyranose substitutes (Teramoto & Fuchigami, 2000). For galactomannan, mannose to galactose ratio varies from 1:2 to 20:1, with the tendency for (1→6)–α–linked galactose to affect galactomannan solubility and viscosity, as well as integrity with other matrix polysaccharides. For GGM, a ratio between galactose, glucose and mannose of 0.1÷1:1:3÷4 has been reported (Berglund et al., 2019). Glucomannan consists mainly of (1→4)–β–linked mannopyranose and glucopyranose in a ratio of 1.6÷2.3:1 (Lerouxel et al., 2006). The incorporation of glucose and mannose into glucomannan is thought to be determined by their actual concentrations in Golgi, but there is no *in vivo* validation (Scheller & Ulvskov, 2010). Biosynthesis of mannans is also catalyzed by certain proteins (mannan synthase, galactosyltransferase) of the CESA–like family (Rodriquez-Gacio et al., 2012).

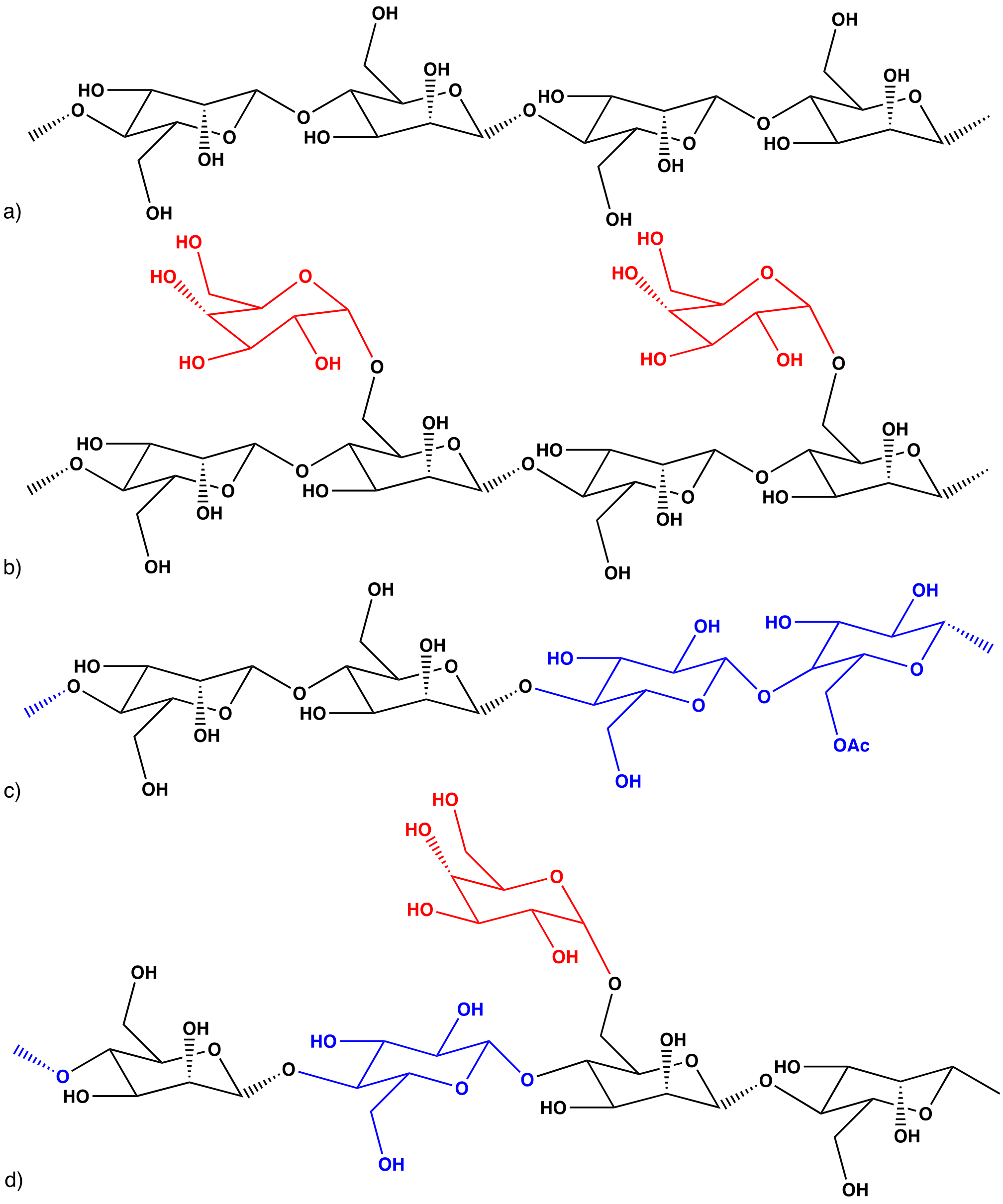

Fig.3. Chemical structure of mannan oligosaccharides: a) linear mannan, b) galactomannan, c) glucomannan, d) galactoglucomannan. (1→4)–β–D–mannopyranose units marked with black, (1→6)–β–galactopyranose substitutes – with red, (1→4)–β–glucopyranose units – with blue colour).

Arabinoxylan is a common PCW hemicellulose of monocotyledons consisting predominantly of (1→4)–β–D–linked xylose units with O2 and/or O3 arabinose substitutes. The arabinose sidechains are irregularly distributed along the xylan backbone and are generally defined by three possible structural patterns – O2–substituted, O3–substituted and O2–O3–substituted (Fig.4). The average molecular weight of arabinoxylan ranges from 65 to 5000 kDa, depending on PCW type, plant species and extraction method. Arabinoxylan is synthesized by arabinoxylan synthase (xylan backbone), arabinosyl transferases (arabinose sidechains) and arabinoxylan feruloyl transferase (ferulic acids).

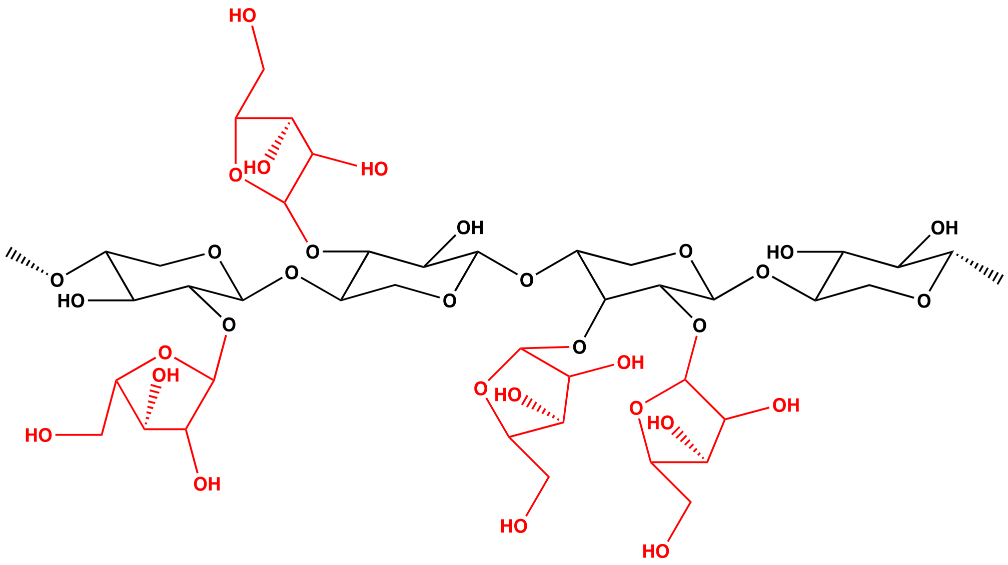

Fig.4. Chemical structure of arabinoxylan oligosaccharide. (1→4)–β–D–xylose backbone is marked with black, O2 and/or O3 arabinose substitutes are marked with red colour.

1.2. Concepts of cellulose–hemicellulose interactions *in muro*

The matrix components of PCW may transmit its architecture in different ways, depending on the individual interaction patterns of cellulose, hemicellulose and pectin (Martinez-Sanz, Pettolino, et al., 2017; Thomas et al., 2013). *In vivo*, the arrangement of cellulose fibers ensures the presence of microspaces filled with matrix polysaccharides, depending on the cell type (Ochoa-Villarreal et al., 2012). In addition, cellulose fibers have randomly distributed hydrophilic and hydrophobic zones that allow them to form interactions with PCW matrix hemicelluloses and pectin (Broxterman & Schols, 2018; Doineau et al., 2020; Martinez-Sanz, Pettolino, et al., 2017). Up to early 2010th, **xyloglucan** was thought to be the major hemicellulose forming the cellulose–hemicellulose network in PCW, forming 20–40 nm long connections between contiguous fibers (Albersheim et al., 2011; Park & Cosgrove, 2015; York et al., 1986). At that time, the stiffness of PCW was assumed to be defined solely by these connections, leading to the development of numerous PCW models. However, the other possible mechanisms of xyloglucan–cellulose binding were revealed, such as xyloglucan entrapment during cellulose crystallization, interfiber hydrogen bonding, xyloglucan adsorption, tethering, covalent linking, etc. (Carpita & Gibeaut, 1993; Keegstra et al., 1973; Probine & Barber, 1966; Talbott & Ray, 1992). As for direct cellulose–xyloglucan bonds, visual bonds have been observed in poplar cells, but they have no justified effect on the PCW mechanobiology (Itoh & Ogawa, 1993). Other microscopy studies on the uppermost lamellae of epidermal tissue of *Allium cepa* showed that xyloglucan covers the cellulose fibers in reasonable amounts, allowing the definition of PCW mechanobiology with these adsorbed mediators (Zheng et al., 2018).

Significant progress in understanding the role of cellulose–xyloglucan interactions *in muro* was demonstrated by *in vivo* suppression of xyloglucan biosynthesis. Some discoveries state that the absence of xyloglucan in *Arabidopsis thaliana* single mutants result in only minor phenotypic changes, suggesting that the aberrant form of xyloglucan could not be detected by standard methods or that it is replaced by a modified β–glucan backbone or some pectin components (Cavalier et al., 2008). Continuing along this path, research on a xyloglucan–deficient *Arabidopsis thaliana* double mutant show significant phenotypic changes. These manifest in an altered organization of cellulose microfibers, a possible decrease in cellulose content and a sensitivity of the mutant to external mechanical changes. Atomic force microscopy and field emission scanning electron microscopy studies reveal wavy linear patterns of separate cellulose fibers, suggesting the role of xyloglucan in the homogeneous distribution of cellulose fibers in PCW as a means of strengthening the microfibers. A bilateral explanation for the absence of xyloglucan affect cellulose organization both physically and by deactivating PCW integrity sensors (Xiao et al., 2016).

Recent advances in the study of xyloglucan–related PCW integrity are related to the enzymolysis of PCW with substrate–specific xyloglucanases to study its degradation. Introductory studies in this field have shown that both xyloglucan endotransglycosylase/ hydrolase (XEGH) enzymes break non–covalent hemicellulose–cellulose interactions, hydrolyze xyloglucan and cut off its non–bonded parts (Eklöf & Brumer, 2010; Farkas et al., 1992; Miedes et al., 2010; J. E. Thompson & Fry, 1997). Substantial work on this approach was carried out by Park and Cosgrove, who reported that XEGH treatment process about 50% of the mass of *Allium cepa* PCW xyloglucan without reducing its strength. The other half of the xyloglucan appear to be unprocessable, resulting in tight cellulose–xyloglucan–cellulose junctions, with xyloglucan layered between individual cellulose fibers. The other prediction is based on the formation of highly disordered zones with deeper xyloglucan penetration and multiple cellulose–xyloglucan splicing, such that the cellulose fibers intertwine with a built–up hydrogen bonding network (Park & Cosgrove, 2012a). Based on aforementioned assumptions, biomechanical hotspot PCW model was proposed, so that defining a vector of further exploration of PCW mechanobiology.

The role of **mannan** in PCW is relatively minor, due to its lower content, compared to xyloglucan. Mannan hemicelluloses may be predominantly found in secondary plant cell wall, as well as some Type I and Type III PCW. Thus, entrenched thoughts on the role of xyloglucan in binding cellulose fibers may be questioned by the ability of glucomannan to form cross–links with cellulose (Cosgrove, 2000). Theoretical predictions state that xyloglucan is not necessarily a structural hemicellulose in Type I PCW with substantial amounts of GGM (Carpita & Gibeaut, 1993). Like xyloglucan, mannan can also form hydrogen bonds with cellulose *in muro* depending on the degree of substitution (DS) (Kabel et al., 2007). The more challenging fact is that galactomannan with different degrees of galactosylation may bind cellulose differently, which is crucial for the mechanobiology of PCW. Galactose substitution increases the solubility of mannan and enhances water uptake, which is critical for seed germination. Conversely, linear mannan provides seed hardness and good storage properties due to its high hydrophobicity (Reid & Bewley, 1979). *In vivo* results declare mannan from the endosperm of *Schizolobium parahybae* not as a reserve polysaccharide, but as a structural one. The absence of cellulose, the presence of mannan and the almost constant amount of mannan during germination declare mannan as a structural polysaccharide instead of cellulose (Petkowicz et al., 2007).

Due to the specific patterns of PCW formation, GGM may reduce the crystallinity of cellulose and increase its flexibility. However, studies on *Arabidopsis thaliana* mutants lacking detectable glucomannan reported minor changes in PCW strength. The basic idea is that plants may adapt to the lack of a particular PCW polysaccharide by replacing it with another or by changing its own structure (Goubet et al., 2003). In this case, the lack of mannan may be compensated by an increased synthesis of other β–glucans (Mora-Montes et al., 2007).

The patterns of interaction of **arabinoxylan** with other polysaccharides have been reported to vary, such that a single arabinoxylan chain may contain domains bonded with cellulose as well as other arabinoxylan molecules and/or unbonded domains (Hartley et al., 1990). When the arabinoxylan content *in muro* is high, the PCW properties are also influenced by the degree of arabinosylation, the distribution of substitutes within the xylan backbone, and the number of ferulic acid cross–links. The multipath structure of arabinoxylan is thought to be a predominant factor for poor cellulose–arabinoxylan binding *in vitro*, leading to the suggestion that arabinoxylan–cellulose and arabinoxylan–arabinoxylan hydrogen bonding *in muro* is possible especially with low–arabinosylated arabinoxylan (Toole et al., 2009). Nevertheless, covalent arabinoxylan–lignin and cellulose–xylan hydrogen bonds have been reported for some plant cell walls (Popper & Fry, 2008). In addition, arabinoxylan branching has been reported to be related to the remodeling of PCW in wheat endosperm during grain filling, thus altering its mechanobiology. It is hypothesized that the overall decreasing degree of arabinosylation during grain filling is due to two different mechanisms: incorporation of low–arabinosylated arabinoxylan *in muro* or remodeling of an existing branched arabinoxylan.

1.3. Studies of bacterial cellulose–hemicellulose interactions in plant cell wall analogues

In terms of origin, structure and preparation methods, cellulose materials are divided into four main categories: crystalline nanocellulose (3–20 nm in diameter, 0.05–5 μm in length), cellulose nanofibers (tangled nanofiber network, usually plant–isolated), bacterial cellulose (BC; highly porous, randomly oriented fiber network), and hairy nanocellulose (rod–like, disordered structure) (Chi & Catchmark, 2017; Van De Ven & Sheikhi, 2016).

Bacterial cellulose (BC) is produced by a number of bacterial genera, such as *Agrobacterium*, *Aerobacter*, *Rhizobium*, etc. (Andrade et al., 2010; S. Q. Chen et al., 2018). *Komagataeibacter xylinus* (up to 2012 – *Gluconacetobacter xylinus*) is commonly used for BC biosynthesis due to the similarities of biosynthesis with that *in planta*, the ultrafine fiber network structure and its chemical purity (S. Q. Chen et al., 2018; Mikkelsen & Gidley, 2010). *In planta*, cellulose in the cell wall matrix precipitates with constant composition, and the same effect is achieved with BC biosynthesis. Cellulose synthesizing complexes are located on the bacteria surface near the cell membrane pores, where cellulose is extruded and forms a ribbon consisting of about 46 nanofibers (Lin et al., 2013). Subsequently, the ribbons aggregate into microfibers by crystallization of the glucan chains (Andrade et al., 2010). **The development of composites of interconnected bacterial cellulose (BC) and PCW hemicelluloses can serve as a tool to achieve a simplified macroscale representations of PCW that have a homogeneous structure, are pure, chemically similar to PCW and repeatable. In addition, its production, handling and storage are more straightforward, as compared to PCW extracted materials.** Such a parallels between *in planta* and bacterial synthesis of cellulose fiber networks allow researchers to modify the “cell wall environment” by studying the effects of each specific matrix polysaccharide on the properties of the cellulose fiber network. Moreover, such BC–based PCW models are cultured in macroscale so that their mechanical performance can be studied in details. Despite several limitations of this approach, it is translucent enough to understand the major processes occurring in PCW (Mikkelsen & Gidley, 2010).The very first studies exploring the interaction patterns of BC and hemicelluloses reported that mainly all PCW polysaccharides with (1→4)–β–linked backbone may alter BC morphology (Haigler et al., 1982). Later research confirmed that hemicellulose in PCW fuses with cellulose, co–crystallizes and defects the fiber structure, resulting in a decrease in fiber width due to its greater affinity for the cellulose domain structure (K. I. Uhlin et al., 1995). Further studies in this field have shown that the physicochemical properties of hemicelluloses, such as DP, DS, monosaccharide composition, lead to different cellulose–hemicellulose interaction patterns, so that a differentiated approach should be taken in further research, according to the structural pattern of each hemicellulose.

Preliminary studies show that the addition of xyloglucan with different degree of polymerization (DP) and the degree of substitution (DS) hinders the aggregation of microfibers by adhering to their surface (Hirai et al., 1998). In addition, adhesion may be drastically limited by the solubility of xyloglucan and the diffusivity associated with DS. Another possibility is that xyloglucan with high DP forms a broad cross–linking with BC and thus improves fiber attachment (Whitney et al., 2006). The same has been observed for an high DP xyloglucan with a fucose substitutes (Lopez et al., 2010).

The role of xyloglucan in ternary cellulose–xyloglucan–pectin PCW analogues is complex and is largely determined by its ratio to pectin. A low ratio leads to thinning of cellulose fibers, while an inverse ratio reduces the crystallinity of cellulose and promotes the formation of longer cellulose chains (Cybulska et al., 2010, 2011; Szymańska-Chargot et al., 2017). One possible mechanism is that pectin makes it more difficult for xyloglucan to coat the cellulose fibers, along with competitive invasion into the fibers (Szymańska-Chargot et al., 2011). Other data suggest that xyloglucan and pectin do not mix at high polysaccharide concentration, but form microdomains with majority/minority of one of these components (Zykwinska et al., 2008). Some parallels are reported for cellulose–xyloglucan and cellulose–arabinoxylan binding patterns, as both xyloglucan and arabinoxylan domains exist on the BC surface and interact with it through non–specific adsorption mechanisms (Martinez-Sanz et al., 2016). Other studies show that the affinity of arabinoxylan to cellulose generally increases with decreasing DS and increasing DP. However, a further decrease in DS limits the solubility of arabinoxylan, which may lead to phase separation (Winter et al., 2005).

Mannan hemicelluloses are shown to bind bacterial cellulose in multiple ways – both by cellulose binding (Whitney et al., 1998), co–crystallization with cellulose (Park et al., 2014), adsorption on its surface (Tan et al., 2016), adhesion to it (Mikkelsen & Gidley, 2010), as well as cellulose cross–linking (Berglund, 2018). Research on co–crystallization of BC and mannan confirms that mannan binds BC in a soft manner, which is due to the limited solubility of high DP mannan (K. I. Uhlin et al., 1995). Mannan inhibits tight aggregation of cellulose ribbons during aggregation of multiple subelementary fibers and/or ribbon formation (Tokoh et al., 2002). Although mannan reduces the crystallinity of cellulose, it does not greatly alter cellulose fibers because the structural differences of mannan and cellulose prevent association processes (K. I. Uhlin et al., 1995). In BC cultured in acetylglucomannan medium, a reduction of DS_{Ac} affects the solubility of mannan by preventing aggregation and/or co–crystallization of mannan chains, resulting in the formation of intertwined cellulose fibers gathered in loose bundles (Berglund, 2018; Brown, 1982). Here, mannan is reported to form an amorphous substance, molded in BC corresponding to the looseness component.

The decreasing degree of galactosylation in galactomannan is inversely related to its incorporation into BC. Based on the structural features of galactomannans, kinetic (entanglement of BC–BC binding region) and thermodynamic (lowest free energy state) controls have been proposed to explain the influence of mannans on fiber association (Whitney et al., 1998). It has been observed that both konjac glucomannan and low–galactose galactomannan form a highly heterogeneous structure consisting of an indistinguishable BC–mannan mash, apparent BC–mannan patterns and a separate mannan network (Whitney et al., 1998).

1.4. Mechanical properties of bacterial cellulose–hemicellulose plant cell wall analogues

The mechanical properties of BC fiber networks largely depend on several crucial factors, such as the amount of fibers, their length, diameter and crystallinity, the homogeneity of fiber distribution within the network and the moisture content. In general, BC hydrogels are more extensible and have lower failure stresses and elastic moduli compared to dried fiber networks. This is due to the moisture–induced lubricating effect, so that the adsorbed moisture limits the stiff interactions between the fibers (Sanchavanakit et al., 2006).

The introduction of hemicellulose into the fiber network may result in a shift in mechanical properties of both the stresses and moduli of the corresponding PCW analogues. Usually, pectin and xyloglucan additives increase the elongation at break and decrease the stress at break compared to bare BC fiber network. The increase in elongation at break is explained by the hydration of xyloglucan and pectin, which allows relaxation of the cellulose network during elongation (Cybulska et al., 2010). Increased moisture uptake is generally reported when hydrophilic and amorphous hemicelluloses are incorporated into the cellulose network (Chanliaud et al., 2002).

Another consideration for the mechanical properties of BC–hemicellulose PCW analogues is that matrix polysaccharides may partially take over the load from the cellulose, resulting in increased uniaxial extensibility (Chanliaud et al., 2002; Cybulska et al., 2023). However, modeling studies consider hemicellulose load–bearing effect as low (Kha et al., 2008).

Uniaxial compression of BC–hemicellulose PCW analogues shows its viscoelastic and elastic behavior at slow strain rate, and elastic at high strain rate (Lopez-Sanchez et al., 2015). The presence of any hemicellulose enhances resistance to cramping at slow strain rate. It is reported that the compressed structure is highly destructive assuming that the mechanical response of BC–hemicellulose PCW analogues is highly dependent on the heterogeneous nature of the additives (Lopez-Sanchez et al., 2015).

1.5. Atomistic modelling of cellulose and hemicellulose chains and their interactions

Atomistic modeling considers each PCW β–glucan as an ensemble of individual atoms coupled by a springs corresponding to a single bonds. In terms of PCW modeling, the current approach is crucial to verify and complement experimental measurements of structural and energetic properties and to gain a fundamental understanding of interaction patterns. In the

PCW simulation, modelling of an intra– and interchain hydrogen bonding patterns of different cellulose allomorphs (Iα, Iβ, amorphous) and the interactions with water and other β–glucans using molecular modeling (MM) and molecular dynamics (MD) is a high priority.

The results of all–atom modeling show that cellulose of both Iα and Iβ allomorphs mainly forms $O_3 - H \cdots O_5$ and $O_2 - H \cdots O_6$ intrachain hydrogen bonds, while interchain bonding occurs for every glucose unit via $O_6 - H \cdots O_3$ mechanism (Poma et al., 2015, 2016). Compared to the intra– and interchain hydrogen bonds, intersheet hydrogen bonds are much weaker in both allomorphs due to the predominant $C - H \cdots O$ bonding mechanism combined with the local chain perturbations (Mazeau, 2005). However, the binding patterns differ when water is introduced into the system. It was observed that Iβ cellulose is stiffer when simulated hydrated. Thus, fiber stiffness is related to water–mediated hydrogen bonding and conformational disorder of the surface hydroxyl groups (Petridis et al., 2014). Another predicted mechanism of cellulose–water interaction could arise from the hydration of non–polar cellulose surfaces with a top localization of aliphatic hydrogen atoms (Matthews et al., 2006). Both water binding patterns are thought to be strong enough to limit the diffusion of matrix molecules around the cellulose (Matthews et al., 2006).

While the cellulose chain is considered to be conformationally stable, the hemicellulose chains are rather flexible. Modelling results indicate that in hemicelluloses, glycosidic bonds of glucose exist in one possible conformation, while those of mannose can exist in two and those of xylose – in three possible conformations (Berglund, 2018; Berglund et al., 2016). Theoretically, hydrogen bond network could force glycosidic chains into the most rigid (energetically strained) conformation, but the effect of moisture presence predominates there. The sidechains also provide some additional stiffness to the backbone, but not by hydrogen bonding, but rather by changing the conformation of the glycosidic bonds to a more stable form (Berglund et al., 2019).

Such an ensemble of β–glucan chain properties allow the nature and atomistic properties of cellulose–hemicellulose interactions to be discovered *in silico*. In general, the binding patterns between cellulose and hemicellulose are highly dependent on hydrogen bonding, van der Waals forces and the presence of hemicellulose sidechains (Besombes & Mazeau, 2005; Lau et al., 2018). To a large extent, moisture introduced into a system can also influence β–glucan interactions, presumably by adsorbing to both cellulose and hemicellulose and migrating within hydrogen bonds (Vrublevskaya et al., 2017).

In the early days of the modelling era, it was shown that the planar chain regions of xyloglucan are a dominant factor for cellulose binding. The proposed mechanism is that the binding of xyloglucan to cellulose is initiated over a short (2–3 monosaccharides) span, followed by binding propagation, coupled with backbone and sidechain conformational changes (Levy et al., 1997). Conformation–based adsorption is thought to be dependent on both the backbone and sidechains (Levy et al., 1997; Q. Zhang et al., 2011; Zhao et al., 2014). However, large side chains are highly unlikely to transition to a flat conformation due to steric hindrances, so this may potentially determine the desorption of xyloglucan and/or readsorption to other cellulose surfaces (Hanus & Mazeau, 2006). The introduction of water into a modelling system results in the adsorption of hemicellulose being determined by van der Waals forces rather than electrostatic interactions (Q. Zhang et al., 2011). Under these conditions, xyloglucan preferentially binds to the hydrophobic cellulose surface through hydrophobic interactions (Zhao et al., 2014).

Similar to xyloglucan, xylan sidechains (namely glucuronic acid) stabilize the binding to cellulose by limiting mobility of the backbone (Pereira et al., 2017) so that leading from a threefold to a twofold screw conformation (Martínez-Abad et al., 2017). However, the opposite effect is reported for arabinose substitutes (Martínez-Abad et al., 2017). Kinking on the cellulose surface is reported for unsubstituted xylan (Li et al., 2015). Another similarity between xylan and xyloglucan is that the interactions of xylan with parallel oriented sidechains with the hydrophobic cellulose surface are stronger than with the hydrophilic one. This is explained by an increasing effect of hydrophobic interactions, which also stabilize the xylan backbone (Martínez-Abad et al., 2017). What is of particular interest for xylans is the fact that calcium ions generate glucuronic acid crosslinks in the interchain junctions, which also stabilize the xylan bonding to cellulose (Pereira et al., 2017).

Despite progress in understanding the structural and interaction patterns of cellulose/hemicellulose, existing models and approaches may not be complete and suitable to provide all relevant data, as the agreement between model predictions and experimental data is highly context–dependent (Geitmann, 2010).

1.6. Atomistic modeling of cellulose and hemicellulose chain mechanics

Atomistic molecular dynamics (MD) simulations of cellulose fibers show that for an infinitely long cellulose chain, non–bonded interactions determine the elasticity of the chain at low strain values (Wu et al., 2011), such that removal of non-bonded interactions can reduce the elastic properties of a chain by up to 40% (Djahedi et al., 2015; Habibi et al., 2010). In contrast, the bonded interactions determine the elasticity of the chain at high strain values. Thus, the effect of hydrogen and covalent bonds on chain stiffness is hidden in the effect of cooperative bonding (Altaner et al., 2014).

Crucial to the mechanobiology of PCW is that the contribution of hydrogen bonds to the elasticity of the cellulose chain decreases with increasing DP (Djahedi et al., 2016; Wu et al., 2011). A comparison of the chain stiffness of Iα and Iβ cellulose show that for Iα cellulose, the removal of hydrogen bonds lead to a decrease in chain stiffness values compared to Iβ cellulose (Eichhorn & Davies, 2006), which could be due to the chain stiffness of Iβ cellulose on its hydrophilic side (Glass et al., 2012). However, when modelling the stretching of a bundle of cellulose chains, the hydrogen bonds determine poor deformation recovery due to the slip–stick behaviour of the newly formed hydrogen bonds (W. Chen et al., 2004).

Various simulation approaches have reported that the elastic moduli of the simulated cellulose fibers are consistent with the experimental values (Djahedi et al., 2016; Glass et al., 2012; X. M. Zhang et al., 2013). Despite the similarities in the elasticity of different cellulose allomorphs, the regulatory mechanisms may differ. For example, the effect of bond stretching is predominant in Iβ cellulose compared to II_0 and III_I cellulose, while angle bending is similar in all three cases, albeit at different atoms (C_1 for III_I, O_1 for Iβ and II_0). This important point lead to the understanding that the tensile deformation in the different cellulose allomorphs is provided by the main role of one degree of freedom, while the other degrees of freedom play a minor role (Djahedi et al., 2015).

The other issue affecting mechanical properties of cellulose fiber is its ability to form periodical longitude kinks, possibly caused by an energy decrease in kinking zones, coupled with torsional and van der Waals interactions (Fan & Maranas, 2015). Such a kinking correspond to both predefining locations for the biomechanical hotspots of cellulose–hemicellulose fiber network (Park & Cosgrove, 2012b), as well as predetermine cellulose Iα–Iβ interconversion (Jarvis, 2000).

Regarding cellulose–hemicellulose interactions, both interfiber contact area, hydrogen bonding, and hemicellulose covalent bonds are defined as a crucial parameters of the stiffness of cellulose–hemicellulose interactions (N. Zhang et al., 2015). When cellulose is bridged by hemicelluloses, both hydrogen bonds and hemicellulose chains are considered to stretch counterforcing shear deformation. As for the loop interactions, hemicellulose contact surface acts like a sticker for cellulose, reducing any surface sliding. Random cellulose–hemicellulose interactions are assumed to provide too low contact surface, being ineffective to oppose shear forces standalone (N. Zhang et al., 2015).

1.7. Modeling of plant cell wall structures

Unfortunately, development of a fully–atomistic PCW model won’t be possible in the nearest future due to computational limitations. Thus, it allows researches within the field to apply particle–based approaches on modelling of both cellulose and hemicellulose fibers. Such a modelling approach consider fiber as a beam of separate particles, coupled by an imaginary spring which correspond to a reservoir of overall energy of an individual bonds, at the same time defining fiber stiffness. And what is known with certainty today is that the mechanical properties of PCW are determined by the microstructure and the physicochemical properties of the cellulose–hemicellulose fiber network, which, for our luck, can be modelled with such a particle–based approach. However, as this was only a hypothesis at the time and computational capabilities were limited, fiber networks of a very simple, paper–like structures with random length and distribution of fibers began to be developed. Such models were based on the finite element method, where the fibers were modeled as homogeneous, linearly elastic, straight rods randomly distributed in 2D or 3D. Interfiber connections were generally treated as rigid or flexible spring connections. These pioneering researches enabled the investigation of patterns of network stiffness (Yang, 1975), axial stress distribution (Rigdahl et al., 1984), the role of fiber orientation on opposing mechanical loads (Hamlen, 1991), bond strength (Åström & Niskanen, 1993), etc. Subsequent studies confirmed the crucial role of the spatial distribution of fibers, curvature and sliding interfiber interactions as decisive factors for the mechanical response of the fiber network (Heyden, 2000). The density of the network has been found to positively affect its stiffness, but the functions describing this are different for 2D and 3D networks. The overall stiffness is negatively related to the fiber curvature, which also depends on the network density. The current investigations have been extended in the present time, in that the elastic modulus of such a fiber networks increases with increasing fiber length, fiber modulus, bond density and network density, but decreases with increasing fiber diameter and fiber curvature (Mao et al., 2017). Although such a models of fiber networks provided crucial insights into the mechanobiology of PCW, a number of constraints critical to PCW organization (type of binding, presence of linkers and matrix constituents) allowed such models to be considered idealized.

Specific modeling of PCW–like structures began in the late 2000^{s} (Kha et al., 2008, 2010). Still taking a purely mechanistic view of PCW architecture, tethered and multinet network models were conceptually revised. It was found that the role of hemicellulose as a load–bearing agent increases with increasing size of PCW, with no suggestions regarding the binding and unbinding mechanism of cellulose–hemicellulose interactions. The current approach has been extended to the mechanical responses of PCW by revising the role of hydrogen bonds, declaring the hydrogen bond between cellulose and hemicellulose as the weakest structural component of PCW (Yi et al., 2012, 2013; Yi & Puri, 2012).

As far as the biomechanical hotspot PCW model was proposed in 2012, research focused on defining the molecular (particle–based) principles hidden in PCW mechanobiology rather than moving forward with a classical mechanics approach. As a result, current PCW models are built according to the principles of MD, particle dynamics or the discrete element method. Methodologically, the structure of such a fiber networks is defined both by cellulose/hemicellulose/pectin fibers (discretized by beads), spring interactions between successive intrafiber beads (with introduction of axial, bending or torsional stiffness) and interactions between interfiber beads (with repulsive and attractive potentials). To date, such an approach has led to three particle–based examinations of PCW mechanobiology. In the very first, Nili et al. investigated a biomechanical hotspot cell wall model, which is almost an *in silico* reduplication of the research of (Park & Cosgrove, 2012a) with XEGH PCW degradation (Nili et al., 2015). The results of simulation showed that, on average, 3.75 xyloglucan links per cellulose fiber is a lowest critical value for PCW integrity, which is consistent with Park and Cosgrove's predictions (≈0.3% wt. xyloglucan fraction at a cellulose:xyloglucan ratio of 1:1). However, simulations unveiled that cellulose–hemicellulose PCW network is not sufficient to counteract the turgor pressure by itself, suggesting pectin–based mechanisms involved in regulation of PCW stiffness (Yi & Puri, 2014). The following research was conducted by (Mani et al., 2020), who developed a coarse–grained (CG) model of layered PCW based on the dissipative particle dynamics technique to investigate the relationships between the fiber movement and the initial phase of PCW deformation. Here, the authors modeled cellulose and pectin as bead–spring chains, while xyloglucan was modeled as a single bead connecting two fibers. The simulations showed that all lamellar components undergo a collective reorientation when force is applied, while the cellulose fibers predominantly buckle transverse to the direction of elongation. Somehow in contrast to the research of (Nili et al., 2015) the length of the pectin chains, simulated over a range of values, showed almost no influence on the movement of the cellulose fibers, so that declaring the role of xyloglucan and pectin as cellulose fiber coating and background matrix, respectively. A modern CG model of PCW was proposed by (Y. Zhang et al., 2021) to simulate the mechanics of epidermal PCW of *Allium cepa* at the nanoscale. In this model, both cellulose, xyloglucan and pectin were randomly distributed in separate lamellae, thus mimicking the CESA deposition of PCW components. The current research has shown that the cellulose fibers counteract stress most and the sliding of the fibers determines the plastic deformation of the PCW. In addition, the structural parameters of xyloglucan and pectin hardly determined the mechanical properties of PCW, as they assumed the role of cellulose interfiber mediators.

2. Research hypotheses and the aims of study

The above literature review shows a very complex structure of the natural plant cell wall, in which hemicelluloses interact with cellulose and the resulting composite acts as the load-bearing network of the cell wall. Bacterial cellulose provides a useful scaffold into which various polysaccharides can be incorporated to mimic the structure of plant cell wall. A major advantage of the plant cell wall analogues produced is the possibility of macroscopic evaluation of the mechanical properties of the composite. Furthermore, it must be pointed out that the model of the plant cell wall is not yet accepted and that an instrument for investigating the structural properties of the cell wall still needs to be developed. Therefore, a combined approach is proposed in this dissertation, where the experimental study on bacterial cellulose-plant hemicellulose composites is used to build and validate the computational model of the fiber network, which is representing plant cell wall load-bearing network. This approach made it possible to interpret the specific effects of the individual hemicelluloses on the cell wall properties. The developed model can be further used (most likely by adding pectin into account) to study the structure-related mechanics of the plant cell wall.

Research hypotheses

1. Structural properties and mechanical responses of hemicellulose-cellulose composites depends on the type of hemicellulose.
2. Interfiber interaction is the main factor affecting the mechanical properties of cellulose-hemicellulose composites.

Aim of the study

To create structural model of cellulose-hemicellulose assembly relevant to plant cell wall and capable on description of plant cell wall mechanobiology from single fiber to whole fiber network.

Specific aims of the study

1. To characterize the effect of one of xylan, arabinoxylan, xyloglucan, and glucomannan on structural, molecular and mechanical properties of bacterial cellulose-hemicellulose plant cell wall analogues on both nano- and macroscale with respect to the content of hemicellulose.
2. To establish a numerical model based on a coarse-grained molecular dynamics that evaluates the mechanical properties of bacterial cellulose-hemicellulose plant cell wall analogues.
3. To validate a mechanical properties of a numerical model obtained against the nano- and macroscale mechanical properties of bacterial cellulose-hemicellulose plant cell wall analogues, depending on specific type of hemicellulose and its content present.

3. Results

3.1. Overview of published studies

In the published manuscripts P1, P2, P3, P4 and yet unpublished research P5, an exhaustive analysis of an existing information on structure and mechanical properties of cellulose–hemicellulose fiber networks, concepts of plant cell wall structure, as well as its numerical models, was provided. It allowed to proceed with a bacterial cellulose–hemicellulose fiber networks as a plant cell wall analogues, replicating the patterns of cellulose-hemicellulose interactions *in muro*. Research methodologies were developed in a way to provide a full-scale characterization of an established plant cell wall analogues, with a focus on its chemical (high-performance liquid chromatography, enzymatic treatment), structural (atomic force microscopy), molecular (Raman spectroscopy), and mechanical (tensile tests with constant and cyclic strain rates, nanoindentation tests) properties.

Particle-based modeling of cellulose-hemicellulose fiber networks according to hotspot plant cell wall model was achieved by means of coarse-grained molecular dynamics simulation. As a key element of a current work, mechanical properties of a simulated network were validated according to the structural and mechanical properties of an established bacterial cellulose-hemicellulose plant cell wall analogues. In addition, sensitivity analysis of an established numerical model was conducted according to its structural (fiber length, fiber diameter), and mechanical (force constant of interfiber interaction, fiber modulus) parameters.

Below, the main conclusions of each publication are summarized. The full manuscripts are attached at the end of dissertation.

3.2. Manuscript P1 (Tailor-Made Biosystems – Bacterial Cellulose-Based Films with Plant Cell Wall Polysaccharides)

Chibrikov, V., Pieczywek, P. M., Zdunek, A., 2023. Tailor-Made Biosystems Bacterial Cellulose-Based Films with Plant Cell Wall Polysaccharides. Polymer Reviews, 63(1), 40-66. DOI: 10.1080/15583724.2022.2067869

The aim of the review manuscript P1 was an explicit summarization of an existing researches regarding specific paths of the preparation of BC–hemicellulose PCW analogues, as well as structural and mechanical properties of the networks of bacterial cellulose, hemicelluloses, as well as BC–hemicellulose PCW analogues. A particular overview of structural and mechanical properties of hemicelluloses and BC–hemicellulose PCW analogues were focused predominantly on xylan, arabinoxylan, xyloglucan and glucomannan hemicelluloses as the most distributed one of monocotyledons and dicotyledons.

BC fiber networks appear as a multi-layered structures of in-plane homogeneously and randomly distributed fibers of high chemical purity. Variability of its structural properties is largely determined by the network formation, which can be enhanced or limited by biological factors (metabolic activity of bacteria strains, presence of other microorganisms), as well as chemical (composition of the medium) and physical (viscosity of the medium, cultivation temperature, static or dynamic type of cultivation) one. Mechanical response of BC hydrogels is generally weaker, compared to dried one, in terms of the stresses applied, being highly determined by the moisture-induced plasticization. Collapsing upon drying lead to an increased interfiber interaction, thus making the network stronger and less extensible.

Casted hemicellulose films oppose stresses in a matter comparable to BC, which rely on density of hemicellulose chain packing, and is positively correlated with DP, and the presence of sidechain substitutions of hemicellulose backbone. However, strain response of hemicellulose casted films is higher, compared to bacterial cellulose, which is determined by moisture-induced plasticization of amorphous hemicelluloses.

Hemicelluloses provide to formation of a fine-structured BC. However, versatility of structural and mechanical properties of BC–hemicellulose PCW analogues is determined by the patterns of cellulose-hemicellulose interactions, which affect both packaging of cellulose fibers, microfibers, and chains. Those interaction patterns include hemicellulose adsorption and aggregation on cellulose fiber/microfiber (both reversible and irreversible), cross-link formation, intertwining cellulose fibers/microfibers, etc., and are highly dependent of polymerization and substitution degrees of subsequent hemicelluloses. As a general trend, mechanical properties of BC–hemicellulose PCW analogues are higher for the one with hemicelluloses of higher DP (reinforcing effect) and DS (enhanced flexibility and interconnectivity). Alteration of the biosynthesis with an addition of hemicelluloses to culturing medium is another factor to be considered while establishing BC–hemicellulose PCW analogues, being dependent on the viscosity of culturing medium, as well as ability of cellulose-synthesizing bacteria to utilize hemicelluloses.

3.3. Manuscript P2 (*In silico* studies of plant primary cell walls - structure and mechanics)

Pieczywek, P. M., Chibrikov, V., Zdunek, A., 2023. In silico studies of plant primary cell walls-structure and mechanics. Biological Reviews, 98(3), 887-899. DOI: 10.1111/brv.12935

Review manuscript P2 aimed to overview and generalize existing physical and biomechanical aspects of PCW architecture. Since the late 1960^{s}, when the first concepts of PCW structure were reported, scientific community evolved throughout various suggestions of plant cell wall architecture, each defined by a structure- and property-related patterns of the main plant cell wall polysaccharides - cellulose, hemicelluloses and pectin. At the very first tries, only cellulose fibers were considered to define plant cell wall integrity, while the role of hemicelluloses and pectin was neglected to some matrix polysaccharides. The following suggestions on plant cell wall structure considered the role of hemicelluloses and pectin, and especially interaction of those with cellulose, in defining PCW strength and extensibility. While one models suggested hemicellulose (or rather specific one of - xyloglucan) to maintain cellulose integrity via road-like tethers (Fig.5c), the other considered plant cell wall structure as a sandwich of interconnected cellulose, hemicelluloses and pectin (Fig.5a-b). The latest commonly recognized model of PCW architecture is called a biomechanical hotspot model (Fig.5d). According to it, plant cell wall integrity is defined by a xyloglucan-linking amalgam, located in a close proximity to the contact surfaces of adjacent cellulose fibers. Such a cellulose-xyloglucan-cellulose interaction hotspots are short (dozen on nanometers), require low amount (appr. 0.3% wt.) of all xyloglucan present in PCW and are thought to define PCW strength and extensibility prior to the bulk viscosity of matrix polysaccharides.

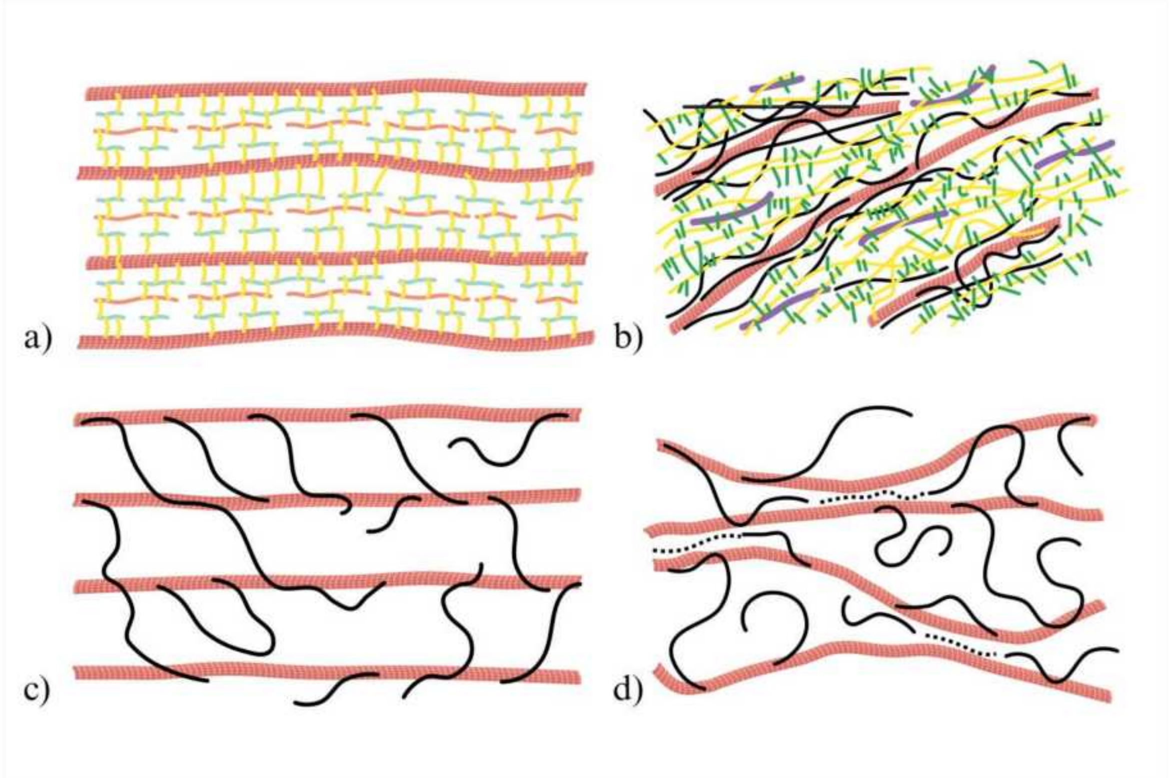

Fig.5. Models of PCW: a) model with covalently linked matrix, b) multi-coat model, c) tethered network, d) biomechanical hotspot model. Red lines represent cellulose fibers, black – hemicellulose (xyloglucan), yellow – pectin. Redrawn after (Pieczywek et al., 2023)

An additional aim of current work was to concisely overview an existing numerical models of polysaccharide interactions in PCW with a regard to the fine structure of network, its supramolecular properties and polysaccharide binding affinity. The very first assumptions on the patterns which define PCW strength and extensibility were explored with a random fiber networks, which allowed to define the contribution of fiber stiffness, length, and diameter, together with network and bond densities (Fig.6).

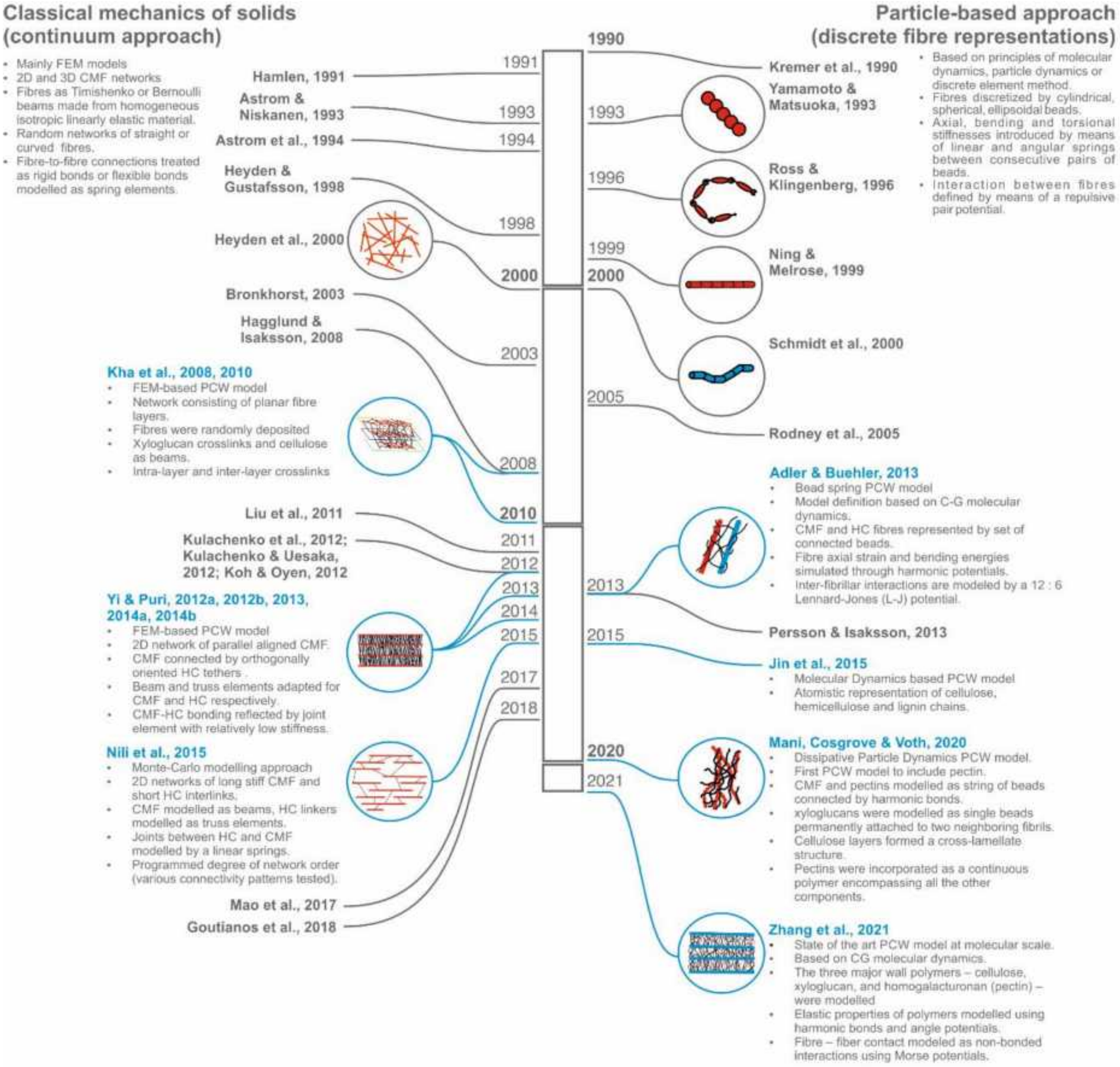

Classical mechanics of solids (continuum approach)

- Mainly FEM models
- 2D and 3D CMF networks
- Fibres as Timishenko or Bernoulli beams made from homogeneous isotropic linearly elastic material.
- Random networks of straight or curved fibres.
- Fibre-to-fibre connections treated as rigid bonds or flexible bonds modelled as spring elements.

Kha et al., 2008, 2010

- FEM-based PCW model
- Network consisting of planar fibre layers.
- Fibres were randomly deposited
- Xyloglucan crosslinks and cellulose as beams.
- Intra-layer and inter-layer crosslinks

Yi & Puri, 2012a, 2012b, 2013, 2014a, 2014b

- FEM-based PCW model
- 2D network of parallel aligned CMF.
- CMF connected by orthogonally oriented HC tethers .
- Beam and truss elements adapted for CMF and HC respectively.
- CMF-HC bonding reflected by joint element with relatively low stiffness.

Nili et al., 2015

- Monte-Carlo modelling approach
- 2D networks of long stiff CMF and short HC interlinks.
- CMF modelled as beams, HC linkers modelled as truss elements.
- Joints between HC and CMF modelled by a linear springs.
- Programmed degree of network order (various connectivity patterns tested).

Particle-based approach (discrete fibre representations)

- Based on principles of molecular dynamics, particle dynamics or discrete element method.
- Fibres discretized by cylindrical, spherical, ellipsoidal beads.
- Axial, bending and torsional stiffnesses introduced by means of linear and angular springs between consecutive pairs of beads.
- Interaction between fibres defined by means of a repulsive pair potential.

Adler & Buehler, 2013

- Bead spring PCW model
- Model definition based on C-G molecular dynamics.
- CMF and HC fibres represented by set of connected beads.
- Fibre axial strain and bending energies simulated through harmonic potentials.
- Inter-fibrillar interactions are modeled by a 12 : 6 Lennard-Jones (L-J) potential.

Jin et al., 2015

- Molecular Dynamics based PCW model
- Atomistic representation of cellulose, hemicellulose and lignin chains.

Mani, Cosgrove & Voth, 2020

- Dissipative Particle Dynamics PCW model.
- First PCW model to include pectin.
- CMF and pectins modelled as string of beads connected by harmonic bonds.
- xyloglucans were modelled as single beads permanently attached to two neighboring fibrils.
- Cellulose layers formed a cross-lamellate structure.
- Pectins were incorporated as a continuous polymer encompassing all the other components.

Zhang et al., 2021

- State of the art PCW model at molecular scale.
- Based on CG molecular dynamics.
- The three major wall polymers – cellulose, xyloglucan, and homogalacturonan (pectin) – were modelled
- Elastic properties of polymers modelled using harmonic bonds and angle potentials.
- Fibre – fiber contact modeled as non-bonded interactions using Morse potentials.

Fig.6. Timeline showing the development of fiber network and PCW models. The models are split into two major categories based on applied modelling methodologies. Both are briefly characterized with bullet point descriptions of model/modelling principles. Grey lines indicate general models of fibrous structures (paper, nano-paper, other cellulose networks). Blue lines indicate models specific to PCWs. CG, coarse grained; CMF, cellulose microfiber; FEM, finite element model; HC, hemicelluloses. The pictograms in the circles represent the main ideas of how PCW structures are represented in models–from linear continuous structures to discrete representation using beads of different shapes. Colours correspond to main PCW structural polysaccharides: cellulose (red, blue), hemicelluloses (black), pectin (yellow). Redrawn after (Pieczywek et al., 2023).

First computation models, focused exclusively on mechanobiology of PCW, examined cellulose-hemicellulose scaffold according to both tethered and biomechanical hotspot models. Despite gaining insights on structure-dependent response of cellulose-hemicellulose scaffold on opposing mechanical loads, the first approaches used were too general. In such a studies, clearly mechanistic modeling prevailed, considering cellulose fibers as beams, connected by fixed-point hemicellulose trusses. Such a modeling limitations allowed to define a bottleneck of mechanistic approach – modeling of fiber motion, bonding–debonding interactions of plant cell wall polysaccharides, and the role of PCW matrix in governing cell wall stiffness.

The following modeling approaches revised PCW architecture by the particle–based representations of plant cell wall polysaccharides and were based on the principles of particle dynamics simulations. Current techniques granted to consider close–to–atomic nature of plant cell wall polysaccharides, as well as to define non–bonded interactions as a part of interfiber interaction forces. Up–to–date implementations of particle dynamics simulation techniques allowed to investigate the patterns of distribution, arrangement, and deformation of PCW polysaccharides, which affect mechanobiology of PCW. However, current modeling implementations are far from complete. The role of pectin and arabinogalactan proteins in PCW responsiveness is barely revealed, as well as there is no practical approach established to simulate growth enhancement and turgor expansion of PCW.

3.4. Manuscript P3 (Evaluation of elasto–plastic properties of bacterial cellulose-hemicellulose composite films)

Chibrikov, V., Pieczywek, P. M., Cybulska, J., Zdunek, A., 2023. Evaluation of elasto–plastic properties of bacterial cellulose–hemicellulose composite films. Industrial Crops and Products, 205, 117578. DOI: 10.1016/j.indcrop.2023.117578

Current research study aimed to investigate the effect of hemicelluloses on the elasto–plastic properties of BC–hemicellulose PCW analogues. According to the hypothesis of current research study, difference in physico–chemical properties of PCW hemicelluloses lead to a different elasto–plastic response of respected PCW analogues. In a current research paper, results on mechanical and molecular properties of an established BC–hemicellulose PCW analogues were presented.

3.4.1. Preparation of bacterial cellulose–hemicellulose plant cell wall analogues

BC–hemicellulose PCW analogues were biosynthesized by *Komagataeibacter xylinus* ATCC–53524 bacteria strain in modified Hestrin–Schramm medium with an addition of the one of birchwood xylan, wheat arabinoxylan, tamarind xyloglucan, or konjac glucomannan hemicelluloses (all – Megazyme, Ireland) at different concentrations.

3.4.2. Elasto–plastic properties of bacterial cellulose–hemicellulose plant cell wall analogues

Mechanical properties of BC–hemicellulose PCW analogues were accessed by means of uniaxial tensile test with cyclic strain rate until failure, with a 0.2% tensile strain increments per cycle. Analysis of a strain–stress curves obtained allowed to define purely mechanistic parameters, such as maximum modulus, maximum stress and maximum strain. In addition, contribution of plastic deformation to overall mechanical response of BC–hemicellulose PCW analogues was evaluated via defining its total plastic strain. For BC–hemicellulose PCW analogues studied, presence of both xylan and arabinoxylan resulted in a statistically significant increase of stresses and moduli, as well as the role of plastic deformation in opposing load applied. For xyloglucan, the role of elastic deformation showed moderate yet statistically significant increase, while for glucomannan, applied loads caused predominantly elastic deformation of respected plant cell wall analogues.

3.4.3. Molecular properties of bacterial cellulose–hemicellulose plant cell wall analogues

Raman spectra of BC–hemicellulose PCW analogues appeared similar to those of plant cellulose and hemicelluloses, with clearly defined bond vibrations within spectral regions of hydrogen bonds (3600 cm^{-1}–3200 cm^{-1}) and structural bonds of polysaccharides (3000 cm^{-1}–2800 cm^{-1} and 1500 cm^{-1}–300 cm^{-1}). Most of bond vibrations observed were attributed to cellulose, while some weak vibrations at 1580 cm^{-1} wavenumber and 100–800 cm^{-1} wavenumber range were assigned to the vibrations of the structural bonds of hemicellulose monosaccharides.

3.4.4. Relation between elasto–plasticity and molecular properties of bacterial cellulose–hemicellulose plant cell wall analogues

To evaluate the effect of specific polysaccharide bonds on elasto–plastic properties of BC–hemicellulose PCW analogues, principal component analysis was applied to establish wavenumber–property correlations. It was defined that elastic deformation of BC–hemicellulose PCW analogues studied were determined by stretching vibrations of structural bonds of cellulose and hemicelluloses, while plastic deformation was a matter of molecular and supramolecular changes occurring at cellulose–hemicellulose fiber network (Fig.7).

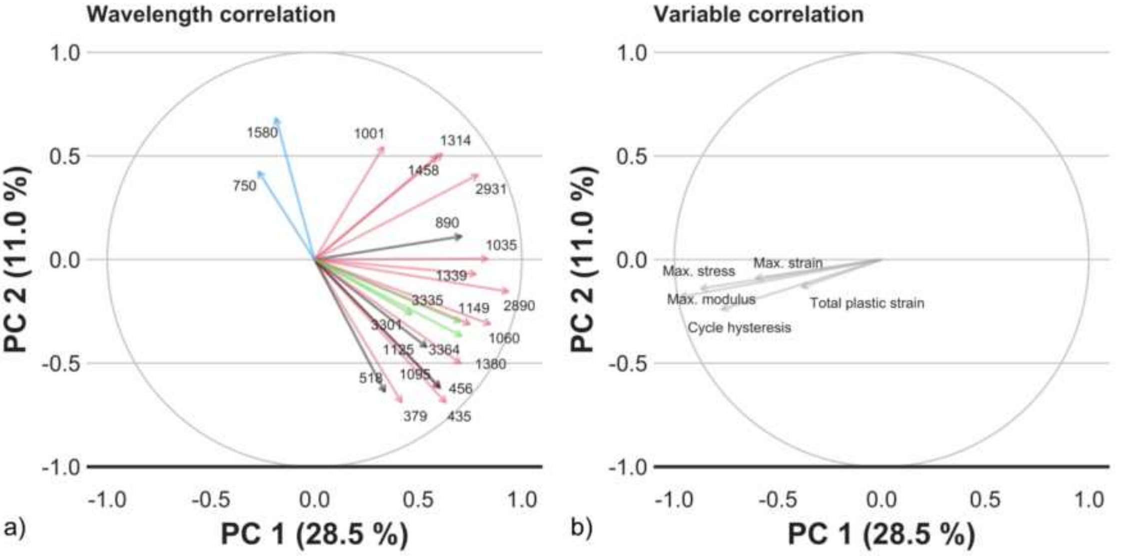

Fig.7. Principal component analysis of spectral data collected from BC–hemicellulose PCW analogues showing: a) correlation between loadings and characteristic spectra wavenumbers. Grey arrows stand for the loadings of the vibrations of glycosidic bonds, red – for ring bond vibrations, green – for hydrogen bond vibrations, blue – for the vibrations of other saccharides; b) correlation between loadings and mechanical properties of BC–hemicellulose PCW analogues. Arrow direction represents correlation between characteristic spectra wavenumber/mechanical property and the PC, and the arrow length represents the strength of the relation between characteristic spectra wavenumber/mechanical property and PC. Redrawn after (Chibrikov et al., 2023).

Correlation matrix allowed to establish overall relations between hemicellulose content in culturing medium, mechanical and molecular properties of BC–hemicellulose PCW analogues (Table 1). Positive correlations between glucomannan content and vibrations of the structural bonds of BC–glucomannan PCW analogues defined its increasing role in elastic deformation. In contrast, correlation trends were opposite for BC–xylan and BC–arabinoxylan PCW analogues, revealing its predominantly plastic deformation for the loads applied.

Table 1 Heatmap representation of Pearson correlation values for the relation of the hemicellulose polysaccharide content and mechanical property or peak of characteristic wavenumber. Heatmap colors represent the Pearson correlation ranges, from cyan (negative correlation), passing through white (no correlation), to mustard (positive correlation) hues. Abbreviation NA stands for *not applicable*. Redrawn after (Chibrikov et al., 2023).

Physical quantity		Molecular structure	Functional group	Hemicellulose			
				AX	KGM	XGY	XYL
Mechanical	Maximum	NA	NA	0.38	-0.64		0.75
	Maximum stress			0.43	-0.74		0.73
	Maximum strain				-0.63		
	Total plastic strain				-0.63		
	Cycle hysteresis				-0.66	-0.35	0.40
Wavenumber	379	Ring bonds	C-C-C, C-O, and C-C-O bending vibrations		0.44	-0.45	-0.47
	435		C-C-C, and C-C-O bending vibrations		0.60	-0.44	-0.39
	456		C-C-C, and C-C-O bending vibrations		0.55	-0.49	
	1001		H-C-H rocking bending vibrations			0.48	-0.35
	1035		C-C and C-O stretching vibrations		0.70	0.31	-0.41
	1060		C-C and C-O stretching vibrations		0.68		-0.60
	1149		C-C, C-O asymmetric stretching vibrations		0.65		-0.53
	1314		H-C-C, H-C-H, C-O-H, H-C-O bending vibrations	-0.33	0.51	0.65	-0.65
	1339		H-C-C, H-C-H, C-O-H, H-C-O bending vibrations	-0.52	0.60	-0.39	-0.56
	1380		H-C-H, H-C-C, H-O-C, C-O-H bending vibrations		0.67	-0.45	-0.32
	1458		H-C-H scissoring bending vibrations	-0.69	0.47		
	2890		C-H and H-C-H stretching vibrations	-0.46	0.78	-0.39	-0.64
	2931		C-H and H-C-H stretching vibrations	-0.57	0.65		-0.49
	3301	Hydrogen bonds	Inter- and intrachain hydrogen bonds		0.39		-0.32
	3335		Inter- and intrachain hydrogen bonds		0.53	-0.37	-0.47
	3364		Inter- and intrachain hydrogen bonds		0.58		-0.50
	750	Hemicellulose	C-O-H, C-C-H, and O-C-H bending vibrations of	0.51	-0.42	0.81	-0.51
	1580		C-O stretching vibrations of galactose		-0.47	0.61	
	518	Glycosidic bonds	C-O-C bending vibrations		0.52	-0.49	
	890		C-O-C stretching vibrations		0.71	0.64	-0.33
	1095		C-O-C asymmetric stretching vibrations		0.63	-0.33	-0.47
	1125		C-O-C symmetric stretching vibrations		0.55		-0.63

3.5. Manuscript P4 (Coarse–grained molecular dynamics model to evaluate the mechanical properties of bacterial cellulose–hemicellulose composites)

Chibrikov, V., Pieczywek, P. M., Cybulska, J., Zdunek, A., 2024. Coarse–grained molecular dynamics model to evaluate the mechanical properties of bacterial cellulose–hemicellulose composites. Carbohydrate Polymers, 121827. DOI: 10.1016/j.carbpol.2024.121827

Current research study aimed to establish a numeric model of BC–hemicellulose PCW analogues to evaluate its mechanical properties. According to the hypothesis of current research study, force of interfiber interaction, which is defined by the hemicelluloses mediating such interactions, is the main factor affecting the mechanical properties of cellulose–hemicellulose fiber networks. In a current research paper, results on mechanical properties of an established BC–hemicellulose PCW analogues were presented. In addition, numeric model, based on coarse–grained molecular dynamics, was established, and validated according to the structural and mechanical properties of BC–hemicellulose PCW analogues.

3.5.1. Nanoscale structural and mechanical properties of bacterial cellulose-hemicellulose plant cell wall analogues

Nanoscale structural and mechanical properties of single fibers of BC–hemicellulose PCW analogues were accessed by means of atomic force microscopy surface topography imaging and nanoindentation tests, respectively. The width of individual fibers decreased statistically significant for BC–xylan PCW analogues, while increasing for BC–arabinoxylan and BC–glucomannan one. Experimental data of nanoindentation tests were fitted according to the Hertz model of the indenter–surface interaction. It showed statistically significant increase with the presence of xylan and xyloglucan, and a statistically significant decrease with an increasing content of glucomannan in culturing medium.

3.5.2. Numerical model

Numerical model was established according to the principles of coarse–grained molecular dynamics simulation, with fibers simulated with bead–spring approach (Fig.8). Intrafiber interactions were defined via harmonic and angular bond potentials, while interfiber interactions – via two–step truncated harmonic potentials. The latter one allowed fibers to rearrange against each other, so that producing dynamic attractive–repulsive forces. A narrow ~1.5 nm range of attractive forces mimicked interfiber interactions according to biomechanical hotspot model of plant cell wall. For the generated and equilibrated models, uniaxial tensile test was simulated according to the conditions of a laboratory test. Strain–stress curves of simulation were comparable to those of laboratory tests, with clearly visible regions of sample elastic and plastic deformation. Current model showed fibers undergo several main types of fiber movements – reorientation, straightening, curving, and sliding along the applied force.

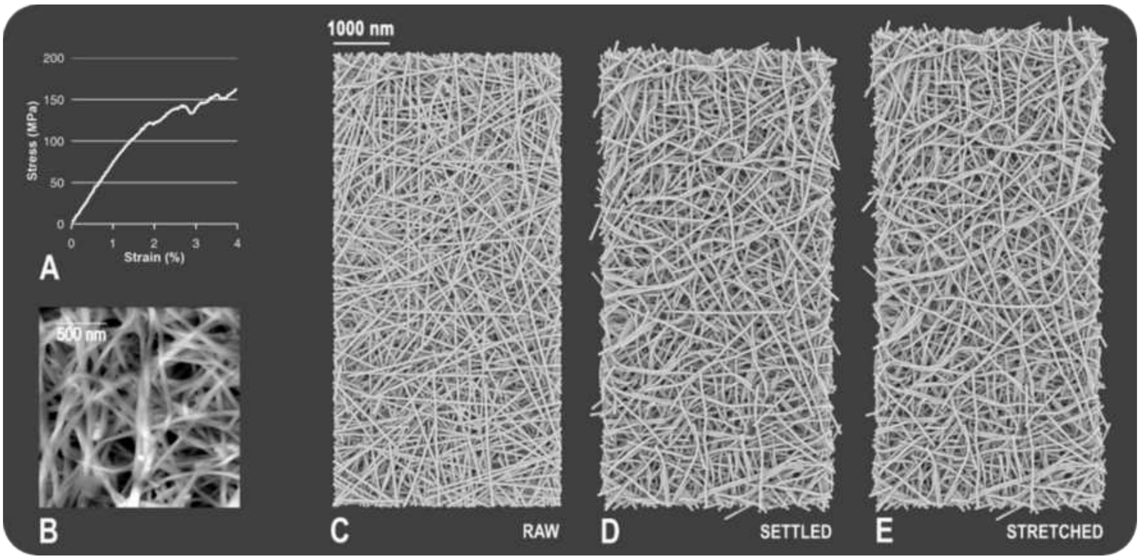

Fig.8. Stages of fiber network modeling: a) stress–strain curve from simulation, b) atomic force microscopy surface topography image of pure BC, c) raw model of BC generated based on atomic force microscopy data, d) model of BC after energy equilibration procedure, and e) model of BC subjected to uniaxial tensile test at constant strain rate. Redrawn after (Chibrikov et al., 2024).

3.5.3. Model sensitivity

Sensitivity of the model was evaluated according to the four input parameters, which contribute mechanical response of fiber network the most – force constant of interfiber interaction, fiber modulus, fiber length, and fiber diameter. Increase of fiber stiffness resulted stresses of elastic deformation to increase in a statistically significant manner, indicating elastic deformation of stiff fiber network is defined by fiber bending resistance. However, with a transition to plastic deformation, respected moduli and stresses showed statistically significant decrease. It is governed by the fact that plastic deformation of stiff fiber network is primarily defined by a number of interfiber contacts (total force of interfiber interaction), amount of which is fewer for less entangled structures. Change in fiber diameter showed lack of statistically significant changes in mechanical response related to elastic deformation within the values tested. In this case, decreasing number of interfiber contacts with an increasing fiber diameter was mitigated by an increasing contact area. However, moduli and stresses of simulated fiber networks decreased with an increasing fiber diameter. To huge extend, it is governed by the logics of the formation of simulated network, in which the volume occupied by the fibers was constant. It resulted in a lower number of thick fibers within the networks, compared to the network of thin fibers, leading to a decrease in total force of interfiber interaction. Extension of fiber length resulted in a statistically significant increase in stresses and moduli within the both regions of elastic and plastic deformation, which was governed not only by an increase in a number of interfiber contacts (total force of interfiber interaction), but also by prolonged phase of fiber reorganization. The most prominent changes were observed with the modification of the force constant of interfiber interactions. While increase in stresses and strains was linear, changes in Young’s moduli and strain hardening moduli were steep for low and high force constants of interfiber interaction, respectively. Rapid initial change in Young's modulus as some lower force constants of interfiber interactions was determined by a network formation conditions, in which increase in force constant caused enhanced fiber adhesion up to some practical limit. In contrast, rapid increase in strain hardening modulus at some high force constants of interfiber interaction defined sensitivity of plastic deformation of such a network structures to supramolecular changes occurring.

3.5.4. Macroscale mechanical properties of bacterial cellulose–hemicellulose plant cell wall analogues – explanatory analysis

Macroscale mechanical properties of BC–hemicellulose PCW analogues were assessed by means of uniaxial tensile tests with constant strain rate. Analysis of a strain–stress curves obtained allowed to define mechanistic parameters of BC–hemicellulose PCW analogues, such as Young's modulus, strain hardening modulus, strain at elastic limit, stress at elastic limit and maximum stress. The results showed that both Young's modulus, strain hardening modulus and maximum stress of BC–xylan and BC–arabinoxylan PCW analogues showed statistically significant increase with an increasing content of respected hemicelluloses. In contrast, BC–xyloglucan and BC–glucomannan PCW analogues showed lack and moderate statistically significant decrease of aforementioned mechanical properties with an increasing content of respected hemicelluloses. Data on mechanical properties of BC–hemicellulose PCW analogues correlated well with the modeling studies. In major cases, mechanical properties of BC–hemicellulose PCW analogues were governed by the force constant of interfiber interaction, which, according to biomechanical hotspot model, is defined by the presence of interfiber hemicellulose mediates. However, in certain cases (BC–xyloglucan and BC–glucomannan PCW analogues) mechanical properties also positively correlated with the change in nanostructural (fiber diameter) and nanomechanical (fiber modulus) properties of cellulose fibers.

4. Supplementary research (The effect of hemicellulose–specific enzymes on the structure and mechanical performance of cellulose-hemicellulose hydrogels)

Chibrikov, V., Pieczywek, P. M., Cybulska, J., Zdunek, A. The effect of hemicellulose–specific enzymes on the structure and mechanical performance of cellulose–hemicellulose hydrogels.

4.1. Introduction

Plant cell wall is highly specialized structure composed predominantly of cellulose, hemicelluloses and pectin (Cosgrove & Jarvis, 2012). While cellulose is considered to be the main load–bearing element of PCW, hemicelluloses have high affinity to cellulose due to the structural similarity, so that mediating interfiber interactions – both directly or indirectly (Khodayari et al., 2021). It resulted in numerous studies suggesting various polysaccharide arrangements in PCW, defining key role of hemicelluloses in maintaining the entirety of plant cell wall scaffold (Carpita & Gibeaut, 1993; Keegstra et al., 1973; Park & Cosgrove, 2012a, 2012b; Probine & Barber, 1966; Talbott & Ray, 1992). Various approaches have already been tested to reveal the insights o cellulose–hemicellulose interactions *in muro* – decomposition of the constituents (Hervé et al., 2009), inhibition of biosynthesis (Park & Cosgrove, 2012b), solubilisation (Goulao & Oliveira, 2008), or its chemical modification (Kozioł et al., 2017).

In current work, another approach was applied – *in vitro* enzymolysis of PCW hemicelluloses in BC–based PCW analogues. It allowed to investigate the effect of hemicellulose additives on the process of biosynthesis, its yield, as well as composition, structure and mechanical properties of BC–hemicellulose PCW analogues. It was hypothesized in current work, that since hemicelluloses differ in structure and chemical composition, their incorporation in cellulose fiber network and enzymatic degradation affect the load–bearing junctions in cellulose–hemicellulose PCW analogues, so that affecting its structure and mechanical properties. In current work, PCW analogues were studied as a water swollen network, providing an analogy to *in vivo* plant cell wall.

4.2. Materials and methods

4.2.1. Sample preparation

4.2.1.1. Biosynthesis of bacterial cellulose–hemicellulose plant cell wall analogues

BC–hemicellulose PCW analogues were synthesized in Hestrin–Schramm medium, modified with hemicellulose additives of a monosaccharide composition and weight average molecular weight, provided in Table 2. Current samples were further defined as *raw*.

Table 2. Monosaccharide composition and weight average molecular weight of hemicelluloses, used in current study. Abbreviation of *Araf* stands for arabinose, *Gal* – galactose, *Glc* – glucose, *GlcA* – glucuronic acid, *Man* – mannose, *Xyl* – xylose. Asterisk sign * refers to data from (Franková & Fry, 2021).

Hemicellulose	Monosaccharide composition (% dry polysaccharide mass)							Weight average molecular weight (kDa)
	Araf	*Gal*	*Glc*	*GlcA*	*Man*	*Xyl*	Other	
Xylan				11.3		86.1	2.6	158.3
Arabinoxylan	37.8					61.7	0.5	323.0
Xyloglucan	2.0	17.0	45.0			34.0	2.0	802.5
Glucomannan			40.0		60.0			950.0*

4.2.1.2. Alkali and enzymatic treatment

To ensure depolymerization and removal of hemicelluloses of bacterial cellulose–hemicellulose plant cell wall analogues, sequential treatment with 0.1M NaOH and enzyme solutions were applied. According to the respected hemicellulose additives (Table 3), BC–hemicellulose PCW analogues were immersed in 10 U/mL enzyme solutions (1 U stands for conversion of 1 μmol of substrate per minute) and treated at both room temperature and 40±1 ºC for overall 8 h. Pure bacterial cellulose was treated with 0.1M sodium phosphate buffer (pH=6) under the same conditions. Enzymolyses were terminated by washing bacterial cellulose–hemicellulose plant cell wall analogues first in respected buffer, followed by deionized water. Current samples were further defined as *treated*.

Table 3. Hemicelluloses, hemicellulose-specific enzymes used, the composition of the enzyme solutions, and the reactions catalysed by enzymes. EC – Enzyme Commission number, BSA – bovine serum albumin.

Hemicellulose	Enzyme	Solution composition	Reaction catalyzed
Arabinoxylan	Endo–β–1→4–xylanase (EC 3.2.1.8)	0.1M sodium phosphate buffer (pH=6), 0.5 mg/mL BSA	Enzymolysis of xylan to oligosaccharides
	α–L–arabinofuranosidase (EC 3.2.1.55)	0.1M sodium acetate buffer (pH=4)	Enzymolysis of α–1→2– and α–1→3–linked L–arabinofuranosyl sidechains of arabinoxylan
Glucomannan	Endo–1→4–β–mannanase (EC 3.2.1.78)	0.1M sodium acetate buffer (pH=4)	Enzymolysis of β–1→4–D–mannosidic linkages of glucomannan
Xyloglucan	Xyloglucan–specific endo–β–1→4–glucanase (EC 3.2.1.151)	0.1M sodium acetate buffer (pH=5.5), 1 mg/mL BSA	Enzymolysis of β–1→4–D–glycosidic linkages of xyloglucan
Xylan	Endo–β–1→4–xylanase (EC 3.2.1.8)	0.1M sodium phosphate buffer (pH=6), 0.5 mg/mL BSA	Enzymolysis of xylan to oligosaccharides

4.2.2. Determination of monosaccharide composition

Monosaccharide composition of both raw and treated BC–hemicellulose PCW analogues was assessed with high–performance liquid chromatography according to the protocol of (S. Zhang et al., 2018) with slight modifications. Determination of monosaccharides and uronic acids (arabinose, fucose, galactose, galacturonic acid, glucose, glucuronic acid, mannose, rhamnose, and xylose) in BC–hemicellulose PCW analogues was conducted in triplicate.

4.2.3. Surface topography imaging

Surface topography imaging of BC–hemicellulose PCW analogues was performed by means of atomic force microscopy tapping mode in dry state. Obtained images were processes for the correction of data artefacts, and root mean square roughness and an average fiber width were evaluated.

4.2.4. Uniaxial tensile test with cyclic load

Macroscale mechanical properties of BC–hemicellulose PCW analogues were accessed by means of uniaxial tensile tests with cyclic strain rate (Fig.9). Maximum stress and maximum strain were defined at the cycle with the highest force. Maximum modulus was defined as the maximum value of the slope of the linear part of the stress strain curve in a single test. The total plastic strain was given as a sum of the irreversible strains in each cycle.

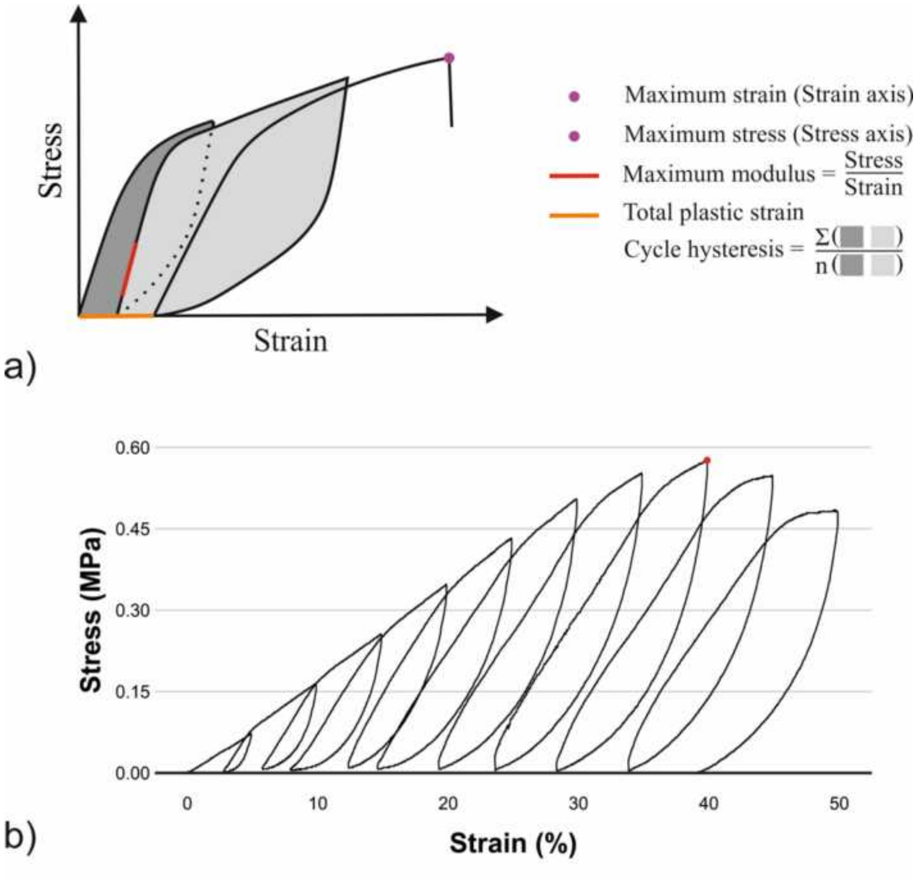

Fig.9. Uniaxial tensile test with cyclic load of BC–hemicellulose PCW analogues: a) schematic three–cycle stress–strain curve. The colored lines, points and areas define mechanical properties evaluated, while the annotation on the right provides the definition; b) experimental stress–strain curve. The single deformation cycle was divided into a loading (up to a maximum stress reached within the applied strain increment), and an unloading (up to zero stress reached) stages. Deformation cycles were repeated with the constant tensile strain increments up to decrease of maximum force within two consecutive cycles. The maximum stress and maximum strain was defined as that, reached at the cycle with the highest stress value (marked with red point).

4.3. Results and discussion

4.3.1. Dry yield of biosynthesis of bacterial cellulose-hemicellulose plant cell wall analogues

BC–hemicellulose PCW analogues appeared as a smooth semi–transparent pellicles with a dry yield of biosynthesis of 1.2–3.8 g/L on average (Fig.10). An increase in dry yield of biosynthesis of BC–hemicellulose PCW analogues was observed, possibly defined by an ability of *Komagataeibacter xylimus* bacteria strain to utilize xylose for bacteria replication (Cavka et al., 2013). In contrast, presence of arabinose sidechains suggested to stabilize xylan backbone, preventing it from degradation, so decreasing dry yield of biosynthesis of bacterial cellulose–arabinoxylan plant cell wall analogues via limited nutrient mobility (Fang & Catchmark, 2015; Kiziltas et al., 2015). Presence of both xyloglucan and glucomannan in culturing medium showed statistically significant decrease in dry yield of biosynthesis of respected plant cell wall analogues, being determined by an increase in medium viscosity, limited mobility of nutrients, and medium over supplementation (Gu & Catchmark, 2012; Hu et al., 2013; Kishani et al., 2020; Vandamme et al., 1998).

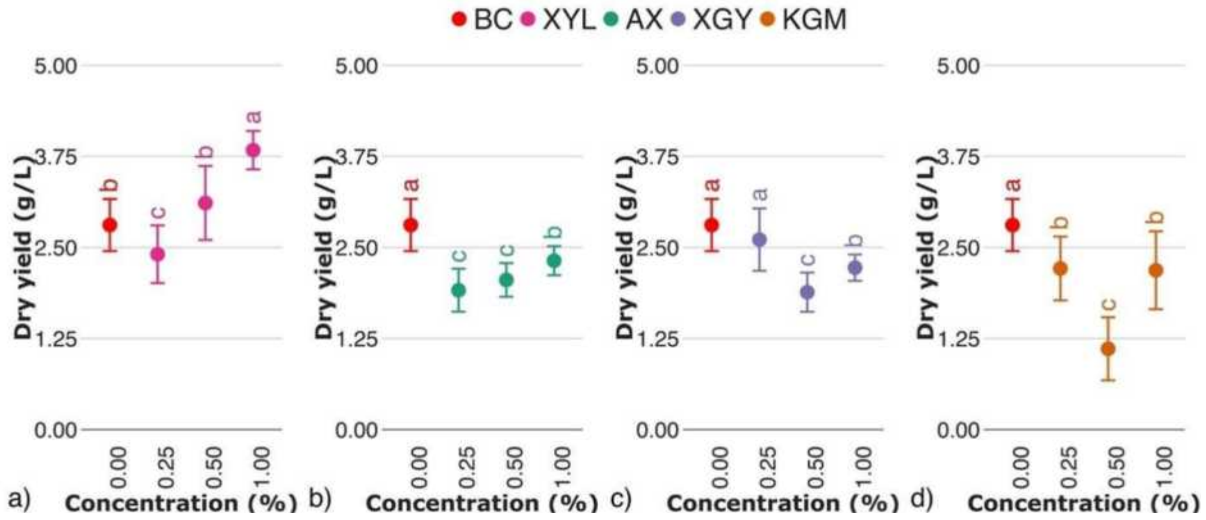

Fig.10. Dry yield of biosynthesis of BC–hemicellulose PCW analogues in relation to the presence of a) xylan (XYL), b) arabinoxylan (AX), c) xyloglucan (XGY), and d) glucomannan (KGM) in culturing medium. The control sample (BC) is marked with red colour. For the estimated parameters, the data points and bars refer to the mean values and standard deviation, respectively. Treatments with the same letter show a lack of statistically significant differences.

4.3.2. Monosaccharide composition of raw and treated bacterial cellulose-hemicellulose plant cell wall analogues

Apart from glucose as a main cellulose monosaccharide, other monosaccharides, spesific for the respected hemicellulose additives, were denoted for BC–hemicellulose PCW analogues (Fig.11). Hemicelluloses incorporated within cellulose fiber network in content–dependent manner, as evidenced by statistically significant increase in the content of respected hemicellulose monosaccharides with an increasing hemicellulose concentration. Enzymolysis was considered to be effective, yet not complete, as evidenced by statistically significant decrease but not complete removal of respected hemicellulose monosaccharides for treated PCW analogues. It was suggested that some part of hemicelluloses was enzyme–inaccessible, and was treated as an integral part of respected PCW analogues (Park & Cosgrove, 2012a; Pauly et al., 1999). Another crucial conclusion that may be drawn here is that no predominant mechanism of cellulose–hemicellulose interactions was observed since an amount of both enzyme-accessible and enzyme–inaccessible hemicelluloses were increasing in a statistically significant manner with an increasing hemicellulose content.

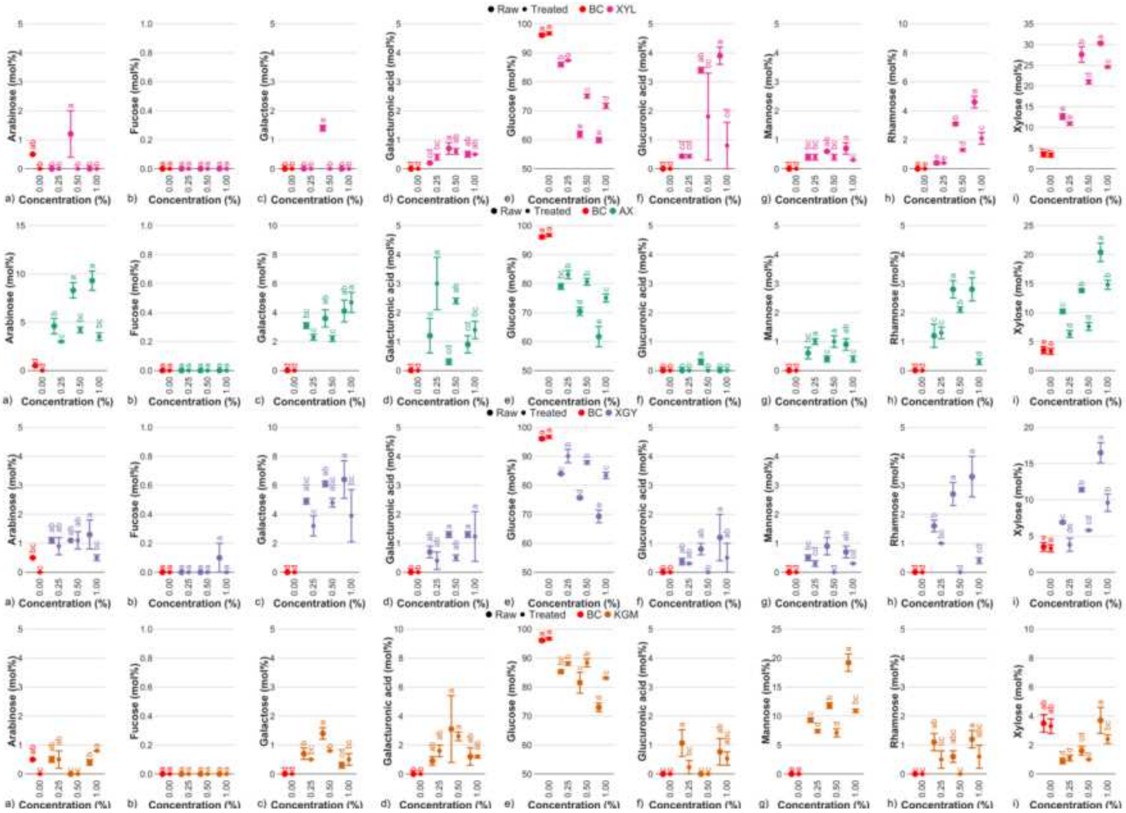

Fig.11. Monosaccharide composition of raw and treated BC–hemicellulose PCW analogues in relation to the presence of xylan (XYL), arabinoxylan (AX), xyloglucan (XGY), and glucomannan (KGM) in culturing medium. Subsequent figures represent the content of a) arabinose, b) fucose, c) galactose, d) galacturonic acid, e) glucose, f) glucuronic acid, g) mannose, h) rhamnose, and i) xylose in samples studied. Raw and treated samples are indicated by the bullet points of bigger and smaller sizes, respectively. The control sample (BC) is marked with red colour. For the estimated parameters, the data points and bars refer to the mean values and standard deviation, respectively. Treatments with the same letter show a lack of statistically significant differences.

4.3.3. Surface topography of raw and treated bacterial cellulose-hemicellulose plant cell wall analogues

Surface topography images revealed both raw and treated BC–hemicellulose PCW analogues were organized as a network of in–plane randomly distributed fibers (Fig.12-13). Fiber width tended not to show statistically significant changes for both raw and treated BC–xylan PCW analogues (Fig.14a), supposing xylan to be predominantly enzyme–inaccessible.

In contrast, increasing content of arabinoxylan in culturing medium resulted fiber width to show statistically significant increase, yet with no effect for treated samples (Fig.14b). It was suggested that removal of arabinose increase affinity of arabinoxylan backbone to cellulose (Mikkonen et al., 2012), leading to lack of statistically significant change of fiber width. Fiber width tended to increase for both BC–xyloglucan (Fig.14c) and BC–glucomannan (Fig.14d) PCW analogues, yet the mechanisms were suggested to be different. While plateau reached for the fiber width of treated BC–glucomannan PCW analogues defined complete removal of surface–deposited enzyme–accessible glucomannan, decrease in fiber width of treated BC–xyloglucan PCW analogues was smooth linear. Data of fiber width is somehow correlated with one of surface roughness, which, despite moderacy of statistical differences, was on average lower for treated samples, compared to raw (Fig.15). Together with a lower data deviation for treated sampled, current data may provide to a conclusion that smoother surface of oven-dried bacterial cellulose-hemicellulose hydrogels may be a matter of the removal of enzyme-accessible hemicelluloses.

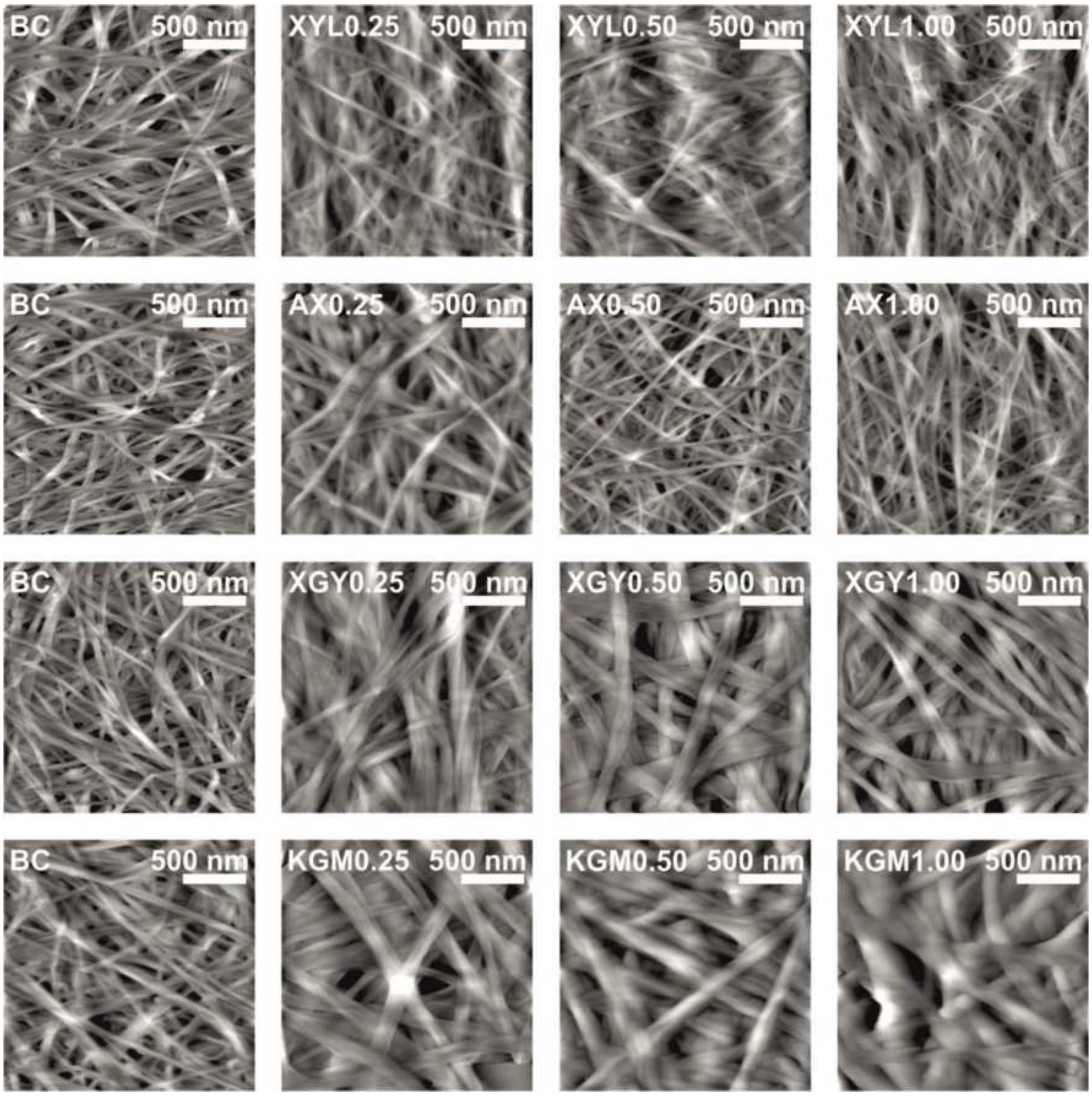

Fig.12. Atomic force microscopy surface topography images of raw BC–hemicellulose PCW analogues in a dry state. Images are divided into rows according to the type of hemicellulose additive, while column indicate the amount of hemicellulose additive (% mass) in culturing medium. For each image, abbreviation and scale are provided.

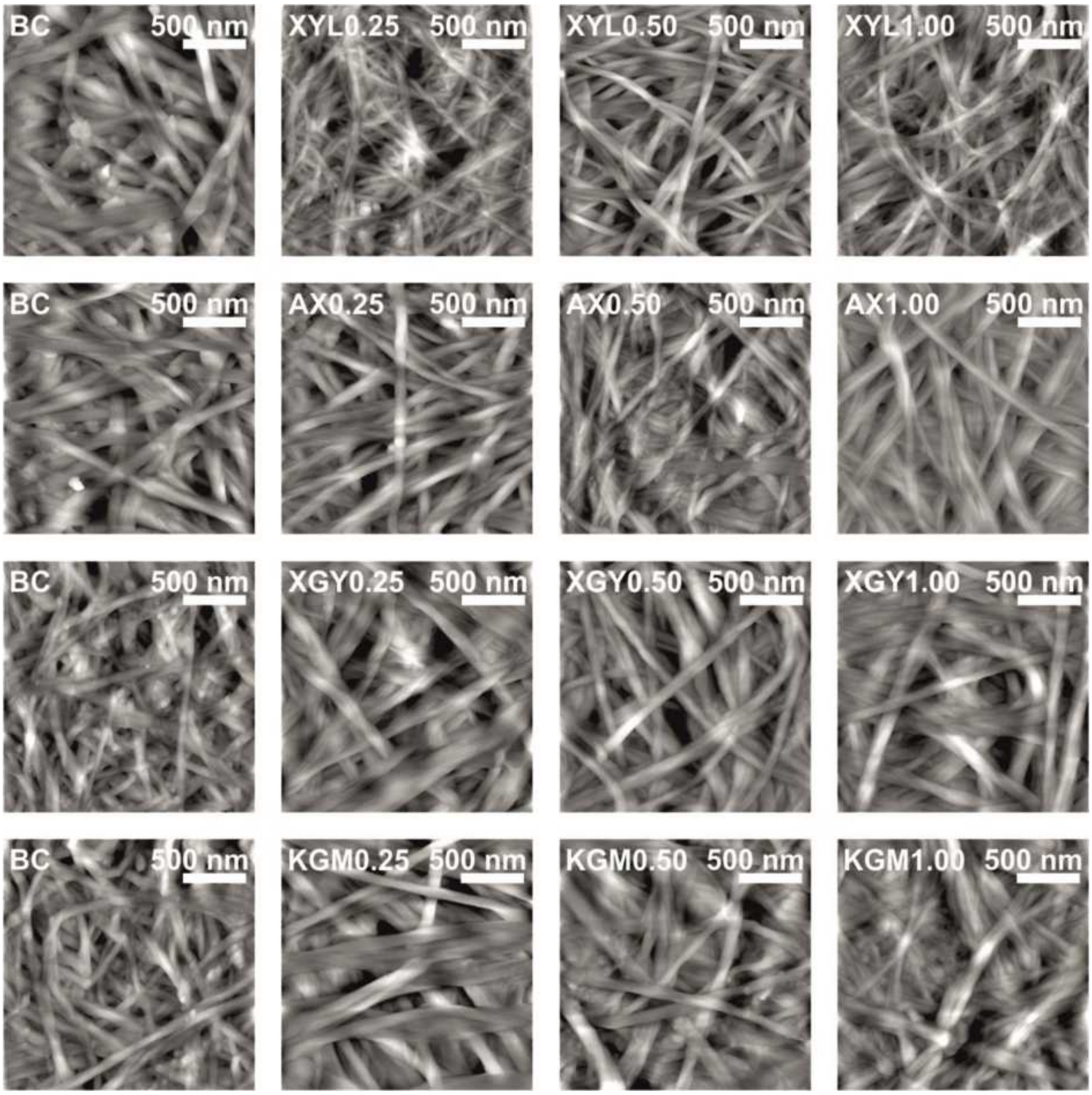

Fig.13. Atomic force microscopy surface topography images of treated BC–hemicellulose PCW analogues in a dry state. Images are divided into rows according to the type of hemicellulose additive, while column indicate the amount of hemicellulose additive (% mass) in culturing medium. For each image, abbreviation and scale are provided.

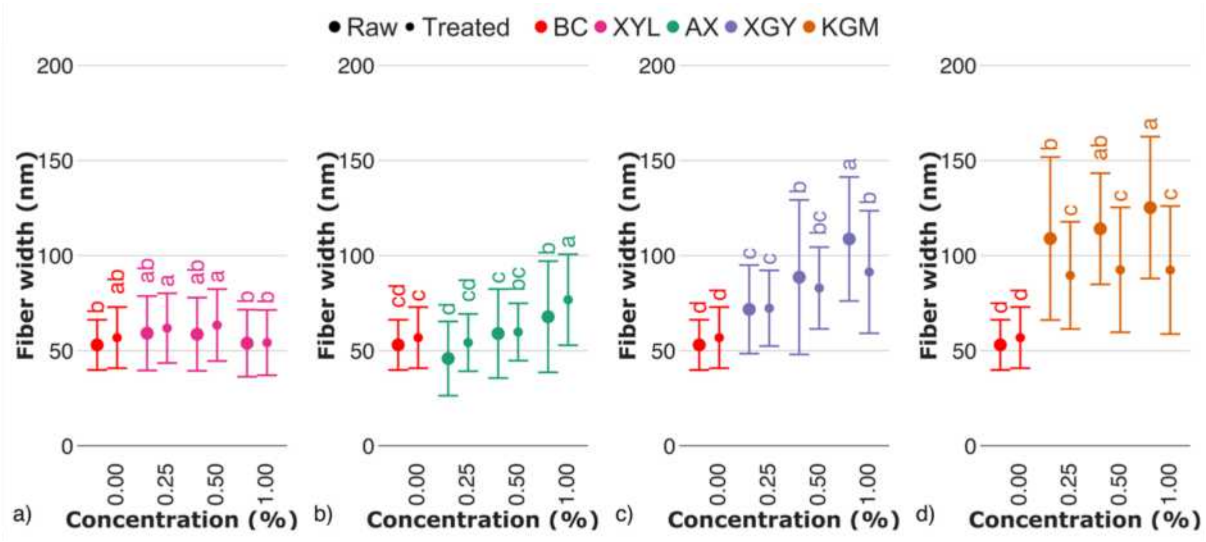

Fig.14. Cellulose fiber width of raw and treated BC–hemicellulose PCW analogues with a) xylan (XYL), b) arabinoxylan (AX), c) xyloglucan (XGY), and d) glucomannan (KGM) in the dry state. Raw and treated samples are indicated by the bullet points of bigger and smaller sizes, respectively. The control sample (bacterial cellulose, BC) is marked with red color. For the estimated parameters, the data points and bars refer to mean values and standard deviation, respectively. Treatments with the same letter show a lack of statistically significant differences.

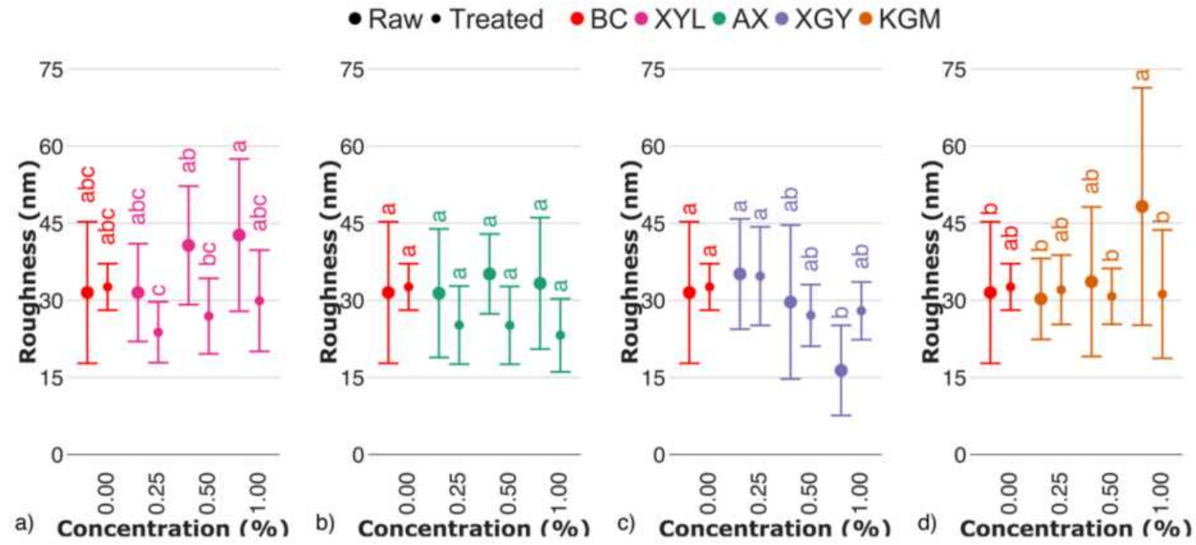

Fig.15. Root mean square roughness of raw and treated bacterial cellulose-hemicellulose hydrogels in relation to the presence of xylan (XYL), arabinoxylan (AX), xyloglucan (XGY), and glucomannan (KGM) in culturing medium. Subsequent figures represent the content of a) arabinose, b) fucose, c) galactose, d) galacturonic acid, e) glucose, f) glucuronic acid, g) mannose, h) rhamnose, and i) xylose in samples studied. Raw and treated samples are indicated by the bullet points rectangles, respectively. The control sample (BC) is marked with red colour. For the estimated parameters, the data points and bars refer to the mean values and standard deviation, respectively. Treatments with the same letter show a lack of statistically significant differences.

4.3.4. Mechanical properties of raw and treated bacterial cellulose-hemicellulose plant cell wall analogues

Moduli and stresses of BC–xylan PCW analogues showed statistically significant decrease with an increasing content of xylan in culturing medium, while being statistically higher for treated samples, compared to raw (Fig.15). The later fact was suggested to be related to the occurrence of direct interfiber interactions, while xylan domains degrade with enzymolysis.

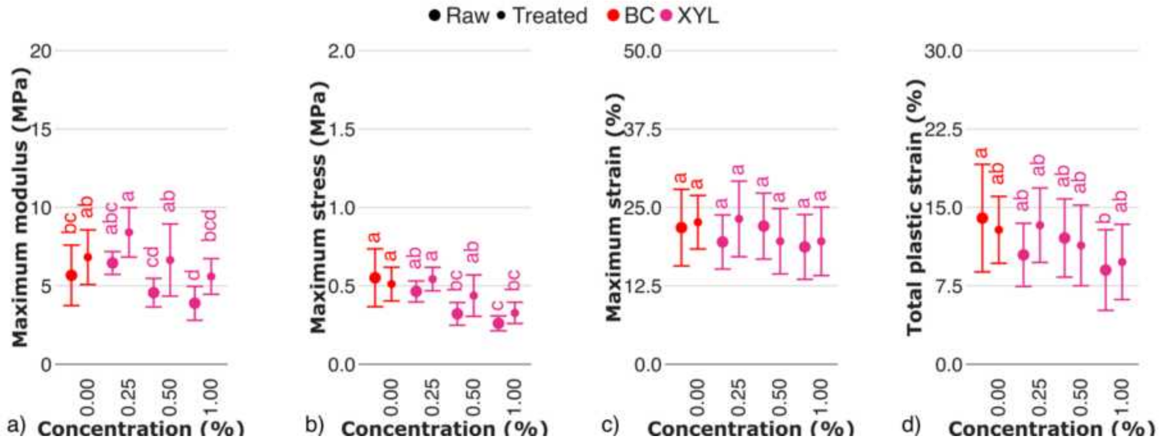

Fig.15. Mechanical properties of raw and treated BC–xylan PCW analogues evaluated by cyclic tests: a) maximum modulus, b) maximum stress, c) maximum strain, d) total plastic strain. The control sample (BC) is marked in red. Raw and treated samples are indicated by bigger and smaller bullet points, respectively. For the estimated parameters, data points and bars refer to the mean and standard deviation, respectively. Treatments with the same letter show no statistically significant differences.

In contrast, moduli, and stresses of BC–arabinoxylan PCW analogues showed statistically significant increase with an increasing arabinoxylan content (Fig.16). The key role here was suggested for arabinose sidechains, which limit arabinoxylan incorporation onto cellulose fiber (Martinez-Sanz, Mikkelsen, et al., 2017), adsorbing on cellulose surface (Martinez-Sanz et al., 2016). Aforementioned mechanical properties showed statistically significant increase for treated BC–arabinoxylan PCW analogues, being consistent with a reinforcing effect, coupled with a reduced moisture–induced plastic deformation of low–arabinosylated arabinoxylan with low degree of polymerization (Hoije et al., 2008; Sternemalm et al., 2008).

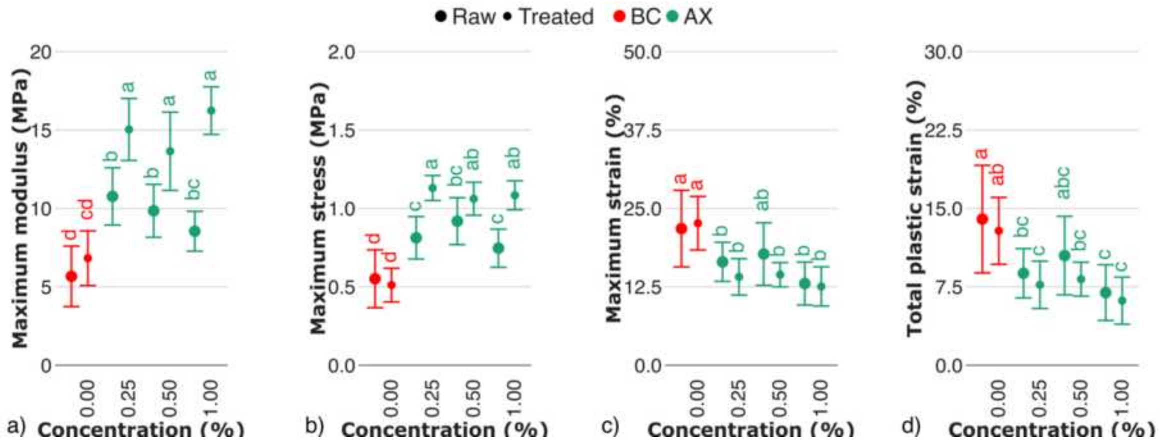

Fig.16. Mechanical properties of raw and treated BC–arabinoxylan PCW analogues evaluated by cyclic tests: a) maximum modulus, b) maximum stress, c) maximum strain, d) total plastic strain. The control sample (BC) is marked in red. Raw and treated samples are indicated by bigger and smaller bullet points, respectively. For the estimated parameters, data points and bars refer to the mean and standard deviation, respectively. Treatments with the same letter show no statistically significant differences.

Increasing content of xyloglucan in culturing medium resulted in a statistically significant decrease in moduli, stresses, and strains of the respected PCW analogues (Fig.17). It was considered to be determined by a decreasing number of direct cellulose–cellulose contacts in favor to weaker cellulose–xyloglucan interactions. Trends on data change of moduli and stresses allowed to assume that increasing xyloglucan content levelled out the effect of enzyme–accessible xyloglucan on mechanical response of respected plant cell wall analogues in favor of enzyme–inaccessible one. However, the effect of the former one xyloglucan was sufficient enough to define statistically significant change on strain component between both raw and treated BC–xyloglucan PCW analogues. It allowed to suggest enzyme–accessible xyloglucan to some extend defined plastic response of the respected PCW analogues.

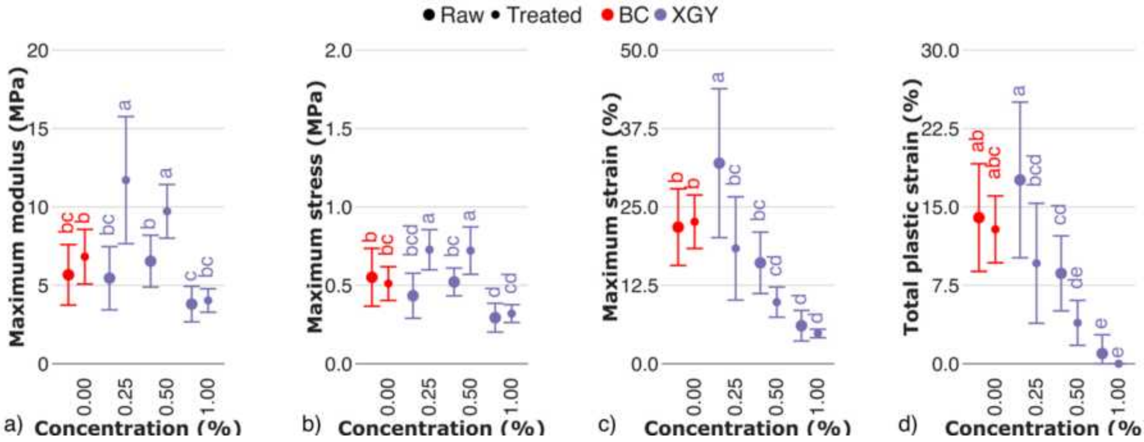

Fig.17. Mechanical properties of raw and treated BC–xyloglucan PCW analogues evaluated by cyclic tests: a) maximum modulus, b) maximum stress, c) maximum strain, d) total plastic strain. The control sample (BC) is marked in red. Raw and treated samples are indicated by bigger and smaller bullet points, respectively. For the estimated parameters, data points and bars refer to the mean and standard deviation, respectively. Treatments with the same letter show no statistically significant differences.

Increasing content of glucomannan resulted in a statistically significant decrease of the mechanical properties of BC–glucomannan PCW analogues – moderate for moduli and stresses, and drastic for strains (Fig.18). Such a decrease was defined by a glucomannan deposition on cellulose surface, so that preventing direct interfiber slippage (Berglund, 2018; Iwata et al., 1998; Tokoh et al., 1998; Whitney et al., 1998). Brittleness and predominantly elastic response of BC–glucomannan PCW analogues with an increasing glucomannan content was defined by its both direct and indirect effects – increased hydrogen bonding, coupled with increased interfiber friction of thick cellulose fibers. Lack of statistically significant differences was reported for both raw and treated BC–glucomannan PCW analogues, defining the crucial role of enzyme–inaccessible glucomannan on tuning interfiber interactions.

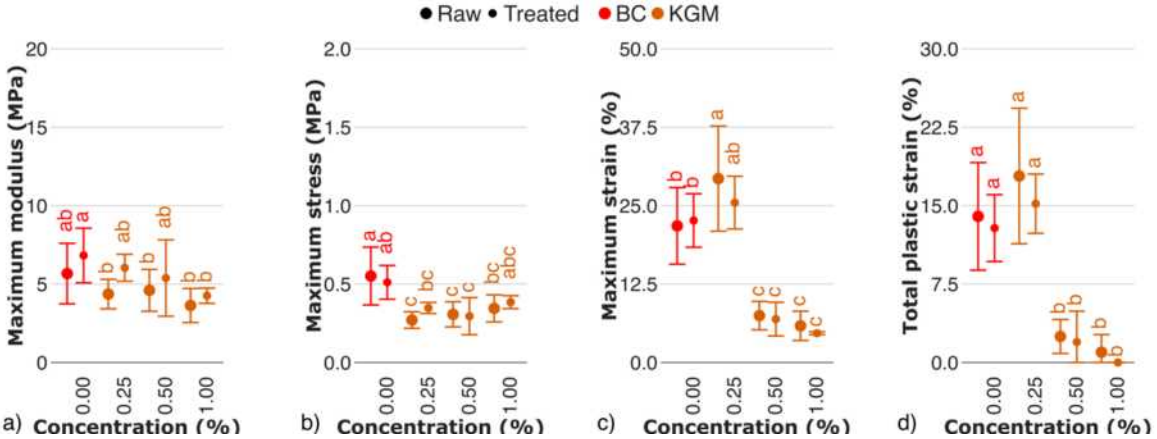

Fig.18. Mechanical properties of raw and treated BC–glucomannan PCW analogues evaluated by cyclic tests: a) maximum modulus, b) maximum stress, c) maximum strain, d) total plastic strain. The control sample (BC) is marked in red. Raw and treated samples are indicated by bigger and smaller bullet points, respectively. For the estimated parameters, data points and bars refer to the mean and standard deviation, respectively. Treatments with the same letter show no statistically significant differences.

4.4. Conclusions

Incorporation of hemicellulose polysaccharides to cellulose fiber network allowed to define the patterns of its interactions, with a specific focus on its structure–related nature. The effect of xylan presence in respected PCW analogues showed minor statistical changes on its structure and mechanical properties. To some extent, removal of enzyme–accessible xylan allowed to establish some stiff cellulose–cellulose junctions, so that increasing mechanical properties of respected PCW analogues, compared to raw one. The effects observed for BC–arabinoxylan PCW analogues were quite opposite. It was suggested that mechanical properties of raw BC–arabinoxylan PCW analogues were defined by the reinforcing effect of arabinoxylan chains. In case of treated PCW analogues, the effects of reduced moisture–induced plastic deformation, and increase in polysaccharide crystallinity were considered.

In contrast to xylan and arabinoxylan additives, presence of xyloglucan and glucomannan in respected PCW analogues resulted in both increase in fiber width, coupled with a general decrease in its mechanical performance.

The obtained results indicated that with increasing xyloglucan content, the mechanical properties of BC–xyloglucan PCW analogues were governed by weaker xyloglucan–cellulose interactions rather than stronger cellulose–cellulose interactions, leading to a decrease in its stresses and moduli. Removal of enzyme–accessible xyloglucan allowed cellulose–cellulose interactions to be re–established, resulting in increase in PCW moduli and stresses. The decrease in mechanical properties of BC–glucomannan PCW analogues with increasing glucomannan content was attributed to an alteration of fiber network formation via glucomannan deposition – both on and within cellulose fiber. It resulted the effect of enzymolysis on BC–glucomannan PCW analogues was comparable to that of xyloglucan, but less pronounced, supposedly by its higher affinity to cellulose surface.

The results obtained supported an idea of enzymolysis of cellulose–hemicellulose fiber networks as an applicable tool for an exploration of its mechanobiology. Current results provided an evidence for a structure–dependent mechanisms of cellulose–hemicellulose interactions, suggesting the specific structural role of the latter.

5. Summary

The literature review has shown that current understanding of the mechanics of plant cell wall is insufficient. Therefore, this research focused on the interfiber interaction between cellulose and one of the four types of hemicelluloses abundant in plant cell walls. As a model for natural plant cell walls, bacterial cellulose-hemicellulose plant cell wall analogues were prepared for experimental studies and the numerical model based on coarse-grained molecular dynamics was established to test the fiber network properties. By implementing these tools, it was possible to verify the research hypotheses and show that the type of hemicellulose plays an important role in the structural and mechanical responses of their composites with cellulose. In addition, it was possible to evaluate the role of interfiber interactions on the mechanics of these composites and to show that the force of interfiber interaction is also determined by the morphological characteristics of BC–hemicellulose PCW analogues, such as fiber width/length/modulus. The results of these studies contribute to the knowledge of the structure and mechanics of plant cell walls and may have implications for the development of composites of cellulose and other natural polysaccharides inspired by plant cell walls.

Based on the results of the conducted research, the following general conclusions can be drawn:

1. Elastic deformation of BC–hemicellulose PCW analogues is governed predominantly by the stretching vibrations of structural bonds of cellulose and hemicelluloses.
2. Plastic deformation of BC–hemicellulose PCW analogues is defined by supramolecular changes occurring in fiber network (fracturing of polysaccharide chains, degradation of hydrogen bond network).
3. Presence of xylan and arabinoxylan resulted in an increase in plastic deformation, moduli and stresses of the respected plant cell wall analogues, being opposite to the effects of xyloglucan and glucomannan.
4. No predominant mechanism of hemicellulose incorporation in BC fiber network is defined.
5. Hemicelluloses, incorporated in bacterial cellulose fiber network, exist as both enzyme–accessible and enzyme–inaccessible. Enzyme–inaccessible hemicelluloses define trends on data change of the mechanical properties of the respected PCW analogues, while enzyme–accessible hemicelluloses define data fluctuation.
6. Mechanical properties of BC–hemicellulose PCW analogues are not determined by the deformation of hemicelluloses itself, but mainly by the deformation of cellulose fibers, mediated by hemicelluloses.
7. Such a mediates, conceptually similar to biomechanical hotspots occurring *in muro,* change the force of interfiber interaction, being the main factor affecting the mechanical properties of BC–hemicellulose PCW analogues.
8. Force of interfiber interaction is also defined by the morphological features of BC–hemicellulose PCW analogues, such as fiber width/length/modulus.
9. Mechanical properties of BC–hemicellulose PCW analogues correspond to those of simulated networks, confirming applicability of the latter for the exploration of the mechanobiology of cellulose–based fiber networks.

6. Content of manuscripts

6.1. Manuscript P1.

6.1.1. Content of the manuscript P1.

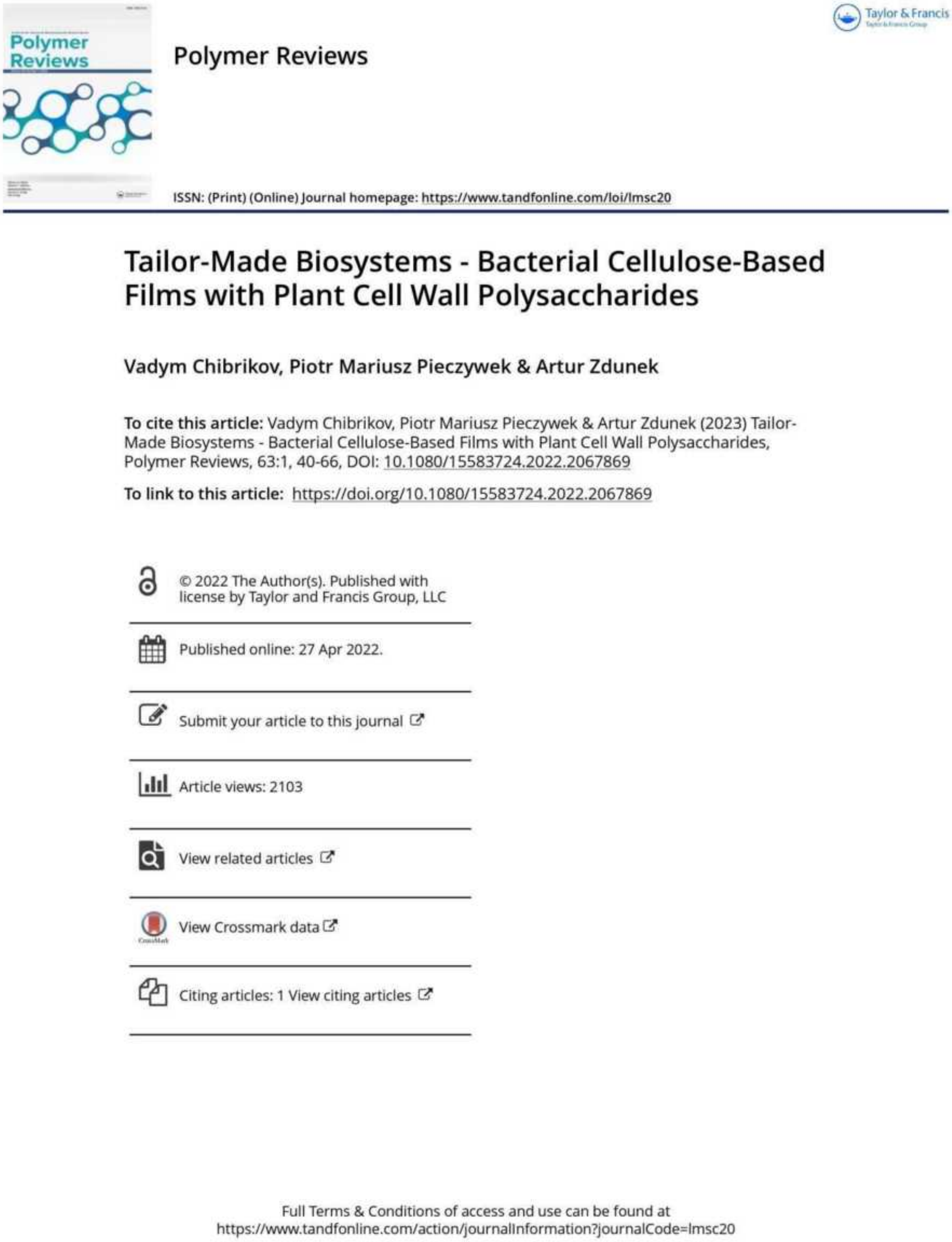

Polymer Reviews

Taylor & Francis

ISSN: (Print) (Online) Journal homepage: https://www.tandfonline.com/loi/lmsc20

Tailor-Made Biosystems - Bacterial Cellulose-Based Films with Plant Cell Wall Polysaccharides

Vadym Chibrikov, Piotr Mariusz Pieczywek & Artur Zdunek

To cite this article: Vadym Chibrikov, Piotr Mariusz Pieczywek & Artur Zdunek (2023) Tailor-Made Biosystems - Bacterial Cellulose-Based Films with Plant Cell Wall Polysaccharides, Polymer Reviews, 63:1, 40-66, DOI: 10.1080/15583724.2022.2067869

To link to this article: https://doi.org/10.1080/15583724.2022.2067869

POLYMER REVIEWS
2023, VOL. 63, NO. 1, 40–66
https://doi.org/10.1080/15583724.2022.2067869

Taylor & Francis
Taylor & Francis Group

REVIEW

Tailor-Made Biosystems - Bacterial Cellulose-Based Films with Plant Cell Wall Polysaccharides

Vadym Chibrikov, Piotr Mariusz Pieczywek, and Artur Zdunek

Institute of Agrophysics, Polish Academy of Sciences, Lublin, Poland

ABSTRACT

Bacterial cellulose (BC) is a natural biopolymer metabolized by Gram-negative bacteria strains in carbon- and nitrogen-rich media. Due to its natural purity, biodegradability, biocompatibility and outstanding mechanical properties, it is considered to be an exceptional biomaterial with versatile scientific and commercial applications. The current review presents data concerning the assembly, structural properties and mechanical behavior of specific biosystems based on bacteria-produced cellulose and polysaccharides derived from plant cell walls. Bacterial cellulose, hemicellulose, their binary composites and ternary composites with pectin are described with respect to the mechanical properties of the obtained materials. The properties of one-component and composite films are discussed with respect to the type of polysaccharides used, their origin and applied pretreatments, as well as various methodological approaches to bacterial cellulose synthesis. This work is focused entirely on the relationship between production methods and composition, and the resulting properties of the obtained materials, it constitutes a universal source of knowledge for specialists from various fields of science and industry.

ARTICLE HISTORY
Received 5 October 2021
Accepted 11 April 2022

KEYWORDS
bacterial cellulose; hemicelluloses; pectin; mechanical properties

1. Introduction

Bacterial cellulose (BC) is a biopolymer produced as a primary metabolite by several strains of bacteria using glucose, fructose, sucrose, mannitol, among others, as carbon sources.[1,2] In terms of chemical structure, bacterial cellulose is identical to the cellulose produced by plants. BC is a linear polysaccharide composed of β-D-glucopyranose monomers linked by β-1,4-glycosidic linkages, forming molecules of cellobiose.[3] As is the case with plants, bacterial cellulose exists mainly in cellulose I crystallographic form, with two coexisting sub-allomorphs, triclinic Iα and monoclinic Iβ structures.[4] Metastable Iα cellulose is the dominant structure, comprising up to 80% of BC.[5] Compared to plant-produced cellulose, BC has a lower degree of polymerization ranging between 2000-6000 (with 13,000 – 14,000 for plants). BC is produced in the pores located in the cytoplasmic membranes and extruded in the form of protofibrils, 2-4 nm in diameter.[6–8] Then, protofibrils may assemble, forming nanofibrils with typical

CONTACT Piotr Mariusz Pieczywek p.pieczywek@ipan.lublin.pl Institute of Agrophysics, Polish Academy of Sciences, ul. Doświadczalna 4, 20–290 Lublin, Poland

widths in range of 5–20 nanometers and micrometer scale lengths or microfibrils up to 100 nm in diameter.[9] Fibrils, that include both of nano- and microfibrils, may also aggregate, creating fibers – multi-scale structures, composed of well-organized fibrils with diameter up to 50 μm and length in several milimeters.[10,11]

BC is assembled in the form of highly hydrated (99% of water), high crystallinity (84-90%) and high purity cellulose membranes at the surface of a carbon- and nitrogen-containing medium.[12–15] The resulting pellicles are constituted by an ultrafine network structure of highly entangled cellulose fibrils.[5,9,16,17]

Bacterial cellulose-based membranes and films show outstanding mechanical properties and a large specific surface area, comparable with materials obtained with plant-based cellulose. BC is characterized by a high degree of crystallinity, reduced fibril diameter and uniform chemical structure, which lead to stiff fibril connections. Applications have already been found for BC in tissue engineering, biosensor fabrication, antimicrobial and biodegradable film production and as a texture improver.[18,19] BC does not cause allergic reactions, so its suitability for the role of being used as a temporary skin substitute, artificial blood vessel etc. is already being investigated.[6,16] BC composites have been used for wound dressing, vessel regeneration.[20] Also, some approaches involving BC-laser sensitized magnetic particle use were applied for breast cancer treatment.[21] Kwak and others reported healing acceleration in burned rat skin with the application of BC membranes.[22] Cellulose fibers, incorporated with hemicelluloses, also demonstrated the stimulation of fibroblast growth and proliferation.[23] Another potential area for hemicellulose use is in the production of biodegradable and antibacterial films for food storage.[24] A brief review of BC-based food packaging material was provided by Cazon and Vasques.[25] They summarized reports concerning the great potential for BC modification with its high degree of porosity, which allows for modifying agents to be immersed in the material.

Among many applications, BC composites with plant cell-wall polysaccharides have gained particular importance in studies concerning the properties of plant cell walls (PCW). This has been attributed to the chemical similarity of BC to natural cellulose, which allows for the creation of what are widely known as plant cell-wall analogues – polysaccharide assemblies which have a composition and structure that mimics those of PCW. The idea of BC use for PCW modeling was firstly proposed in 1982 by Haigler et al.[26–28] Since then, pectin, xyloglucan, glucomannan, arabinoglucuroxylan and arabinogalactan have been added to the culture medium and their effects on the bacterial cellulose structure as well as their mechanical properties have been shown by several groups.[29–34]

With the use of precise techniques, such an approach allows one to minimize the limitations of the method used to determine the qualitative composition of PCW analogues, cellulose crystallinity or physical properties of the network (thickness, density, permeability).[35] The synthesis of bacterial cellulose (BC) in the presence of hemicelluloses and/or pectins allows for the attainment of films, which may be varied in their composition or/and structure, according to research necessities. This synthetic approach allows researchers to modify the cell-wall environment and to study the impact of each specific compound on the properties of the cellulose-based material. Production, handling and storage are more straightforward, as compared to plant cell-wall-extracted materials.[36] BC-based composites may be considered to be a model object of PCW, this has been confirmed by numerous scientific investigations. A number of papers, dedicated to the determination of PCW structure and mechanical properties have already been published.[37–39]

Therefore the scope of this paper is focused exclusively on data concerning the structural and mechanical properties of BC films, BC-hemicellulose binary and BC-hemicellulose-pectin ternary composites, thereby providing information that may be useful not only to scientists from the cell wall community, but in general, for researchers concerned with plant polysaccharide-based composites.

2. Structural and mechanical properties of bacterial cellulose

BC-producing bacteria include a number of genera.[26,40] *Komagataeibacter xylinum* (previously known as *Acetobacter* or *Gluconacetobacter xylinum*) is a widely used bacteria strain for BC biosynthesis, this is due to its plant-like synthesis, high yields, ultrafine structure and chemical purity.[24,33] In general, the mechanical characteristics of films improve with the growing concentration of BC. *Komagataeibacter* BC hydrogels with a higher percentage of BC are entirely opaque, compared to low-BC samples, which contribute both opaque and transparent regions. High-BC hydrogels provide superior levels of stress resistance and Young's modulus, but the maximum strain measurements are not changed significantly. However, low-BC samples showed a higher level of moisture uptake per unit weight.

K. rhaeticus BC films show a more homogeneous distribution of cellulose fibers, as compared to the *K. xylinum* one, being much closer to the PCW-like structure. Comparing both, *K. xylinum* films exhibit a higher tensile strength and Young's modulus in the dried state, whereas elongation is higher for *K. rhaeticus* samples. This difference may be explained by the higher degree of porosity of the *K. rhaeticus* film (looser structure, lower degree of hydrogen bonding), lower fibril orientation and decreased crystallinity. The opposite relationship was obtained for BC samples in their wet state, which also indicated that some *Komagataeibacter* strains are sensitive to post-production treatment.[41]

Kombucha (*Komagataeibacter* strains) untreated BC films show a bulky low-crystalline structure. However, NaOH-washed samples showed a sufficient increase (3 to 20 times) in mechanical properties and crystallinity level up to about 47%.[40,41] Such a tendency was further explained by stronger nanoparticle interconnections and fibril entanglements.[42]

The classic medium for *K. xylinum* growth was established in 1954 by Hestrin and Schramm (HS medium), it includes glucose, bactopeptone, yeast extract, agar (for solid medium), with a pH value of 4.5-6 and a temperature of 25-30 °C.[43–46] Bacteria synthesize cellulose as a primary metabolite. The main sources of carbon and nitrogen for cellulose growth are glucose/fructose/sucrose/mannitol and peptone/yeast extract, respectively, the effect of additives is assumed to be negligible.[17] Volova et al. reported that fibril shape parameters are closely dependent on the growth medium used, with thin low-crystalline fibrils being obtained from a galactose-enriched medium, while the thickest one were obtained from the sucrose one. The mechanical properties of the film directly depend on fibril diameter growth only to a minor degree.[47] An informative

Table 1. BC film mechanical properties (measurement conditions: RH –relative humidity of air, T – air temperature).

Composition	Source	Tensile strength (MPa)	Strain at break (%)	Youngs modulus (MPa)	RH (%)	T (°C)	References
$\text{BC}_{\text{air-dried}}$	*K. xylinum*	256.0	1.07	16900	65	20	[4]
$\text{BC}_{\text{hot-pressed}}$	*AJ 12368*	91-260	0.8-1.9	16400-17500			
BC	*K. xylinum*	0.33-0.54	17.5-40.0				[31]
BC	*K. xylinum*	1.57	18.0				[29]
BC_{dried}	*K. xylinum*	5.21	3.75				[52]
$\text{BC}_{\text{swollen}}$		1.56	8.0				
BC	*K. xylinum ATCC 23769*	32.0 ± 5.0	3.4			RT	[53]
$\text{BC}_{\text{pinned}}$		28.0 ± 5.0	1.7				
BC	*K. xylinum ATCC 53524*	1.2-2.0	23.0-30.0	10.0-14.2			[54]
$\text{BC}_{\text{NaOH treat.}}$		1.2-1.6	21.0-26.0	9.1-13.2			
BC	*K. xylinum*	150 ± 16.0	4.5 ± 0.5	3700 ± 800	30	20	[55]
BC	*K. xylinum ATCC 53582*	1.7	>33.0			25	[30]
Crystalline bacterial cellulose	*G. hansenii ATCC 23769*	33.0	76.0	5200.0	50	25	[42]
BC	*K. xylinum ATCC 1765*	194.4	3.4	11400.0	40	23	[56]
$\text{BC}_{\text{ATCC 700178}}$	*K. xylinum, G. hansenii*	0.15 ± 0.08	20.7 ± 8.3	1.1 ± 0.38			[26]
$\text{BC}_{\text{ATCC 10245}}$		0.36 ± 0.08	18.6 ± 8.0	2.87 ± 1.33			
$\text{BC}_{\text{ATCC 23769}}$		0.12 ± 0.04	18.0 ± 5.0	1.26 ± 0.66			
$\text{BC}_{\text{NBRC 13693}}$		0.62 ± 0.17	18.7 ± 3.3	3.08 ± 0.66			
$\text{BC}_{\text{ATCC 53524}}$		0.68 ± 0.13	20.7 ± 6.0	5.56 ± 2.29			
$\text{BC}_{\text{KTH 5655}}$		0.62 ± 0.16	16.2 ± 2.91	3.83 ± 1.08			
BC	*K. xylinum B-12068*		10.1-15.2	3.7-5.5		RT	[47]
$\text{BC}_{\text{untreat.}}$	*K. xylinum*	27.9 ± 1.7	45.2 ± 1.4	43.7			[57]
$\text{BC}_{\text{H2O pretreat.}}$		75.8 ± 7.8	8.4 ± 2.5	950.0			
$\text{BC}_{\text{NaOH pretreat.}}$		73.7 ± 11.8	5.5 ± 4.6	1069.1			
$\text{BC}_{\text{K. xylinus (dry)}}$	*K. xylinum, K.rhaet. TJPU03*	141 ± 70	4.0	10100 ± 800		RT	[41]
$\text{BC}_{\text{K. xylinus (wet)}}$		0.1 ± 0.01	22.0 ± 1.0	6.1			
$\text{BC}_{\text{K. rhaet. (dry)}}$		70 ± 6	5.0	5300 ± 400			
$\text{BC}_{\text{K. rhaet. (wet)}}$		0.16 ± 0.01	27.0 ± 2.0	0.0083			
$\text{BC}_{\text{diff. H2O act.}}$	*K. xylinum*	15.5-22.3	1.4-3.7	650-1800			[25]

summary of BC production under different cultural conditions has been provided by Lin et al.[48]

Since *K. xylinum* is an aerobic bacteria, growing techniques may include forced aeration. Static conditions allow for the attainment of uniform and smooth films with defined characteristics.[49] Agitation reduces the degree of polymerization, the cellulose Iα content and total crystallinity. Chemically, the BC produced under agitation, is equivalent to one produced in static conditions, but with curved and entangled fibrils, which results in an enhanced density and water-holding capacity but up to a 20% decrease in Youngs modulus.[49–51]

Cellulose synthesizing complexes are located on the bacteria surface close to the cell membrane pores. Cellulose is extruded with an approximate speed 2 µm/min and forms a ribbon composed of nearly 46 microfibrils, each containing 18-36 cellulose chains. Ribbons tear from their forming sites possibly due to lateral stress and aggregate into fibrils via glucan chain crystallization. The resulting BC fibril length is approximately 1.6-5.8 µm.[48]

Generalized data concerning BC film mechanical properties are given in Table 1. Yamanaka et al. provided one of the first reports about BC dedicated to the relationship between its structural and mechanical properties, and determined that the Young's modulus of the BC film to be higher than 15 GPa. They also reported the presence of structural "three-way branching points" along fibrils, which was indicated by continued cellulose excretion during bacteria cell division. Structurally, BC is deposited in the pellicle in a number of thin fibrillar layers, with a thickness estimated to be approximately 0.1 µm. Such layers are believed to be connected via an interfibril hydrogen bond network, which is quite dense due to its enhanced contact area.[4]

The isotropic randomized structure of the pellicle was observed for BC produced by *K. xylinum*. Under the high strain-rate deformation of the pellicles, double stress peaks were observed, this was attributed to the failure of the short and long fibrils. Slow deformation revealed similar stress values with one peak only, indicating the presence of strain-dependent mechanical properties connected with inter-fiber slippage and disentanglement.[54] Such a fracturing behavior was previously observed by Astley et al. (2003), who reported BC layers sliding past each other during deformation.[29]

BC pellicles behave as a highly hydrophilic material, holding up to 100 times its dry weight in water.[43] Sanchavanakit et al. reported water swollen films that show a strain which is twice as high at its breaking point and a Young's modulus which decreased by a factor of three when compared to the dried films.[52] Rambo et al. (2008) declared that water swelling decreased inter-fibril hydrogen bonding, thereby degrading the mechanical properties of the film.[53]

Cybulska et al. (2010) reported the pure BC network to be porous and consist of branched nanofibrils, distributed randomly with an average length and diameter of 1 µm and 10-20 nm, respectively.[32] Chi and Catchmark also reported porous BC film with ribbons of about 30-60 nm in diameter. Crystalline bacterial cellulose (CBC), which is acid treated BC with removed amorphous regions was observed as rod-shaped particles 0.1-2 µm and 2-14 nm in length and height, respectively.[42] Bendaoud et al. (2017) reported the attainment of non-porous BC pellicles, which were characterized by linear elastic stress-strain behavior, a low strain at break and exhibiting brittle fracturing. The rigid and brittle behavior of the network was potentially attributed to its vitreous polymer state.[58]

Wang et al. described a BC film which was processed with wet-stretching and shaking to provide a highly linear structure. Stretching led to the creation of a densely packed aligned cellulose network. During network elongation, BC changed its arrangement from a layered one to fibril needlelike bundles. Denser packaging promoted the formation of an enhanced hydrogen bond network, which resulted in an increased Young's modulus (4.4 times), tensile strength – (5 times) and strain at break – (1.3 times). Also, the stretched films showed lower water adsorption, improved toughness and strength, which were explained through decreased defect size and the enhanced hydrogen bond network.[56] Dayal et al. reported that its water binding capacity enhanced the mechanical properties of BC films.[30]

BC films also demonstrated the non-linear dependence of mechanical properties under different water activities. Young's modulus and the tensile strength increase with growing water activity, reaching its maximum value at $a_w = 0.43$. At lower moisture contents, water adsorbs on cellulose, easing the mobility of both crystalline and amorphous cellulose regions, promoting fibril reorganization and improving chain resistance under axial deformation. With further water addition, the hydrogen bond network degrades in conjunction with fibril swelling, the plasticizing of the cellulose film and the enhancement of fibril movement within the network.[25]

3. Structural and mechanical properties of hemicelluloses

Hemicelluloses are defined as polysaccharides, they can be water- or alkali-extracted from plants[59], they are able to link cellulose via hydrogen bonding.[60] Hemicellulose composition may vary between plant species.[61] Common hemicellulose monosaccharides are D-xylose, L-arabinose, D-glucose, D-galactose, D-mannose, D-glucuronic acid etc.[59]

In PCW, there are several main types of hemicelluloses – xyloglucan XG, xylans and mannans. XG is a major PCW hemicellulose component, which consists of a β-(1,4)-D-glucan backbone, decorated with xylose sidechains. Xylose residues may have some galactose- and fucose- grafted substitutes.[62] Compared to other PCW hemicelluloses, the XG structure is highly regular. The majority of higher plants produce repeatable XG of the XXXG-type (X – glucose unit with xylose residue, G – glucose unit), with the X unit prone to further substitutions.[63] Widely used in experimental studies, tamarind XG is composed of XXXG, XXLG, LXG and XLLG units in a ratio of 1.4:3:1:5.4, respectively.[64] Analysis of polysaccharide subunits in different plants and tissues shows predominant composition of XXXG, XXLG, XLXG and XXFG, which means attribution of the main chain with β-(1,2)-D-galactopyranoses and α-(1,2)-L-fucopyranoses. Plant cell wall XG is usually fucosylated, whether substitutes with fucosyl attributes also has biological activity effect in PCW.[40,65] Hoffman et al. (2005) provided comprehensive overview on structures of XG in various plant species according to type of subunit and tissue.[63] The molecular weight (MW) of XG is in the range of 650-2500 kDa.[66] In its solid state, XG has a flat, two-fold twisted backbone, similar to cellulose.[67]

Xylans are linear polymers of β-(1,4)-linked xylose. According to the type of backbone α-(1,2)-substitutes used, several xylan groups, such as glucuronoxylan (GX), methyl glucuronoxylan (MGX), arabinoxylan (AX) are known. AX is the main hemicellulose of commelinid monocots.[66] It contains O2 and/or O3 arabinose substitutes, irregularly distributed along the backbone. The average MW is 65-5000 kDa. Xylans have various randomly distributed backbone substitutes, which are difficult to determine. Its biosynthetic pathway is complex[68], but predicted to be similar to XG.[69]

Mannans are a group of polysaccharides, composed of (1,4)-β-D-mannopyranoses with a low degree of galactose substitution (linear mannan), high-galactose substitutes (galactomannan), glucopyranose (glucomannan) and galactose-glucopyranose (galactoglucomannan GGM) incorporation.[70] The glucose to mannose ratio for GGM is reported to be 1:1.6.[71] GGM and glucomannan in small amounts exist in dicot PCW.[72] Konjac and spruce glucomannans are widely used in experimental studies by acting as a model polysaccharides.[73] Konjac glucomannan (KGM) contains randomly distributed β-(1,4)-linked D-mannose and β-(1,4)-linked D-glucose in 3:1 ratio with a low degree of α-(1,6) branching and degree of polymerization of 200.[73,74] Softwood mannans is a low galactosyl substituted glucomannan with degree of polymerization of 510 with a sugar ratio of galactose:glucose:mannose 0.03:1:3.4.[75] Both Konjac and

Table 2. Mechanical properties of XG films (measurement conditions: RH –relative humidity of air, T – air temperature).

Composition	Source	Tensile strength (MPa)	Strain at break (%)	Young's modulus (MPa)	RH (%)	T (°C)	Reference
XG	Tamarind	61.0 ± 8.6	4.8 ± 3.6	4300 ± 230	50	RT	[80]
XG	Tamarind	28.0-114.0	2.7-9.2	1630-5950	50	RT	[36]
XG	Tamarind	78.0 ± 8.6	5.7 ± 3.6	4597 ± 164	50	RT	[81]
XG	Tamarind	92.9 ± 5.8	8.9 ± 2.0	4100 ± 150	50	23	[82]
XG	Tamarind			1500-3500	50	25	[58]
XG	Tamarind	78.0 ± 8.6	5.7 ± 3.6	4597 ± 164	50	23	[83]

spruce glucomannan provide structures similar to low-galactosylated GGM, with an ability to be extracted with a reasonable yields, even from residues of papermaking industry.[70,71,73] High content of mannans in Konjac and softwood allow to reduce mannans degradation by lowering its yield.[73]

Hemicellulose distribution in the plant cell wall is still an open question, especially from the viewpoint of accepted PCW models. Hemicelluloses are synthesized in Golgi, targeting the plasma membrane for newly synthesized cellulose fibrils.[59] According to the most recent views developed by researchers, hemicelluloses are recognized as tethers/hotspot linkers, which enhance cellulosic network properties. Nonetheless, some sort of hemicellulose-only networks were observed in pea root cells.[76] In a similar way, hemicelluloses are reported to form separate microdomains in PCW [38], or they form a hydrogen bond network.[71,72] Networks consisting entirely of hemicellulose are fragile for the most part due to their short polysaccharide backbones and branched substitutes.[77] Also, it is necessary to declare the role of lignin (copolymers of p-hydroxyphenyl, guaiacyl and syringyl units) on plant cell wall network.[78] Plant cell wall lignin is suggested to be more associated with xylans, compare to the other cell wall polysaccharides. Higher lignin content in cell wall decrease its mechanical properties due to decreased aggregation of other plant cell wall polysaccharides.[79] There are relatively few published reports dedicated to this theme. Here, we will evaluate the current data concerning the structural and mechanical properties of hemicellulose films.

3.1. Xyloglucan

Generalized data concerning the mechanical properties of XG are given in Table 2. Kochumalayil et al. (2010) reported that uniformly casted XG films are only produced in negligible quantities.[80] High-MW XG may form cast films on its own, whereas low-MW XG requires external plasticizing agents. High-MW XG networks show robustness with a smooth surface. Young's modulus for dry XG films is approximately 6 GPa, which is defined by strong intermolecular connections and low free volume.[26] With moisture uptake, the intermolecular bonds of branched XG degrade, however, they are still strong enough to oppose mechanical loads. Bendaoud reported that XG films exhibit linear elastic stress-strain behavior, but have a low strain at break value and brittle fracturing. Cross-sections of XG networks showed a smooth structure with uniform fibril dispersion and few aggregates. Stress at break and Young's modulus for the XG films were 1.5-1.8 times higher, compared to the BC control.[58]

Table 3. Mechanical properties of xylan films (DS – degree of substitution; DP – degree of polymerization, measurement conditions: RH –relative humidity of air, T – air temperature).

Composition	Source	Tensile strength (MPa)	Strain at break (%)	Youngs modulus (MPa)	RH (%)	T (°C)	Reference
Xylan	Maize bran	10.0-11.0	8.0-38.0	57.0-118.0		19 ± 1	[86]
Xylan	Cotton stalk	1.1-1.4	45.5-56.7		40 ± 4	20 ± 2	[87]
Xylan	Bamboo	10.02 ± 2.01	1.28 ± 0.5	780 ± 420			[88]
Xylan	Birchwood	19.3 ± 1.4	0.8 ± 0.1	2400 ± 200	50	23	[89]
Xylan	Sugarcane bagasse	9.2-22.3	0.7-1.3	8.9-38.9			[90]
Glucuronoxylan	Cotton stalks	14.0	12.0				[91]
AX	Maize bran	26.5 ± 4.1	7.4 ± 2.9	72.4 ± 35.2	54	25	[92]
AX	Corn hull	53.8 ± 0.4	6.2 ± 1.6	1316 ± 90	54	22	[93]
AX	Barley husks	50.0	2.5	2930	50	23	[94]
AX	Barley husks	40.0	1.4	2800	50	23	[59]
AX	Rye flour	52.4 ± 5.9	4.7 ± 1.8	1750 ± 740	50	23	[95]
AX$_{\text{(high DS)}}$	Rye flour	58.0 ± 11.0	8.1 ± 3.3	2500 ± 400	50	30	[96]
AX$_{\text{(low DS)}}$		32.0 ± 3.0	2.1 ± 0.3	2200 ± 200			
AX	Rye bran	15.7	6.1	533.0	50	23	[97]
AX	Rye flour	42.5 ± 6.5	11.9 ± 4.3	2300 ± 200	50 ± 2	23 ± 1	[98]
AX$_{\text{(high DP, high DS)}}$	Rye flour	63.0	12.4	1800.0	50	23	[99]
AX$_{\text{(low DP, high DS)}}$		47.0	5.2	1890.0			
AX$_{\text{(high DP, low DS)}}$		60.0	12.2	1700.0			
AX$_{\text{(low DP, low DS)}}$		36.5	4.0	1900.0			
AX	Rye flour	62.0 ± 3.0	4.0 ± 0.9	3100 ± 200	50	23	[100]
AX	Wheat flour	8.1-98.0	7.1-39.0	325-2475	59	25 ± 1	[101]
AX	Rye flour	16.0	6.0	550.0	50	23	[102]
AcAX	Rye flour	65.1 ± 4.2	21.0 ± 3.1	2160 ± 80	50	23	[103]
AX	Corncob	53.54 ± 12.8	7.08 ± 1.3	1662 ± 268	50	25	[104]
AX	Wheat flour	61.0-131.0	22.0-46.0		59	20	[105]
AX	Oat spelt	25.0 ± 4.1	6.0 ± 0.8	626 ± 126	50	23	[106]
AX	Sorghum bagasse	32.0-34.0	2.0-2.6	2299-3400	50	23	[107]

Pre-sonicated XG solutions form casted films with improved mechanical characteristics, as compared to non-sonicated ones.[84] It is clear that more dense dispersions of polymer chains in a network enhance its properties via hydrogen bond densification and fibril sticking.

3.2. Xylans

Aspen, birchwood, corncob and grass xylans were shown to have non-network-forming polysaccharides.[85] Data concerning the mechanical properties of xylan films are summarized in Table 3. A number of xylan networks with lignin/pectin additives have been reported. Under the same network density, xylan concentration is directly proportional to tensile strength, strain at break (increased amount of entrapped water) and Youngs modulus.[87] Da Silva Braga et al. reported dense xylan-lignin networks with reduced surface roughness.[90] The contiguous glucuronoxylan network with lignin additives, obtained by Bancegul et al. showed a high degree of extensibility with elongations reaching up to 12%. The presence of approximately 1% lignin and pectin impurities improves the xylan network-forming properties due to its dispersibility, thereby increasing Youngs modulus but decreasing strain at break. Lignin improve network elongation properties by creation of intermolecular ester and ether bonds with xylan. Both compounds act as natural plasticizers, and produce an effect similar to increasing the degree of acetylation.[89]

As far as AX film-forming properties are concerned, there are far more promising candidates than glucuronoxylan, a number of studies were conducted in this field. Pure AX films were reported to be smooth with uniformly distributed arabinoxylan chains.[93,99,100] The AX branched structure enhanced plastification through the use of substitutes such as xylitol and sorbitol. Water was also reported to be a good AX plasticizer.[59]

Pure alkali-extracted AX films were cohesive, but also brittle with minor insoluble particles of denaturated proteins.[95,98] The authors determined the mechanical properties of AX films to be highly dependent on AX extraction methods.[95] The same authors reported that mild acid and heat treatment partially degrades arabinose side-chains.[94,95] Low-arabinose AX films showed a cracked surface, in contrast to amorphous high-arabinose samples (arabinose substitutes prohibit xylan backbone interactions). Non-treated high-arabinose AX films showed enhanced mechanical properties. Being amorphous, xylan chains disentangle and become orientated in the direction of the applied force. The decreased degree of arabinosylation resulted in crystallinity growth, which positively contributed to the desirable mechanical behavior of the film. With further AX dearabinosylation, the film softens due to increased moisture uptake.[95] Stevanic et al. reported arabinoxylan debranching to increase crystallinity by about 20% and provide excessive embrittlement. Debranching also resulted in a decrease in strain at break by 45%.[100]

Sarossy showed that co-extracted β-glucan improves the mechanical behavior of AX film. Enhancement occurs due to the increase in the density of the composite structure. After β-glucan removal, the authors reported a 50% drop in tensile strength, a 40% drop in strain at break and 20% lower values of Young̀s modulus.[98] Being a natural polymer, AX films are highly hydrophobic.[92] Mikkonen et al. reported that the storage modulus of AX films decreases with growing relative humidity, which indicates moisture-induced plasticization. The higher number of AX substituents degrades the hydrogen bond network, which results in enhanced composite flexibility.[96] An increase in both the degree of polymerization and in the degree of substitution of AX resulted in an increase in tensile strength and Young̀s modulus, with the first parameter being affected the most.[99] Changes in the degree of substitution of AX did not affect the elongation at break. An increase in the number of unsubstituted xylopyranoses also lead to an increase in AX crystallinity.[106]

3.3. Glucomannan

As with AX, glucomannan forms films without any additives. Generalized data concerning KGM mechanical properties are given in Table 4. Pure KGM films are reported to be mainly smooth, with small pores and cracks visible in cross-sections and obvious crystalline regions and numerous aggregates in its body, formed by high-MW glucomannan fractions.[108,109,111,114] The films showed mechanical behavior characteristic of brittle materials. As for all polysaccharide chains, a number of factors affect its

Table 4. Mechanical properties of Konjac glucomannan films (measurement conditions: RH –relative humidity of air, T – air temperature).

Composition	Source	Tensile strength (MPa)	Strain at break (%)	Youngs modulus (MPa)	RH (%)	T (°C)	Reference
KGM	Konjac	10.1	7.7		47	5	[108]
KGM	Konjac	20.1	8.0		63	RT	[109]
KGM	Konjac	2.3-3.4	7.8-12.2		0-100	RT	[110]
KGM	Konjac	8.2	1.8				[101]
KGM	Konjac	57.0	11.0	1914.0	54		[111]
KGM	Konjac	40.0	7.0		50		[112]
KGM $_{\text{deacetylated}}$	Konjac	36.2	9.0		67	25	[113]
KGM	Konjac	30.2 ± 1.1	32.0 ± 3.1		50		[114]
KGM	Konjac	61.0 ± 3.0	25.0 ± 0.5	1200.0	50	20	[115]
KGM	Konjac	41.47 ± 1.79	7.46 ± 0.75		50	25	[116]

mechanical properties, such as the flexibility and mobility of the backbone, degree of entanglement, segmental motion and antiplasticization of low-MW tailings.

Extensive backbone entanglements cause fragmentary chain alignment, which may increase tensile strength and decrease elongation with decreasing MW. However, it may go the other way, as low-MW chains limit entangling abilities. Antiplasticization with low-MW chains/water enhance the desirable mechanical behavior of the film, possibly acting as a slippage area for long chains or this may be due to structure compaction.[110]

4. Structural and mechanical properties of binary BC-hemicellulose composites

Structural and mechanical properties of BC-hemicellulose composites differ significantly, according to the method of composite production. The most frequently used methods of BC-hemicellulose composite production are medium growth and casting. Medium growth method is the same as for the pure BC growth, with the difference that corresponding quantities of hemicellulose are diluted in growth medium before autoclaving and bacteria inoculation.[34]

BC-hemicellulose composites, produced by casting are often called reconstituted or regenerated composites, which refers to the production method.[96,99,117] Generally, scraps of never-dried BC are mechanically treated and dispersed in ultrapure water, with further addition of hemicellulose solution. Also, instead of BC, commercial cellulose fibrils are often used. Additional treatment may allow vacuum filtration of pulp and degassing by ultrasonication *in vacuo*.[96,118] On the last step, pulp is deposited on sterile Petri dishes and dried for 23-60 °C from 4 h to several days.[99,117,118]

As it will be shown in the next chapters, casted BC-hemicellulose composites show improved mechanical properties, compared to medium grown, due to better hemicellulose dispersion, denser film structure and improved fiber-to-fiber interconnectivity.

4.1. BC-xyloglucan

For approximately 50 years, XG was thought to be the main hemicellulose to form a cellulose-hemicellulose network in PCW, causing 20-40 nm links to form between

Table 5. Mechanical properties of BC-XG composites (measurement conditions: RH –relative humidity of air, T – air temperature).

Composition	Hemicellulose source	Fabrication method	Tensile strength (MPa)	Strain at break (%)	Youngs modulus (MPa)	RH (%)	T (°C)	Reference
BC-XG	Tamarind	Grown in medium	0.14-0.33	38.0-58.0				[31]
BC-XG	Tamarind	Grown in medium	0.18	48.0				[122]
BC-XG	Tamarind	Grown in medium	0.09	42.0				[29]
BC-XG $_{\text{(high-MW)}}$	Tamarind	Grown in medium	0.18	48.0				[123]
BC-XG $_{\text{(Gal-depleted)}}$			0.09-0.15	16.0-25.0				
BC $_{\text{(reconstituted)}}$-XG	Tamarind	Casted	92.0-130.0	1.6-2.6	8300-11000	50	RT	[117]
BC-XG	Tamarind	Grown in medium	18.2 ± 2.7	0.29 ± 0.1	4300 ± 1400	>33	35	[124]
BC-XG	Tamarind	Grown in medium	2.7-37.7	>25.0			25	[125]
BC $_{\text{(reconstituted)}}$-XG	*Guibourtia hymenifolia*	Casted	59.0 ± 11.0	2.4 ± 0.55	4750 ± 230	50 ± 5	RT	[118]
BC-XG	Tamarind	Grown in medium	3.1	37.0	7.5			[34]
CBC-XG	Tamarind	Casted	52.0	77.0	9700			[42]
Cellulose $_{\text{cryst.}}$-XG	Tamarind	Casted			2650-4750	50	25	[58]

contiguous fibrils. A number of *in vitro* and *in situ* cellulose-XG interactions were observed, such as cellulose tethering[119], fibrils coverage[120] or the formation of covalent links between them.[121] The mechanical properties of BC-XG composites are provided in Table 5.

Structurally, XG appears in binary composite form as a thin ladder rung-like structure, 30-50 nm long. Also, some substantial links longer than 70 nm occur between diverged cellulose ribbons.[119] Measurements of XG link lengths showed that they may link three or more cellulose fibrils together. As for the incorporation level, several different studies reported a BC:XG ratio in the binary network ranging from 1:0.1 to 1:0.7.[29,32,106,108] Gu et al. reported several differences between BC-XG composite and pure BC, like thicker BC fibrils, a denser pellicle structure and lower porosity.[109,114] Chain length, sidechain pattern and the degree of XG acetylation influence its bonding to CBC. The XG binding rate increases with its length, with a minimum of 12 glucosyl residues, which are necessary for bonding. The degree of XG acetylation does not have any impact on binding with cellulose, while the presence of fucosyl third saccharide substitutes improves XG flexibility thereby increasing its exposure to the cellulose surface.[126]

XG provides interfibril adhesion to form a binary casted composite with cellulose.[117] XG chains are reported to obstruct nanofibril aggregation, which may be explained through its adsorption on the fibril surface. However, XG may have some issues with adhesion on the BC surface, this is related to its diffusion abilities (presence of side branches) and hydrogen binding with BC.[127]

The presence of high-MW XG in its binary cellulose-based composite causes the formation of highly organized cross-linked structures. Addition of low-MW XG to the growth medium leads to a higher level of incorporation into the cellulose network with almost no lateral organization of cellulose fibrils and abundant XG cross-bridges. XG may participate in the formation of more than one cross-link, with the lengths of the cross-links and aligned regions having similar values.[40]

BC which is synthesized in the presence of hemicelluloses is more accessible to enzymatic hydrolysis. This effect is related to the structure of fibrils packed into ribbons or bundles, and to the general structure of the composite, where fibrils synthesized in hemicellulose-containing medium aggregate less tightly as compared to pure BC.[128] A comparison between the measured cellulose:XG ratio and the number of cross-bridges, suggested that only a small fraction of XG is involved in bridge formation with the majority of it presumably becoming aligned with cellulose.[119] Other authors reported that XG is partially responsible for creating cellulose interchain bindings and also partially responsible for binding cellulose during its synthesis through reactions with inner hydroxyl groups.[129]

The addition of any kind of XG to the growth medium decrease cellulose crystallinity in general by lowering Iα BC and increasing Iβ content at the early stage of BC-XG composite growth.[119] An increased level of Iβ cellulose was also indicated for CBC-XG films, as compared to pure CBC.[42] The tendency for cellulose Iβ formation in the presence of XG was explained by decreases in shear stress, which normally occurs during ribbon twisting when fibrils assemble.[127]

Binary 1:1 BC:XG networks showed enhanced mechanical properties, compared to pure polysaccharide films. Based on XG content, networks may be classified into several structural types – continuous BC networks (<40% XG content), co-continuous networks (≈40-50% XG) and continuous XG ones (>50% XG). In continuous BC networks, the amorphous XG is well dispersed, thereby reinforcing it and increasing its Young's modulus. In the case of BC dispersion in the XG network, mechanical properties are dominated by the XG component. The mechanical behavior of the co-continuous network may be explained through the lubricating action of XG, increasing stress and strain at break. Such an effect was also observed for the BC-xylan co-continuous matrix.[58]

Compared to pure BC, lower failure stresses and higher failure strains were observed for BC-XG networks, grown in XG-containing medium.[31] Stress-strain tests on the BC-XG network showed that at both low and high compressive strain-rates, the XG network was stronger and provided a significantly more robust mechanical response as compared to the BC sample. Both the viscoelastic and elastic properties were observed for the XG material at low and high-strain deformation rates.[125]

The extensibility of the BC-XG composite grown in hemicellulose-containing medium was reported to increase by up to 300% as compared to pure BC.[27,106] High-MW XG promotes the greater extensibility of the composite under uniaxial and biaxial tensions. This has contributed to the alignment of cross-linked domains with tensile direction, resulting in the restraint of cellulose-XG knots at greater strains.[29,116]

Xyloglucan composites with bacterial cellulose prepared by casting showed higher tensile strength, compared to composites grown in the liquid medium (Table 5). This effect was explained by better fibril dispersion and better fiber-to-fiber interconnectivity, in case of casted films.[117,118] However, the scarcity of data makes it impossible to draw decisive conclusions on the remaining mechanical parameters.

4.2. BC-xylans

The mechanical properties of BC-xylan composites are summarized in Table 6. Xylans are known to form intertwined networks with BC. BC-xylan composites exhibit increased fibril length, with a lower level of cellulose crystallinity and a lower average

Table 6. Mechanical properties of BC-xylan composites (AGX - arabino-4-O-methyl glucuronoxylan; GX – glucuronoxylan; DS – degree of substitution; DP – degree of polymerization, measurement conditions: RH –relative humidity of air, T – air temperature).

Composition	Hemicellulose source	Fabrication method	Tensile strength (MPa)	**Strain at break** (%)	**Youngs modulus (MPa)**	**RH** (%)	**T** (°**C**)	Reference
BC-AX $_{\text{(high DS)}}$	Rye endosperm	Casted	53.0-68.0	3.3-8.3	2700-3200	50	30	[96]
BC-AX $_{\text{(low DS)}}$			46.0-49.0	2.8 ± 1.3	3100-3700			
CMF-AX $_{\text{(high DP, high DS)}}$	Rye endosperm	Casted	90.0	10.9	2520.0	50	23	[99]
CMF-AX $_{\text{(high DP, low DS)}}$			83.0	11.0	1900.0			
CMF-AX $_{\text{(low DP, high DS)}}$			57.0	3.7	2680.0			
CMF-AX $_{\text{(low DP, low DS)}}$			42.0	4.2	1780.0			
CNF-AX	Rye endosperm	Casted	108-143	6.0-7.2	4800-7300	50	23	[100]
CNF-AcAX	Rye endosperm	Casted	72.5-90.1	10.5-19.2	2390-3330	50	23	[103]
BC-AX	Wheat flour	Grown in medium	0.98-10.2	18.0			25	[125]
CNF-xylan	Birchwood	Casted	23.0-57.0	0.6-1.1	5200-7600	50	23	[130]
CBC-xylan	Beechwood	Grown in medium	42.0	71.0	7300	50	25	[42]
CNF-xylan	Beechwood	Casted	45.0-100.0	1.2 ± 0.4	5800-10100			[131]
Cellulose $_{\text{(regenerated)}}$-AGX	Spruce wood	Casted	19.0-75.0	2.8-24.8	400-2150	30-90	25	[99]
BC-AGX	Softwood	Grown in medium	0.67	100.0	0.4 ± 0.1			[73]
BC-GX $_{\text{(acetylated)}}$			0.82	100.0	0.7 ± 0.1			

diameter of fibril at the same time, compared to pure BC. It was hypothesized that xylan and XG may convert localized amorphous cellulose regions into more uniformly distributed ones, resulting in a higher resistance to complete hydrolysis.[42] Xylans may act as fillers of BC in a binary composite, by mainly aggregating on the cellulose surface.[131] Linder et al. discovered that xylan aggregates may adsorb on a cellulose surface via unsubstituted regions of both chains.[132] Apart from the random uniform distribution of xylans and fibril bundles in films, xylans were observed to interact mainly with amorphous cellulose.[130,133]

The Youngs modulus of BC-xylan composite decreases with increasing xylan content. This effect contributed to weakened cellulose interfibril interactions.[131] An improvement in mechanical properties was reported with the increase in cellulose nanofibril (CNF) content in casted xylan films. The best mechanical performance was reported for xylan films with 5-10% vol. CNF. The further addition of CNF resulted in diminished mechanical properties for the casted composites. Cellulose acetylation improves mechanical behavior by increasing tensile strength and Youngs modulus, but decreases tensile strain with increases in cellulose concentration.[134]

However some researchers have reported that CBC film of BC grown in xylan presence show 27% and 40% higher tensile strength and Youngs modulus, respectively, as compared to pure BC. The enhanced mechanical properties were explained in this case by the enlarged hydrogen bond network of BCNC and flexible long-chained xylans (nanoreinforcing fillers).[42]

The structural and mechanical properties of BC-AX composite, cultivated in Hestrin-Schramm medium with AX presence, indicate different types of AX-cellulose interactions, as compared to XG or pectin. Binary AX-BC composites were shown to have diminished mechanical properties as compared to pure cellulose samples. AX was shown to form microscale grains, closely bonded to cellulose.[125] Such AX domains existing on the BC surface, were reported to interact via nonspecific adsorption mechanisms.[135]

Köhnke et al. reported that AX adsorbs irreversibly on the cellulose surface according to a substitution pattern. The adsorption and affinity of AX to BC only increases with a decreasing Ara:Xyl ratio. However, further reductions in the of Ara:Xyl ratio will decrease AX solubility, which may lead to composite phase separation. Also, substitution patterns have an impact on the viscoelastic properties of samples with lower amounts of arabinan. Reports have shown that AX adsorption on crystalline regions of cellulose is irreversible, and depends on the AX concentration in solution and the degree of arabinose substitution.[99]

Adsorption is enhanced with increases in the MW of AX, as well as in the presence of lignin. AX slightly decreases the crystallinity of BC, with lignin intensifying this process. It has been shown that lignin can promote AX aggregation in ternary composites, thereby intensifying AX adsorption, while improving the incorporation of AX at low quantities.[136]

Egues et al. showed that the presence of lignin and arabinose-xylose enhances composite formation in alkaline-extracted hemicelluloses. For BC films, grown with addition of alkaline extracted hemicelluloses with lignin impurities, lignin promotes the formation of thicker composites, with a dense structure and a reduced number of cracks. Lignin promotes the formation of thicker composites, with a dense structure and a reduced number of cracks.[137] Upon attachment to cellulose, branched AX may rearrange itself into extended conformations, thereby entrapping another AX.[86] In an AX-continuous matrix, reinforcement of cellulose nanofibrils increases film surface roughness. Cellulose nanofibrils addition leads to the formation of heterogeneous lamellar CNF structures coated by thin pore-clogging AX layers.[100]

The AX presence in growth medium does not affect the level of Iβ cellulose to the same extent as compared to BC (38 and 40%, respectively).[125] Debranching of arabinoxylan causes an increase in the degree of crystallinity. Also, only backbone residues of xylans may take part in the crystallization and show co-crystallizing properties under conditions of relatively low arabinose concentration.[96]

The BC-AX composite shows both viscoelastic and elastic properties at slow strain-rates and elastic properties at high-strain rates.[125] Stevanic et al. demonstrated that BC additives enhance the mechanical behavior of AX films.[96] This effect was also observed for AX-CNF casted films.[100,103] For cellulose microfibrils (CMF) a significant increase in tensile strength was only reported for mixtures with a high content of AX with high degree of polymerization.[99] In general, stiffer, stronger and more ductile films were obtained for cellulose-AX composites, as compared to pure AX films. Moisture sorption and the associated moisture-induced softening were both reduced with increased cellulose reinforcement content. AX debranching decreased the strength and breaking strain, resulting in more brittle films.[96] BC-arabinoglucuronoxylan (AGX) composites, produced by casting technique, demonstrated a smooth structure with a multilayered porous cross section. AGX may be adsorbed on the cellulose network as well as agglomerating in empty voids. Blended BC-AGX composites showed a higher degree of stiffness as compared to pure BC, which may be explained by cellulose-AGX hydrogen bonding.[138]

Table 7. Mechanical properties of BC-glucomannan composites (measurement conditions: RH –relative humidity of air, T – air temperature).

Composition	Hemicellulose source	Fabrication method	Tensile strength(MPa)	Strain at break(%)	Youngs modulus(MPa)	RH (%)	T(°C)	Reference
CNF-KGM	Konjac	Casted	73.0-118.0	6.7-10.8		50	23	[131]
BC-GGM	Softwood	Grown in medium	0.6	91.0	0.7 ± 0.2			[73]
BC-AcGGM			0.97	53.0	2.4 ± 0.3			
CNF-GGM	Spruce wood	Hot-pressed	50.8 ± 7.2		400.0 ± 45.0	50	23	[140]
CNF-KGM	Konjac	Casted	95.0-135.0	5.9 ± 2.0	6400-7700			[131]

Cellulose-xylan composites prepared by casting, showed higher tensile strength and Youngs modulus, compared to the composites grown in medium (Table 6). Better mechanical properties were contributed to the extended hydrogen bond network of fibrillated cellulose and flexible long-chained xylans that act as nano-reinforcing fillers.[42] However, casted films were less extensible, showing lower strain at break, than composites grown in medium. Degree of AX polymerization showed positive correlation with composite mechanical properties. This effect was attributed to increased interconnectivity between xylan chains, which enabled longer chains to slide across each other.[96,99] An increase in relative humidity decreased mechanical properties of cellulose-xylan composites, as a result of moisture-induced plasticization.[99]

4.3. BC-glucomannan

Studies concerning BC-mannans co-crystallization have suggested that mannans bind to BC via weak interactions.[139] The mechanical properties of BC-glucomannan composites are provided in Table 7. Berglund has shown that intercalated acetylated galactoglucomannan (acGGM) and GGM is incorporated into the BC network.[73] GGM shows a good affinity to cellulose nanofibrils by forming rigid layers on its surface.

Also, the similarity between the cellulose and GGM surface charges resulted in a smooth lubricating effect for the fibrils coated with GGM.[140] However, low-MW (20-40 kDa) glucomannans are not capable of coating or tethering cellulose fibrils due to their relatively short chains.[141] A reduction in the galactose content of galactomannan inversely relates to the level of incorporation into the BC network. Due to the structural features of galactomannans, kinetic (entanglement of BC-BC bonding region fibrils) and thermodynamic (lowest free energy state) controls are proposed to explain mannan impact on fibril association. It has been reported that for low-Gal mannans, fibril annealing resulted in BC-mannans-BC bonding.[142]

Pure BC, produced in a Haigler-Benziman medium, formed a twisted-ribbon-like structure, whereas BC, grown in the presence of acetylated glucomannans resulted in the formation of interwined fibrils, gathered in loose bundles.[28] Tokoh et al. discovered that acetylated glucomannan in the medium prevents the assembly of BC fibrils.[143]

A lower number of acetate substitutes stimulate adsorption, water solubility and thermal degradability, whereas close substitutions may result in stronger interactions.[73] The adsorption of mannans, as well as that of all of hemicelluloses, is highly dependent on its concentration and on the composition of cellulose nanofibrils.[144] GGM adsorbs on the nanofibril surface in a rigid conformation with a tight association due to the lower water content in the GGM layer. It has been shown that the affinity of GGM to cellulose does not correlate with the presence of xylan, moreover, the opposite relationship with xylan was observed.[86]

Carob and Konjac glucomannan adsorption on crystalline regions of cellulose decreases the accessibility of cellulases to cellulose.[145] A higher Gal:Man ratio may lower the adsorption of mannans, but branched mannans result in steric hindrances for cellulases.[146]

In casted binary composites, KGM acts as a filler, intertwining with BC fibrils. At relatively low concentrations, KGM mixes well with BC, forming multilayered smooth structures without visible aggregates.[131] The content of KGM in the binary composite has an inverse relationship with material phase separation. However, with increasing concentrations of KGM, a number of egg-like structures on the composite surface were reported, they were possibly formed by agglomerations of high-MW KGM.

As with XG and xylan, mannans in the composite decrease BC crystallinity. The structural differences between mannans and cellulose hinder the cellulose association processes and decrease its crystal size, thereby limiting the changes occurring in the crystalline lattice of the cellulose.[147] Whitney showed that KGM and low-galactose galactomannan reduce cellulose crystallinity in the BC-mannans composite, cultured in mannans presence, from 80-85% to 25%.[142] After that, Tokoh et al. reported that BC grown in mannan-containing medium resulted in a significantly reduced Iα cellulose level, as compared to the control samples.[148]

The presence of mannans had a significant effect on the mechanical properties of their binary composites with BC. The plasticity of hemicellulose films is enhanced by the high degree of substitution of GGM.[86] GGM addition improves the BC composite strength in its wet state. An increase in tensile strength and toughness by 170% was reported after the addition of 2% wt. GGM. A moderate increase in Young's modulus (33%) was observed after the addition of mannan polysaccharides.[140] Acetylated GGM increased Youngs modulus due to its tendency to co-crystallize with BC.[73] The mechanical behavior of composites made from regenerated cellulose-KGM showed a minor decrease in mechanical properties with the increase in KGM concentration. It was observed that mainly low-MW chains of both cellulose and KGM form the continuous matrix base. KGM additives improved the mechanical behavior of the CNF-KGM casted composite, which was attributed to the favorable dispersibility of KGM in cellulose fibrils.[131]

Composites prepared with casting method and fibrillated cellulose showed improved mechanical properties, compared to the composites, grown in medium (Table 7). Studies showed that glucomannans better penetrate into fibril network in casted films, due to glucomannan-mediated interactions facilitating uniform fibril distribution during composite formation.[140]

5. Structural and mechanical properties of BC-hemicellulose-pectin ternary composites

Most recent studies suggest that pectin forms its own wall network with plasticizing and water-binding properties, providing physical strength to PCW.[138,139] The crosslinking of pectin polysaccharides with other wall components provides additional structural and functional complexity to the wall.[145] Susanne E. Broxterman provided a comprehensive overview of most reported cross-links between cellulose, hemicellulose and pectins. To date, several types of these have been recognized in the cellulose-hemicellulose-pectin system, such as covalent linkages, adsorption by H-bonds, diferulic bridges, calcium bridges, borate-diol ester linkages etc.[149]

At high polysaccharide concentrations, XG and pectin do not mix, but rather, form micro domains. In vitro adsorption experiments onto cellulose fibrils have shown that XG and pectin bind to cellulose both simultaneously and competitively.[38] Haas et al. suggested the double-role of pectin – both as a minor cellulose bonding component in XG-rich walls and as a prime cellulose association mediating component in XG-poor walls.[150] In the second scenario, in areas of PCW lacking XG, the pectin establishes contacts between the fibrils, and takes over the tethering role of XG.[149,151,152] Covalent linkages of cellulose and galactose/arabinose rhamnogalacturonan I (RGI) sidechains were observed for carrot samples. It was proposed that RGI and xylans were present in covalently linked complexes of some fruit species.[149] However, the pectin-cellulose supramolecular complexes have yet to be determined.[153]

Structural studies on binary/ternary PCW analogues prepared by addition of XG and/or pectin to growth medium showed that the BC fibrils in the BC-pectin composite are drastically thinner (110 ± 33 nm, 45 ± 9 nm and 123 ± 29 nm for pure BC, BC-pectin and BC-pectin-XG, respectively). Studies have shown that pectin and some hemicelluloses act as inhibitors of microfibril association, while XG promotes their association through surface coating and the establishment of interfibril linkages.[154]

Several polysaccharide ratios in the ternary BC-XG-pectin composite were tested, such as 26% BC, 44% pectin and 20% XG[155]; 63% cellulose, 22% pectin and 15% XG.[122] Irrespective of the component ratio, binary BC-pectin composites were generally thicker than ternary composites, suggesting the existence of stronger bonds of cellulose XG to cellulose.[155]

According to the research of Gu and Catchmark, pectins show a 2.5 times lower adsorption rate, compared to xylans, both being non-comparable with XG. Due to structural differences (shorter sidechains) pectin binds more easily to porous cellulose, occupying a lower surface area.[156] In the BC-XG-pectin composite, grown in medium with 0.5% w/v addition of XG and pectin, XG may interact with all of pre-crystallized, crystallized and preferably amorphous BC, while pectin preferentially binds with crystalline regions.[33]

The effect of the composition of BC-XG-pectin composites on BC crystallinity is unclear. Some studies concerning BC-XG-pectin composites grown in Hestrin-Schramm medium with polysaccharide additives have shown that BC crystallinity has dropped significantly in the presence of XG and pectin additives. However, the ternary composites of other studies showed a higher degree of cellulose crystallinity, compared to pure BC. Researchers have hypothesized that the pectin network may contribute to simultaneous coating of the fibrils by XG.[157] Raman and FT-IR spectra have shown that the content of Iβ cellulose increases with XG content (up to 73%) and decreases with pectin concentration in the composite.[34] The XG:pectin ratio in BC-XG-pectin ternary composites grown in liquid medium with polysaccharide addition was shown to have an influence on the mechanical properties of the composite. The lower XG:pectin ratio resulted in a thinning of the cellulose fibrils and an increase in Youngs modulus. Studies have also shown that the removal of pectin significantly reduces composite tensile strength, which was not observed in the case of XG removal. Experimental results indicated that PCW stiffness is dependent on the XG:pectin ratio, in which pectin play a dominant role in the strengthening of ternary composites.[34] Introducing xyloglucan into a cellulose/pectin composite led to very compliant materials characterized by time-dependent creep behavior and high failure strains.[122]

6. Conclusion

Plant-like synthesis, high yields, an ultrafine structure and chemical purity have resulted in bacteria-produced cellulose being widely used in many scientific fields. The structural and chemical similarity with plant-based cellulose allows for the production of so-called plant cell-wall analogues and the study of the role of individual polysaccharides in PCW. Studies have shown that the materials produced are sensitive to the conditions of bacteria growth and require a carefully controlled growth process. It has also been demonstrated that BC synthesis in the presence of other plant-based polysaccharides such as hemicelluloses or pectin induces structural and chemical modifications in final composites. Structural changes induced by composition and growth conditions were directly reflected in the mechanical and thermal properties of the films, thereby providing a set of versatile materials. As they are relatively easy to modify, BC-based composites have a great potential in finely-tuned biosystems, the properties of which are ideally suited to targeted applications.

Disclosure statement

No potential conflict of interest was reported by the authors.

Funding

This study was supported by the National Science Center, Poland (Project no. 2019/35/D/NZ9/00555).

References

1. Ramana, K. V.; Tomar, A.; Singh, L. Effect of Various Carbon and Nitrogen Sources on Cellulose Synthesis by Acetobacter Xylinum. *World J. Microbiol. Biotechnol* **2000**, *16*, 245–248. . DOI: 10.1023/A:1008958014270.
2. Heo, M.-S.; Son, H.-J. Development of an Optimized, Simple Chemically Defined Medium for Bacterial Cellulose Production by Acetobacter Sp. A9 in Shaking Cultures. *Biotechnol. Appl. Biochem.* **2002**, *36*, 41–45. DOI: 10.1042/ba20020018.
3. Martínez-Sanz, M.; Pettolino, F.; Flanagan, B.; Gidley, M. J.; Gilbert, E. P. Structure of Cellulose Microfibrils in Mature Cotton Fibres. *Carbohydr. Polym.* **2017**, *175*, 450–463. DOI: 10.1016/j.carbpol.2017.07.090.

4. Yamanaka, S.; Watanabe, K.; Kitamura, N.; Iguchi, M.; Mitsuhashi, S.; Nishi, Y.; Uryu, M. The Structure and Mechanical Properties of Sheets Prepared from Bacterial Cellulose. *J. Mater. Sci.* **1989**, *24*, 3141–3145. DOI: 10.1007/BF01139032.
5. Reiniati, I.; Hrymak, A. N.; Margaritis, A. Recent Developments in the Production and Applications of Bacterial Cellulose Fibers and Nanocrystals. *Crit. Rev. Biotechnol.* **2017**, *37*, 510–524. DOI: 10.1080/07388551.2016.1189871.
6. Jonas, R.; Farah, L. F. Production and Application of Microbial Cellulose. *Polym. Degrad. Stab* **1998**, *59*, 101–106. DOI: 10.1016/S0141-3910(97)00197-3.
7. Lee, K. Y.; Buldum, G.; Mantalaris, A.; Bismarck, A. More than Meets the Eye in Bacterial Cellulose: Biosynthesis, Bioprocessing, and Applications in Advanced Fiber Composites. *Macromol. Biosci.* **2014**, *14*, 10–32. DOI: 10.1002/mabi.201300298.
8. Gregory, D. A.; Tripathi, L.; Fricker, A. T. R.; Asare, E.; Orlando, I.; Raghavendran, V.; Roy, I. Bacterial Cellulose: A Smart Biomaterial with Diverse Applications. *Mater. Sci. Eng. R Reports* **2021**, *145*, 100623. DOI: 10.1016/j.mser.2021.100623.
9. Iguchi, M.; Yamanaka, S.; Budhiono, A. Bacterial Cellulose - a Masterpiece of Nature's Arts. *J. Mater. Sci.* **2000**, *35*, 261–270. DOI: 10.1023/A:1004775229149.
10. Chinga-Carrasco, G. Microscopy and Computerized Image Analysis of Wood Pulp Fibres Multi-Scale Structures. In *Microscopy: Science, Technology, Applications and Education*; A. Méndez-Vilas, J. Díaz; Formatex: Badajoz, 2010, 2182–2189.
11. Chinga-Carrasco, G. Cellulose Fibres, Nanofibrils and Microfibrils: The Morphological Sequence of MFC Components from a Plant Physiology and Fibre Technology Point of View. *Nanoscale Res. Lett.* **2011**, *6*, 417–417. DOI: 10.1186/1556-276X-6-417.
12. Czaja, W.; Romanovicz, D.; Brown, R. m. Structural Investigations of Microbial Cellulose Produced in Stationary and Agitated Culture. *Cellulose* **2004**, *11*, 403–411. DOI: 10.1023/B:CELL.0000046412.11983.61.
13. Wan, W. K.; Hutter, J. L.; Milion, L.; Guhados, G. Bacterial Cellulose and Its Nanocomposites for Biomedical Applications. *ACS Symp. Ser.* **2006**, *938*, 221–241. DOI: 10.1021/bk-2006-0938.ch015.
14. Huang, Y.; Zhu, C.; Yang, J.; Nie, Y.; Chen, C.; Sun, D. Recent Advances in Bacterial Cellulose. *Cellulose* **2014**, *21*, 1–30. DOI: 10.1007/s10570-013-0088-z.
15. Cazón, P.; Vázquez, M. Improving Bacterial Cellulose Films by Ex-Situ and in-Situ Modifications: A Review. *Food Hydrocoll.* **2021**, *113*, 106514. DOI: 10.1016/j.foodhyd.2020.106514.
16. Klemm, D.; Schumann, D.; Udhardt, U.; Marsch, S. Bacterial Synthesized Cellulose - Artificial Blood Vessels for Microsurgery. *Prog. Polym. Sci* **2001**, *26*, 1561–1603. DOI: 10.1016/S0079-6700(01)00021-1.
17. Castro, C.; Zuluaga, R.; Putaux, J. L.; Caro, G.; Mondragon, I.; Gañán, P. Structural Characterization of Bacterial Cellulose Produced by Gluconacetobacter Swingsii Sp. from Colombian Agroindustrial Wastes. *Carbohydr. Polym* **2011**, *84*, 96–102. DOI: 10.1016/j.carbpol.2010.10.072.
18. Machado, R. T. A.; Gutierrez, J.; Tercjak, A.; Trovatti, E.; Uahib, F. G. M.; Moreno, GdP.; Nascimento, A. P.; Berreta, A. A.; Ribeiro, S. J. L.; Barud, H. S. Komagataeibacter Rhaeticus as an Alternative Bacteria for Cellulose Production. *Carbohydr. Polym.* **2016**, *152*, 841–849. DOI: 10.1016/j.carbpol.2016.06.049.
19. Portela, R.; Leal, C. R.; Almeida, P. L.; Sobral, R. G. Bacterial Cellulose: A Versatile Biopolymer for Wound Dressing Applications. *Microb. Biotechnol.* **2019**, *12*, 586–610. DOI: 10.1111/1751-7915.13392.
20. Esa, F.; Tasirin, S. M.; Rahman, N. A. Overview of Bacterial Cellulose Production and Application. *Agric. Agric. Sci. Procedia* **2014**, *2*, 113–119. DOI: 10.1016/j.aaspro.2014.11.017.
21. Zhang, L. K.; Du, S.; Wang, X.; Jiao, Y.; Yin, L.; Zhang, Y.; Guan, Y. Q. Bacterial Cellulose Based Composites Enhanced Transdermal Drug Targeting for Breast Cancer Treatment. *Chem. Eng. J.* **2019**, *370*, 749–759. DOI: 10.1016/j.cej.2019.03.216.

22. Kwak, M. H.; Kim, J. E.; Go, J.; Koh, E. K.; Song, S. H.; Son, H. J.; Kim, H. S.; Yun, Y. H.; Jung, Y. J.; Hwang, D. Y. Bacterial Cellulose Membrane Produced by Acetobacter Sp. A10 for Burn Wound Dressing Applications. *Carbohydr. Polym.* **2015**, *122*, 387–398. DOI: 10.1016/j.carbpol.2014.10.049.
23. Liu, J.; Chinga-Carrasco, G.; Cheng, F.; Xu, W.; Willför, S.; Syverud, K.; Xu, C. Hemicellulose-Reinforced Nanocellulose Hydrogels for Wound Healing Application. *Cellulose* **2016**, *23*, 3129–3143. DOI: 10.1007/s10570-016-1038-3.
24. Zhao, J.; Sun, H.; Yang, B.; Weng, Y. Hemicellulose-Based Film: Potential Green Films for Food Packaging. *Polymers (Basel)***2020**, *12*, 1775. DOI: 10.3390/polym12081775.
25. Cazón, P.; Velázquez, G.; Vázquez, M. Bacterial Cellulose Films: Evaluation of the Water Interaction. *Food Packag. Shelf Life* **2020**, *25*, 100526. DOI: 10.1016/j.fpsl.2020.100526.
26. Chen, S. Q.; Lopez-Sanchez, P.; Wang, D.; Mikkelsen, D.; Gidley, M. J. Mechanical Properties of Bacterial Cellulose Synthesised by Diverse Strains of the Genus Komagataeibacter. *Food Hydrocoll.* **2018**, *81*, 87–95. DOI: 10.1016/j.foodhyd.2018.02.031.
27. Brown, R. M. *Cellulose and Other Natural Polymer Systems: Biogenesis, Structure, and Degradation*, 1st ed.; Springer: US, **1982**. DOI: 10.1007/978-1-4684-1116-4.
28. Haigler, C. H.; White, A. R.; Brown, R. M.; Cooper, K. M. Alteration of in Vivo Cellulose Ribbon Assembly by Carboxymethylcellulose and Other Cellulose Derivatives. *J. Cell Biol.* **1982**, *94*, 64–69. DOI: 10.1083/jcb.94.1.64.
29. Astley, O. M.; Chanliaud, E.; Donald, A. M.; Gidley, M. J. Tensile Deformation of Bacterial Cellulose Composites. *Int. J. Biol. Macromol.* **2003**, *32*, 28–35. DOI: 10.1016/S0141-8130(03)00022-9.
30. Dayal, M. S.; Catchmark, J. M. Mechanical and Structural Property Analysis of Bacterial Cellulose Composites. *Carbohydr. Polym.* **2016**, *144*, 447–453. DOI: 10.1016/j.carbpol.2016.02.055.
31. Whitney, S. E. C.; Gothard, M. G. E.; Mitchell, J. T.; Gidley, M. J. Roles of Cellulose and Xyloglucan in Determining the Mechanical Properties of Primary Plant Cell Walls. *Plant Physiol.* **1999**, *121*, 657–663. DOI: 10.1104/pp.121.2.657.
32. Cybulska, J.; Vanstreels, E.; Ho, Q. T.; Courtin, C. M.; Craeyveld, V.; Van; Nicolaï, B.; Zdunek, A.; Konstankiewicz, K. Mechanical Characteristics of Artificial Cell Walls. *J. Food Eng.* **2010**, *96*, 287–294. DOI: 10.1016/j.jfoodeng.2009.08.001.
33. Gu, J.; Catchmark, J. M. Impact of Hemicelluloses and Pectin on Sphere-like Bacterial Cellulose Assembly. *Carbohydr. Polym.* **2012**, *88*, 547–557. DOI: 10.1016/j.carbpol.2011.12.040.
34. Szymańska-Chargot, M.; Chylińska, M.; Cybulska, J.; Kozioł, A.; Pieczywek, P. M.; Zdunek, A. Simultaneous Influence of Pectin and Xyloglucan on Structure and Mechanical Properties of Bacterial Cellulose Composites. *Carbohydr. Polym.* **2017**, *174*, 970–979. DOI: 10.1016/j.carbpol.2017.07.004.
35. Popper, Z. A. *The Plant Cell Wall: Materials and Protocols*;Humana Press: Totowa, New Jersey, **2011**. DOI: 10.1007/978-1-61779-008-9.
36. Kochumalayil J., J. Xyloglucan-Based Polymers and Nanocomposites – Modification, Properties and Barrier Film Applications. Doctoral dissertation, KTH Royal Institute of Technology: Stockholm, Sweden, **2012**.
37. Cosgrove, D. J.; Jarvis, M. C. Comparative Structure and Biomechanics of Plant Primary and Secondary Cell Walls. *Front. Plant Sci.* **2012**, *3*, 204–206. DOI: 10.3389/fpls.2012.00204.
38. Zykwinska, A.; Thibault, J. F.; Ralet, M. C. Competitive Binding of Pectin and Xyloglucan with Primary Cell Wall Cellulose. *Carbohydr. Polym.* **2008**, *74*, 957–961. DOI: 10.1016/j.carbpol.2008.05.004.
39. Park, Y. B.; Cosgrove, D. J. Changes in Cell Wall Biomechanical Properties in the Xyloglucan-Deficient Xxt1/Xxt2 Mutant of Arabidopsis. *Plant Physiol.* **2012**, *158*, 465–475. DOI: 10.1104/pp.111.189779.
40. Whitney, S. A. C. The Interaction of Cellulose with Xyloglucan and Other Glucan-Binding Polymers. Doctoral dissertation, University of Stirling: Stirling, Scotland, 1996.

41. He, X.; Meng, H.; Song, H.; Deng, S.; He, T.; Wang, S.; Wei, D.; Zhang, Z. Novel Bacterial Cellulose Membrane Biosynthesized by a New and Highly Efficient Producer Komagataeibacter Rhaeticus TJPU03. *Carbohydr. Res.* **2020**, *493*, 108030. DOI: 10.1016/j.carres.2020.108030.
42. Chi, K.; Catchmark, J. M. The Influences of Added Polysaccharides on the Properties of Bacterial Crystalline Nanocellulose. *Nanoscale* **2017**, *9*, 15144–15158. DOI: 10.1039/c7nr05615j.
43. Andrade, F.K.; Pertile, R.A.N.; Dourado F.; Gama, F.M. Bacterial Cellulose: Properties, Production and Applications. In *Cellulose: Structure and Properties, Derivatives and Industrial Uses*; A. Lejeune, T. Deprez; Nova Science Publishers: Hauppauge, New York, 2010, 427–458.
44. Hestrin, S.; Schramm, M. Synthesis of Cellulose by Acetobacter Xylinum. II. Preparation of Freeze-Dried Cells Capable of Polymerizing Glucose to Cellulose. *Biochem. J.* **1954**, *58*, 345–352. DOI: 10.1042/bj0580345.
45. Pecoraro, É.; Manzani, D.; Messaddeq, Y.; Ribeiro, S. J. L. Bacterial Cellulose from Glucanacetobacter Xylinus: Preparation, Properties and Applications. In *Monomers, Polymers and Composites from Renewable Resources*; M. N. Belgacem, A. Gandini; Elsevier: Amsterdam, **2008**, 369–383. DOI: 10.1016/B978-0-08-045316-3.00017-X.
46. Embuscado, M. E.; Marks, J. S.; BeMiller, J. N. Bacterial Cellulose. II. Optimization of Cellulose Production by Acetobacter Xylinum through Response Surface Methodology. *Top. Catal* **1994**, *8*, 419–430. DOI: 10.1016/S0268-005X(09)80085-4.
47. Volova, T. G.; Prudnikova, S. V.; Sukovatyi, A. G.; Shishatskaya, E. I. Production and properties of bacterial cellulose by the strain Komagataeibacter xylinus B-12068. Appl. Microbiol. Biotechnol. **2018**, 102(17), 7417–7428. DOI: 10.1007/s00253-018-9198-8.
48. Lin, S. P.; Loira Calvar, I.; Catchmark, J. M.; Liu, J. R.; Demirci, A.; Cheng, K. C. Biosynthesis, Production and Applications of Bacterial Cellulose. *Cellulose* **2013**, *20*, 2191–2219. DOI: 10.1007/s10570-013-9994-3.
49. Silvestre, A. J. D.; Freire, C. S. R.; Neto, C. P. Do Bacterial Cellulose Membranes Have Potential in Drug-Delivery Systems? *Expert Opin. Drug Deliv.* **2014**, *11*, 1113–1124. DOI: 10.1517/17425247.2014.920819.
50. Okiyama, A.; Motoki, M.; Yamanaka, S. Bacterial Cellulose II. Processing of the Gelatinous Cellulose for Food Materials. *Top. Catal* **1992**, *6*, 479–487. DOI: 10.1016/S0268-005X(09)80033-7.
51. Watanabe, K.; Tabuchi, M.; Morinaga, Y.; Yoshinaga, F. Structural Features and Properties of Bacterial Cellulose Produced in Agitated Culture. *Cellulose* **1998**, *5*, 187–200. . DOI: 10.1023/A:1009272904582.
52. Sanchavanakit, N.; Sangrungraungroj, W.; Kaomongkolgit, R.; Banaprasert, T.; Pavasant, P.; Phisalaphong, M. Growth of Human Keratinocytes and Fibroblasts on Bacterial Cellulose Film. *Biotechnol. Prog.* **2006**, *22*, 1194–1199. DOI: 10.1021/bp060035o.
53. Rambo, C. R.; Recouvreux, D. O. S.; Carminatti, C. A.; Pitlovanciv, A. K.; Antônio, R. V.; Porto, L. M. Template Assisted Synthesis of Porous Nanofibrous Cellulose Membranes for Tissue Engineering. *Mater. Sci. Eng. C.* **2008**, *28*, 549–554. DOI: 10.1016/j.msec.2007.11.011.
54. McKenna, B. A.; Mikkelsen, D.; Wehr, J. B.; Gidley, M. J.; Menzies, N. W. Mechanical and Structural Properties of Native and Alkali-Treated Bacterial Cellulose Produced by Gluconacetobacter Xylinus Strain ATCC 53524. *Cellulose* **2009**, *16*, 1047–1055. DOI: 10.1007/s10570-009-9340-y.
55. Zhijiang, C.; Guang, Y. Optical Nanocomposites Prepared by Incorporating Bacterial Cellulose Nanofibrils into Poly(3-Hydroxybutyrate). *Mater. Lett.* **2011**, *65*, 182–184. DOI: 10.1016/j.matlet.2010.09.055.
56. Wang, S.; Li, T.; Chen, C.; Kong, W.; Zhu, S.; Dai, J.; Diaz, A. J.; Hitz, E.; Solares, S. D.; Li, T.; Hu, L. Transparent, Anisotropic Biofilm with Aligned Bacterial Cellulose Nanofibers. *Adv. Funct. Mater.* **2018**, *28*, 1707491. DOI: 10.1002/adfm.201707491.

57. Sederavičiūtė, F.; Bekampienė, P.; Domskienė, J. Effect of Pretreatment Procedure on Properties of Kombucha Fermented Bacterial Cellulose Membrane. *Polym. Test* **2019**, *78*, 105941. DOI: 10.1016/j.polymertesting.2019.105941.
58. Bendaoud, A.; Kehrbusch, R.; Baranov, A.; Duchemin, B.; Maigret, J. E.; Falourd, X.; Staiger, M. P.; Cathala, B.; Lourdin, D.; Leroy, E. Nanostructured Cellulose-Xyloglucan Blends via Ionic Liquid/Water Processing. *Carbohydr. Polym.* **2017**, *168*, 163–172. DOI: 10.1016/j.carbpol.2017.03.080.
59. Gröndahl, M.; Gatenholm, P. Oxygen Barrier Films Based on Xylans Isolated from Biomass. *ACS Symp. Ser.* **2007**, *954*, 137–152. DOI: 10.1021/bk-2007-0954.ch009.
60. York, W. S.; Darvill, A. G.; McNeil, M.; Stevenson, T. T.; Albersheim, P. Isolation and Characterization of Plant Cell Walls and Cell Wall Components. *Methods Enzymol.* **1986**, *118*, 3–40. DOI: 10.1016/0076-6879(86)18062-1.
61. Gabrielii, I.; Gatenholm, P.; Glasser, W. G.; Jain, R. K.; Kenne, L. Separation, Characterization and Hydrogel-Formation of Hemicellulose from Aspen Wood. *Carbohydr. Polym* **2000**, *43*, 367–374. DOI: 10.1016/S0144-8617(00)00181-8.
62. Tuomivaara, S. T.; Yaoi, K.; O'Neill, M. A.; York, W. S. Generation and Structural Validation of a Library of Diverse Xyloglucan-Derived Oligosaccharides, Including an Update on Xyloglucan Nomenclature. *Carbohydr. Res.* **2015**, *402*, 56–66. DOI: 10.1016/j.carres.2014.06.031.
63. Hoffman, M.; Jia, Z.; Peña, M. J.; Cash, M.; Harper, A.; Blackburn, A. R.; Darvill, A.; York, W. S. Structural Analysis of Xyloglucans in the Primary Cell Walls of Plants in the Subclass Asteridae. *Carbohydr. Res.* **2005**, *340*, 1826–1840. DOI: 10.1016/j.carres.2005.04.016.
64. York, W. S.; van Halbeek, H.; Darvill, A. G.; Albersheim, P. Structural Analysis of Xyloglucan Oligosaccharides by 1H-n.m.r. Spectroscopy and Fast-Atom-Bombardment Mass Spectrometry. *Carbohydr. Res.* **1990**, *200*, 9–31. DOI: 10.1016/0008-6215(90)84179-X.
65. McDougall, G. J.; Fry, S. C. Structure-Activity Relationships for Xyloglucan Oligosaccharides with Antiauxin Activity. *Plant Physiol.* **1989**, *89*, 883–887. DOI: 10.1104/pp.89.3.883.
66. Lima, D. U.; Loh, W.; Buckeridge, M. S. Xyloglucan-Cellulose Interaction Depends on the Sidechains and Molecular Weight of Xyloglucan. *Plant Physiol. Biochem.* **2004**, *42*, 389–394. DOI: 10.1016/j.plaphy.2004.03.003.
67. Zhou, Q.; Rutland, M. W.; Teeri, T. T.; Brumer, H. Xyloglucan in Cellulose Modification. *Cellulose* **2007**, *14*, 625–641. DOI: 10.1007/s10570-007-9109-0.
68. Faik, A. Xylan Biosynthesis: News from the Grass. *Plant Physiol.* **2010**, *153*, 396–402. DOI: 10.1104/pp.110.154237.
69. Rennie, E. A.; Scheller, H. V. Xylan Biosynthesis. *Curr. Opin. Biotechnol.* **2014**, *26*, 100–107. DOI: 10.1016/j.copbio.2013.11.013.
70. Moreira, L. R. S.; Filho, E. X. F. An Overview of Mannan Structure and Mannan-Degrading Enzyme Systems. *Appl. Microbiol. Biotechnol.* **2008**, *79*, 165–178. DOI: 10.1007/s00253-008-1423-4.
71. Takigami, S. *Konjac Mannan*; Woodhead Publishing Limited: Sawston, Cambridge, **2009**. DOI: 10.1533/9781845695873.889.
72. Schröder, R.; Atkinson, R. G.; Redgwell, R. J. Re-In terpreting the Role of Endo-Beta-Mannanases as Mannan Endotransglycosylase/Hydrolases in the Plant Cell Wall. *Ann. Bot.* **2009**, *104*, 197–204. DOI: 10.1093/aob/mcp120.
73. Berglund, J. Wood Hemicelluloses-Fundamental Insights on Biological and Technical Properties. Doctoral dissertation, KTH Royal Institute of Technology: Stockholm, Sweden, 2018.
74. Katsuraya, K.; Okuyama, K.; Hatanaka, K.; Oshima, R.; Sato, T.; Matsuzaki, K. Constitution of Konjac Glucomannan: Chemical Analysis and 13C NMR Spectroscopy. *Carbohydr. Polym.* **2003**, *53*, 183–189. DOI: 10.1016/S0144-8617(03)00039-0.

75. Zhang, Y.; Li, J.; Lindström, M. E.; Stepan, A.; Gatenholm, P. Spruce Glucomannan: Preparation, Structural Characteristics and Basic Film Forming Ability. *Nord. Pulp Pap. Res. J.* **2013**, *28*, 323–330. DOI: 10.3183/npprj-2013-28-03-p323-330.
76. Ropitaux, M.; Bernard, S.; Follet-Gueye, M. L.; Vicré, M.; Boulogne, I.; Driouich, A. Xyloglucan and Cellulose Form Molecular Cross-Bridges Connecting Root Border Cells in Pea (Pisum Sativum). *Plant Physiol. Biochem.* **2019**, *139*, 191–196. DOI: 10.1016/j.plaphy.2019.03.023.
77. Gröndahl, M.; Eriksson, L.; Gatenholm, P. Material Properties of Plasticized Hardwood Xylans for Potential Application as Oxygen Barrier Films. *Biomacromolecules* **2004**, *5*, 1528–1535. DOI: 10.1021/bm049925n.
78. Grabber, J. H. How Do Lignin Composition, Structure, and Cross-Linking Affect Degradability? A Review of Cell Wall Model Studies. *Crop Sci.* **2005**, *45*, 820–831. DOI: 10.2135/cropsci2004.0191.
79. Zhang, S. Y.; Wang, C. G.; Fei, B. H.; Yu, Y.; Cheng, H. T.; Tian, G. L. Mechanical Function of Lignin and Hemicelluloses in Wood Cell Wall Revealed with Microtension of Single Wood Fiber. *BioResources* **2013**, *8*, 2376–2385. DOI: 10.15376/biores.8.2.2376-2385.
80. Kochumalayil, J.; Sehaqui, H.; Zhou, Q.; Berglund, L. A. Tamarind Seed Xyloglucan - A Thermostable High-Performance Biopolymer from Non-Food Feedstock. *J. Mater. Chem.* **2010**, *20*, 4321–4327. DOI: 10.1039/c0jm00367k.
81. Kochumalayil, J. J.; Zhou, Q.; Kasai, W.; Berglund, L. A. Regioselective Modification of a Xyloglucan Hemicellulose for High-Performance Biopolymer Barrier Films. *Carbohydr. Polym.* **2013**, *93*, 466–472. DOI: 10.1016/j.carbpol.2012.12.041.
82. Kochumalayil, J. J.; Bergenstråhle-Wohlert, M.; Utsel, S.; Wågberg, L.; Zhou, Q.; Berglund, L. A. Bioinspired and Highly Oriented Clay Nanocomposites with a Xyloglucan Biopolymer Matrix: Extending the Range of Mechanical and Barrier Properties. *Biomacromolecules* **2013**, *14*, 84–91. DOI: 10.1021/bm301382d.
83. Kochumalayil, J. J.; Berglund, L. Xyloglucan film. US patent 20160251488A1, filed October 23, 2014.
84. Rodrigues, D. C.; Cunha, A. P.; Silva, L. M. A.; Rodrigues, T. H. S.; Gallão, M. I.; Azeredo, H. M. C. Emulsion Films from Tamarind Kernel Xyloglucan and Sesame Seed Oil by Different Emulsification Techniques. *Food Hydrocoll.* **2018**, *77*, 270–276. DOI: 10.1016/j.foodhyd.2017.10.003.
85. Gabrielii, I.; Gatenholm, P. Preparation and Properties of Hydrogels Based on Hemicellulose. *J. Appl. Polym. Sci* **1998**, *69*, 1661–1667. DOI: 10.1002/(sici)1097-4628(19980822)69:8 < 1661::aid-app19 > 3.3.co;2-k.
86. Fredon, E.; Granet, R.; Zerrouki, R.; Krausz, P.; Saulnier, L.; Thibault, J. F.; Rosier, J.; Petit, C. Hydrophobic Films from Maize Bran Hemicelluloses. *Carbohydr. Polym* **2002**, *49*, 1–12. DOI: 10.1016/S0144-8617(01)00312-5.
87. Goksu, E. I.; Karamanlioglu, M.; Bakir, U.; Yilmaz, L.; Yilmazer, U. Production and Characterization of Films from Cotton Stalk Xylan. *J. Agric. Food Chem.* **2007**, *55*, 10685–10691. DOI: 10.1021/jf071893i.
88. Rao, J.; Gao, H.; Guan, Y.; Li, W. q.; Liu, Q. Fabrication of Hemicelluloses Films with Enhanced Mechanical Properties by Graphene Oxide for Humidity Sensing. *Carbohydr. Polym.* **2019**, *208*, 513–520. DOI: 10.1016/j.carbpol.2018.12.099.
89. Morais De Carvalho, D.; Marchand, C.; Berglund, J.; Lindström, M. E.; Vilaplana, F.; Sevastyanova, O. Impact of Birch Xylan Composition and Structure on Film Formation and Properties. *Holzforschung* **2020**, *74*, 184–196. DOI: 10.1515/hf-2018-0224.
90. Plengnok, U.; Jarukumjorn, K. Preparation and Characterization of Nanocellulose from Sugarcane Bagasse. *Biointerface Res. Appl. Chem.* **2020**, *10*, 5675–5678. DOI: 10.33263/BRIAC103.675678.
91. Bahcegul, E.; Özkan, N.; Bakir, U. Production of Hemicellulose-Based Biodegradable Films from Agricultural Wastes. *N. Biotechnol.* **2009**, *25*, S278–S278. DOI: 10.1016/j.nbt.2009.06.626.

92. Péroval, C.; Debeaufort, F.; Despré, D.; Voilley, A. Edible Arabinoxylan-Based Films. 1. Effects of Lipid Type on Water Vapor Permeability, Film Structure, and Other Physical Characteristics. *J. Agric. Food Chem.* **2002**, *50*, 3977–3983. DOI: 10.1021/jf0116449.
93. Zhang, P.; Whistler, R. L. Mechanical Properties and Water Vapor Permeability of Thin Film from Corn Hull Arabinoxylan. *J. Appl. Polym. Sci* **2004**, *93*, 2896–2902. DOI: 10.1002/app.20910.
94. Höije, A.; Gröndahl, M.; Tømmeraas, K.; Gatenholm, P. Isolation and Characterization of Physicochemical and Material Properties of Arabinoxylans from Barley Husks. *Carbohydr. Polym.* **2005**, *61*, 266–275. DOI: 10.1016/j.carbpol.2005.02.009.
95. Höije, A.; Sternemalm, E.; Heikkinen, S.; Tenkanen, M.; Gatenholm, P. Material Properties of Films from Enzymatically Tailored Arabinoxylans. *Biomacromolecules* **2008**, *9*, 2042–2047. DOI: 10.1021/bm800290m.
96. Mikkonen, K. S.; Heikkinen, S.; Soovre, A.; Peura, M.; Serimaa, R.; Talja, R.; Helen, H.; Hyvonen, L.; Tenkanen, M. Films from Oat Spelt Arabinoxylan Plasticized with Glycerol and Sorbitol. *Cellulose* **2012**, *19*, 467–480. DOI: 10.1002/app.
97. Sárossy, Z. Production and Utilization of Hemicelluloses from Renewable Resources for Sustainable Advanced Products. Doctoral Dissertation, Technical University of Denmark: Kongens Lyngby, Denmark, **2011**.
98. Sárossy, Z.; Blomfeldt, T. O. J.; Hedenqvist, M. S.; Koch, C. B.; Ray, S. S.; Plackett, D. Composite Films of Arabinoxylan and Fibrous Sepiolite: Morphological, Mechanical, and Barrier Properties. *ACS Appl. Mater. Interfaces* **2012**, *4*, 3378–3386. DOI: 10.1021/am3002956.
99. Mikkonen, K. S.; Pitkänen, L.; Liljeström, V.; Mabasa Bergström, E.; Serimaa, R.; Salmén, L.; Tenkanen, M. Arabinoxylan Structure Affects the Reinforcement of Films by Microfibrillated Cellulose. *Cellulose* **2012**, *19*, 467–480. DOI: 10.1007/s10570-012-9655-y.
100. Stevanic, J. S.; Bergström, E. M.; Gatenholm, P.; Berglund, L.; Salmén, L. Arabinoxylan/Nanofibrillated Cellulose Composite Films. *J. Mater. Sci.* **2012**, *47*, 6724–6732. DOI: 10.1007/s10853-012-6615-8.
101. Ying, R.; Rondeau-Mouro, C.; Barron, C.; Mabille, F.; Perronnet, A.; Saulnier, L. Hydration and Mechanical Properties of Arabinoxylans and β-d-Glucans Films. *Carbohydr. Polym.* **2013**, *96*, 31–38. DOI: 10.1016/j.carbpol.2013.03.090.
102. Sárossy, Z.; Tenkanen, M.; Pitkänen, L.; Bjerre, A. B.; Plackett, D. Extraction and Chemical Characterization of Rye Arabinoxylan and the Effect of β-Glucan on the Mechanical and Barrier Properties of Cast Arabinoxylan Films. *Food Hydrocoll.* **2013**, *30*, 206–216. DOI: 10.1016/j.foodhyd.2012.05.022.
103. Stepan, A. M.; Ansari, F.; Berglund, L.; Gatenholm, P. Nanofibrillated Cellulose Reinforced Acetylated Arabinoxylan Films. *Compos. Sci. Technol.* **2014**, *98*, 72–78. DOI: 10.1016/j.compscitech.2014.04.010.
104. Egüés, I.; Stepan, A. M.; Eceiza, A.; Toriz, G.; Gatenholm, P.; Labidi, J. Corncob Arabinoxylan for New Materials. *Carbohydr. Polym.* **2014**, *102*, 12–20. DOI: 10.1016/j.carbpol.2013.11.011.
105. Ying, R.; Saulnier, L.; Bouchet, B.; Barron, C.; Ji, S.; Rondeau-Mouro, C. Multiscale Characterization of Arabinoxylan and β-Glucan Composite Films. *Carbohydr. Polym.* **2015**, *122*, 248–254. DOI: 10.1016/j.carbpol.2015.01.014.
106. Heikkinen, S. Biodegradable films from cereal arabinoxylans. Doctoral dissertation, University of Helsinki: Helsinki, Finland, **2016**.
107. Stoklosa, R. J.; Latona, R. J.; Bonnaillie, L. M.; Yadav, M. P. Evaluation of Arabinoxylan Isolated from Sorghum Bran, Biomass, and Bagasse for Film Formation. *Carbohydr. Polym.* **2019**, *213*, 382–392. DOI: 10.1016/j.carbpol.2019.03.018.
108. Xiao, C.; Gao, S.; Wang, H.; Zhang, L. Blend Films from Chitosan and Konjac Glucomannan Solutions. *J. Appl. Polym. Sci.* **2000**, *76*, 509–515. DOI: 10.1002/(SICI)1097-4628(20000425)76:4 < 509::AID-APP8 > 3.0.CO;2-2.

109. Xiao, C.; Gao, S.; Zhang, L. Blend Films from Konjac Glucomannan and Sodium Alginate Solutions and Their Preservative Effect. *J. Appl. Polym. Sci* **2000**, *77*, 617–626. DOI: 10.1002/(SICI)1097-4628(20000718)77:3 < 617::AID-APP17 > 3.0.CO;2-1.
110. Cheng, L. H.; Abd Karim, A.; Seow, C. C. Effects of Acid Modification on Physical Properties of Konjac Glucomannan (KGM) Films. *Food Chem* **2007**, *103*, 994–1002. DOI: 10.1016/j.foodchem.2006.09.052.
111. Mikkonen, K. S.; Mathew, A. P.; Pirkkalainen, K.; Serimaa, R.; Xu, C.; Willför, S.; Oksman, K.; Tenkanen, M. Glucomannan Composite Films with Cellulose Nanowhiskers. *Cellulose* **2010**, *17*, 69–81. DOI: 10.1007/s10570-009-9380-3.
112. Wu, C.; Peng, S.; Wen, C.; Wang, X.; Fan, L.; Deng, R.; Pang, J. Structural Characterization and Properties of Konjac Glucomannan/Curdlan Blend Films. *Carbohydr. Polym.* **2012**, *89*, 497–503. DOI: 10.1016/j.carbpol.2012.03.034.
113. Wei, X.; Pang, J.; Zhang, C.; Yu, C.; Chen, H.; Xie, B. Structure and Properties of Moisture-Resistant Konjac Glucomannan Films Coated with Shellac/Stearic Acid Coating. *Carbohydr. Polym.* **2015**, *118*, 119–125. DOI: 10.1016/j.carbpol.2014.11.009.
114. Wu, C.; Li, Y.; Du, Y.; Wang, L.; Tong, C.; Hu, Y.; Pang, J.; Yan, Z. Preparation and Characterization of Konjac Glucomannan-Based Bionanocomposite Film for Active Food Packaging. *Food Hydrocoll* **2019**, *89*, 682–690. DOI: 10.1016/j.foodhyd.2018.11.001.
115. Wang, L.; Lin, L.; Chen, X.; Tong, C.; Pang, J. Synthesis and Characteristics of Konjac Glucomannan Films Incorporated with Functionalized Microcrystalline Cellulose. *Colloids Surfaces A Physicochem. Eng. Asp* **2019**, *563*, 237–245. DOI: 10.1016/j.colsurfa.2018.12.015.
116. Liu, Z.; Shen, R.; Yang, X.; Lin, D. Characterization of a Novel Konjac Glucomannan Film Incorporated with Pickering Emulsions: Effect of the Emulsion Particle Sizes. *Int. J. Biol. Macromol.* **2021**, *179*, 377–387. DOI: 10.1016/j.ijbiomac.2021.02.188.
117. De Souza, C. F.; Lucyszyn, N.; Woehl, M. A.; Riegel-Vidotti, I. C.; Borsali, R.; Sierakowski, M. R. Property Evaluations of Dry-Cast Reconstituted Bacterial Cellulose/Tamarind Xyloglucan Biocomposites. *Carbohydr. Polym.* **2013**, *93*, 144–153. DOI: 10.1016/j.carbpol.2012.04.062.
118. Lucyszyn, N.; Ono, L.; Lubambo, A. F.; Woehl, M. A.; Sens, C. V.; de Souza, C. F.; Sierakowski, M. R. Physicochemical and in Vitro Biocompatibility of Films Combining Reconstituted Bacterial Cellulose with Arabinogalactan and Xyloglucan. *Carbohydr. Polym.* **2016**, *151*, 889–898. DOI: 10.1016/j.carbpol.2016.06.027.
119. Whitney, S. E. C.; Brigham, J. E.; Darke, A. H.; Reid, J. S. G.; Gidley, M. J. In Vitro Assembly of Cellulose/Xyloglucan Networks: Ultrastructural and Molecular Aspects. *Plant J.* **1995**, *8*, 491–504. DOI: 10.1046/j.1365-313X.1995.8040491.x.
120. Zheng, Y.; Wang, X.; Chen, Y.; Wagner, E.; Cosgrove, D. J. Xyloglucan in the Primary Cell Wall: Assessment by FESEM, Selective Enzyme Digestions and Nanogold Affinity Tags. *Plant J.* **2018**, *93*, 211–226. DOI: 10.1111/tpj.13778.
121. Herburger, K.; Franková, L.; Pičmanová, M.; Loh, J. W.; Valenzuela-Ortega, M.; Meulewaeter, F.; Hudson, A. D.; French, C. E.; Fry, S. C. Hetero-Trans-β-Glucanase Produces Cellulose-Xyloglucan Covalent Bonds in the Cell Walls of Structural Plant Tissues and Is Stimulated by Expansin. *Mol. Plant* **2020**, *13*, 1047–1062. DOI: 10.1016/j.molp.2020.04.011.
122. Chanliaud, E.; Burrows, K. M.; Jeronimidis, G.; Gidley, M. J. Mechanical Properties of Primary Plant Cell Wall Analogues. *Planta* **2002**, *215*, 989–996. DOI: 10.1007/s00425-002-0783-8.
123. Whitney, S. E. C.; Wilson, E.; Webster, J.; Bacic, A.; Grant Reid, J. S.; Gidley, M. J. Effects of Structural Variation in Xyloglucan Polymers on Interactions with Bacterial Cellulose. *Am. J. Bot.* **2006**, *93*, 1402–1414. DOI: 10.3732/ajb.93.10.1402.
124. Gu, J.; Catchmark, J. M. Roles of Xyloglucan and Pectin on the Mechanical Properties of Bacterial Cellulose Composite Films. *Cellulose* **2014**, *21*, 275–289. DOI: 10.1007/s10570-013-0115-0.

125. Lopez-Sanchez, P.; Cersosimo, J.; Wang, D.; Flanagan, B.; Stokes, J. R.; Gidley, M. J. Poroelastic Mechanical Effects of Hemicelluloses on Cellulosic Hydrogels under Compression. *PLoS One* **2015**, *10*, e0122132–19. DOI: 10.1371/journal.pone.0122132.
126. Lopez, M.; Bizot, H.; Chambat, G.; Marais, M. F.; Zykwinska, A.; Ralet, M. C.; Driguez, H.; Buléon, A. Enthalpic Studies of Xyloglucan-Cellulose Interactions. *Biomacromolecules* **2010**, *11*, 1417–1428. DOI: 10.1021/bm1002762.
127. Hirai, A.; Tsuji, M.; Yamamoto, H.; Horii, F. Situ Crystallization of Bacterial Cellulose III. Influences of Different Polymeric Additives on the Formation of Microfibrils as Revealed by Transmission Electron Microscopy. *Cellulose* **1998**, *5*, 201–213. DOI: 10.1023/A:1009233323237.
128. Penttilä, P. A.; Imai, T.; Hemming, J.; Willför, S.; Sugiyama, J. Enzymatic Hydrolysis of Biomimetic Bacterial Cellulose-Hemicellulose Composites. *Carbohydr. Polym.* **2018**, *190*, 95–102. DOI: 10.1016/j.carbpol.2018.02.051.
129. Martínez-Sanz, M.; Lopez-Sanchez, P.; Gidley, M. J.; Gilbert, E. P. Evidence for Differential Interaction Mechanism of Plant Cell Wall Matrix Polysaccharides in Hierarchically-Structured Bacterial Cellulose. *Cellulose* **2015**, *22*, 1541–1563. DOI: 10.1007/s10570-015-0614-2.
130. Hansen, N. M. L.; Blomfeldt, T. O. J.; Hedenqvist, M. S.; Plackett, D. V. Properties of Plasticized Composite Films Prepared from Nanofibrillated Cellulose and Birch Wood Xylan. *Cellulose* **2012**, *19*, 2015–2031. DOI: 10.1007/s10570-012-9764-7.
131. Yu, J.; Zhu, Y.; Ma, H.; Liu, L.; Hu, Y.; Xu, J.; Wang, Z.; Fan, Y. Contribution of Hemicellulose to Cellulose Nanofiber-Based Nanocomposite Films with Enhanced Strength, Flexibility and UV-Blocking Properties. *Cellulose* **2019**, *26*, 6023–6034. DOI: 10.1007/s10570-019-02518-6.
132. Linder, A.; Bergman, R.; Bodin, A.; Gatenholm, P. Mechanism of Assembly of Xylan onto Cellulose Surfaces. *Langmuir* **2003**, *19*, 5072–5077. DOI: 10.1021/la0341355.
133. Long, L.; Shen, F.; Wang, F.; Tian, D.; Hu, J. Synthesis, Characterization and Enzymatic Surface Roughing of Cellulose/Xylan Composite Films. *Carbohydr. Polym.* **2019**, *213*, 121–127. DOI: 10.1016/j.carbpol.2019.02.086.
134. Gordobil, O.; Egüés, I.; Urruzola, I.; Labidi, J. Xylan-Cellulose Films: Improvement of Hydrophobicity, Thermal and Mechanical Properties. *Carbohydr. Polym.* **2014**, *112*, 56–62. DOI: 10.1016/j.carbpol.2014.05.060.
135. Martínez-Sanz, M.; Gidley, M. J.; Gilbert, E. P. Hierarchical Architecture of Bacterial Cellulose and Composite Plant Cell Wall Polysaccharide Hydrogels Using Small Angle Neutron Scattering. *Soft Matter* **2016**, *12*, 1534–1549. DOI: 10.1039/c5sm02085a.
136. Winter, H.; Barakat, A.; Cathala, B.; Saake, B. Preparation of Arabinoxylan and Its Sorption on Bacterial Cellulose during Cultivation. *Macromol. Symp* **2005**, *232*, 74–84. DOI: 10.1002/masy.200551409.
137. Egüés, I.; Eceiza, A.; Labidi, J. Effect of Different Hemicelluloses Characteristics on Film Forming Properties. *Ind. Crops Prod* **2013**, *47*, 331–338. DOI: 10.1016/j.indcrop.2013.03.031.
138. Sundberg, J.; Toriz, G.; Gatenholm, P. Effect of Xylan Content on Mechanical Properties in Regenerated Cellulose/Xylan Blend Films from Ionic Liquid. *Cellulose* **2015**, *22*, 1943–1953. DOI: 10.1007/s10570-015-0606-2.
139. Uhlin, K. I.; Atalla, R. H.; Thompson, N. S. Influence of Hemicelluloses on the Aggregation Patterns of Bacterial Cellulose. *Cellulose* **1995**, *2*, 129–144. DOI: 10.1007/BF00816385.
140. Lucenius, J.; Valle-Delgado, J. J.; Parikka, K.; Österberg, M. Understanding Hemicellulose-Cellulose Interactions in Cellulose Nanofibril-Based Composites. *J. Colloid Interface Sci.* **2019**, *555*, 104–114. DOI: 10.1016/j.jcis.2019.07.053.
141. Fengel, D. Ideas on the Ultrastructural Organization of the Cell Wall Components. *J. Polym. Sci., C Polym. Symp.* **1971**, *36*, 383–392. DOI: 10.1002/polc.5070360127.

142. Whitney, S. E. C.; Brigham, J. E.; Darke, A. H.; Reid, J. S. G.; Gidley, M. J. Structural Aspects of the Interaction of Mannanbased Polysaccharides with Bacterial Cellulose. *Carbohydr. Res* **1998**, *307*, 299–309. DOI: 10.1016/S0008-6215(98)00004-4.

143. Tokoh, C.; Takabe, K.; Fujita, M.; Saiki, H. Cellulose Synthesized by Acetobacter Xylinum in the Presence of Acetyl Glucomannan. *Cellulose* **1998**, *5*, 249–261. DOI: 10.1023/A:1009211927183.

144. Eronen, P.; Österberg, M.; Heikkinen, S.; Tenkanen, M.; Laine, J. Interactions of Structurally Different Hemicelluloses with Nanofibrillar Cellulose. *Carbohydr. Polym.* **2011**, *86*, 1281–1290. DOI: 10.1016/j.carbpol.2011.06.031.

145. Caffall, K. H.; Mohnen, D. The Structure, Function, and Biosynthesis of Plant Cell Wall Pectic Polysaccharides. *Carbohydr. Res.* **2009**, *344*, 1879–1900. DOI: 10.1016/j.carres.2009.05.021.

146. Lin, D.; Lopez-Sanchez, P.; Selway, N.; Gidley, M. J. Viscoelastic Properties of Pectin/Cellulose Composites Studied by QCM-D and Oscillatory Shear Rheology. *Food Hydrocoll* **2018**, *79*, 13–19. DOI: 10.1016/j.foodhyd.2017.12.019.

147. Uhlin, K. I. The Influence of Hemicelluloses on the Structure of Bacterial Cellulose. Doctoral dissertation, Institute of Paper Science and Technology: Atlanta, USA, **1990**.

148. Tokoh, C.; Takabe, K.; Sugiyama, J.; Fujita, M. CP/MAS 13C NMR and Electron Diffraction Study of Bacterial Cellulose Structure Affected by. *Cell Wall Polysaccharides. Cellulose* **2002**, *9*, 351–360. DOI: 10.1023/A:1021150520953..

149. Broxterman, S.E. The architecture of the primary plant cell wall: the role of pectin reconsidered. Doctoral dissertation, Wageningen University: Wageningen, The Netherlands, **2018**.

150. Haas, K. T.; Wightman, R.; Meyerowitz, E. M.; Peaucelle, A. Pectin Homogalacturonan Nanofilament Expansion Drives Morphogenesis in Plant Epidermal Cells. *Science* **2020**, *367*, 1003–1007. DOI: 10.1126/science.aaz5103.

151. Popper, Z. A.; Fry, S. C. Xyloglucan-Pectin Linkages Are Formed Intra-Protoplasmically, Contribute to Wall-Assembly, and Remain Stable in the Cell Wall. *Planta* **2008**, *227*, 781–794. DOI: 10.1007/s00425-007-0656-2.

152. Dyson, R. J.; Band, L. R.; Jensen, O. E. A Model of Crosslink Kinetics in the Expanding Plant Cell Wall: Yield Stress and Enzyme Action. *J. Theor. Biol.* **2012**, *307*, 125–136. DOI: 10.1016/j.jtbi.2012.04.035.

153. Wang, T.; Hong, M. Solid-State NMR Investigations of Cellulose Structure and Interactions with Matrix Polysaccharides in Plant Primary Cell Walls. *J. Exp. Bot.* **2016**, *67*, 503–514. DOI: 10.1093/jxb/erv416.

154. Fanta, S. W.; Vanderlinden, W.; Abera, M. K.; Verboven, P.; Karki, R.; Ho, Q. T.; De Feyter, S.; Carmeliet, J.; Nicolaï, B. M. Water Transport Properties of Artificial Cell Walls. *J. Food Eng.* **2012**, *108*, 393–402. DOI: 10.1016/j.jfoodeng.2011.09.010.

155. Cybulska, J.; Konstankiewicz, K.; Zdunek, A.; Skrzypiec, K. Nanostructure of Natural and Model Cell Wall Materials. Int Agrophys 2010, 24(2), 107–114.

156. Gu, J.; Catchmark, J. M. The Impact of Cellulose Structure on Binding Interactions with Hemicellulose and Pectin. *Cellulose* **2013**, *20*, 1613–1627. DOI: 10.1007/s10570-013-9965-8.

157. Szymańska-Chargot, M.; Cybulska, J.; Zdunek, A. Sensing the Structural Differences in Cellulose from Apple and Bacterial Cell Wall Materials by Raman and FT-IR Spectroscopy. *Sensors (Basel)* **2011**, *11*, 5543–5560. DOI: 10.3390/s110605543.

6.2.Manuscript P2.

6.2.1. Content of the manuscript P2.

BIOLOGICAL
REVIEWS

Cambridge
Philosophical Society

Check for updates

Biol. Rev. (2023), **98**, pp. 887–899.
doi: 10.1111/brv.12935

In silico studies of plant primary cell walls – structure and mechanics

Piotr Mariusz Pieczywek*, Vadym Chibrikov and Artur Zdunek

Institute of Agrophysics, Polish Academy of Sciences, ul. Doświadczalna 4, Lublin, 20-290, Poland

ABSTRACT

Primary plant cell wall (PCW) is a highly organized network, its performance is dependent on cellulose, hemicellulose and pectic polysaccharides, their properties, interactions and assemblies. Their mutual relationships and functions in the cell wall can be better understood by means of conceptual models of their higher-order structures. Knowledge unified in the form of a conceptual model allows predictions to be made about the properties and behaviour of the system under study. Ongoing research in this field has resulted in a number of conceptual models of the cell wall. However, due to the currently limited research methods, the community of cell wall researchers have not reached a consensus favouring one model over another. Herein we present yet another research technique – numerical modelling – which is capable of resolving this issue. Even at the current stage of development of numerical techniques, due to their complexity, the *in silico* reconstruction of PCW remains a challenge for computational simulations. However, some difficulties have been overcome, thereby making it possible to produce advanced approximations of PCW structure and mechanics. This review summarizes the results concerning the simulation of polysaccharide interactions in PCW with regard to network fine structure, supramolecular properties and polysaccharide binding affinity. The *in silico* mechanical models presented herein incorporate certain physical and biomechanical aspects of cell wall architecture for the purposes of undertaking critical testing to bring about advances in our understanding of the mechanisms controlling cells and limiting cell wall expansion.

Key words: cellulose, hemicellulose, cell wall model, modelling, mechanics.

CONTENTS

I. INTRODUCTION

The primary plant cell wall (PCW) is a highly ordered and specialized network that developed to protect the cell and manage the mechanical responses, strengths and flexibility of both the individual cell and the plant as a whole (O'Neill & York, 2018). PCW is formed mainly of polysaccharides (up to 90% dry mass), glycoproteins (threonine and hydroxyproline-rich glycoproteins, up to 10% dry mass), phenolic compounds, minerals and enzymes (endo- and

---

* Author for correspondence (E-mail: p.pieczywek@ipan.lublin.pl)

exoglycanases, transglycosylases, peroxidases) (Carpita & Gibeaut, 1993). In the wet state, water makes up to 60–65% by volume of the PCW (Jackman & Stanley, 1995; Pettolino *et al.*, 2012). The dry matter generally contains 15–40% by mass cellulose, 30–50% pectins and 20–30% hemicelluloses (Cosgrove & Jarvis, 2012). The most abundant hemicelluloses are xyloglucan (XG), xylan and glucomannan, while galactoglucomannan (GGM) and arabinoxylan (AX) are much less common and only occur in particular types of PCW and specific tissues. The structure of pectic polysaccharides is based on three main polymers, homogalacturonan (HG), rhamnogalacturonan I (RGI) and rhamnogalacturonan II (RGII). The main unit comprising approximately 70% of all pectin is D-galacturonic acid (GalA), while the remaining 30% consists of a rich family of neutral sugars (O'Neill & York, 2018). With regard to hemicellulose in the PCW, there are two main types of primary walls: Type I (containing XG and/or GGM and pectin), and Type II (rich in AX and pectin) (Carpita & Gibeaut, 1993; Carpita, 1996). Mannan-rich walls with a low pectin content are classified as Type III walls (Silva *et al.*, 2011).

Cellulose and hemicellulose are considered to be key compartments forming the mechanical scaffold of the PCW. To date, a number of idealized models of cell wall structure have been proposed to enhance our understanding of the mechanics of this system (Probine & Barber, 1966; Keegstra *et al.*, 1973; Talbott & Ray, 1992; Ha, Apperley & Jarvis, 1997; Park & Cosgrove, 2012*a*,*b*). Various concepts of cell wall structure raise specific questions about the role of hemicellulose and pectin in determining its structure. In some models, hemicellulose chains crosslink cellulose fibres, hypothetically separating them from each other. However, it is unknown if hemicellulose is stiff enough mechanically to separate cellulose or whether it acts as a space filler. Another open question concerns the structure, nature and strength of cellulose–hemicellulose bonds and whether their collective contribution is sufficient to maintain the integrity of the turgor-exposed cell wall. Although the role of interfibre links in PCWs is commonly recognized, direct measurements of the adhesive forces between nanoscale cellulose fibres have only been reported recently (Dolan *et al.*, 2019). Even for well-established conceptual models of the interactions of PCW basic components such as hemicellulose and cellulose, recent discoveries have led to new conceptions of PCW polysaccharide assemblies (Park & Cosgrove, 2012*a*).

Studies concerning PCWs in their intact state encounter a number of difficulties which make it almost impossible to provide clear estimations of the individual contributions of specific PCW compounds to the various mechanical properties *in planta*. An alternative approach to solving this problem is to provide *in silico* representations of biological systems by means of numerical methods. Numerical modelling uses a wide range of methods, from classical mechanics to quantum-field theories to resolve the current state of the simulated system and its evolution over time under the influence of changing environmental conditions (Zhao *et al.*, 2014; Berglund *et al.*, 2016, 2019). In this context, revision of current PCW conceptual models may be achieved *via* a new approach based on multiscale robust computational modelling tools.

The aim of this review is to provide a brief overview of the most significant achievements in the field of the numerical modelling of PCW mechanics. In this review we assign importance to the cellulose–hemicellulose complex as the main component of the primary PCW mechanical system. We begin with a summary of the current knowledge concerning basic PCW polysaccharides and their structure and properties. Next we briefly discuss both historical and current conceptual views on their spatial assemblies in PCW. We present various PCW conceptual models that have been developed based on experimental data.

The final section presents both the historical and the latest advances in numerical modelling of wall-like structures. It should be emphasized that only a handful of PCW numerical models have been developed to date. Therefore we expand our overview to include models of random fibre networks. This decision was motivated by the fact that these systems share many similarities in terms of their structure–mechanics relationships. Moreover, the random fibre networks developed much earlier laid the conceptual foundations for the PCW models described below.

II. PCW LOAD-BEARING POLYSACCHARIDES

Cellulose is the main building block of PCWs. It is a paracrystalline array of two to three dozen polymer chains, made up of 7000–15,000 β-D-glucosyl-(1→4) units, which oscillate at an angle of 180°, with a twofold screw conformation (Carpita, 2011; Berglund *et al.*, 2019). Equatorial β-(1→4)-linkages and surface hydroxyl groups lead to the formation of cellulose–cellulose and cellulose–water hydrogen bonds, in turn causing microfibrils to organize themselves into a ribbon-like structure (Martínez-Sanz *et al.*, 2017). Cellulose biosynthesis is carried out in terminal complexes and facilitated by complex cellulose synthase (CESA) proteins (Endler & Persson, 2011; Fernandes *et al.*, 2011; Pauly *et al.*, 2013; Braidwood, Breuer & Sugimoto, 2014). CESA proteins move along fibrils on the plasma membrane and deposit fibrils onto the cell wall (McFarlane, Döring & Persson, 2014).

Separate cellulose units (18 according to modern predictions, 24 and 36 according to earlier references) may become coordinated to create microfibrils, which can form crystalline, para-crystalline, and non-crystalline domains (Martínez-Sanz *et al.*, 2017; Purushotham, Ho & Zimmer, 2020; Yang & Kubicki, 2020). Different diameters of cellulose microfibrils have been reported, ranging from 2–5 nm in the case of plant fibrils, 4–8 nm for bacterial cellulose, greater than 15 nm for algal cellulose, and up to 40 nm in the case of wood fibrils (Newman, Hill & Harris, 2013; Thomas *et al.*, 2013). The native crystallographic form of plant cellulose (cellulose I) exhibits structural heterogeneity with two different para-crystalline forms – a triclinic system with one chain per unit cell (cellulose Iα) and a more stable monoclinic system with two chains per unit cell (cellulose Iβ) – the distribution of which, within the cell wall, remains unclear (Matthews *et al.*, 2006). Other cellulose crystal formations are formed after cellulose mercerization (cellulose II) or treatment with hot liquid ammonia or amines (cellulose III). Cellulose microfibrils have regularly distributed definite hydrophilic and hydrophobic surfaces, making it possible for them to interact with other polysaccharides such as hemicelluloses (Martínez-Sanz *et al.*, 2017; Broxterman & Schols, 2018).

Hemicelluloses are a chemically heterogeneous class of polysaccharides of medium chain length, with glucose, mannose and xylose β-(1→4)-linked backbones (Uhlin, Atalla & Thompson, 1995; Scheller & Ulvskov, 2010). Although hemicelluloses have different component sugars, their backbones are structurally similar (York *et al.*, 1990; Tuomivaara *et al.*, 2015). All hemicelluloses have straight β-(1→4)-linked backbones with an equatorial configuration at C1 and C4. The three main families of hemicellulose polysaccharides (XG, AX and GGMs) can be found in the cell walls of fruit and vegetables, hardwood, annual plants, cereals, and herbs (Spiridon & Popa, 2008; Ren & Sun, 2010; Scheller & Ulvskov, 2010; Yu *et al.*, 2022). Among these, XG is the most abundant primary cell wall hemicellulose, with AX and GGM generally present in significantly smaller proportions according to the species in question. XG represents about 20–25% of the primary wall (Lima, Loh & Buckeridge, 2004). XG consists of β-D-glucosyl-(1→4) units ramified at O-6 by α-D-xylosyl monomers, regularly organized into blocks. It can be further extended by galactose, fucose, arabinose, xylose or uronic acid residues as side-chains. However, the side chains attached to the backbone are short – usually just one sugar long – and protrude from the sides of the backbone. GGM consists of β-D-glucosyl-(1→4) and β-D-mannosyl-(1→4) residues either alternating or as blocks more or less ramified at the O-6 of glucose or mannose by galactose and di-galactose (Melton *et al.*, 2009). GGM is particularly prominent in tomato fruit (about 6% of the cell wall dry mass) (Prakash *et al.*, 2012) and is a minor hemicellulose in other fruits, such as kiwi, apple and banana (Schröder *et al.*, 2001; Cheng *et al.*, 2009; Ray *et al.*, 2014; Colodel, Vriesmann & de Oliveira Petkowicz, 2018). AX is a common hemicellulose present in the flesh and peel of fruit and vegetables (Marcelin, Williams & Brillouet, 1993). It consists of β-D-xylosyl-(1→4) units substituted at O-2 and O-3 by α-L-arabinosyl units, and at O-2 by α-D-glucuronic acid which also occurs as its 4-O methyl ether derivative (Hao & Mohnen, 2014; Chen *et al.*, 2019). Apart from some reports on mannan (Mackie & Preston, 1968), there is no evidence for self-aggregation of hemicelluloses into long, close-packed crystalline fibrils in the manner of cellulose. However, hemicellulose polysaccharide chains can form significant hydrogen-bonded associations with each other in the cell wall, particularly between regions of the chains with few side branches or axial hydroxyl groups (McNiel *et al.*, 1975). Importantly, the structural similarity to cellulose facilitates a close, non-covalent association of hemicellulose with cellulose microfibrils, resulting in the formation of a cellulose–hemicellulose network which is believed to play a major role PCW mechanics (Scheller & Ulvskov, 2010).

III. CONCEPTS OF PCW POLYSACCHARIDE INTERACTIONS

Several models of PCW structure have been established according to cellulose–cellulose and cellulose–hemicellulose physicochemical and mechanical interactions. These models were designed to explain how the cell wall maintains its integrity under turgor pressure, and most importantly, how such rigid structures allow plant cells to grow (Cosgrove, 2000, 2014; Thompson, 2005; Cosgrove & Jarvis, 2012). The first theory proposed visualized PCW as a template of cellulose fibrils, loosely incorporated into the amorphous wall matrix (the 'multinet model') (Probine & Barber, 1966). The model assumed that about 10% of the PCW volume is occupied by cellulose, which has long fibrils that cause many contact and adhesion points with neighbouring fibrils or they may even twist around each other (Roelofsen, 1958). Matrix polysaccharides (hemicellulose and pectin) were considered to be partly immobilized, and partly arranged in fibrils.

In the cell wall structure proposed by Keegstra *et al.* (1973) hemicelluloses coat the microfibrils and interact with other fibrils *via* covalently linked matrix polymers and PCW proteins (Fig. 1A). In this case, XGs are attached to the galactan side chains of pectic polysaccharides (RGs), while pectic polysaccharides are attached to the wall proteins through arabinogalactan chains (Albersheim *et al.*, 2011). The proposed structure was supported in part by the observed degradation of cell walls during the selective enzymatic hydrolysis of matrix polysaccharides. However, the lack of evidence for the presence of other key hypothetical linkages predicted by this model finally led to the rejection of this concept.

Talbott & Ray (1992) proposed a multi-coat cell wall model in which cellulose microfibrils are covered with XG, followed by successive layers of less closely bound pectic polysaccharides (Fig. 1B). In their concept, XG does not form crosslinks between the cellulose molecules, therefore cleavage of XG is not a necessary condition for wall expansion. The PCW structure is held together by interactions between the matrix polymers. Other authors modified this multi-coat model to include structures in which layers of cellulose are crosslinked by XG and separated by lamellae of pectic polysaccharides (Ha *et al.*, 1997).

A simplified view of PCW structure was proposed in the tethered network model (Carpita & Gibeaut, 1993). In this model the cellulose fibrils are separated from each other by XG chains, which crosslink fibrils into a load-bearing network *via* 20–40 nm long tethers (Fig. 1C). According to this

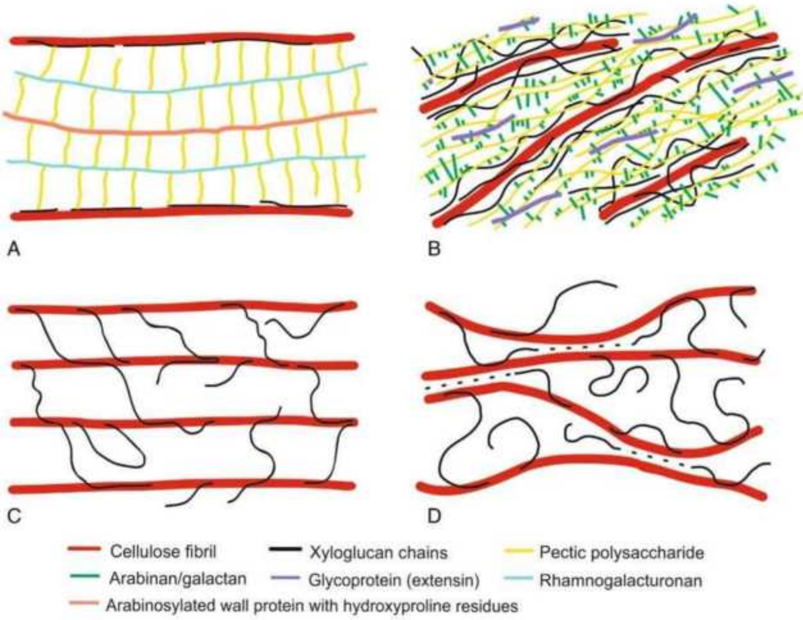

Fig. 1. Models of plant primary cell wall. (A) Model with covalently linked matrix. (B) Multi-coat cell wall model. (C) Tethered network. (D) Biomechanical hotspot cell wall model.

hypothesis, XG is a key component of PCW, providing mechanical strength and integrity. Pectic polysaccharides and structural proteins, although physically entangled with the cellulose–XG network, create separate networks which are not covalently bound. The loosening of the cell wall structure and its growth can be achieved through the hydrolysis of hemicellulose connections. This model was supported by a series of studies confirming the affinity of XG to cellulose and the presence of relatively long XG chains, of sufficient length to pass through neighbouring cellulose fibrils (Hayashi, Marsden & Delmer, 1987; Hayashi, Ogawa & Mitsuishi, 1994; Fry, 1989; Hayashi, 1989; McCann, Wells & Roberts, 1990; Fry *et al.*, 1992; Hayashi & Kaida, 2011).

Despite being widely supported and accepted by many researchers, some experimental results have challenged the concept of the tethered network model. Experiments on primary PCWs using enzymes targeting XG tethers showed no wall extension or mechanical weakening, while enzymes with the ability to cut both XG and cellulose were effective at loosening the wall (Park & Cosgrove, 2012*a*,*b*). At the same time, research with XG-deficient *Arabidopsis* mutants showed that XG is not necessary to maintain PCW mechanical integrity, which would be expected for a critical load-bearing component of the expanding cell wall (Cavalier *et al.*, 2008; Park & Cosgrove, 2012*b*; Uluisik *et al.*, 2016). Based on data that contradicted the assumptions of the tethered model, a new cell wall model was conceived where tethers, although present, do not play a significant role in PCW mechanics. Instead of crosslinking tethers, mechanically important XGs are located in close proximity to two adjacent cellulose fibrils, forming lateral tight load-bearing junctions called biomechanical hotspots (Fig. 1D) (Park & Cosgrove, 2012*a*,*b*; Zhang *et al.*, 2014; Cosgrove, 2018). According to this model, the mechanical load is transmitted between fibrils not through the XG backbone but rather due to lateral interactions generated by the contact surfaces of XG sandwiched between cellulose fibrils. The biomechanical hotspot concept has the implication that wall extensibility is controlled by limited, specific junctions between microfibrils rather than by the bulk viscoelasticity of the matrix. Despite promising results there remain questions to be answered with regard to the formation, density, location and strength of these cellulose–hemicellulose junctions as well as the nature of the role of other PCW polysaccharides.

In order to achieve this goal, *in silico* mechanical models of cell walls need to incorporate physical and biomechanical aspects of cell wall architecture before critical testing and refinement by a combination of numerical approaches in order to improve our understanding of the mechanisms controlling cells and limiting cell wall expansion.

IV. COMPUTATIONAL MODELS OF PCWS

(1) Random fibre networks – precursors of cell wall models

The first studies dedicated to the simulation of wall-like cellulose networks involved two-dimensional (2D) paper structures with a random fibre length and distribution (Rigdahl, Westerlind & Hollmark, 1984; Åström *et al.*, 1994). Although these models were initially simple and designed for industrial use, they provided valuable insights into the structure–mechanics relationships of fibre-based networks. Subsequently, many publications have modelled cellulose networks as 2D and three-dimensional (3D) random fibre networks. In these models, all fibres are straight, with the same diameter and length, and randomly distributed in 2D or 3D. The interspace between the fibres is considered as an empty void that cannot dissipate strain energy. Fibre-to-fibre connections are treated as rigid or flexible bonds modelled as spring elements (Rigdahl *et al.*, 1984; Åström *et al.*, 1994; Heyden, 2000; Bronkhorst, 2003; Hägglund & Isaksson, 2008; Liu *et al.*, 2011; Koh & Oyen, 2012; Kulachenko & Uesaka, 2012; Kulachenko *et al.*, 2012; Mao *et al.*, 2017; Deogekar & Picu, 2018; Goutianos, Mao & Peijs, 2018) (see Fig. 2).

Heyden (2000) summarized the results of simulations of the mechanical properties of cellulose fibre fluff. 2D and 3D finite element method network models were used to determine the relationship between network stiffness and fibre and bond stiffness, network density, fibre curl and length. Networks were generated by placing fibres randomly in space. Single fibres were modelled using a Bernoulli beam, while fibre–fibre interactions were approximated using an artificial spring element connecting fibres. Bonds were designed to exhibit non-linear stick–slip fracture behaviour.

The models showed that the elastic modulus of the network rises rapidly with increases in its density and number of inter-fibre contacts, while Poisson's ratio showed a weaker response, being less affected by network structural changes. Networks consisting of curled fibres were less stiff due to the lower axial stiffness of the curled beam segments. Long fibres resulted in stiffer networks, with stiffer responses along the preferred fibre orientation.

An interesting observation was that the overall network fracture mechanism was more sensitive to fibre failure than to bond disruption. In the case of fibre failure, the load-bearing path was completely interrupted. However, due to the possibility of the fibre being entangled with other fibres or connected by more than two bonds, bond disruption results in a lower decrease in network strength. These conclusions may be applied to PCW growth, where structural expansion requires its partial loosening, but not complete disintegration. According to both the tethered network and biomechanical hotspot models, loosening is achieved by the degradation of the hemicellulose connections, which corresponds to elastic bonds between fibres in the model used by Heyden (2000). Results showed that the partial degradation of the cellulose–hemicellulose network would allow the cell wall to expand without the risk of damaging its integrity. Moreover, simulation results showed that structural loosening progressed much faster when the cellulose fibres were interrupted, which corresponds with the hotspot hypothesis, assuming the simultaneous degradation of cellulose and hemicelluloses (Park & Cosgrove, 2012*b*).

Nevertheless, the model had several limitations that distinguished it from conceptual PCW models. Bonds were modelled as contact points rather than crosslinks, suggesting that this approach should rather be interpreted as a representation of a biomechanical hotspot model. Moreover, potential slippage of inter-fibre bonds was limited. Once broken, they did not form new connections, which is a departure from the previously discussed models of hemicellulose adsorption.

Heyden's (2000) modelling approach was further explored with variations of 2D or 3D models of cellulose networks. Kulachenko & Uesaka (2012) and Kulachenko *et al.* (2012) used a 2D and 3D nano-paper finite element model (FEM) and found generally similar conclusions to those of Heyden (2000). The elastic modulus of the network, strength and strain-to-failure were mainly influenced by fibre length. Bond stiffness had a negligible impact on network stiffness if it varied within a reasonable range. Similar findings had been reported by Rigdahl *et al.* (1984) who noted that bond stiffness did not play a role in stress transfer, unless it was below some critical value indicating rapid deterioration. Mao *et al.* (2017) developed a 2D FEM of a fibrous network to investigate the impact of network structural properties on its elastic modulus. Their 2D modelling approach used fibres in the form of linear elastic Timoshenko beam elements and point-wise fibre–fibre bonds that could not slide or separate under strain; thus this is an example of an idealized biomechanical hotspot PCW model. A simulation showed that the network elastic modulus increases with fibre length (thereby enhancing stress-transfer capability and number of contacts), fibre modulus, bond density and network density (multiple contacts). However, it decreases with increasing fibre diameter (due to the decreasing number of fibres but with an overall constant fibril volume) and with fibre waviness. Goutianos *et al.* (2018) developed a 3D extension of this model to examine the effects of inter-fibre bonds. Bonds were assumed to be damageable non-linear springs, which only carry axial loads (truss elements). The spring damage was irreversible – once broken, the bonds neither carry a load nor re-establish connections. It was found that the Young's modulus of the network increased with the growing number and strength of inter-fibre bonds. On the other hand, both parameters only had a minor effect on the cellulose network strain-to-failure relationship.

(2) PCW models with classical beam theory representations of fibres

Despite intensive research concerning the mechanics of random fibre networks, the value of numerical simulations as a research tool has only been recognized by the PCW

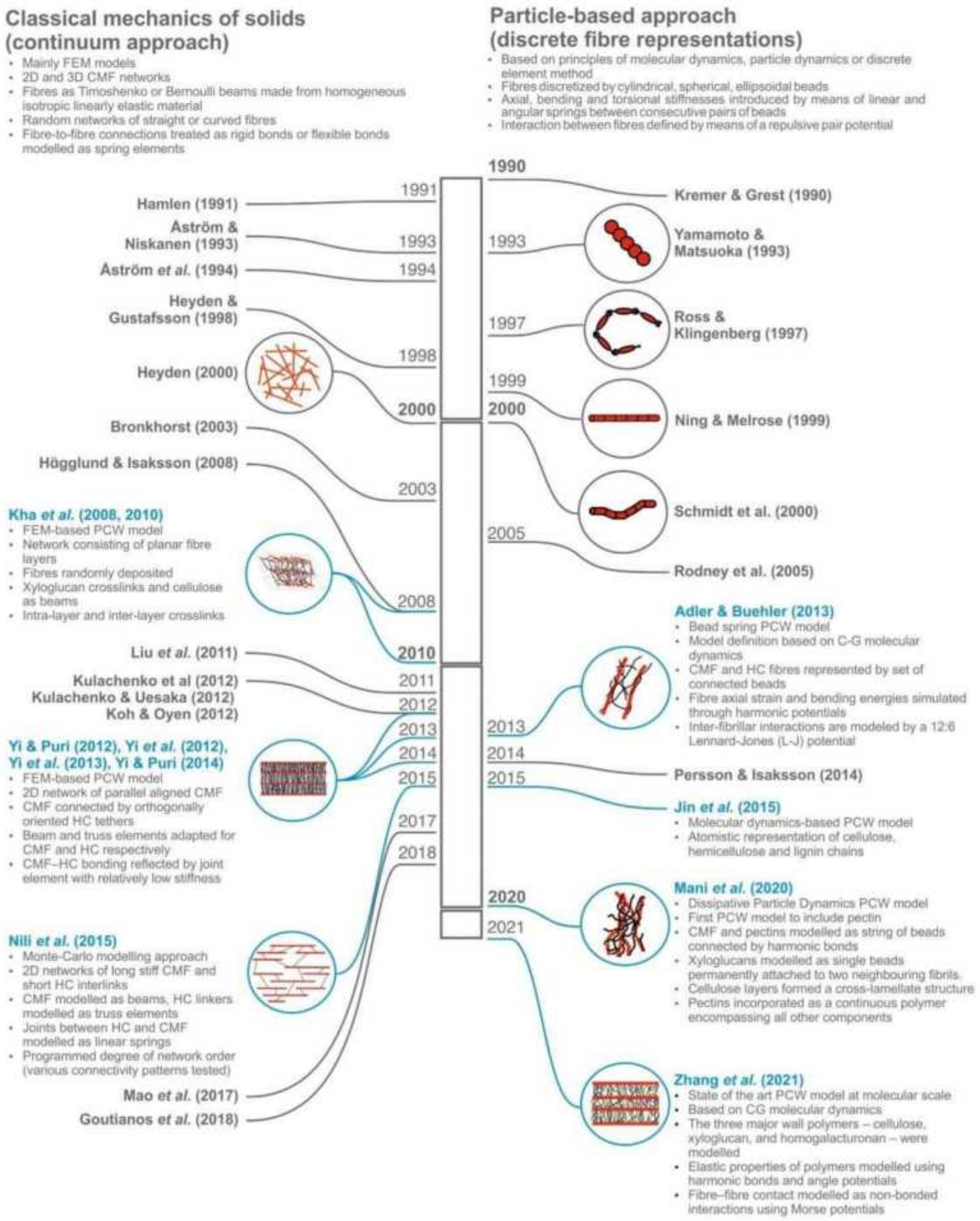

Fig. 2. Timeline showing the development of fibre network and plant cell wall (PCW) models. The models are split into two major categories based on applied modelling methodologies. Both are briefly characterized with bullet point descriptions of model/modelling principles. Grey lines indicate general models of fibrous structures (paper, nano-paper, other cellulose networks). *(Figure legend continues on next page.)*

community relatively recently (see Fig. 2). Conceptual models have had a profound influence on the way numerical models of cell walls were constructed. All models to a greater or lesser degree have attempted to recreate one of the idealized concepts of PCW. Major findings and limitations of PCW models can be found in Table 1.

One of the first structural models designed exclusively to simulate PCW mechanical behaviour was presented by Kha *et al.* (2008, 2010). This novel modelling approach was aimed at the reconstruction of multilayered cellulose–hemicellulose networks, resembling a fine-structure, interlinked tethered PCW model. The FEM-based model fibrils were organized into separate flat and parallel layers of cellulose networks. Randomly deposited cellulose fibres were crosslinked by XG chains, which were also modelled as beams. XG chains, which were inserted into the cellulose network were constrained to crosslinking with only two cellulose fibrils each. As for the previously described random fibre networks, simulations showed that structures with a higher number of, or longer, cellulose fibres were stiffer. Cell wall stiffness was positively correlated with XG stiffness. The structures were stiffer in the direction parallel to cellulose alignment, as compared to the perpendicular direction or a random orientation. Despite its novelty, this approach suffered from several limitations. The models were designed to simulate relatively small cell wall deformations with the thickness of the structure being limited to 100 nm. More importantly, the cellulose–hemicellulose connections were designed to act as permanent crosslinks with no bonding–debonding mechanism, which is crucial for the reproduction of PCW viscoelastic properties.

This approach was extended by Yi & Puri (2012, 2014) and Yi, Zamil & Puri (2012, 2013) who developed a tethered network computational model to explore the PCW hydrogen-bond hypothesis. The 2D representation of the PCW network consisted of cellulose microfibrils in a parallel alignment which were connected by orthogonally oriented hemicellulose tethers. Classical beam theory was adapted to reflect the physical properties of both PCW components. Two-node beam elements were used to describe the capabilities of cellulose microfibrils to resist axial and lateral loading, while truss elements were used to model the single molecular backbone of hemicellulose, which were considered to be too weak to resist lateral forces. In order to consider the effect on cellulose–hemicellulose of hydrogen bonding between cellulose and hemicellulose, both structures were connected indirectly *via* intermediate linearly elastic joint elements, with a spring constant equivalent to the stiffness of a hydrogen bond. The results showed that cellulose–hemicellulose hydrogen bonds experienced the highest value of strain energy, being the weakest structural component. Cellulose–hemicellulose interactions *via* hydrogen bond equivalent structures were recognized as crucial components of cell wall network mechanics. Model sensitivity analysis showed that the stiffness of these structures contributed up to 75% of the overall stiffness of the PCW, while hemicellulose stiffness alone contributed ~25% overall. Variations in cellulose microfibril (CMF) stiffness showed a marginal impact (1%) on overall cell wall mechanical performance. The results were explained by the possibility of CMF–hemicellulose bonds acting as growth regulators. Based on the theoretical hydrogen bond energy and strain energies of the cellulose–hemicellulose links, it was concluded that at 1% cell wall strain hydrogen bonding was not strong enough to maintain the integrity of the cell wall. The necessity for other, and more importantly, stronger load-bearing mechanisms was postulated to maintain the overall shape of the cell. Among various possibilities, the authors identified the biomechanical hotspot concept of Park & Cosgrove (2012*b*), as well as additional interactions with the pectin matrix.

The same model-building concept was used by Nili *et al.* (2015), who examined the biomechanical hotspot cell wall model with an almost *in silico* duplication of Park & Cosgrove (2012*a*). Simulations of uniaxial tensile tests were carried out with a decreasing number of linkers per fibril, showing that disorder in cellulose distribution had a greater impact on PCW stiffness than the degree of disorder in the cellulose–hemicellulose crosslinks. PCW integrity decay was also disorder dependent, so that the highly disordered networks required more links per fibre to maintain the same level of stiffness as the ordered network. The simulation showed 3.75 XG links per cellulose fibril to be a critical value for system integrity, which correlates with the Park & Cosgrove (2012*a*) predictions for the mass fraction of biomechanical hotspots in PCW (≈0.3%). However, the corresponding PCW network stiffness was not enough to maintain its structural integrity under loads generated by turgor pressure. Similar to the theories of Yi & Puri (2014), the authors hypothesized another mechanism governing cell wall stiffness (a more important role of pectin, or a different nature of the hotspot linkage).

(3) PCW models with particle-based representation of fibres

Early PCW models and random fibre networks, which were based on classical continuum mechanics, shared the same limitations. For instance, certain modelling approaches take into account adhesion and failure between cellulose nanofibrils but do not include self-healing induced by reformation bonds, which is an important phenomenon in cell walls.

(Figure legend continued from previous page.)
Blue lines indicate models specific to PCWs. CG, coarse grained; CMF, cellulose microfibril; FEM, finite element model; HC, hemicelluloses. The pictograms in the circles represent the main ideas of how PCW structures are represented in models – from linear continuous structures to discrete representation using beads of different shapes. Colours correspond to main PCW structural polysaccharides: cellulose (red), hemicelluloses (black), pectin (yellow).

Table 1. Summary of major findings and limitations of plant cell wall (PCW) models. CMF, cellulose microfibril.

Reference	Technique	Major findings	Limitations
Kha *et al.* (2008, 2010)	Finite element method	• Walls with CMFs parallel to each other and to enforced displacements were found to be stiffer than those with randomly oriented CMFs • Walls with CMFs parallel to each other but perpendicular to enforced displacements had the lowest stiffness • Structures with a higher number or longer cellulose fibres were stiffer	• Limited size of simulated structures • Cellulose–hemicellulose connections as permanent fixed-point crosslinks • No bonding–debonding mechanism • Limited to small cell wall deformations • Cellulose and hemicellulose represented as stiff rods • Dynamic interactions of PCW components not considered
Yi & Puri (2012, 2014); Yi *et al.* (2012, 2013)	Finite element method	• Cellulose–hemicellulose interactions *via* hydrogen bond equivalent structures were recognized as crucial components of cell wall network mechanics • Cellulose–hemicellulose interactions act as a major regulatory mechanism to manipulate PCW compliance • Hemicellulose degradation alone had marginal effects on PCW stiffness • Hydrogen bonding alone was not strong enough to maintain the integrity of the cell wall • Results suggested the existence of other load-bearing mechanisms governing cell wall stiffness than cellulose–hemicellulose interactions	• Limited capabilities in simulating fibril motions • Simplified 2D representation of PCW • Stress relaxation and creep behaviour not considered • Cell wall rupture not considered
Nili *et al.* (2015)	Finite element method	• Hydrogen bond network stiffness generated by tethered model was not sufficient to maintain PCW structural integrity under turgor pressure • More efficient deployment of xyloglucan was suggested – as multiple, short, parallel strands rather than a single long strand (as in the tethered network model) • Highly disordered networks required more links per fibre to maintain the same level of stiffness as the ordered network • Results suggested pectin-based mechanism governing cell wall stiffness	
Jin *et al.* (2015)	Molecular dynamics/ atomistic model	• Stress–strain curve connected with the dynamics of the matrix–cellulose interfacial H-bonds • Wall matrix stiffer under higher loading rates • Molecular structure of lignin had no effect on wall mechanical behaviour • Dominant interaction within lignin matrix is the squeezing and separation between atoms	• Limited to relatively small time and length scales • Atomistic model limiting simulations to local effects only
Adler & Buehler (2013)	Coarse-grained molecular dynamics	• Cell wall material under shear loading deforms in an elastic and then plastic manner • Plastic deformation regime divides into two parts: yielding of the hemicellulose matrix and sliding of matrix along the cellulose surface • Three-regime behaviour and microfibril angle–strain relationship are derived from inter-fibrillar shearing • Microfibril angle decreases as wall strain increases • Hemicellulose hydrogel matrix relaxation is the most frequent mechanism of irreversible deformation	• Difficulties with simulating objects with a large difference in size (thick cellulose fibres and thin chains of pectin and hemicelluloses) • Simplified coarse-grained representations of cellulose microfibrils, xyloglucans and pectin • Proteins not included • Covalent bonding of matrix polysaccharides to cellulose was not considered

(Continues on next page)

Table 1. *(Cont.)*

Reference	Technique	Major findings	Limitations
Mani *et al.* (2020)	Dissipative particle dynamics	• Varying pectin chain length had negligible effects on cellulose fibril motions • Suggestion that interactions between pectin and fibrils are limited to weak non-covalent interactions • Fibril motions are dependent on its net alignment with respect to stretch direction	• Entrapment of matrix polysaccharides within cellulose microfibrils was not considered • Limited simulated strains • Cell wall rupture not considered
Zhang *et al.* (2021)	Coarse-grained particle dynamics	• Cellulose microfibrils carry most of PCW stress • Cellulose microfibrils sliding contributes the most to irreversible PCW deformation, with a smaller influence of straightening and angular reorientation • Xyloglucan length, pectin length and cross-linking had little effect on tensile PCW response • Length, density and distribution of cellulose microfibrils had substantial effects on PCW mechanical performance • Cellulose–cellulose interactions at close proximity shaped the properties of PCW	• Simplified interactions between polysaccharides (e.g. pectin–pectin, pectin–xyloglucan, pectin–cellulose, and xyloglucan–xyloglucan interactions simulated using the same binding energy)

Awareness of these issues led to the development of an alternative approach based on the principles of particle dynamics (Fig. 2). In this approach, fibres were represented using modified bead–spring models adopted from particle dynamics simulations (Rodney, Fivel & Dendievel, 2005; Persson & Isaksson, 2014). In the bead–spring model, fibres were discretized by nodes, whose number was equal to a fibre aspect ratio. Axial and bending stiffnesses were introduced by means of linear and angular springs between consecutive pairs of nodes. Interaction between the fibres was defined by means of a repulsive pair potential. Other variations of the bead–spring technique included various bead–bead interaction potentials (Yamamoto & Matsuoka, 1993) or spring potentials (Kremer & Grest, 1990). Bead–spring models also allowed for modifications to bead shape from spherical to prolate spheroids (Ross & Klingenberg, 1997), cylindrical (Ning & Melrose, 1999) or cylindrical with hemispherical end caps (Schmid, Switzer & Klingenberg, 2000).

A milestone in the field of PCW modelling was the work of Adler & Buehler (2013), who described a mesoscale bead–spring model of the wall mechanics of various wood species. Their model included cellulose and hemicellulose only, thus providing a universal representation of cellulose–hemicellulose networks, similar to the tethered PCW model. Cellulose and hemicellulose chains were divided into segments, approximated by spherical beads – a simplified representation of large number of connected molecules. Harmonic bond potentials between beads were established to simulate the axial strain and bending energies of the fibres. Inter-fibrillar interactions were modelled by means of Lennard-Jones (LJ) potentials. The application of LJ interaction potentials made this model the first to allow users to simulate the process of desorption and adsorption of hemicelluloses freely during the deformation of the cell wall; this is significant because it had a key influence on the shape of the force–strain characteristics obtained during uniaxial tensile experiments. The authors reported so-called 'slip–stick' behaviour between the cellulose and hemicellulose, which was indicated by three regimes of tensile behaviour of the deformed cell wall: (*i*) initial elastic deformation, (*ii*) yielding of the matrix polysaccharides and (*iii*) plastic deformation caused by the sliding of the matrix along the cellulose. The resulting binomial stress–strain curve is characteristic for plant materials and was observed on larger scales for wood and plant tissues (Spatz, Köhler & Niklas, 1999; Köhler, 2000; Keunecke *et al.*, 2008). The cell wall yield and the resulting plastic deformation was explained by the continuous process of cellulose–hemicellulose bonding and debonding. After exceeding the critical values of shear strain, the locally overloaded hydrogen bonds broke, allowing for short-term fibre slippage and relaxation. During the slip event the hemicellulose re-attached in a new location along the cellulose, thereby creating a new bond which again contributed to overall PCW stiffness. The implementation of structural self-healing allowed for the reconstruction of the general behaviour of the PCW material, and also reproduced the trend of increasing stiffness with decreases in the microfibril angle. This mechanism was further explored and confirmed at the molecular level with a wood cell wall model approximated by a 'cellulose-xylan-lignin-xylan-cellulose' double sandwich-like structure (Jin, Qin & Buehler, 2015).

Another coarse-grained (CG) model based on dissipative particle dynamics (DPD) principles was developed by Mani, Cosgrove & Voth (2020) to investigate changes in the arrangement and spatial distribution of basic PCW polysaccharides during the initial phase of forced deformation. The cell wall included cellulose (in the form of bead–spring chains) and hemicelluloses (single bead, interconnecting with two fibrils). Unlike the previous models, pectin molecules were also included in the PCW molecular structure. The cellulose was arranged into separate layers which varied according to fibril orientation, all of which was submerged in the pectin matrix. XGs were modelled as linkers between two neighbouring cellulose fibres, connected by permanent bonds. All of the PCW constituents showed a collective response to forced stretching, with the mode of deformation varying with respect to orientation, which in general followed the diverse range of motions under a series of well-defined extensions observed in experiments (Zhang *et al.*, 2017). Fibres aligned with the stretching direction exhibited mainly angular reorientations. Fibres with a transverse direction predominantly showed a kinking movement due to the existence of compressive loads in a direction orthogonal to the stretching vector. The mesoscale phenomenological model developed was one of the first to recognize explicitly the presence of pectin. Simulations of chains with a wide range of lengths had almost no impact on the fibril motions. These findings suggested that the interactions between pectin and fibrils are limited to weak non-covalent interactions. The negligible effects of pectin on fibril motion is in line with indirect observations of a lower binding affinity of pectin to cellulose fibrils compared to that of XGs for cell wall analogues, as well as cucumber hypocotyl walls in which mechanics predominantly was determined by contacts involving XGs and cellulose (Whitney *et al.*, 1995; Chanliaud & Gidley, 1999; Park & Cosgrove, 2012*a*). However, it should be emphasized that the adopted force field works exclusively by means of repulsive potentials. Therefore, the results obtained were specific to certain simulation conditions, which are only capable of reflecting a limited range of interactions. The developed simulation affirmed roles for XG and pectin as a cellulose fibril coating and background matrix, respectively.

Recently a state-of-the-art research process developed a CG model based on polymer physics which aimed to simulate the mechanics of epidermal cell walls at a nanoscale level (Zhang *et al.*, 2021). The methodology used shared a conceptual basis with the model developed by Adler & Buehler (2013), and belongs to the same category as the bead–spring models derived from CG molecular dynamics (CGMD), with the elastic properties of PCW polysaccharides being modelled using harmonic bonds and angle potentials between beads, and fibre-to-fibre contacts modelled as non-bonded interactions using Morse potentials.

The onion epidermal cell wall was modelled as a polylamellate structure of cellulose microfibrils (four lamellae) with varied orientation angles, mimicking surface deposition by synthase complexes, and embedded in matrix polysaccharides (XG and HG). Both matrix polysaccharides were initially randomly dispersed in a simulation domain, following which the whole system was dynamically equilibrated, resulting in structures resembling PCW in terms of organization as observed using an atomic force microscope.

Simulations showed that cellulose fibrils support most cell wall stress, highly dependent on fibril length and density; there was little response to XG and HG length and HG crosslinking, in line with previous experimental studies (Park & Cosgrove, 2012*a*; Zhang *et al.*, 2019). The modulus of the uniaxially stretched PCW model showed a non-linear response to applied strain, being constant up to ≈1% strain, and increasing up to ≈8% with a further drop due to the plastic deformation of selected wall components. An analysis of tensile stress distribution showed the highest values for lamellae aligned most closely to the stretching direction and decreasing with alignment angle. The simulations provided unprecedented insight into structural changes in the deformation system, thereby allowing three main microfibril movements associated with epidermis stretching to be distinguished. Straightening was observed at low CMF orientation angles (0–30°) and low strains, then this ceased and was replaced by sliding at high strains, marking the beginning of the plastic yield point. Bending was observed for 60–90° orientation angles irrespective of the strain rate, due to cell wall compression in the transverse direction. For lamellae with intermediate CMF orientation angles, reorientation was observed due to increased microfibril bundling at higher strains. Modelling of the cyclic extension of the wall showed irreversible deformation for the first cycle, whereas subsequent loading was reversible. Fibril sliding made a major contribution to irreversible extension, which increased with strain and CMF alignment in the stretching direction. The breakage and reforming of non-covalent bonding between cell wall polysaccharides was considered to govern cell wall elastic behaviour under subsequent loading. Despite some simplifications in the representation of PCW polysaccharides (CGMD representation, pectin was modelled as a HG due to the lack of other PCW constituents), this model is the most detailed depiction of supramolecular morphology and the tensile behaviour of PCWs to date.

Despite these successes and promising results, the current models are far from complete. The next challenge is to incorporate pectic polysaccharides into future computational models of the PCW. A number of recent studies have indicated an important role of pectin on the mechanical performance and growth of the PCW (Peaucelle, Braybrook & Höfte, 2012; Wolf & Greiner, 2012). Liu, Talbot & Llewellyn (2013) showed that some of the specific polymethyl esterase isoforms were expressed throughout rapid cotton fibre elongation and so may be contributing to cell wall loosening by lowering wall pH and assisting turgor-driven wall extension. The growth enhancement reported for the low-MW *Arabidopsis thaliana* mutant with a lower molecular weight of HG chains was correlated with increased esterification, reduced crosslinking, and increased aggregation of interfibrillar pectins and weaker HG–CMF interactions (Phyo *et al.*, 2017). Another study with an arabinan-deficient *Arabidopsis thaliana* mutant indicated an influence of arabinan structures on responsiveness of PCW to an imposed mechanical stress (Verhertbruggen *et al.*, 2013). Haas *et al.* (2020) reported the presence of pectin nanofilaments in cell walls that possess an intrinsic expansion capacity. Using growth models containing such structures it was shown that a complex plant cell shape can arise from chemically induced local and polarized expansion of the pectin nanofilaments without turgor-driven growth. To take this complexity into account, future models must consider not only the pectin structure itself in unprecedented detail, but also the dynamics of changes in its structure over time. Current cell wall models take into account the presence of only HG at best, thus ignoring the true diversity of pectin. One possible solution to this problem is the application of multiscale and multi-physics modelling (Fish, Wagner & Keten, 2021). With multiscale modelling, the target system is described simultaneously by multiple models at different scales. On the other hand, multi-physics simulations allow capturing different aspects of a physical system such as mechanical stress and fluid dynamics at the same time. Both modelling techniques allow the formulation of models that couple together different scales and modelling techniques, offering new possibilities for modelling complex systems with reasonable accuracy and efficiency. Regardless of the strategy adopted, the initial path has been set and awaits researchers ready to take on this challenge.

V. CONCLUSIONS

(1) The primary plant cell wall (PCW) is a complex system whose structure and functions are the subject of ongoing studies. The available and currently widely recognized conceptual models of PCWs facilitate the idealization of this biological system and the interpretation of experimental results. However, their experimental validation is hindered due to a lack of techniques to enable the assessment of individual mechanical contributions of PCW components in planta.

(2) The first models of PCW were based on the experience gained by researchers with random fibre networks. Despite achieving considerable successes, their development was ultimately limited by the conceptual assumptions imposed by the applied methodology. An alternative methodology developed at the same time was based on particle dynamics, and due to its flexibility and relatively straightforward implementation, this has led to far more accurate PCW modelling.

(3) The role of major wall polysaccharides and mechanisms of hemicellulose and pectin incorporation should be investigated using modern computational methods. Modelling allows for the exploration of conditions that it may not be possible to measure experimentally. Further developments in this field await the extension of current PCW numerical models or approaches that include the molecular backgrounds of cell wall plasticity, elasticity, softening, loosening and the key mechanical and regulatory molecules in order to understand the nature of PCW processes. However, the exploration of spatiotemporal organization, the mechanisms of wall polymer synthesis as well as degradation and cell wall constituent assembly remain a challenge even with the most sophisticated modelling techniques.

VI. ACKNOWLEDGEMENTS

This study was supported by the National Science Centre, Poland (Project no. 2019/35/D/NZ9/00555).

VII. REFERENCES

Adler, D. C. & Buehler, M. J. (2013). Mesoscale mechanics of wood cell walls under axial strain. *Soft Matter* **9**, 7138–7144.

Albersheim, P., Darvill, A., Roberts, K., Sederoff, R. & Staehelin, A. (2011). *Plant Cell Walls: A Renewable Material Resource*. Garland Science, Taylo & Francis Group, New York.

Åström, J. & Niskanen, K. (1993). Symmetry-breaking fracture in random fibre networks. *Europhysics Letters* **21**, 557–562.

Åström, J., Saarinen, S., Niskanen, K. & Kurkijärvi, J. (1994). Microscopic mechanics of fiber networks mechanics of fiber networks. *Journal of Applied Physics* **75**, 2383–2392.

Berglund, J., Angles d'Ortoli, T., Vilaplana, F., Widmalm, G., Bergenstråhle-Wohlert, M., Lawoko, M., Henriksson, G., Lindström, M. & Wohlert, J. (2016). A molecular dynamics study of the effect of glycosidic linkage type in the hemicellulose backbone on the molecular chain flexibility. *Plant Journal* **88**, 56–70.

Berglund, J., Azhar, S., Lawoko, M., Lindström, M., Vilaplana, F., Wohlert, J. & Henriksson, G. (2019). The structure of galactoglucomannan impacts the degradation under alkaline conditions. *Cellulose* **26**, 2155–2175.

Braidwood, L., Breuer, C. & Sugimoto, K. (2014). My body is a cage: mechanisms and modulation of plant cell growth. *New Phytologist* **201**, 388–402.

Bronkhorst, C. A. (2003). Modelling paper as a two-dimensional elastic - plastic stochastic network. *International Journal of Solids and Structures* **40**, 5441–5454.

Broxterman, S. E. & Schols, H. A. (2018). Interactions between pectin and cellulose in primary plant cell walls. *Carbohydrate Polymers* **192**, 263–272.

Carpita, N. C. (1996). Structure and biogenesis of the cell walls of grasses. *Annual Review of Plant Physiology and Plant Molecular Biology* **47**, 445–476.

Carpita, N. C. (2011). Update on mechanisms of plant cell wall biosynthesis: how plants make cellulose and other (1→4)-β-D-Glycans. *Plant Physiology* **155**, 171–184.

Carpita, N. C. & Gibeaut, D. M. (1993). Structural models of primary cell walls in flowering plants: consistency of molecular structure with the physical properties of the walls during growth. *Plant Journal* **3**, 1–30.

Cavalier, D. M., Lerouxel, O., Neumetzler, L., Yamauchi, K., Reinecke, A., Freshour, G., Zabotina, O. A., Hahn, M. G., Burgert, I., Pauly, M., Raikhel, N. V. & Keegstra, K. (2008). Disrupting two *Arabidopsis thaliana* xylosyltransferase genes results in plants deficient in xyloglucan, a major primary cell wall component. *Plant Cell* **20**, 1519–1537.

Chanliaud, E. & Gidley, M. J. (1999). In vitro synthesis and properties of pectin/*Acetobacter xylinus* cellulose composites. *Plant Journal* **20**, 25–35.

Chen, Z., Li, S., Fu, Y., Li, C., Chen, D., Chen, H., Ara, G., Ara, X. & Ara, A. (2019). Arabinoxylan structural characteristics, interaction with gut microbiota and potential health functions. *Journal of Functional Foods* **54**, 536–551.

Cheng, G., Duan, X., Jiang, Y., Sun, J., Yang, S., Yang, B., He, S., Liang, H. & Luo, Y. (2009). Modification of hemicellulose polysaccharides during ripening of postharvest banana fruit. *Food Chemistry* **115**, 43–47.

Colodel, C., Vriesmann, L. C. & de Oliveira Petkowicz, C. L. (2018). Cell wall polysaccharides from Ponkan mandarin (*Citrus reticulata* Blanco cv. Ponkan) peel. *Carbohydrate Polymers* **195**, 120–127.

Cosgrove, D. J. (2000). Expansive growth of plant cell walls. *Plant Physiology and Biochemistry* **38**, 109–124.

Cosgrove, D. J. (2014). Re-constructing our models of cellulose and primary cell wall assembly. *Current Opinion in Plant Biology* **22**, 122–131.

Cosgrove, D. J. (2018). Diffuse growth of plant cell walls. *Plant Physiology* **176**, 16–27.

Cosgrove, D. J. & Jarvis, M. C. (2012). Comparative structure and biomechanics of plant primary and secondary cell walls. *Frontiers in Plant Science* **3**, 1–6.

Deogekar, S. & Picu, R. C. (2018). On the strength of random fiber networks. *Journal of the Mechanics and Physics of Solids* **116**, 1–16.

Dolan, G. K., Cartwright, B., Bonilla, M. R., Gidley, M. J., Stokes, J. R. & Yakubov, G. E. (2019). Probing adhesion between nanoscale cellulose fibres using AFM lateral force spectroscopy: the effect of hemicelluloses on hydrogen bonding. *Carbohydrate Polymers* **208**, 97–107.

Endler, A. & Persson, S. (2011). Cellulose synthases and synthesis in arabidopsis. *Molecular Plant* **4**, 199–211.

Fernandes, A. N., Thomas, L. H., Altaner, C. M., Callow, P., Forsyth, V. T., Apperley, D. C., Kennedy, C. J. & Jarvis, M. C. (2011). Nanostructure of cellulose microfibrils in spruce wood. *Proceedings of the National Academy of Sciences of the United States of America* **108**, 1195–1203.

Fish, J., Wagner, G. J. & Keten, S. (2021). Mesoscopic and multiscale modelling in materials. *Nature Materials* **20**, 774–786.

Fry, S. C. (1989). The structure and functions of xyloglucan. *Journal of Experimental Botany* **40**, 1–11.

Fry, S. C., Smith, R. C., Renwick, K. F., Martin, D. J., Hodge, S. K. & Matthews, K. J. (1992). Xyloglucan endotransglycosylase, a new wall-loosening enzyme activity from plants. *Biochemical Journal* **282**, 821–828.

Goutianos, S., Mao, R. & Peijs, T. (2018). Effect of inter-fibre bonding on the fracture of fibrous networks with strong interactions. *International Journal of Solids and Structures* **136–137**, 271–278.

Ha, M. A., Apperley, D. C. & Jarvis, M. C. (1997). Molecular rigidity in dry and hydrated onion cell walls. *Plant Physiology* **115**, 593–598.

Haas, K. T., Wightman, R., Meyerowitz, E. M. & Peaucelle, A. (2020). Pectin homogalacturonan nanofilament expansion drives morphogenesis in plant epidermal cells. *Science* **367**, 1003–1007.

Hägglund, R. & Isaksson, P. (2008). On the coupling between macroscopic material degradation and interfiber bond fracture in an idealized fiber network. *International Journal of Solids and Structures* **45**, 868–878.

Hamlen, R.C. (1991). *Paper structure, mechanics, and permeability: computer-aided modeling.* PhD Thesis: University of Minnesota, USA.

Hao, Z. & Mohnen, D. (2014). A review of xylan and lignin biosynthesis: foundation for studying Arabidopsis irregular xylem mutants with pleiotropic phenotypes. *Critical Reviews in Biochemistry and Molecular Biology* **49**, 212–241.

Hayashi, T. (1989). Xyloglucans in the primary cell wall. *Annual Review of Plant Physiology and Plant Molecular Biology* **40**, 139–168.

Hayashi, T. & Kaida, R. (2011). Functions of xyloglucan in plant cells. *Molecular Plant* **4**, 17–24.

Hayashi, T., Marsden, M. P. F. & Delmer, D. P. (1987). Pea xyloglucan and cellulose. *Plant Physiology* **83**, 384–389.

Hayashi, T., Ogawa, K. & Mitsuishi, Y. (1994). Characterization of the adsorption of xyloglucan to cellulose. *Plant and Cell Physiology* **35**, 1199–1205.

Heyden, S. (2000). *Network modelling for the evaluation of mechanical properties of cellulose fluff.* PhD Thesis: Lund University, Sweden.

Heyden, S. & Gustafsson, P. J. (1998). Simulation of fracture in a cellulose fibre network. *Journal of Pulp and Paper Science* **24**, 160–165.

Jackman, R. L. & Stanley, D. W. (1995). Perspectives in the textural evaluation of plant foods. *Trends in Food Science and Technology* **6**, 187–194.

Jin, K., Qin, Z. & Buehler, M. J. (2015). Molecular deformation mechanisms of the wood cell wall material. *Journal of the Mechanical Behavior of Biomedical Materials* **42**, 198–206.

Keegstra, K., Talmadge, K. W., Bauer, W. D. & Albersheim, P. (1973). The structure of plant cell walls: III. A model of the walls of suspension-cultured sycamore cells based on the interconnections of the macromolecular components. *Plant Physiology* **51**, 188–197.

Keunecke, D., Eder, M., Burgert, I. & Niemz, P. (2008). Micromechanical properties of common yew (*Taxus baccata*) and Norway spruce (*Picea abies*) transition wood fibers subjected to longitudinal tension. *Journal of Wood Science* **54**, 420–422.

Kha, H., Tuble, S., Kalyanasundaram, S. & Williamson, R. E. (2008). Finite element analysis of plant cell wall materials. *Advanced Materials Research* **32**, 197–202.

Kha, H., Tuble, S. C., Kalyanasundaram, S. & Williamson, R. E. (2010). WallGen, software to construct layered cellulose-hemicellulose networks and predict their small deformation mechanics. *Plant Physiology* **152**, 774–786.

Koh, C. T. & Oyen, M. L. (2012). Branching toughens fibrous networks. *Journal of the Mechanical Behavior of Biomedical Materials* **12**, 74–82.

Köhler, L. (2000). Biphasic mechanical behaviour of plant tissues. *Materials Science and Engineering C* **11**, 51–56.

Kremer, K. & Grest, G. S. (1990). Dynamics of entangled linear polymer melts: a molecular-dynamics simulation. *The Journal of Chemical Physics* **92**, 5057–5086.

Kulachenko, A., Denoyelle, T., Galland, S. & Lindström, S. B. (2012). Elastic properties of cellulose nanopaper. *Cellulose* **19**, 793–807.

Kulachenko, A. & Uesaka, T. (2012). Direct simulations of fiber network deformation and failure. *Mechanics of Materials* **51**, 1–14.

Lima, D. U., Loh, W. & Buckeridge, M. S. (2004). Xyloglucan-cellulose interaction depends on the sidechains and molecular weight of xyloglucan. *Plant Physiology and Biochemistry* **42**, 389–394.

Liu, J. X., Chen, Z. T., Wang, H. & Li, K. C. (2011). Elasto-plastic analysis of influences of bond deformability on the mechanical behavior of fiber networks. *Theoretical and Applied Fracture Mechanics* **55**, 131–139.

Liu, Q., Talbot, M. & Llewellyn, D. J. (2013). Pectin methylesterase and pectin remodelling differ in the fibre walls of two *Gossypium* species with very different fibre properties. *PLoS One* **8**, e65131.

Mackie, W. & Preston, R. D. (1968). The occurrence of mannan microfibrils in the green algae *Codium fragile* and *Acetabularia crenulata*. *Planta* **79**, 249–253.

Mani, S., Cosgrove, D. J. & Voth, G. A. (2020). Anisotropic motions of fibrils dictated by their orientations in the lamella: a coarse-grained model of a plant cell wall. *Journal of Physical Chemistry B* **124**, 3527–3539.

Mao, R., Goutianos, S., Tu, W., Meng, N., Chen, S. & Peijs, T. (2017). Modelling the elastic properties of cellulose nanopaper. *Materials and Design* **126**, 183–189.

Marcelin, O., Williams, P. & Brillouet, J. M. (1993). Isolation and characterisation of the two main cell-wall types from guava (*Psidium guajava* L.) pulp. *Carbohydrate Research* **240**, 233–243.

Martínez-Sanz, M., Pettolino, F., Flanagan, B., Gidley, M. J. & Gilbert, E. P. (2017). Structure of cellulose microfibrils in mature cotton fibres. *Carbohydrate Polymers* **175**, 450–463.

Matthews, J. F., Skopec, C. E., Mason, P. E., Zuccato, P., Torget, R. W., Sugiyama, J., Himmel, M. E. & Brady, J. W. (2006). Computer simulation studies of microcrystalline cellulose Iβ. *Carbohydrate Research* **341**, 138–152.

McCann, M. C., Wells, B. & Roberts, K. (1990). Direct visualization of cross-links in the primary plant cell wall. *Journal of Cell Science* **96**, 323–334.

McFarlane, H. E., Döring, A. & Persson, S. (2014). The cell biology of cellulose synthesis. *Annual Review of Plant Biology* **65**, 69–94.

McNiel, M., Albersheim, P., Taiz, L. & Jones, R. L. (1975). The structure of plant cell walls. *Plant Physiology* **55**, 64–68.

Melton, L. D., Smith, B. G., Ibrahim, R. & Schröder, R. (2009). Mannans in primary and secondary plant cell walls. *New Zealand Journal of Forestry Science* **39**, 153–160.

Newman, R. H., Hill, S. J. & Harris, P. J. (2013). Wide-angle x-ray scattering and solid-state nuclear magnetic resonance data combined to test models for cellulose microfibrils in mung bean cell walls. *Plant Physiology* **163**, 1558–1567.

Nili, A., Yi, H., Crespi, V. H. & Puri, V. M. (2015). Examination of biological hotspot hypothesis of primary cell wall using a computational cell wall network model. *Cellulose* **22**, 1027–1038.

Ning, Z. & Melrose, J. R. (1999). A numerical model for simulating mechanical behavior of flexible fibers. *Journal of Chemical Physics* **111**, 10717–10726.

O'Neill, M. A. & York, W. S. (2018). The composition and structure of plant primary cell walls. In *Annual Plant Reviews Online 8* (ed. J. K. C. Rose), pp. 1–54. John Wiley & Sons, United States.

Park, Y. B. & Cosgrove, D. J. (2012*a*). A revised architecture of primary cell walls based on biomechanical changes induced by substrate-specific endoglucanases. *Plant Physiology* **158**, 1933–1943.

Park, Y. B. & Cosgrove, D. J. (2012*b*). Changes in cell wall biomechanical properties in the xyloglucan-deficient xxt1/xxt2 mutant of *Arabidopsis*. *Plant Physiology* **158**, 465–475.

Pauly, M., Gille, S., Liu, L., Mansoori, N., de Souza, A., Schultink, A. & Xiong, G. (2013). Hemicellulose biosynthesis. *Planta* **238**, 627–642.

Peaucelle, A., Braybrook, S. & Höfte, H. (2012). Cell wall mechanics and growth control in plants: the role of pectins revisited. *Frontiers in Plant Science* **3**, 1–6.

Persson, J. & Isaksson, P. (2014). A mechanical particle model for analyzing rapid deformations and fracture in 3D fiber materials with ability to handle length effects. *International Journal of Solids and Structures* **51**, 2244–2251.

Pettolino, F. A., Walsh, C., Fincher, G. B. & Bacic, A. (2012). Determining the polysaccharide composition of plant cell walls. *Nature Protocols* **9**, 1590–1607.

Phyo, P., Wang, T., Xiao, C., Anderson, C. T. & Hong, M. (2017). Effects of pectin molecular weight changes on the structure, dynamics, and polysaccharide interactions of primary cell walls of *Arabidopsis thaliana*: insights from solid-state NMR. *Biomacromolecules* **18**, 2937–2950.

Prakash, R., Johnston, S. L., Boldingh, H. L., Redgwell, R. J., Atkinson, R. G., Melton, L. D., Brummell, D. A. & Schröder, R. (2012). Mannans in tomato fruit are not depolymerized during ripening despite the presence of endo-β-mannanase. *Journal of Plant Physiology* **169**, 1125–1133.

Probine, M. & Barber, N. (1966). The structure and plastic properties of the cell wall of nitella in relation to extension growth. *Australian Journal of Biological Sciences* **19**, 439.

Purushotham, P., Ho, R. & Zimmer, J. (2020). Architecture of a catalytically active homotrimeric plant cellulose synthase complex. *Science* **369**, 1089–1094.

Ray, S., Vigouroux, J., Quémener, B., Bonnin, E. & Lahaye, M. (2014). Novel and diverse fine structures in LiCl-DMSO extracted apple hemicelluloses. *Carbohydrate Polymers* **108**, 46–57.

Ren, J. & Sun, R. (2010). *Cereal Straw as a Resource for Sustainable Biomaterials and Biofuels: Chemistry, Extractives, Lignins, Hemicelluloses and Cellulose*, 1st Edition, pp. 73–130. Elsevier, Amsterdam.

Rigdahl, M., Westerlind, B. & Hollmark, H. (1984). Analysis of cellulose networks by the finite element method. *Journal of Materials Science* **19**, 3945–3952.

Rodney, D., Fivel, M. & Dendievel, R. (2005). Discrete modeling of the mechanics of entangled materials. *Physical Review Letters* **95**, 2–5.

Roelofsen, P. A. (1958). Cell-wall structure as related to surface growth some supplementary remarks on multinet growth. *Acta Botanica Neerlandica* **7**, 77–89.

Ross, R. F. & Klingenberg, D. J. (1997). Dynamic simulation of flexible fibers composed of linked rigid bodies. *Journal of Chemical Physics* **106**, 2949–2960.

Scheller, H. V. & Ulvskov, P. (2010). Hemicelluloses. *Annual Review of Plant Biology* **61**, 263–289.

Schmid, C. F., Switzer, L. H. & Klingenberg, D. J. (2000). Simulations of fiber flocculation: effects of fiber properties and interfiber friction. *Journal of Rheology* **44**, 781–809.

Schröder, R., Nicolas, P., Vincent, S. J. F., Fischer, M., Reymond, S. & Redgwell, R. J. (2001). Purification and characterisation of a galactoglucomannan from kiwifruit (*Actinidia deliciosa*). *Carbohydrate Research* **331**, 291–306.

Silva, G. B., Ionashiro, M., Carrara, T. B., Crivellari, A. C., Tiné, M. A. S., Prado, J., Carpita, N. C. & Buckeridge, M. S. (2011). Cell wall polysaccharides from fern leaves: evidence for a mannan-rich type III cell wall in *Adiantum raddianum*. *Phytochemistry* **72**, 2352–2360.

Spatz, H. C., Köhler, L. & Niklas, K. J. (1999). Mechanical behaviour of plant tissues: composite materials or structures? *Journal of Experimental Biology* **202**, 3269–3272.

Spiridon, I. & Popa, V. (2008). Chapter 13 - hemicelluloses: major sources, properties and applications. In *Monomers, Polymers and Composites from Renewable Resources* (eds M. N. Belgacem and A. Gandini), pp. 289–304. Elsevier Science, Amsterdam.

Talbott, L. D. & Ray, P. M. (1992). Molecular size and separability features of pea cell wall polysaccharides: implications for models of primary wall structure. *Plant Physiology* **98**, 357–368.

Thomas, L. H., Trevor Forsyth, V., Šturcová, A., Kennedy, C. J., May, R. P., Altaner, C. M., Apperley, D. C., Wess, T. J. & Jarvis, M. C. (2013). Structure of cellulose microfibrils in primary cell walls from collenchyma. *Plant Physiology* **161**, 465–476.

Thompson, D. S. (2005). How do cell walls regulate plant growth? *Journal of Experimental Botany* **56**, 2275–2285.

Tuomivaara, S. T., Yaoi, K., O'Neill, M. A. & York, W. S. (2015). Generation and structural validation of a library of diverse xyloglucan-derived oligosaccharides, including an update on xyloglucan nomenclature. *Carbohydrate Research* **402**, 56–66.

Uhlin, K. I., Atalla, R. H. & Thompson, N. S. (1995). Influence of hemicelluloses on the aggregation patterns of bacterial cellulose. *Cellulose* **2**, 129–144.

Uluisik, S., Chapman, N. H., Smith, R., Poole, M., Adams, G., Gillis, R. B., Besong, T. M. D., Sheldon, J., Stiegelmeyer, S., Perez, L., Samsulrizal, N., Wang, D., Fisk, I. D., Yang, N., Baxter, C., et al. (2016). Genetic improvement of tomato by targeted control of fruit softening. *Nature Biotechnology* **34**, 950–952.

Verhertbruggen, Y., Marcus, S. E., Chen, J. & Knox, J. P. (2013). Cell wall pectic arabinans influence the mechanical properties of *Arabidopsis thaliana* inflorescence stems and their response to mechanical stress. *Plant and Cell Physiology* **54**, 1278–1288.

Whitney, S. E. C., Brigham, J. E., Darke, A. H., Reid, J. S. G. & Gidley, M. J. (1995). In vitro assembly of cellulose/xyloglucan networks: ultrastructural and molecular aspects. *The Plant Journal* **8**, 491–504.

Wolf, S. & Greiner, S. (2012). Growth control by cell wall pectins. *Protoplasma* **249**, 169–175.

Yamamoto, S. & Matsuoka, T. (1993). A method for dynamic simulation of rigid and flexible fibers in a flow field. *The Journal of Chemical Physics* **98**, 644–650.

Yang, H. & Kubicki, J. D. (2020). A density functional theory study on the shape of the primary cellulose microfibril in plants: effects of C6 exocyclic group conformation and H-bonding. *Cellulose* **27**, 2389–2402.

Yi, H. & Puri, V. M. (2012). Architecture-based multiscale computational modeling of plant cell wall mechanics to examine the hydrogen-bonding hypothesis of the cell wall network structure model. *Plant Physiology* **160**, 1281–1292.

Yi, H. & Puri, V. M. (2014). Contributions of the mechanical properties of major structural polysaccharides to the stiffness of a cell wall network model. *American Journal of Botany* **101**, 244–254.

Yi, H., Zamil, M. S. & Puri, V. M. (2012). Structure based computational plant cell wall model. In *American Society of Agricultural and Biological Engineers Annual International Meeting* (Volume **2012**), pp. 1195–1199. St. Joseph, Michigan.

Yi, H., Zamil, M. S. & Puri, V. M. (2013). Investigation of the plant cell wall's molecular structure models using the finite element modeling. In *American Society of Agricultural and Biological Engineers Annual International Meeting* (Volume **2013**), pp. 488–493. St. Joseph, Michigan.

York, W. S., van Halbeek, H., Darvill, A. G. & Albersheim, P. (1990). Structural analysis of xyloglucan oligosaccharides by 1H-N.M.R. spectroscopy and fast-atom-bombardment mass spectrometry. *Carbohydrate Research* **200**, 9–31.

Yu, L., Yoshimi, Y., Cresswell, R., Wightman, R., Lyczakowski, J. J., Wilson, L. F. L., Ishida, K., Stott, K., Yu, X., Charalambous, S., Wurman-Rodrich, J., Terrett, O. M., Brown, S. P., Dupree, R., Temple, H., et al. (2022). Eudicot primary cell wall glucomannan is related in synthesis, structure, and function to xyloglucan. *The Plant Cell* **34**, 4600–4622.

Zhang, T., Mahgsoudy-Louyeh, S., Tittmann, B. & Cosgrove, D. J. (2014). Visualization of the nanoscale pattern of recently-deposited cellulose microfibrils and matrix materials in never-dried primary walls of the onion epidermis. *Cellulose* **21**, 853–862.

Zhang, T., Tang, H., Vavylonis, D. & Cosgrove, D. J. (2019). Disentangling loosening from softening: insights into primary cell wall structure. *Plant Journal* **100**, 1101–1117.

Zhang, T., Vavylonis, D., Durachko, D. M. & Cosgrove, D. J. (2017). Nanoscale movements of cellulose microfibrils in primary cell walls. *Nature Plants* **3**, 1–6.

Zhang, Y., Yu, J., Wang, X., Durachko, D. M., Zhang, S. & Cosgrove, D. J. (2021). Molecular insights into the complex mechanics of plant epidermal cell walls. *Science* **372**, 607–711.

Zhao, Z., Crespi, V. H., Kubicki, J. D., Cosgrove, D. J. & Zhong, L. (2014). Molecular dynamics simulation study of xyloglucan adsorption on cellulose surfaces: effects of surface hydrophobicity and side-chain variation. *Cellulose* **21**, 1025–1039.

(*Received 24 March 2022; revised 16 December 2022; accepted 13 January 2023; published online 24 January 2023*)

6.3. Manuscript P3

6.3.1. Graphical abstract of the manuscript P3

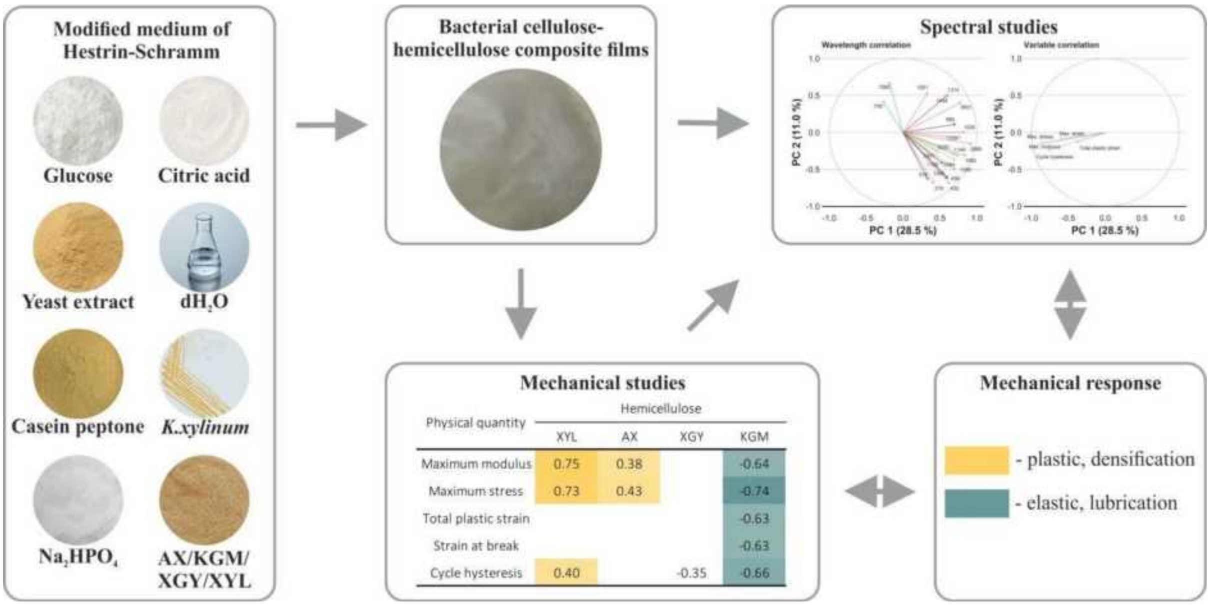

Physical quantity	Hemicellulose			
	XYL	AX	XGY	KGM
Maximum modulus	0.75	0.38		-0.64
Maximum stress	0.73	0.43		-0.74
Total plastic strain				-0.63
Strain at break				-0.63
Cycle hysteresis	0.40		-0.35	-0.66

6.3.2. Content of the manuscript P3.

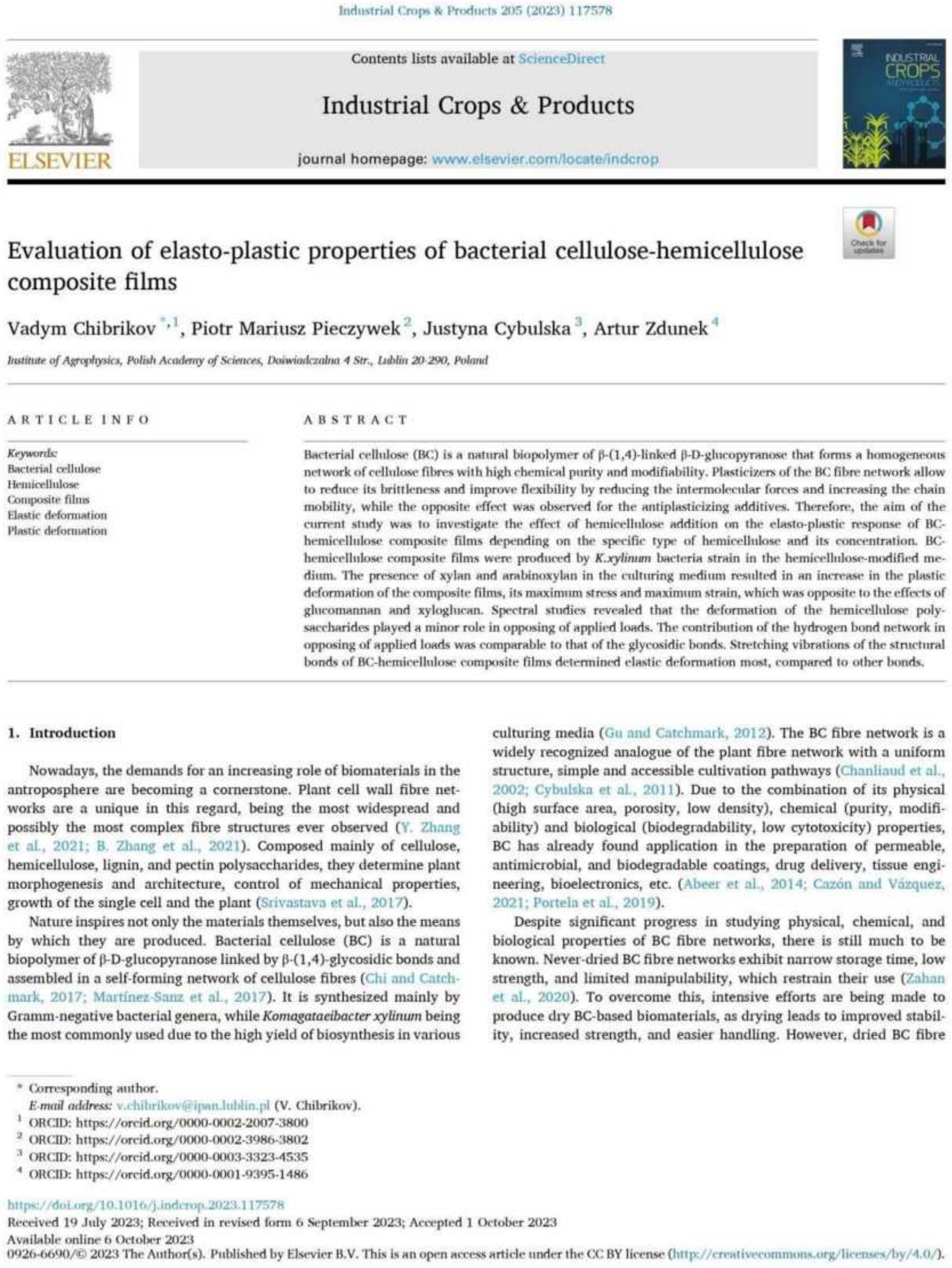

Industrial Crops & Products 205 (2023) 117578

Contents lists available at ScienceDirect

Industrial Crops & Products

journal homepage: www.elsevier.com/locate/indcrop

Evaluation of elasto-plastic properties of bacterial cellulose-hemicellulose composite films

Vadym Chibrikov [*,1], Piotr Mariusz Pieczywek [2], Justyna Cybulska [3], Artur Zdunek [4]

Institute of Agrophysics, Polish Academy of Sciences, Doświadczalna 4 Str., Lublin 20-290, Poland

A R T I C L E I N F O

Keywords:
Bacterial cellulose
Hemicellulose
Composite films
Elastic deformation
Plastic deformation

A B S T R A C T

Bacterial cellulose (BC) is a natural biopolymer of β-(1,4)-linked β-D-glucopyranose that forms a homogeneous network of cellulose fibres with high chemical purity and modifiability. Plasticizers of the BC fibre network allow to reduce its brittleness and improve flexibility by reducing the intermolecular forces and increasing the chain mobility, while the opposite effect was observed for the antiplasticizing additives. Therefore, the aim of the current study was to investigate the effect of hemicellulose addition on the elasto-plastic response of BC-hemicellulose composite films depending on the specific type of hemicellulose and its concentration. BC-hemicellulose composite films were produced by *K.xylinum* bacteria strain in the hemicellulose-modified medium. The presence of xylan and arabinoxylan in the culturing medium resulted in an increase in the plastic deformation of the composite films, its maximum stress and maximum strain, which was opposite to the effects of glucomannan and xyloglucan. Spectral studies revealed that the deformation of the hemicellulose polysaccharides played a minor role in opposing of applied loads. The contribution of the hydrogen bond network in opposing of applied loads was comparable to that of the glycosidic bonds. Stretching vibrations of the structural bonds of BC-hemicellulose composite films determined elastic deformation most, compared to other bonds.

1. Introduction

Nowadays, the demands for an increasing role of biomaterials in the antroposphere are becoming a cornerstone. Plant cell wall fibre networks are a unique in this regard, being the most widespread and possibly the most complex fibre structures ever observed (Y. Zhang et al., 2021; B. Zhang et al., 2021). Composed mainly of cellulose, hemicellulose, lignin, and pectin polysaccharides, they determine plant morphogenesis and architecture, control of mechanical properties, growth of the single cell and the plant (Srivastava et al., 2017).

Nature inspires not only the materials themselves, but also the means by which they are produced. Bacterial cellulose (BC) is a natural biopolymer of β-D-glucopyranose linked by β-(1,4)-glycosidic bonds and assembled in a self-forming network of cellulose fibres (Chi and Catchmark, 2017; Martínez-Sanz et al., 2017). It is synthesized mainly by Gramm-negative bacterial genera, while *Komagataeibacter xylinum* being the most commonly used due to the high yield of biosynthesis in various culturing media (Gu and Catchmark, 2012). The BC fibre network is a widely recognized analogue of the plant fibre network with a uniform structure, simple and accessible cultivation pathways (Chanliaud et al., 2002; Cybulska et al., 2011). Due to the combination of its physical (high surface area, porosity, low density), chemical (purity, modifiability) and biological (biodegradability, low cytotoxicity) properties, BC has already found application in the preparation of permeable, antimicrobial, and biodegradable coatings, drug delivery, tissue engineering, bioelectronics, etc. (Abeer et al., 2014; Cazón and Vázquez, 2021; Portela et al., 2019).

Despite significant progress in studying physical, chemical, and biological properties of BC fibre networks, there is still much to be known. Never-dried BC fibre networks exhibit narrow storage time, low strength, and limited manipulability, which restrain their use (Zahan et al., 2020). To overcome this, intensive efforts are being made to produce dry BC-based biomaterials, as drying leads to improved stability, increased strength, and easier handling. However, dried BC fibre

---

[*] Corresponding author.
E-mail address: v.chibrikov@ipan.lublin.pl (V. Chibrikov).
[1] ORCID: https://orcid.org/0000-0002-2007-3800
[2] ORCID: https://orcid.org/0000-0002-3986-3802
[3] ORCID: https://orcid.org/0000-0003-3323-4535
[4] ORCID: https://orcid.org/0000-0001-9395-1486

https://doi.org/10.1016/j.indcrop.2023.117578
Received 19 July 2023; Received in revised form 6 September 2023; Accepted 1 October 2023

networks have limited ductility and plasticity, which also restrain material applicability.

It has been reported that the mechanical response of BC fibre networks can be tuned to both plastic and elastic with respect to the applied load, if the sufficient plasticizers/anti-plasticizers are set (Barud et al., 2013; Trovatti et al., 2012). Embedding plasticizers in cellulose fibre network, such as glycols, acetins, glycerol, allows to reduce the inherent brittleness and improve the flexibility of dry cellulose fibre networks by reducing the intermolecular forces, and increasing the mobility of polysaccharide chains (Cazón and Vázquez, 2021). The opposite effects on the cellulose fibre network were observed for the anti-plasticizing additives, such as water, zeolites, glucaric acid etc. (Li et al., 2020).

Hemicellulose polysaccharides are the second major group of plant polysaccharides, consisting predominantly of (1,4)-linked β-D-glucose, β-D-glucuronic acid, β-D-xylose, β-D-mannose, α-L-arabinose etc. (Marriott et al., 2016; Scheller and Ulvskov, 2010). Generally accepted models of the primary plant cell wall explain cellulose as the dominant load-bearing element, while hemicellulose polysaccharides mediate the interactions between fibres (Cybulska et al., 2011; Pauly et al., 1999). Owing structural similarity to cellulose, hemicellulose polysaccharides provide the formation of a broad hydrogen bond network in plant cell wall, which is thought to define its architecture, and control mechanical response. Hemicellulose polysaccharides have also been shown to have a high affinity for cellulose, as evidenced by cellulose fibre binding, nonspecific adsorption, and covalent bond formation (Herburger et al., 2020; Linder et al., 2003; Zheng et al., 2018). The patterns of the interaction of hemicellulose polysaccharides with cellulose were shown to be structure-dependent. The general trend defines enhance in cellulose-hemicellulose interactions for substituted hemicellulose polysaccharides of high degree of polymerization (Chibrikov et al., 2022; Szymańska-Chargot et al., 2024). Additionally, the presence of amorphous hemicellulose polysaccharides in the BC fibre network can increase its swelling abilities and cause a moisture-induced plasticization effect (Dammström et al., 2005). Considering the role of hemicellulose polysaccharides in the plant cell wall, such additives may serve to tailor the mechanical properties of cellulose-based biomaterials.

In comparison with low molecular weight plasticizers, the use of hemicellulose polysaccharides may be preferable in terms of its renewability and sustainability (Jia et al., 2016; Ma et al., 2022), low migration abilities and reduced extractability (Bocqué et al., 2016), and compatibility with the other bio based polymers (Müller et al., 2019). Being the second largest group of plant polysaccharides, the sources of hemicellulose polysaccharides are practically unlimited in accessibility. Their amorphousness allow for easier extraction and industrial use, compared to other plant–derived materials (Qaseem et al., 2021). The biorefinery of hemicellulose polysaccharides from plant residues and industrial wastes has also been widely reported (Bahçegül et al., 2020; Banerjee et al., 2019).

The research described in this article aimed to investigate the effects of hemicellulose polysaccharide additives on the elasto-plastic properties of BC-hemicellulose composite films. Four different types of hemicellulose polysaccharides - tamarind (*Tamarindus indica*) xyloglucan, beechwood (*Fagus sylvatica*) xylan, wheat (*Triticum aestivum*) arabinoxylan, and konjac (*Amorphophallus konjac*) glucomannan - were selected as the most widespread, abundant and available of monocotyledons and dicotyledons (Scheller and Ulvskov, 2010; Y. Zhang et al., 2021; B. Zhang et al., 2021). Since plant hemicellulose polysaccharides differ in physicochemical properties (monosaccharide composition, molecular weight etc.) their addition could lead to a different elasto-plastic response of BC-hemicellulose composite films with respect to the applied load, which was a hypothesis of the current study.

To our knowledge, the study described here is the first complex investigation of the effect of hemicellulose polysaccharides on the elasto-plastic properties of BC-based fibre networks using the cyclic load mechanical tests. The novelty of the current article lies in an experimental approach used, which concern exhaustive analysis of the spectral data of bacterial cellulose-hemicellulose composite films in terms of its elasto-plastic properties. A significant amount of the researches in field were analyzed to synthesize the physicochemical patterns of cellulose-hemicellulose interactions, which were previously observed *in vitro*, *in muro*, and *in silico*.

2. Materials and methods

2.1. Sample preparation

Komagataeibacter xylinum ATCC-53524 (LGC Standards, UK) bacteria strain was used for preparation of the BC-hemicellulose composite films. Pure BC was prepared in Hestrin-Schramm (HS) medium containing 2.0% mass of glucose (Sigma-Aldrich, USA), 0.5% mass of casein peptone (Sigma-Aldrich, USA), 0.5% mass of yeast extract (Thermo Fisher Scientific, USA), 0.27% mass of anhydrous disodium phosphate (Sigma-Aldrich, USA), 0.115% mass of citric acid monohydrate (Chempur, Poland), all dissolved in deionized water. The pH of culturing medium was adjusted to 5.0 with 1 M NaOH/HCl (Cybulska et al., 2010). For preparation of BC-hemicellulose composite films, hemicellulose polysaccharides (all - Megazyme, Ireland) of monosaccharide composition and molecular weight, provided in Table 1, were added to the culturing medium prior autoclaving. The content of hemicellulose polysaccharides and abbreviation of each composite film are listed in Table 2.

Culturing media were autoclaved in an Series 2100 autoclave (Prestige Medical, UK) at 121 °C for 11 min and cooled to the room temperature (Mikkelsen and Gidley, 2010). Inoculum was prepared by seeding 2 mg of two-day fresh *Komagataeibacter xylinum* bacteria colonies from HS agar medium in sterile 250 mL Erlenmeyer flasks (SCHOTT, Germany) containing 50 mL of liquid HS medium. Bacteria inoculation was conducted in horizontal laminar flow cabinet (ESCO Technologies Ltd, South Africa), previously cleaned with 96% ethanol (STANLAB, Poland) and sterilized with UV. The composite films were produced statically at 30 ± 1 °C for 10 days in INE 400 precision incubator (Memmert, Germany). To remove the culturing medium, bacteria, and loosely attached hemicellulose polysaccharides, the composite films were washed with deionized water for 4 days. To obtain dry BC-hemicellulose composite films, pellicles were oven-dried in UNB 400 drying cabinet (Memmert, Germany) on sterile polystyrene Petri dishes (NOEX, Poland) at 40 ± 1 °C up to constant mass. Composite films were stored in the dark at a temperature of 20 ± 1 °C and a relative humidity of 33 ± 2% prior to further analysis.

2.2. Mechanical tests

Dried BC-hemicellulose composite films were cut into stripes and their dimensions were measured using an Olympus SZX16 microscope (Olympus Corporation, Japan) with SDF PLAPO 0.5XPF objective and a DMK 21AU04 AS camera (The Imaging Source, Germany). The image resolution was 10 μm per pixel. The width of the individual stripe was calculated as the average of three values along the sample. The thickness of each sample was measured using BAKER IP54 digital micrometre (Baker Gauges India Private Limited, India). Mechanical tests were conducted using a tensile stage microtester (Deben Microtest, UK) equipped with a 200 N load cell (Fig. 1a).

The samples were subjected to uniaxial tension with cyclic load at a strain rate of 100 μm/min until failure, with the tensile strain in increments of 0.2% per cycle (Gindl et al., 2006). The single deformation cycle was divided into a loading, and an unloading stages. Prior to the loading of the first cycle, a pre-load of 0.02 N was applied to ensure un-crimping of the cellulose fibres (Gao et al., 2015). Dwelling time of 10 s was set to ensure stress relaxation of sample between consecutive cycles. For each composite film, tests were performed in 10 replicates at a temperature of 19 ± 1 °C and a relative humidity of 33 ± 2%. Schematic two-cycle stress-strain curve of BC-hemicellulose composite films

Table 1
Monosaccharide composition and molecular weight of hemicellulose polysaccharides, used in current study. Abbreviation of *Araf* stands for arabinose, *Gal* – galactose, *Glc* – glucose, *GlcA* – glucuronic acid, *Man* – mannose, *Xyl* – xylose. Asterisk sign * refers to data from (Franková and Fry, 2021).

Type of hemicellulose polysaccharide	Monosaccharide composition (% dry polysaccharide mass)							Molecular weight (kDa)
	Araf	*Gal*	*Glc*	*GlcA*	*Man*	*Xyl*	Other	
Xylan				11.3		86.1	2.6	158.3
Arabinoxylan	37.8					61.7	0.5	323.0
Xyloglucan	2.0	17.0	45.0			34.0	2.0	802.5
Glucomannan			40.0		60.0			950.0 *

Table 2
Type of the composite films used in the study and their code names. Abbreviation BC stands for pure bacterial cellulose with no hemicellulose polysaccharides, while the other shortenings stand for the type of hemicellulose polysaccharide and its mass fraction.

Type of hemicellulose polysaccharide	Concentration of hemicellulose polysaccharides (% of mass of culturing medium)			
	0.00	0.25	0.50	1.00
Xylan	BC	XYL0.25	XYL0.50	XYL1.00
Arabinoxylan		AX0.25	AX0.50	AX1.00
Xyloglucan		XGY0.25	XGY0.50	XGY1.00
Glucomannan		KGM0.25	KGM0.50	KGM1.00

at cyclic testing are provided in Fig. 1b. Experimental stress-strain curve of pure BC, obtained by uniaxial tension with cyclic load, is provided in Fig. 2. The description of the evaluated parameters of mechanical properties is given in Table 3.

2.3. Raman spectroscopy

Several pieces of each BC-hemicellulose composite film were attached to a microscope glass with a double-sided adhesive tape for further spectroscopy studies. Raman spectra were recorded using the alpha300R confocal Raman microscope (WITec, Germany) in single spectra mode at a temperature of 19 ± 1 °C and a relative humidity of 33 ± 2%. The Raman microscope wavelength of 532 nm at a power of 10 mW was used for excitation through a EC Epiplan-Neoflural 100 X objective (Zeiss, Germany). For each composite film, 40 spectra were

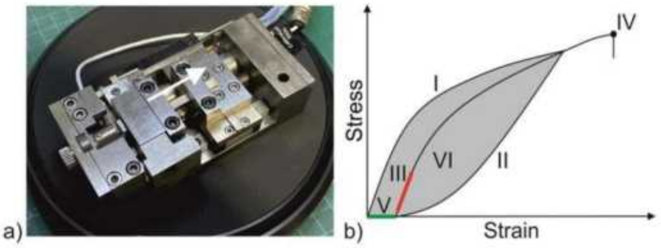

Fig. 1. a) Demonstrative view of tensile stage microtester. Arrow indicates direction of loading; b) Schematic representation of the stages of I) loading, and II) unloading of BC-hemicellulose composite films at cyclic test. Graphical representation of the parameters of mechanical properties: III) slope of maximum modulus, IV) maximum stress and maximum strain, V) total plastic strain, VI) cycle hysteresis.

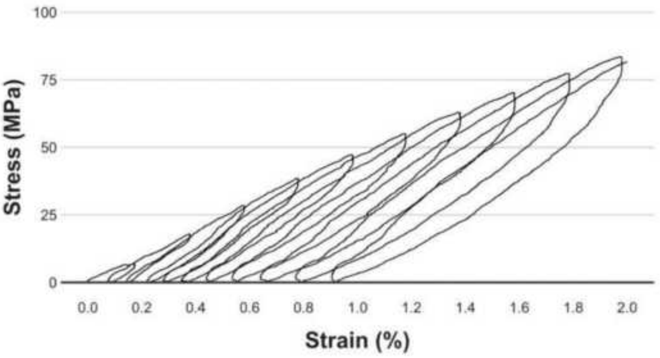

Fig. 2. Experimental stress-strain curve of pure BC, obtained by uniaxial tension with cyclic load. Original curves were captured as elongation-force one, converted to strain-stress curves, following by data smooth with convolution filter. The single deformation cycle was divided into a loading (up to a maximum stress reached within the applied strain increment), and an unloading (up to zero stress reached) stages. Deformation cycles were repeated with the constant tensile strain increments up to the fracture of composite film.

Table 3
Description of the parameters of mechanical properties of BC-hemicellulose composite films, obtained at cyclic testing.

Parameter	Graphical representation	Definition
Maximum modulus	Fig. 1b, III	The maximum value of initial slope of stress-strain curve from all loading cycles.
Maximum stress	Fig. 1b, IV	Maximum value of stress from all loading cycles.
Maximum strain	Fig. 1b, IV	Maximum strain at the last loading cycle.
Total plastic strain	Fig. 1b, V	Cumulative irreversible strain from all loading cycles.
Cycle hysteresis	Fig. 1b, VI	Averaged area between loading and unloading stress-strain curves from all cycles

acquired at random points over the range 4000 cm^{-1} - 150 cm^{-1} with a spectral resolution of 2.1 cm^{-1} Raman shift. Spectral data analysis was carried out using *ChemoSpec* R package (Hanson, 2015). Prior the analysis reflectance spectra were cropped to 3400 cm^{-1} - 350 cm^{-1} range. Next, each spectra was subjected to Savitzky-Golay smoothing filter to remove high frequency noise. Baseline correction was performed using the asymmetric least squares technique, whether the spectra were normalized using the probabilistic quotient normalization method (Dieterle et al., 2006; Peng et al., 2010).

The normalized Raman spectra were processed for principal component analysis (PCA) to reduce the dimensionality of the data. The wavenumbers from 3400 cm^{-1} to 350 cm^{-1} were treated as variables, and the principal component (PC) loading was obtained from the model for the score plots. Differences between loadings were also analyzed using a one-way analysis of variance (ANOVA) and a Tukey test for honest significant differences at a significance level of $p = 0.05$. A total of 520 spectra were used to build a model for PCA.

2.4. Statistical analysis

Statistical analysis of experimental data was performed using RStudio 2022.12.0 software (RStudio Inc., USA). The differences between the mechanical properties of the BC-hemicellulose composite films, as well as principal component loadings were analyzed using ANOVA and a Tukey test for honest significant differences at a significance level of $p = 0.05$.

Pearson correlation coefficients R were calculated to determine the relationship between the mechanical properties and the intensities of peaks of the characteristic wavenumbers as a function of the type of hemicellulose polysaccharide additive and its concentration. The statistical significance of R was determined at $p = 0.05$. Correlation coefficients R with a significance threshold of $-0.3 \geq R$ and $R \geq 0.3$ were presented.

3. Results and discussion

3.1. Sample preparation

Dried BC-hemicellulose composite films appeared as a smooth semi-transparent with an average thickness in range of 20–55 μm, whereas only pure BC appeared as a white, opaque films. Data on dry thickness of BC-hemicellulose composite films are provided in Fig. 3.

Hemicellulose polysaccharides affected production yield of BC by both the type of additive and its concentration in culturing medium, although the values were within the range of the production yields, reported previously (Chen et al., 2017; Gu and Catchmark, 2012).

3.2. Mechanical properties of BC-hemicellulose composite films

Mechanical properties of BC-hemicellulose composite films depended not only on the type of hemicellulose polysaccharide, but also on a concentration factor. With increasing xylan concentration, the maximum modulus and maximum stress of composite films increased to 18.07 ± 4.08 GPa and 146.12 ± 18.25 MPa, respectively (Fig. 4a,b), compared to control. The obtained values were higher than those previously reported (Chi and Catchmark, 2017; Yu et al., 2019). Chi and Catchmark attributed the increase in maximum modulus and maximum stress of cellulose-xylan composite films to a possible nano-reinforcing effect of the xylan embedded in the cellulose fibre network (Chi and Catchmark, 2017). Increased interconnectivity of xylan lead to densification of the network by wrapping it with xylan chain strands, associated with an enlarged network of hydrogen bonds. At a low substitution degree of xylose backbone of xylan (approximately one substitution per eight xylose units), which was used in current study, the xylan chains adsorb to the cellulose surface via stiffer substituted domains of chain (Cosgrove, 2018), while the unsubstituted flexible domains of the xylan chain can physically bind cellulose fibres. Very similar considerations

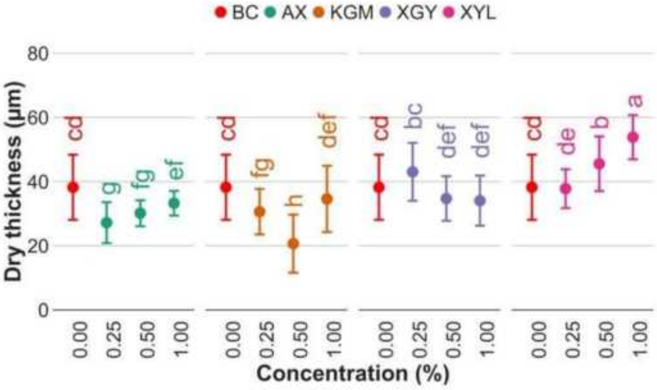

Fig. 3. Dry thickness of BC-hemicellulose composite films as a function of the concentration of arabinoxylan (AX), glucomannan (KGM), xyloglucan (XGY), and xylan (XYL) in culturing medium. The control samples (pure BC) are marked with red color. For all parameters, data points and bars indicate means and standard deviations, respectively. Treatments with the same letter are not significantly different.

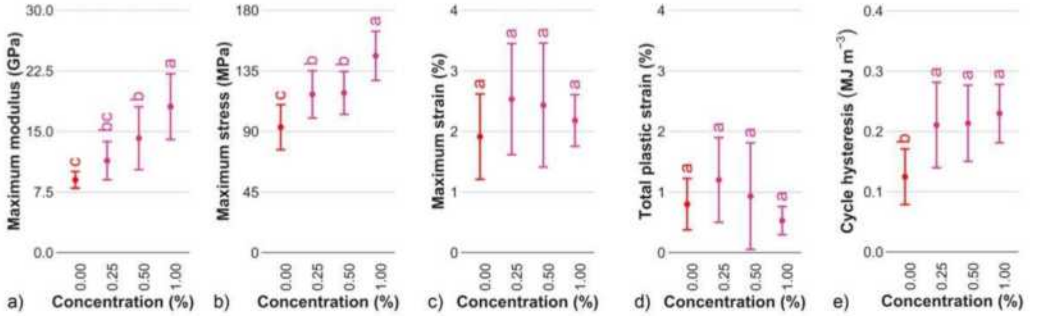

Fig. 4. Mechanical properties of BC-xylan composite films, evaluated by cyclic tests: a) maximum modulus, b) maximum stress, c) maximum strain, d) total plastic strain, e) cycle hysteresis. The control samples (pure BC) are marked with red color. For all parameters, data points and bars indicate means and standard deviations, respectively. Treatments with the same letter are not significantly different.

were reported by Long et al., in which the authors reported that the maximum modulus and maximum stress of cellulose-xylan composite films increase at low xylan content, which can be attributed to fibre reinforcement and increased hydrogen bonding (Long et al., 2019).

In our study, the addition of xylan showed a statistically insignificant, but still noticeable effect on the maximum strain of the composite film. The highest maximum strain was found for the lowest xylan content in the culturing medium, which further decreased with increasing xylan content (Fig. 4c). Yu et al. (2019) reported a statistically insignificant decrease in the strain of cellulose-xylan composite films with increasing concentration of xylan. This is consistent with the mechanical response of binary composite films, where the dominant component (cellulose) determines the mechanical properties of the composite films (Hansen et al., 2012). We assume that at low xylan content in culturing medium, as investigated in the current study, the increase in maximum strain was due to an impeded movement of the cellulose fibres due to an enlarged hydrogen bonding network (Beluns et al., 2022). Moreover, the direct dependence on the xylan content and the brittleness of the BC-xylan composite films is defined by the phenomenon of phase separation, which leads to the formation of a defective structure of the composite films. A similar mechanical response has been observed previously (Beluns et al., 2022).

Increasing the content of xylan in culturing medium resulted in a statistically insignificant change in the total plastic strain of BC-xylan composite films (Fig. 4d). Since xylan is assumed to densify the BC network by wrapping it with xylan chain strands, reversible fibre deformation should be limited due to the decreasing free space caused by adjusting cellulose fibres (Chi and Catchmark, 2017). Thus, structure densification leads to increasing internal friction in the BC-xylan network, which correlates with a larger cycle hysteresis compared to pure BC (Fig. 4e). It defines an increasing role of plastic deformation in the mechanical response of the BC-xylan composite films to the applied load with an increasing concentration of xylan in culturing medium.

Data on mechanical properties of BC-arabinoxylan composite films were comparable to those of BC-xylan. Regardless of arabinoxylan concentration, an increase in the maximum modulus and maximum stress of the composite films was observed (Fig. 5a,b). The data obtained were on average 1.5–4 times larger than those reported elsewhere, while the trends were similar (Mikkonen et al., 2012; Stepan et al., 2014). Stevanic et al. (2012) reported that the addition of arabinoxylan at low concentrations increased both the modulus and maximum stress of a composite films compared to a pure cellulose network. The authors hypothesized that this is due to increased homogeneity of the fibre network, with arabinoxylan reducing lamellar separation and distributing stress more uniformly. Dolan et al. (2019) observed an increase in interfibre adhesion forces by 1.3 times while BC was cultured with the presence of 0.5% w/v of arabinoxylan, which were supposed to be a matter of an increased hydrogen bonding. Despite the structural similarity of arabinoxylan and xylan, the interactions of the both hemicellulose polysaccharides with cellulose differ, which is due to the presence of various sidechains and different substitution degree (Chen et al., 2019). Arabinoxylan has been reported to adsorb nonspecifically on the

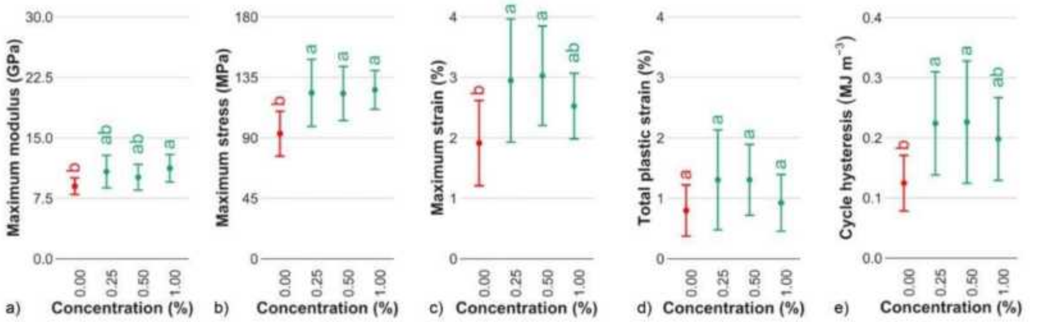

Fig. 5. Mechanical properties of BC-arabinoxylan composite films, evaluated by cyclic tests: a) maximum modulus, b) maximum stress, c) maximum strain, d) total plastic strain, e) cycle hysteresis. The control samples (pure BC) are marked with red color. For all parameters, data points and bars indicate means and standard deviations, respectively. Treatments with the same letter are not significantly different.

surface of BC (Martínez-Sanz et al., 2016, 2015), aggregate on it (Lopez-Sanchez et al., 2015), fill empty voids of a cellulose network (Sundberg et al., 2015), cross-link other arabinoxylan via diferulic acid bridges (Ralph et al., 1994), and form separate arabinoxylan domains (Martínez-Sanz et al., 2016). In our study, we suppose that similar to xylan, the stiffer domains of the arabinoxylan chains predominantly adsorb on cellulose fibres, while the unsubstituted domains provide additional interfibre interactions. This leads to an overall increase in the maximum modulus and maximum stress of composite films, but not as much as for BC-xylan composite films.

The effect of the arabinoxylan addition on the maximum strain of a composite films (Fig. 5c) was comparable to that of xylan. For AX0.25, and AX0.50 composite films, the value of the maximum strain was the highest compared to other composite films, being 2.95 ± 1.02%, and 3.03 ± 0.82%, respectively. The obtained values were at least two times lower, compared to one reported by Stevanic et al., which can be attributed to the fabrication method (Stevanic et al., 2012). Maximum strain of cellulose-arabinoglucuronoxylan composites, casted from spruce wood polysaccharides is comparable to the current study (Sundberg et al., 2015). Since most of the domains of the arabinoxylan chain should be considered rigid, the tight adsorption to the cellulose fibre should lead to a stronger hydrogen bond network, compared to pure BC. This leads to a prolonged strain hardening effect of the BC-arabinoxylan composite films, so that at increasing maximum stress, higher maximum strain was also observed.

BC-arabinoxylan composite films exhibited higher total plastic strain with increasing concentration of the additive compared to the control (Fig. 5d). The nearly twofold increase in cycle hysteresis (Fig. 5e) compared to pure BC revealed the plasticizing effect of the arabinoxylan additive, comparable to that of xylan. Apart from decreasing free volume for fibre movement with the presence of arabinoxylan, as observed for BC-xylan composite films, the increase in the plasticity of BC-arabinoxylan composite films may also be related to the deformation of the arabinoxylan network. Since arabinoxylan, unlike xylan, is a network-forming polysaccharide (Gabrielii and Gatenholm, 1998; Zhang and Whistler, 2004), it is believed to exhibit slip-stick motion, which further contributes to the mechanical properties of the already irreversibly deformed cellulose fibre network (Adler and Buehler, 2013).

The addition of xyloglucan to culturing medium showed no statistically significant change in the maximum modulus and maximum stress of a composite films (Fig. 6a,b), which is in contrast to BC-xylan and BC-arabinoxylan composite films studied. Obtained data are comparable to those previously reported for casted cellulose-xyloglucan composites (De Souza et al., 2013; Lucyszyn et al., 2016). Despite the lack of statistically significant changes in maximum modulus and maximum stress within different BC-xyloglucan composite films, we consider that the mechanical properties of BC-xyloglucan composite films are governed by two opposing processes: xyloglucan-mediated interactions between cellulose fibres, which increases maximum modulus and maximum stress, and local disruption of the network by phase separation with increasing xyloglucan content (De Souza et al., 2013). Xyloglucan-mediated interfibre interactions were shown to be 4.3 times stronger, compared to the pull-off forces of regular cellulose-cellulose interactions, as it was evidenced by Dolan et al. (2019) for bacterial cellulose, cultivated in xyloglucan-enriched medium. Since xyloglucan is the major network-forming hemicellulose polysaccharide of the primary plant cell wall of dicotyledons, its interactions with cellulose and the effects of such interactions on the mechanical properties of cellulose-based networks have been extensively studied. Xyloglucan has been shown to coat cellulose surface (Zheng et al., 2018), form thin interfibre tethers (Whitney et al., 1995), form separate xyloglucan domains (Bendaoud et al., 2017), or covalently bind cellulose (Herburger et al., 2020). Also, xyloglucan was observed to deposit on fibre surface, decreasing the cellulose crystallinity by altering chain gathering, so decreasing the maximum stress of the composite (Gu and Catchmark, 2014).

Increasing the xyloglucan content in the culturing medium resulted in increasing brittleness of composites, as shown by statistically insignificant decrease of maximum strain (Fig. 6c). While BC-xyloglucan composite film can counteract crack formation at low stress, it is ineffective in controlling crack propagation at higher one (De Souza et al., 2013). The same tendency for maximum strain to decrease with increasing xyloglucan content was reported previously (Szymańska-Chargot et al., 2017). The decrease in the maximum strain of BC-xyloglucan composite films with an increasing xyloglucan content may be explained by the increasing content of adsorbed/entrapped xyloglucan, whose interactions with cellulose are weaker, than those of cellulose-cellulose.

The addition of xyloglucan to the culturing medium resulted in a statistically insignificant decrease in the total plastic strain of the BC-xyloglucan composite films compared to the control, which was directly dependent on the concentration of hemicellulose (Fig. 6d). Decrease in cycle hysteresis of BC-xyloglucan composite films showed that the xyloglucan addition increased the role of elastic deformation of the BC fibre network with respect to the applied load (Fig. 6e). This is consistent with the data of Park and Cosgrove, showing that elastic deformations dominate the mechanical response of the *Arabidopsis thaliana* petiole wall, whereas plastic deformations prevail in a xyloglucan-depleted wall (Park and Cosgrove, 2012). We consider that the increasing elasticity of the BC-xyloglucan composite films is defined by the reduction of frictional forces between the adjusting cellulose fibres via amorphous xyloglucan mediators (Bendaoud et al., 2017; Gu

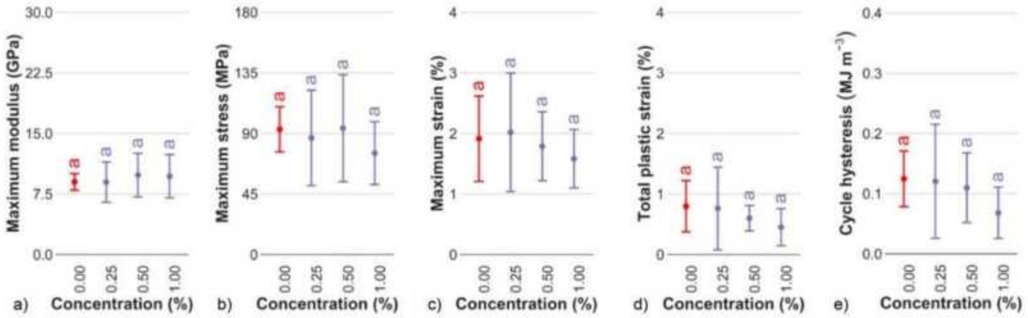

Fig. 6. Mechanical properties of BC-xyloglucan composite films, evaluated by cyclic tests: a) maximum modulus, b) maximum stress, c) maximum strain, d) total plastic strain, e) cycle hysteresis. The control samples (pure BC) are marked with red color. For all parameters, data points and bars indicate means and standard deviations, respectively. Treatments with the same letter are not significantly different.

and Catchmark, 2014). The moderate decrease of cycle hysteresis (Fig. 6e) also shows that the elasticity of the BC-xyloglucan composite films increases with increasing xyloglucan content, as the area between the loading and unloading curves of single cycle tended to zero.

Increasing concentration of glucomannan in culturing medium showed an exceptional effect on the maximum modulus and stress of the BC-glucomannan composite films (Fig. 7a,b), compared to the effect of other hemicellulose polysaccharide additives. The lowest glucomannan concentration in KGM0.25 composite film resulted in a moderate increase in the maximum modulus and maximum stress to 12.55 ± 1.08 GPa and 106.39 ± 37.39 MPa, respectively, compared to 9.00 ± 1.03 GPa and 93.12 ± 16.74 MPa of pure BC. However, further addition of glucomannan resulted in a two- to threefold decrease in maximum modulus and maximum stress. Glucomannan is generally reported to homogeneously incorporate into the cellulose network, facilitating the formation of a smooth composite structure (Berglund et al., 2020; Yu et al., 2019). However, Tokoh et al. (1998) showed that at high content, glucomannan interacts with the fibre surface, and disrupts the cellulose crystal structure. The same properties have been reported for galactomannan (Whitney et al., 1998). We consider that the maximum modulus and maximum stress of BC-glucomannan composite films decrease with increasing glucomannan content due to glucomannan adsorption on cellulose fibre, preventing its direct interaction. It can be supported by our data on the width of cellulose fibre in the BC-glucomannan composite films (data not presented), and by the rate of glucomannan adsorption on apple parenchyma cellulose (Szymańska-Chargot et al., 2024).

Moreover, increasing concentration of glucomannan in the culturing medium resulted in the formation of brittle composite films, as evidenced by the decrease of maximum strain (Fig. 7c). Wang et al. (2019) suggested that the increased brittleness of cellulose-glucomannan composite films was defined by an enhanced hydrogen bonding network and hindered chain movement. However, enhanced hydrogen bonding should lead to energy dissipation, which would at least result in higher values of maximum modulus and maximum stress, which was not observed in the current study. The overall decrease in mechanical properties of BC-glucomannan composite films was determined by the physical altering of BC network by highly dispersible glucomannan (Moreira and Filho, 2008). Together with water swelling, glucomannan assisted a formation of a gelatinous culturing medium that hindered the formation of the BC fibre network, and possibly decreasing degree of cellulose polymerization (Gu and Catchmark, 2012; Liu et al., 2021).

Altered formation of the BC fibre network by glucomannan additives resulted in a lower total plastic strain, compared to pure BC (Fig. 7d). BC-glucomannan composite films responded predominantly elastically to the load, as the cycle hysteresis (Fig. 7e) tended to zero with increasing concentration of glucomannan. By preventing cellulose fibre assembling and mediating their interaction, glucomannan is supposed to provide a lubricating effect to cellulose fibres, ensuring ample room for reversible fibre deformation (Lucenius et al., 2019; Tokoh et al., 1998; Whitney et al., 1998). Lower maximum strain of the BC-glucomannan composite films compared to pure BC indicate inability to undergo sufficient plastic deformation without rupture, which seems to be obvious in terms of limited fibre entanglement. Obtained data are consistent with the simulation studies of deformation of Iβ cellulose, in which, once the first chain fails, the other chains fall without much additional load applied (Wu et al., 2014).

3.3. Relation between molecular structure and elasto-plastic properties of bacterial cellulose-hemicellulose composite films

3.3.1. Raman spectra

The averaged Raman spectra of BC-hemicellulose composite films are described in the Supplementary Materials and shown graphically in Fig.S1. The Raman spectra obtained were comparable to those of plant fibres and BC reported elsewhere (Himmelsbach et al., 1999; Schenzel and Fischer, 2001). Three spectral regions were defined, assigned to hydrogen bonds (3600 cm^{-1} - 3200 cm^{-1}) and polysaccharide backbone (3000 cm^{-1} - 2800 cm^{-1} and 1500 cm^{-1} - 300 cm^{-1}) (Szymańska-Chargot et al., 2011). Characteristic wavenumbers assigned to the vibrations of glycosidic bonds, and bonds of monosaccharide rings were also observed. Due to the structural similarity of glucose and hemicellulose monosaccharides, the determination of minor hemicellulose polysaccharides in BC-hemicellulose composite films is challenging (Szymańska-Chargot et al., 2016). However, several peaks at characteristic wavenumbers of hemicellulose monosaccharides were denoted. The occurrence of the peak at 1580 cm^{-1} wavenumber was attributed to the stretching vibrations of the carbonyl group of galactose (Himmelsbach and Akin, 1998). The peak at 750 cm^{-1} wavenumber was assigned to the C-O-H, C-C-H, and O-C-H bending vibrations of arabinose/galactose/xylose, which differ from those of glucose (Himmelsbach and Akin, 1998; Mathlouthi and Koenig, 1987). In addition, some weak peaks were found in the 1000 cm^{-1} - 800 cm^{-1} wavenumber range, which were previously attributed to the vibrations of structural bonds of hemicellulose monosaccharides (Chu et al., 2010). Detailed information on the decoding of the spectra is provided in Table S1 in Supplementary Materials.

3.3.2. Principal component and correlation analysis

Evaluation of principal components (PC) scores enabled to reduce data dimensionality, and provide a graphical summary of the spectral changes of BC-hemicellulose composite films according to the type of

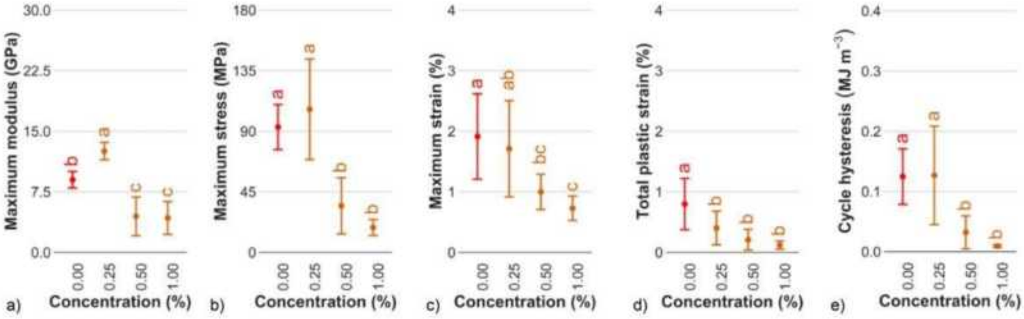

Fig. 7. Mechanical properties of BC-glucomannan composite films, evaluated by cyclic tests: a) maximum modulus, b) maximum stress, c) maximum strain, d) total plastic strain, e) cycle hysteresis. The control samples (pure BC) are marked with red color. For all parameters, data points and bars indicate means and standard deviations, respectively. Treatments with the same letter are not significantly different.

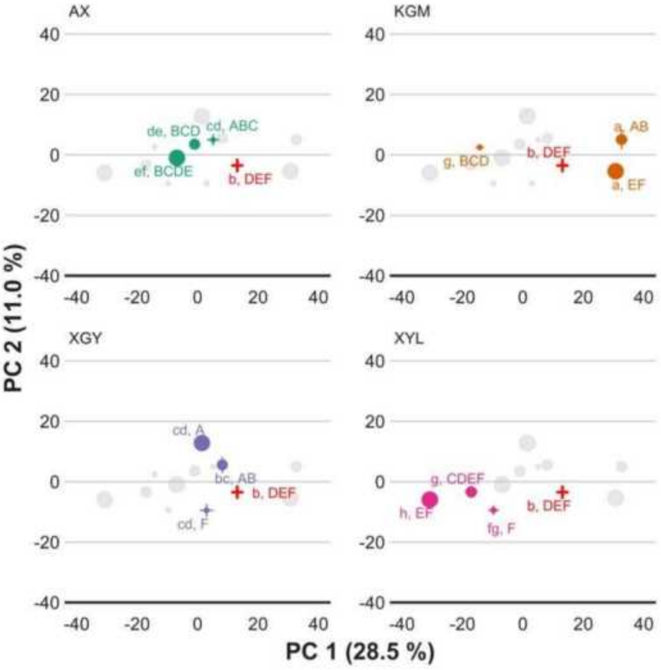

Fig. 8. Principal component analysis of spectral data collected from BC composite films with arabinoxylan (AX), glucomannan (KGM), xyloglucan (XGY), and xylan (XYL), showing two dimensional score plot with average loadings of PC 1 and PC 2 for each type of composite film (points) and standard errors (bars). Amount of hemicellulose polysaccharide added is indicated by size of data point (the bigger the point, the higher the concentration). Data points with different lower case and upper case letters have significantly different PC 1 and PC 2 values, respectively. Control sample (no hemicellulose polysaccharide additives) is marked with the red color.

hemicellulose polysaccharide additive and its concentration. The PC 1 versus PC 2 scores plot (39.5% variance described) are shown in Fig. 8. In the case of BC-xylan and BC-arabinoxylan composite films, the main variability was explained by PC 1. The values of PC1 showed negative correlation with increasing concentration of both hemicellulose polysaccharides. Similar trends in PC 1 shifts of BC-xylan and BC-arabinoxylan composite films confirm the compositional similarity of the following composite films, explaining comparable effect of both on mechanical properties of BC-hemicellulose composite films. The loadings of KGM0.25 composite film were on the negative values of PC 1, similar to those of BC-xylan and BC-arabinoxylan composite films. With an increasing concentration of glucomannan (KGM0.50 and KGM1.00 composite films), loadings shifted to the positive values of PC 1, and showed little difference between them, being in clear contrast to the PC 1 loadings of BC-xylan and BC-arabinoxylan composite films. Contrary to aforementioned composite films, the differences in BC-xyloglucan composite films were mainly explained by PC 2. As the concentration of xyloglucan additive increased, the PC 2 loading changed from negative to positive values. Here, the loading of PC 2 positively correlates with the presence of galactose, arabinose, and other monosaccharides within the aforementioned hemicellulose polysaccharides (Table 1), since xyloglucan provides the most heterogeneous collection of side-chain substitutes among hemicellulose polysaccharides studied (Park and Cosgrove, 2015).

To evaluate the effect of specific polysaccharide bonds on the overall mechanical properties of BC-hemicellulose composite films, PCA-wavenumber and PCA-variable correlation plots were provided (Fig. 9). Most of the wavenumbers assigned to the vibrations of glycosidic bonds (grey arrows), ring bonds (red arrows) and hydrogen bonds (green arrows) showed high (> 0.5) positive correlation with PC 1 (Fig. 9a). This can be attributed to the key role of the aforementioned bonds in elastic deformation of BC-hemicellulose composite films. Stretching vibrations of C-C, C-O, and C-H bonds at 2931 cm^{-1}, 2890 cm^{-1}, 1149 cm^{-1}, 1060 cm^{-1}, and 1035 cm^{-1} wavenumbers, and stretching vibrations of glycosidic bonds at 1125 cm^{-1}, 1095 cm^{-1}, and 890 cm^{-1} wavenumbers showed the highest positive correlation with PC 1, which best defines elastic deformation of BC-hemicellulose composite films. It leads to the conclusion that in case of the extension of the BC-hemicellulose composite films, the stretching vibrations of the structural bonds at the nanoscale predefine the energy dissipation within the structure of composite film, resulting in elastic deformation of the composite film at the macroscale (Eichhorn et al., 2001). However, further energy dissipation is likely to cause molecular and supramolecular changes in the cellulose, such as fracturing of polysaccharide chains or degradation of the hydrogen bond network. Thus, plastic deformation of BC-hemicellulose composite films (Fig. 9b) is hardly defined by the vibrations of the structural bonds (Chen et al., 2004).

The correlations between PC 1 of the intensities of hydrogen bonds peaks (3364 cm^{-1}, 3335 cm^{-1}, and 3301 cm^{-1}) were approximately comparable to those of the glycosidic bonds. This indicates that despite the higher energy of the covalent glycosidic bonds of the cellulose chain compared to the weak electrostatic interactions of hydrogen bonds, the density of the latter contributes statistically significantly to the elastic deformation of the BC-hemicellulose composite films. This is consistent

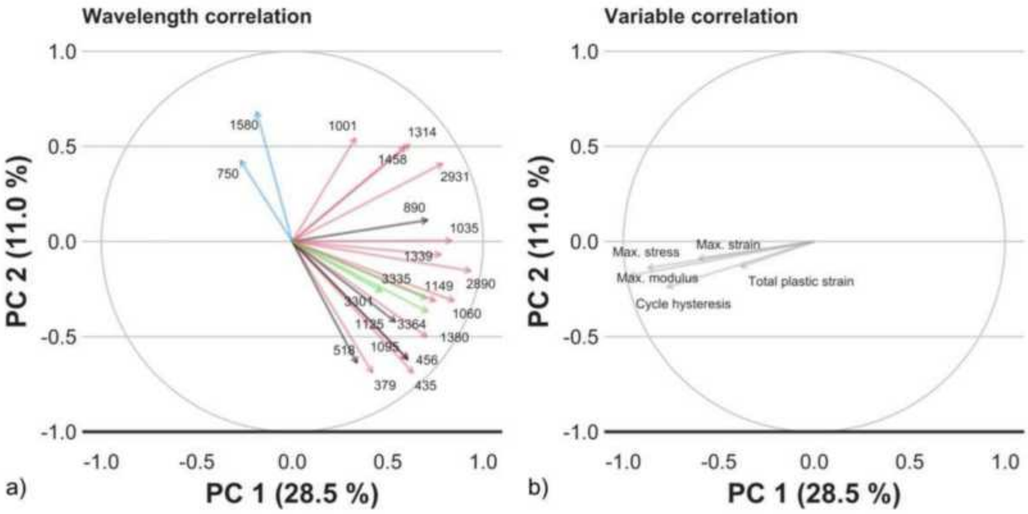

Fig. 9. Principal component analysis of spectral data collected from BC-hemicellulose composite films showing: a) correlation between loadings and characteristic spectra wavenumbers. Grey arrows stand for the loadings of the vibrations of glycosidic bonds, red – for ring bond vibrations, green - for hydrogen bond vibrations, blue – for the vibrations of other saccharides; b) correlation between loadings and mechanical properties of BC-hemicellulose composite films. Arrow direction represents correlation between characteristic spectra wavenumber/mechanical property and the PC, and the arrow length represents the strength of the relation between characteristic spectra wavenumber/mechanical property and PC.

Table 4
Heatmap representation of Pearson correlation values for the relation of the hemicellulose polysaccharide content and mechanical property or peak of characteristic wavenumber. Heatmap colors represent the Pearson correlation ranges, from cyan (negative correlation), passing through white (no correlation), to mustard (positive correlation) hues.

Physical quantity		Molecular structure	Functional group	Hemicellulose			
				AX	KGM	XGY	XYL
Mechanical	Maximum			0.38	-0.64		0.75
	Maximum stress			0.43	-0.74		0.73
	Maximum strain	NA	NA		-0.63		
	Total plastic				-0.63		
	Cycle hysteresis				-0.66	-0.35	0.40
Wavenumber	379	Ring bonds	C-C-C, C-O, and C-C-O bending vibrations		0.44	-0.45	-0.47
	435		C-C-C, and C-C-O bending vibrations		0.60	-0.44	-0.39
	456		C-C-C, and C-C-O bending vibrations		0.55	-0.49	
	1001		H-C-H rocking bending vibrations			0.48	-0.35
	1035		C-C and C-O stretching vibrations		0.70	0.31	-0.41
	1060		C-C and C-O stretching vibrations		0.68		-0.60
	1149		C-C, C-O asymmetric stretching vibrations		0.65		-0.53
	1314		H-C-C, H-C-H, C-O-H, H-C-O bending vibrations	-0.33	0.51	0.65	-0.65
	1339		H-C-C, H-C-H, C-O-H, H-C-O bending vibrations	-0.52	0.60	-0.39	-0.56
	1380		H-C-H, H-C-C, H-O-C, C-O-H bending vibrations		0.67	-0.45	-0.32
	1458		H-C-H scissoring bending vibrations	-0.69	0.47		
	2890		C-H and H-C-H stretching vibrations	-0.46	0.78	-0.39	-0.64
	2931		C-H and H-C-H stretching vibrations	-0.57	0.65		-0.49
	3301	Hydrogen bonds	Inter- and intrachain hydrogen bonds		0.39		-0.32
	3335		Inter- and intrachain hydrogen bonds		0.53	-0.37	-0.47
	3364		Inter- and intrachain hydrogen bonds		0.58		-0.50
	750	Hemicellulose	C-O-H, C-C-H, and O-C-H bending vibrations of	0.51	-0.42	0.81	-0.51
	1580		C-O stretching vibrations of galactose		-0.47	0.61	
	518	Glycosidic bonds	C-O-C bending vibrations		0.52	-0.49	
	890		C-O-C stretching vibrations		0.71	0.64	-0.33
	1095		C-O-C asymmetric stretching vibrations		0.63	-0.33	-0.47
	1125		C-O-C symmetric stretching vibrations		0.55		-0.63

with the simulations of Tashiro and Kobayashi, which showed comparable energy dissipations for glycosidic bonds, ring bonds, and hydrogen bonds of cellulose (Hinterstoisser et al., 2001; Tashiro and Kobayashi, 1991). Djahedi et al. (2016) also evaluated statistically significant contribution of hydrogen bonds to the axial modulus of cellulose chain.

The peaks at the wavenumbers of 1580 cm^{-1} and 750 cm^{-1}, previously assigned to the vibrations of structural bonds of arabinose/galactose/xylose of hemicellulose polysaccharides, showed a significant positive correlation with PC 2. It can be concluded that the mechanical properties of BC-hemicellulose composite films are barely determined by the deformation of hemicellulose polysaccharides itself, but mainly by the deformation of cellulose fibres whose gathering is mediated by hemicellulose polysaccharides. This is consistent with simulation studies, reporting the structural parameters of plant cell wall matrix polysaccharides to have a little effect on the tensile responses of plant cell wall (Mani et al., 2020; Y. Zhang et al., 2021; B. Zhang et al., 2021).

Direct relationships between the hemicellulose content in culturing medium, mechanical properties of composite films and the intensities of characteristic wavenumber peaks are shown by means of correlation matrix (Table 4). The distinct correlation patterns revealed chemometric fingerprints of hemicellulose polysaccharide additives and their relation to the mechanical properties of BC-hemicellulose composite films. A notable negative correlation existed between the mechanical properties of BC-glucomannan composite films and glucomannan content, which was attributed to altering of the formation of composite film. Positive correlations existed between the peaks related to the structural bonds of BC-glucomannan composite films and the glucomannan content. This is consistent with the data on the mechanical properties of BC-glucomannan composite films, which indicate that increasing the glucomannan content enhances the role of elastic deformation of BC-glucomannan composite films in terms of mechanical response to the applied load compared to pure BC. For addition of both xylan and arabinoxylan, correlations were opposite to those of glucomannan - positive with the mechanical properties, and negative with the peaks of the characteristic wavenumbers of the structural bonds. This leads to the conclusion that BC-xylan and BC-arabinoxylan composite films exhibit predominantly plastic deformation compared to pure BC in terms of mechanical response to a load.

The values of correlation coefficients of the peaks of the characteristic wavenumbers of the structural bonds of BC-xyloglucan composite films varied according to xyloglucan content. This is believed to be due to overlay of the spectral peaks of cellulose and xyloglucan monosaccharides with different structures. This is related to the correlation between the peaks of the vibrations of the structural bonds of arabinose/galactose/xylose of hemicellulose polysaccharides, and the type of hemicellulose polysaccharide additive. The observed peaks of characteristic wavenumbers correspond to the chemical composition of the plant cell wall hemicellulose polysaccharides, used in the current study.

4. Conclusions

In this study, we have investigated the role of hemicellulose polysaccharides in the elasto-plastic properties of BC-hemicellulose composite films. Macroscale mechanical studies, supported by spectroscopic studies and PCA allowed us to determine the effect of physicochemical properties of hemicellulose polysaccharides on overall performance of bacterial cellulose-hemicellulose composite films in terms of its elastic and plastic responses.

Addition of arabinoxylan and xylan resulted in statistically significant increase in plasticity, maximum stress and maximum strain of the composite films. Current study supports an idea of an increased inter-fibre friction in BC-hemicellulose composite films with an increasing concentration of xylan and arabinoxylan, resulting an increase in plastic deformations under applied load. The addition of xyloglucan to the culturing medium resulted in a moderate increase in the elasticity of the composite films compared to pure BC, thought to be determined by the lubricating effect of the adsorbed/entrapped xyloglucan. Glucomannan hindered the formation of a cellulose fibre network resulting in an increase in elasticity of BC-glucomannan composite films. Drop in maximum stress and maximum strain of the BC-glucomannan composite films compared to pure BC suggests its inability to undergo sufficient plastic deformation without fracturing.

Mechanical properties of BC-hemicellulose composite films were shown not to be determined by the deformation of hemicellulose polysaccharides themselves, but mainly by the deformation of cellulose fibres, mediated by hemicellulose polysaccharides. Contribution of the hydrogen bond network to the overall mechanical response of the BC-hemicellulose composite films were shown to be comparable to those of the glycosidic bonds. Stretching vibrations of the structural bonds of BC-hemicellulose composite films determined elastic deformation the most, compared to other bonds. Principal component loadings of mechanical properties of BC-hemicellulose composite films were opposite to loadings of the vibrations of structural bonds, showing the crucial effect of the supramolecular changes of composite film structure on the plastic deformation.

Obtained result on tunable elasto-plastic properties of bacterial cellulose-hemicellulose composite films showed that current films may find its further application in production of bio based flexible packaging and electronics (supporting and conductive layers), bioplastics, biodegradable films of agricultural properties (soil microbiota carriers), and products of hygiene and personal care (sheet masks, carrier of skin pigments).

CRediT authorship contribution statement

Vadym Chibrikov: Methodology, Formal analysis, Investigation, Data curation, Writing – original draft, Visualization. **Piotr Mariusz Pieczywek:** Conceptualization, Software, Formal analysis, Data curation, Writing – review & editing, Visualization, Supervision, Project administration, Funding acquisition. **Justyna Cybulska**: Methodology. **Artur Zdunek:** Conceptualization, Writing – review & editing. All authors have read and agreed to the published version of the manuscript.

Declaration of Competing Interest

The authors declare the following financial interests/personal relationships which may be considered as potential competing interests: Piotr Mariusz Pieczywek reports financial support was provided by National Science Centre Poland.

Data Availability

Data will be made available on request.

Acknowledgements

This work was supported by the National Science Centre, Poland [grant number 2019/35/D/NZ9/00555].

Appendix A. Supporting information

Supplementary data associated with this article can be found in the online version at doi:10.1016/j.indcrop.2023.117578.

References

Abeer, M.M., Mohd Amin, M.C.I., Martin, C., 2014. A review of bacterial cellulose-based drug delivery systems: Their biochemistry, current approaches and future prospects. J. Pharm. Pharmacol. 66, 1047–1061. https://doi.org/10.1111/jphp.12234.

Adler, D.C., Buehler, M.J., 2013. Mesoscale mechanics of wood cell walls under axial strain. Soft Matter 9, 7138–7144. https://doi.org/10.1039/c3sm50183c.

Bahçegül, E.G., Bahçegül, E., Özkan, N., 2020. 3D printing of hemicellulosic biopolymers extracted from lignocellulosic agricultural wastes. ACS Appl. Polym. Mater. 2, 2622–2632. https://doi.org/10.1021/acsapm.0c00256.

Banerjee, S., Patti, A.F., Ranganathan, V., Arora, A., 2019. Hemicellulose based biorefinery from pineapple peel waste: Xylan extraction and its conversion into xylooligosaccharides. Food Bioprod. Process. 117, 38–50. https://doi.org/10.1016/j.fbp.2019.06.012.

Barud, H.S., Ribeiro, S.J.L., Carone, C.L.P., Ligabue, R., Einloft, S., Queiroz, P.V.S., Borges, A.P.B., Jahno, V.D., 2013. Optically transparent membrane based on bacterial cellulose/polycaprolactone. Polimeros 23, 135–138. https://doi.org/10.1590/S0104-14282013005000018.

Beluns, S., Gaidukovs, S., Platnieks, O., Barkane, A., Gaidukova, G., Grase, L., Nabels-Sneiders, M., Kovalovs, A., Thakur, V.K., 2022. Clean manufacturing of cellulose nanopapers by incorporating lignin and xylan as sustainable additives. Carbohydr. Polym. Technol. Appl. 3, 1–9. https://doi.org/10.1016/j.carpta.2022.100207.

Bendaoud, A., Kehrbusch, R., Baranov, A., Duchemin, B., Maigret, J.E., Falourd, X., Staiger, M.P., Cathala, B., Lourdin, D., Leroy, E., 2017. Nanostructured cellulose-xyloglucan blends via ionic liquid/water processing. Carbohydr. Polym. 168, 163–172. https://doi.org/10.1016/j.carbpol.2017.03.080.

Berglund, J., Mikkelsen, D., Flanagan, B.M., Dhital, S., Gaunitz, S., Henriksson, G., Lindström, M.E., Yakubov, G.E., Gidley, M.J., Vilaplana, F., 2020. Wood hemicelluloses exert distinct biomechanical contributions to cellulose fibrillar networks. Nat. Commun. 11, 1–16. https://doi.org/10.1038/s41467-020-18390-z.

Bocqué, M., Voirin, C., Lapinte, V., Caillol, S., Robin, J.J., 2016. Petro-based and bio-based plasticizers: chemical structures to plasticizing properties. J. Polym. Sci. Part A Polym. Chem. 54, 11–33. https://doi.org/10.1002/pola.27917.

Cazón, P., Vázquez, M., 2021. Bacterial cellulose as a biodegradable food packaging material: a review. Food Hydrocoll. 113, 106530 https://doi.org/10.1016/j.foodhyd.2020.106530.

Chanliaud, E., Burrows, K.M., Jeronimidis, G., Gidley, M.J., 2002. Mechanical properties of primary plant cell wall analogues. Planta 215, 989–996. https://doi.org/10.1007/s00425-002-0783-8.

Chen, S.Q., Mikkelsen, D., Lopez-Sanchez, P., Wang, D., Martinez-Sanz, M., Gilbert, E.P., Flanagan, B.M., Gidley, M.J., 2017. Characterisation of bacterial cellulose from diverse Komagataeibacter strains and their application to construct plant cell wall analogues. Cellulose 24, 1211–1226. https://doi.org/10.1007/s10570-017-1203-3.

Chen, W., Lickfield, G.C., Yang, C.Q., 2004. Molecular modeling of cellulose in amorphous state. Part I: model building and plastic deformation study. Polymer 45, 1063–1071. https://doi.org/10.1016/j.polymer.2003.11.020.

Chen, Z., Li, S., Fu, Y., Li, C., Chen, D., Chen, H., Ara, G., Ara, X., Ara, A., 2019. Arabinoxylan structural characteristics, interaction with gut microbiota and potential health functions. J. Funct. Foods 54, 536–551. https://doi.org/10.1016/j.jff.2019.02.007.

Chi, K., Catchmark, J.M., 2017. The influences of added polysaccharides on the properties of bacterial crystalline nanocellulose. Nanoscale 9, 15144–15158. https://doi.org/10.1039/c7nr05615j.

Chibrikov, V., Pieczywek, P.M., Zdunek, A., 2022. Tailor-made biosystems - bacterial cellulose-based films with plant cell wall polysaccharides. Polym. Rev. 63, 1–27. https://doi.org/10.1080/15583724.2022.2067869.

Chu, L.Q., Masyuko, R., Sweedler, J.V., Bohn, P.W., 2010. Base-induced delignification of miscanthus x giganteus studied by three-dimensional confocal raman imaging. Bioresour. Technol. 101, 4919–4925. https://doi.org/10.1016/j.biortech.2009.10.096.

Cosgrove, D.J., 2018. Nanoscale structure, mechanics and growth of epidermal cell walls. Curr. Opin. Plant Biol. 46, 77–86. https://doi.org/10.1016/j.pbi.2018.07.016.

Cybulska, J., Vanstreels, E., Ho, Q.T., Courtin, C.M., Craeyveld, V.V., Nicolaï, B., Zdunek, A., Konstankiewicz, K., 2010. Mechanical characteristics of artificial cell walls. J. Food Eng. 96, 287–294. https://doi.org/10.1016/j.jfoodeng.2009.08.001.

Cybulska, J., Zdunek, A., Konstankiewicz, K., 2011. Calcium effect on mechanical properties of model cell walls and apple tissue. J. Food Eng. 102, 217–223. https://doi.org/10.1016/j.jfoodeng.2010.08.019.

Dammström, S., Salmén, L., Gatenholm, P., 2005. The effect of moisture on the dynamical mechanical properties of bacterial cellulose/glucuronoxylan nanocomposites. Polymer 46, 10364–10371. https://doi.org/10.1016/j.polymer.2005.07.105.

De Souza, C.F., Lucyszyn, N., Woehl, M.A., Riegel-Vidotti, I.C., Borsali, R., Sierakowski, M.R., 2013. Property evaluations of dry-cast reconstituted bacterial cellulose/tamarind xyloglucan biocomposites. Carbohydr. Polym. 93, 144–153. https://doi.org/10.1016/j.carbpol.2012.04.062.

Dieterle, F., Ross, A., Schlotterbeck, G., Senn, H., 2006. Probabilistic quotient normalization as robust method to account for dilution of complex biological mixtures. Application in^{1}H NMR metabonomics. Anal. Chem. 78, 4281–4290. https://doi.org/10.1021/ac051632c.

Djahedi, C., Bergenstråhle-Wohlert, M., Berglund, L.A., Wohlert, J., 2016. Role of hydrogen bonding in cellulose deformation: the leverage effect analyzed by molecular modeling. Cellulose 23, 2315–2323. https://doi.org/10.1007/s10570-016-0968-0.

Dolan, G.K., Cartwright, B., Bonilla, M.R., Gidley, M.J., Stokes, J.R., Yakubov, G.E., 2019. Probing adhesion between nanoscale cellulose fibres using AFM lateral force spectroscopy: the effect of hemicelluloses on hydrogen bonding. Carbohydr. Polym. 208, 97–107. https://doi.org/10.1016/j.carbpol.2018.12.052.

Eichhorn, S.J., Sirichaisit, J., Young, R.J., 2001. Deformation mechanisms in cellulose fibres, paper and wood. J. Mater. Sci. 36, 3129–3135. https://doi.org/10.1023/A:1017969916020.

Franková, L., Fry, S.C., 2021. Hemicellulose-remodelling transglycanase activities from charophytes: towards the evolution of the land-plant cell wall. Plant J. 108, 7–28. https://doi.org/10.1111/tpj.15500.

Gabrielii, I., Gatenholm, P., 1998. Preparation and properties of hydrogels based on hemicellulose. J. Appl. Polym. Sci. 69, 1661–1667. https://doi.org/10.1002/(sici)1097-4628(19980822)69:8<1661::aid-app19>3.3.co;2-k.

Gao, X., Shi, Z., Liu, C., Yang, G., Sevostianov, I., Silberschmidt, V.V., 2015. Inelastic behaviour of bacterial cellulose hydrogel: In aqua cyclic tests. Polym. Test. 44, 82–92. https://doi.org/10.1016/j.polymertesting.2015.03.021.

Gindl, W., Martinschitz, K.J., Boesecke, P., Keckes, J., 2006. Structural changes during tensile testing of an all-cellulose composite by in situ synchrotron X-ray diffraction. Compos. Sci. Technol. 66, 2639–2647. https://doi.org/10.1016/j.compscitech.2006.03.020.

Gu, J., Catchmark, J.M., 2012. Impact of hemicelluloses and pectin on sphere-like bacterial cellulose assembly. Carbohydr. Polym. 88, 547–557. https://doi.org/10.1016/j.carbpol.2011.12.040.

Gu, J., Catchmark, J.M., 2014. Roles of xyloglucan and pectin on the mechanical properties of bacterial cellulose composite films. Cellulose 21, 275–289. https://doi.org/10.1007/s10570-013-0115-0.

Hansen, N.M.L., Blomfeldt, T.O.J., Hedenqvist, M.S., Plackett, D.V., 2012. Properties of plasticized composite films prepared from nanofibrillated cellulose and birch wood xylan. Cellulose 19, 2015–2031. https://doi.org/10.1007/s10570-012-9764-7.

Hanson, B.A., 2015. ChemoSpec: An R Package for Chemometric Analysis of Spectroscopic Data (Package Version 4.0.1).

Herburger, K., Franková, L., Pičmanová, M., Loh, J.W., Valenzuela-Ortega, M., Meulewaeter, F., Hudson, A.D., French, C.E., Fry, S.C., 2020. Hetero-trans-β-glucanase produces cellulose–xyloglucan covalent bonds in the cell walls of structural plant tissues and is stimulated by expansin. Mol. Plant 13, 1047–1062. https://doi.org/10.1016/j.molp.2020.04.011.

Himmelsbach, D.S., Akin, D.E., 1998. Near-infrared fourier-transform raman spectroscopy of flax (Linum usitatissimum L.) stems. J. Agric. Food Chem. 46, 991–998. https://doi.org/10.1021/jf970656k.

Himmelsbach, D.S., Khahili, S., Akin, D.E., 1999. Near-infrared - Fourier-transform - Raman microspectroscopic imaging of flax stems. Vib. Spectrosc. 19, 361–367. https://doi.org/10.1016/S0924-2031(98)00065-4.

Hinterstoisser, B., Åkerholm, M., Salmén, L., 2001. Effect of fiber orientation in dynamic FTIR study on native cellulose. Carbohydr. Res. 334, 27–37. https://doi.org/10.1016/S0008-6215(01)00167-7.

Jia, P., Zhang, M., Hu, L., Zhou, Y., 2016. Green plasticizers derived from soybean oil for poly(vinyl chloride) as a renewable resource material. Korean J. Chem. Eng. 33, 1080–1087. https://doi.org/10.1007/s11814-015-0213-9.

Li, D., Wang, Y., Long, F., Gan, L., Huang, J., 2020. Solvation-controlled elastification and shape-recovery of cellulose nanocrystal-based aerogels. ACS Appl. Mater. Interfaces 12, 1549–1557. https://doi.org/10.1021/acsami.9b18569.

Linder, A., Bergman, R., Bodin, A., Gatenholm, P., 2003. Mechanism of assembly of xylan onto cellulose surfaces. Langmuir 19, 5072–5077. https://doi.org/10.1021/la0341355.

Liu, Z., Shen, R., Yang, X., Lin, D., 2021. Characterization of a novel konjac glucomannan film incorporated with Pickering emulsions: Effect of the emulsion particle sizes. Int. J. Biol. Macromol. 179, 377–387. https://doi.org/10.1016/j.ijbiomac.2021.02.188.

Long, L., Shen, F., Wang, F., Tian, D., Hu, J., 2019. Synthesis, characterization and enzymatic surface roughing of cellulose/xylan composite films. Carbohydr. Polym. 213, 121–127. https://doi.org/10.1016/j.carbpol.2019.02.086.

Lopez-Sanchez, P., Cersosimo, J., Wang, D., Flanagan, B., Stokes, J.R., Gidley, M.J., 2015. Poroelastic mechanical effects of hemicelluloses on cellulosic hydrogels under compression. PLoS One 10, e0122132. https://doi.org/10.1371/journal.pone.0122132.

Lucenius, J., Valle-Delgado, J.J., Parikka, K., Österberg, M., 2019. Understanding hemicellulose-cellulose interactions in cellulose nanofibril-based composites. J. Colloid Interface Sci. 555, 104–114. https://doi.org/10.1016/j.jcis.2019.07.053.

Lucyszyn, N., Ono, L., Lubambo, A.F., Woehl, M.A., Sens, C.V., de Souza, C.F., Sierakowski, M.R., 2016. Physicochemical and in vitro biocompatibility of films combining reconstituted bacterial cellulose with arabinogalactan and xyloglucan. Carbohydr. Polym. 151, 889–898. https://doi.org/10.1016/j.carbpol.2016.06.027.

Ma, Y., Song, F., Yu, J., Wang, N., Jia, P., Zhou, Y., 2022. Combining renewable eleostearic acid and eugenol to fabricate sustainable plasticizer and its effect of plasticizing on PVC. J. Polym. Environ. 30, 2099–2108. https://doi.org/10.1007/s10924-021-02341-w.

Mani, S., Cosgrove, D.J., Voth, G.A., 2020. Anisotropic motions of fibrils dictated by their orientations in the lamella: a coarse-grained model of a plant cell wall. J. Phys. Chem. B 124, 3527–3539. https://doi.org/10.1021/acs.jpcb.0c01697.

Marriott, P.E., Gómez, L.D., Mcqueen-Mason, S.J., 2016. Unlocking the potential of lignocellulosic biomass through plant science. N. Phytol. 209, 1366–1381. https://doi.org/10.1111/nph.13684.

Martínez-Sanz, M., Lopez-Sanchez, P., Gidley, M.J., Gilbert, E.P., 2015. Evidence for differential interaction mechanism of plant cell wall matrix polysaccharides in hierarchically-structured bacterial cellulose. Cellulose 22, 1541–1563. https://doi.org/10.1007/s10570-015-0614-2.

Martínez-Sanz, M., Gidley, M.J., Gilbert, E.P., 2016. Hierarchical architecture of bacterial cellulose and composite plant cell wall polysaccharide hydrogels using small angle neutron scattering. Soft Matter 12, 1534–1549. https://doi.org/10.1039/c5sm02085a.

Martínez-Sanz, M., Pettolino, F., Flanagan, B., Gidley, M.J., Gilbert, E.P., 2017. Structure of cellulose microfibrils in mature cotton fibres. Carbohydr. Polym. 175, 450–463. https://doi.org/10.1016/j.carbpol.2017.07.090.

Mathlouthi, M., Koenig, J.L., 1987. Vibrational spectra of carbohydrates. Adv. Carbohydr. Chem. Biochem. 44, 7–89. https://doi.org/10.1016/S0065-2318(08)60077-3.

Mikkelsen, D., Gidley, M.J., 2010. Formation of cellulose-based composites with hemicelluloses and pectins using gluconacetobacter fermentation. Plant Cell Wall 197–208. https://doi.org/10.1007/978-1-61779-008-9.

Mikkonen, K.S., Pitkänen, L., Liljeström, V., Mabasa Bergström, E., Serimaa, R., Salmén, L., Tenkanen, M., 2012. Arabinoxylan structure affects the reinforcement of films by microfibrillated cellulose. Cellulose 19, 467–480. https://doi.org/10.1007/s10570-012-9655-y.

Moreira, L.R.S., Filho, E.X.F., 2008. An overview of mannan structure and mannan-degrading enzyme systems. Appl. Microbiol. Biotechnol. 79, 165–178. https://doi.org/10.1007/s00253-008-1423-4.

Müller, K., Zollfrank, C., Schmid, M., 2019. Natural polymers from biomass resources as feedstocks for thermoplastic materials. Macromol. Mater. Eng. 304, 1–17. https://doi.org/10.1002/mame.201800760.

Park, Y.B., Cosgrove, D.J., 2012. Changes in cell wall biomechanical properties in the xyloglucan-deficient xxt1/xxt2 mutant of Arabidopsis. Plant Physiol. 158, 465–475. https://doi.org/10.1104/pp.111.189779.

Park, Y.B., Cosgrove, D.J., 2015. Xyloglucan and its interactions with other components of the growing cell wall. Plant Cell Physiol. 56, 180–194. https://doi.org/10.1093/pcp/pcu204.

Pauly, M., Albersheim, P., Darvill, A., York, W.S., 1999. Molecular domains of the cellulose/xyloglucan network in the cell walls of higher plants. Plant J. 20, 629–639. https://doi.org/10.1046/j.1365-313X.1999.00630.x.

Peng, J., Peng, S., Jiang, A., Wei, J., Li, C., Tan, J., 2010. Asymmetric least squares for multiple spectra baseline correction. Anal. Chim. Acta 683, 63–68. https://doi.org/10.1016/j.aca.2010.08.033.

Portela, R., Leal, C.R., Almeida, P.L., Sobral, R.G., 2019. Bacterial cellulose: a versatile biopolymer for wound dressing applications. Microb. Biotechnol. 12, 586–610. https://doi.org/10.1111/1751-7915.13392.

Qaseem, M.F., Shaheen, H., Wu, A.M., 2021. Cell wall hemicellulose for sustainable industrial utilization. Renew. Sustain. Energy Rev. 144, 110996 https://doi.org/10.1016/j.rser.2021.110996.

Ralph, J., Quideau, S., Grabber, J.H., Hatfield, R.D., 1994. Identification and synthesis of new ferulic acid dehydrodimers present in grass cell Walls. J. Chem. Soc. Perkin Trans. 1 (23), 3485–3498. https://doi.org/10.1039/P19940003485.

Scheller, H.V., Ulvskov, P., 2010. Hemicelluloses. Annu. Rev. Plant Biol. 61, 263–289. https://doi.org/10.1146/annurev-arplant-042809-112315.

Schenzel, K., Fischer, S., 2001. NIR FT Raman spectroscopy - a rapid analytical tool for detecting the transformation of cellulose polymorphs. Cellulose 8, 49–57. https://doi.org/10.1023/A:1016616920539.

Srivastava, V., McKee, L.S., Bulone, V., 2017. Plant Cell Walls, in: ELS. Chichester, pp. 1–17. https://doi.org/10.1002/9780470015902.a0001682.pub3.

Stepan, A.M., Ansari, F., Berglund, L., Gatenholm, P., 2014. Nanofibrillated cellulose reinforced acetylated arabinoxylan films. Compos. Sci. Technol. 98, 72–78. https://doi.org/10.1016/j.compscitech.2014.04.010.

Stevanic, J.S., Bergström, E.M., Gatenholm, P., Berglund, L., Salmén, L., 2012. Arabinoxylan/nanofibrillated cellulose composite films. J. Mater. Sci. 47, 6724–6732. https://doi.org/10.1007/s10853-012-6615-8.

Sundberg, J., Toriz, G., Gatenholm, P., 2015. Effect of xylan content on mechanical properties in regenerated cellulose/xylan blend films from ionic liquid. Cellulose 22, 1943–1953. https://doi.org/10.1007/s10570-015-0606-2.

Szymańska-Chargot, M., Chylińska, M., Cybulska, J., Kozioł, A., Pieczywek, P.M., Zdunek, A., 2017. Simultaneous influence of pectin and xyloglucan on structure and mechanical properties of bacterial cellulose composites. Carbohydr. Polym. 174, 970–979. https://doi.org/10.1016/j.carbpol.2017.07.004.

Szymańska-Chargot, M., Chylińska, M., Pieczywek, P.M., Rösch, P., Schmitt, M., Popp, J., Zdunek, A., 2016. Raman imaging of changes in the polysaccharides distribution in the cell wall during apple fruit development and senescence. Planta 243, 935–945. https://doi.org/10.1007/s00425-015-2456-4.

Szymańska-Chargot, M., Cybulska, J., Zdunek, A., 2011. Sensing the structural differences in cellulose from apple and bacterial cell wall materials by Raman and FT-IR Spectroscopy. Sensors 11, 5543–5560. https://doi.org/10.3390/s110605543.

Szymańska-Chargot, M., Pękala, P., Myśliwiec, D., Cieśla, J., Pieczywek, P.M., Siemińska-Kuczer, A., Zdunek, A., 2024. A study of the properties fo hemicelluloses adsorbed onto microfibrillar cellulose isolated from apple parenchyma. Food Chem. 1, 137116 https://doi.org/10.2139/ssrn.4424833.

Tashiro, K., Kobayashi, M., 1991. Theoretical evaluation of three-dimensional elastic constants of native and regenerated celluloses: role of hydrogen bonds. Polymer 32, 1516–1526. https://doi.org/10.1016/0032-3861(91)90435-L.

Tokoh, C., Takabe, K., Fujita, M., Saiki, H., 1998. Cellulose synthesized by Acetobacter xylinum in the presence of acetyl glucomannan. Cellulose 5, 249–261. https://doi.org/10.1023/A:1009211927183.

Trovatti, E., Fernandes, S.C.M., Rubatat, L., Freire, C.S.R., Silvestre, A.J.D., Neto, C.P., 2012. Sustainable nanocomposite films based on bacterial cellulose and pullulan. Cellulose 19, 729–737. https://doi.org/10.1007/s10570-012-9673-9.

Wang, J., Chen, X., Zhang, C., Rehman, A., 2019. Transparent konjac gluconannan / cellulose nanofibril composite films with improved mechanical properties and thermal stabilit. Cellulose 26, 3155–3165. https://doi.org/10.1007/s10570-019-02302-6.

Whitney, S.E.C., Brigham, J.E., Darke, A.H., Reid, J.S.G., Gidley, M.J., 1995. In vitro assembly of cellulose/xyloglucan networks: ultrastructural and molecular aspects. Plant J. 8, 491–504. https://doi.org/10.1046/j.1365-313X.1995.8040491.x.

Whitney, S.E.C., Brigham, J.E., Darke, A.H., Reid, J.S.G., Gidley, M.J., 1998. Structural aspects of the interaction of mannan-based polysaccharides with bacterial cellulose. Carbohydr. Res. 307, 299–309. https://doi.org/10.1016/S0008-6215(98)00004-4.

Wu, X., Moon, R.J., Martini, A., 2014. Tensile strength of Iβ crystalline cellulose predicted by molecular dynamics simulation. Cellulose 21, 2233–2245. https://doi.org/10.1007/s10570-014-0325-0.

Yu, J., Zhu, Y., Ma, H., Liu, L., Hu, Y., Xu, J., Wang, Z., Fan, Y., 2019. Contribution of hemicellulose to cellulose nanofiber-based nanocomposite films with enhanced strength, flexibility and UV-blocking properties. Cellulose 26, 6023–6034. https://doi.org/10.1007/s10570-019-02518-6.

Zahan, K.A., Azizul, N.M., Mustapha, M., Tong, W.Y., Rahman, M.S.A., Sahuri, I.S., 2020. Application of bacterial cellulose film as a biodegradable and antimicrobial packaging material. Mater. Today Proc. 31, 83–88. https://doi.org/10.1016/j.matpr.2020.01.201.

Zhang, B., Gao, Y., Zhang, L., Zhou, Y., 2021. The plant cell wall: Biosynthesis, construction, and functions. J. Integr. Plant Biol. 63, 251–272. https://doi.org/10.1111/jipb.13055.

Zhang, P., Whistler, R.L., 2004. Mechanical properties and water vapor permeability of thin film from corn hull arabinoxylan. J. Appl. Polym. Sci. 93, 2896–2902. https://doi.org/10.1002/app.20910.

Zhang, Y., Yu, J., Wang, X., Durachko, D.M., Zhang, S., Cosgrove, D.J., 2021. Molecular insights into the complex mechanics of plant epidermal cell walls. Science 372, 706–711. https://doi.org/10.1126/science.abf2824.

Zheng, Y., Wang, X., Chen, Y., Wagner, E., Cosgrove, D.J., 2018. Xyloglucan in the primary cell wall: assessment by FESEM, selective enzyme digestions and nanogold affinity tags. Plant J. 93, 211–226. https://doi.org/10.1111/tpj.13778.

6.3.3. Supplementary Materials of the manuscript P3

Evaluation of elasto-plastic properties of bacterial cellulose-hemicellulose composite films

Vadym Chibrikov*, Piotr Mariusz Pieczywek, Justyna Cybulska, Artur Zdunek

Institute of Agrophysics, Polish Academy of Sciences, Doświadczalna 4 Str., Lublin 20-290, Poland

*corresponding author: Vadym Chibrikov, Institute of Agrophysics, Polish Academy of Sciences, Doświadczalna 4 *Str.*, 20–290 Lublin, Poland, e-mail: v.chibrikov@ipan.lublin.pl

ORCID
Vadym Chibrikov https://orcid.org/0000-0002-2007-3800
Piotr Mariusz Pieczywek https://orcid.org/0000-0002-3986-3802
Justyna Cybulska https://orcid.org/0000-0003-3323-4535
Artur Zdunek https://orcid.org/0000-0001-9395-1486

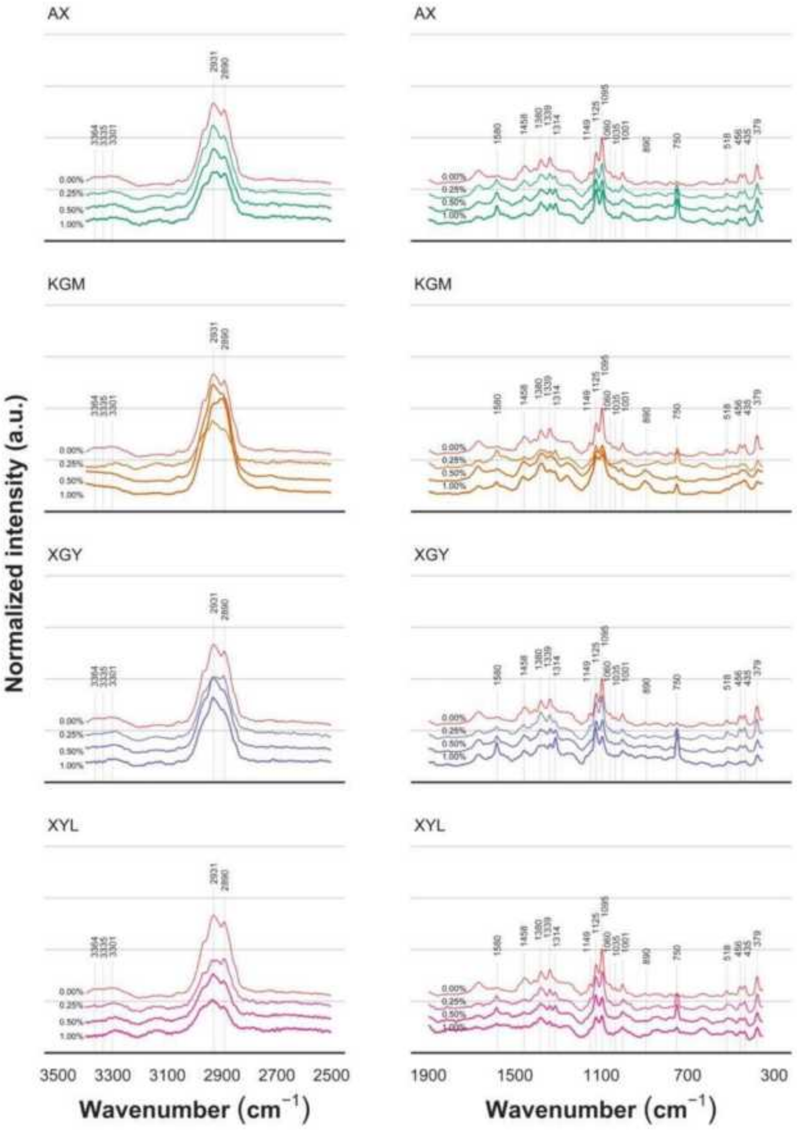

Fig.S1. Averaged Raman spectra of bacterial cellulose composite films with: arabinoxylan (AX), glucomannan (KGM), xyloglucan (XGY) and xylan (XYL). Spectra were shifted vertically according to the concentration of hemicellulose polysaccharide in culturing medium. Concentration of hemicellulose polysaccharide in culturing medium is marked with % mass annotation on left side of specific single spectra. Control sample (0.00% mass of hemicellulose polysaccharide) is marked with the red color. Characteristic spectra wavenumbers were assigned and highlighted with dashed lines.

Table S1. Summary of specific Raman wavenumbers and bond assignments of bacterial cellulose-hemicellulose composite films.

Wavenumber, cm^{-1}	**Assignment**	**Reference**
Hydrogen bond vibrations		
3364	O-H stretching vibrations of hydroxyl groups; Inter- and intramolecular hydrogen bonds	[1,2]
3335	O-H stretching vibrations of hydroxyl groups; Inter- and intramolecular hydrogen bonds	[1]
3301	O-H stretching vibrations of hydroxyl groups; Inter- and intramolecular hydrogen bonds	[1]
Ring bond vibrations		
2931	C-H and H-C-H stretching vibrations	[3,4]
2890	C-H and H-C-H stretching vibrations	[5–7]
1458	H-C-H scissoring bending vibrations	[6–13]
1380	H-C-H, H-C-C, H-O-C, and C-O-H bending vibrations	[1,6,7,12–15]
1339	H-C-H wagging bending vibrations, H-C-C, H-C-O, and C-O-H bending vibrations	[1,12,15]
1314	H-C-H wagging bending vibrations, H-C-C, H-C-O, and C-O-H bending vibrations	[1,4,5,7,12,13, 16,17]
1149	C-C, and C-O asymmetric stretching vibrations	[1,5,6,12]
1060	C-C, and C-O stretching vibrations	[15]
1035	C-C, and C-O stretching vibrations	[12]
1001	H-C-H rocking bending vibrations	[1,4,6,9]
456	C-C-C, and C-C-O bending vibrations	[1,6,12]
435	C-C-C, and C-C-O bending vibrations	[1,6,12]
379	C-C-C, C-O, and C-C-O bending vibrations	[1,6,12,16–18]
Glucosidic bond vibrations		
1125	C_1-O-C_4 symmetric stretching vibrations	[1,6,11,12,15]

1095	C_1-O-C_4 asymmetric stretching vibrations	[1,6,14,15,19,20]
890	C_1-O-C_4 stretching vibrations	[11,16,18]
518	C_1-O-C_4 bending vibrations	[6,12]
Other saccharides		
1580	C=O stretching vibrations of galactose	[7]
750	C-O-H, C-C-H, and O-C-H bending vibrations of arabinose/galactose/xylose	[7,21]

References

[1] M. Szymańska-Chargot, J. Cybulska, A. Zdunek, Sensing the structural differences in cellulose from apple and bacterial cell wall materials by Raman and FT-IR Spectroscopy, Sensors. 11 (2011) 5543–5560. https://doi.org/10.3390/s110605543.

[2] L.X. Wang, A.R. Lee, Y. Yuan, X.M. Wang, T.J. Lu, Preparation and FTIR, Raman and SEM characterizations of konjac glucomannan-KCl electrogels, Food Chem. 331 (2020) 127289. https://doi.org/10.1016/j.foodchem.2020.127289.

[3] D.S. Himmelsbach, S. Khahili, D.E. Akin, Near-infrared - Fourier-transform - Raman microspectroscopic imaging of flax stems, Vib. Spectrosc. 19 (1999) 361–367. https://doi.org/10.1016/S0924-2031(98)00065-4.

[4] M. Kačuráková, N. Wellner, A. Ebringerová, Z. Hromádková, R.H. Wilson, P.S. Belton, Characterisation of xylan-type polysaccharides and associated cell wall components by FT-IR and FT-Raman spectroscopies, Food Hydrocoll. 13 (1999) 35–41. https://doi.org/10.1016/S0268-005X(98)00067-8.

[5] D. Naumann, FT-infrared and FT-Raman spectroscopy in biomedical research, Appl. Spectrosc. Rev. 36 (2001) 239–298. https://doi.org/10.1081/ASR-100106157.

[6] L. Cabrales, N. Abidi, F. Manciu, Characterization of developing cotton fibers by confocal Raman microscopy, Fibers. 2 (2014) 285–294. https://doi.org/10.3390/fib2040285.

[7] D.S. Himmelsbach, D.E. Akin, Near-Infrared Fourier-Transform Raman Spectroscopy of Flax (Linum usitatissimum L.) Stems, J. Agric. Food Chem. 46 (1998) 991–998. https://doi.org/10.1021/jf970656k.

[8] M. Szymańska-Chargot, M. Chylińska, J. Cybulska, A. Kozioł, P.M. Pieczywek, A. Zdunek,

Simultaneous influence of pectin and xyloglucan on structure and mechanical properties of bacterial cellulose composites, Carbohydr. Polym. 174 (2017) 970–979. https://doi.org/10.1016/j.carbpol.2017.07.004.

[9] K. Schenzel, S. Fischer, E. Brendler, New method for determining the degree of cellulose I crystallinity by means of FT Raman spectroscopy, Cellulose. 12 (2005) 223–231. https://doi.org/10.1007/s10570-004-3885-6.

[10] N. Atykyan, V. Revin, V. Shutova, Raman and FT-IR Spectroscopy investigation the cellulose structural differences from bacteria Gluconacetobacter sucrofermentans during the different regimes of cultivation on a molasses media, AMB Express. 10 (2020) 1–11. https://doi.org/10.1186/s13568-020-01020-8.

[11] H. Schulz, M. Baranska, Identification and quantification of valuable plant substances by IR and Raman spectroscopy, Vib. Spectrosc. 43 (2007) 13–25. https://doi.org/10.1016/j.vibspec.2006.06.001.

[12] K. Schenzel, S. Fischer, NIR FT Raman spectroscopy - A rapid analytical tool for detecting the transformation of cellulose polymorphs, Cellulose. 8 (2001) 49–57. https://doi.org/10.1023/A:1016616920539.

[13] M. Chylińska, M. Szymańska-Chargot, A. Zdunek, FT-IR and FT-Raman characterization of non-cellulosic polysaccharides fractions isolated from plant cell wall, Carbohydr. Polym. 154 (2016) 48–54. https://doi.org/10.1016/j.carbpol.2016.07.121.

[14] N. Gierlinger, M. Schwanninger, The potential of Raman microscopy and Raman imaging in plant research, Spectroscopy. 21 (2007) 69–89. https://doi.org/10.1155/2007/498206.

[15] I. Zeise, Z. Heiner, S. Holz, M. Joester, C. Büttner, J. Kneipp, Raman imaging of plant cell walls in sections of cucumis sativus, Plants. 7 (2018) 1–16. https://doi.org/10.3390/plants7010007.

[16] U.P. Agarwal, S.A. Ralph, FT-Raman spectroscopy of wood: Identifying contributions of lignin and carbohydrate polymers in the spectrum of black spruce (Picea mariana), Appl. Spectrosc. 51 (1997) 1648–1655. https://doi.org/10.1366/0003702971939316.

[17] Y. Zeng, J.M. Yarbrough, A. Mittal, M.P. Tucker, T.B. Vinzant, S.R. Decker, M.E. Himmel, In situ label-free imaging of hemicellulose in plant cell walls using stimulated Raman scattering microscopy, Biotechnol. Biofuels. 9 (2016) 1–16. https://doi.org/10.1186/s13068-016-0669-9.

[18] U.P. Agarwal, 1064 nm FT-Raman spectroscopy for investigations of plant cell walls and other

biomass materials, Front. Plant Sci. 5 (2014) 1–12. https://doi.org/10.3389/fpls.2014.00490.

[19] Y.C. Hsieh, H. Yano, M. Nogi, S.J. Eichhorn, An estimation of the Young's modulus of bacterial cellulose filaments, Cellulose. 15 (2008) 507–513. https://doi.org/10.1007/s10570-008-9206-8.

[20] N. Gierlinger, T. Keplinger, M. Harrington, Imaging of plant cell walls by confocal Raman microscopy, Nat. Protoc. 7 (2012) 1694–1708. https://doi.org/10.1038/nprot.2012.092.

[21] M. Mathlouthi, J.L. Koenig, Vibrational spectra of carbohydrates, Adv. Carbohydr. Chem. Biochem. 44 (1987) 7–89. https://doi.org/10.1016/S0065-2318(08)60077-3.

6.4. Manuscript P4

6.4.1. Graphical abstract of the manuscript P4

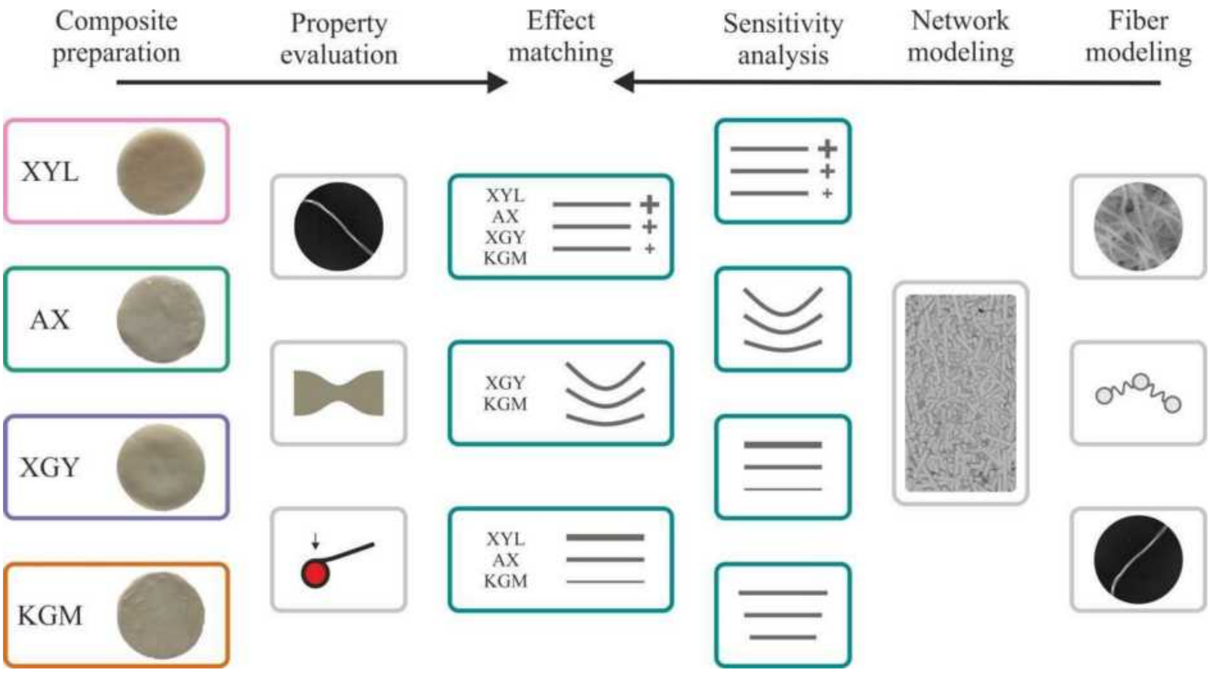

6.4.2. Content of the manuscript P4

Carbohydrate Polymers 330 (2024) 121827

Contents lists available at ScienceDirect

Carbohydrate Polymers

journal homepage: www.elsevier.com/locate/carbpol

Coarse-grained molecular dynamics model to evaluate the mechanical properties of bacterial cellulose–hemicellulose composites

Vadym Chibrikov, Piotr Mariusz Pieczywek, Justyna Cybulska, Artur Zdunek*

Institute of Agrophysics, Polish Academy of Sciences, Doświadczalna 4 Str., 20-290 Lublin, Poland

ARTICLE INFO

Keywords:
Cellulose, hemicellulose
Composite
Structure
Mechanical properties
Computational model

ABSTRACT

The plant cell wall (PCW) inspires the preparation of fiber-based biomaterials, particularly emphasizing exploiting the intrinsic interactions within the load-bearing cellulose and hemicellulose network. Due to experimental difficulties in studying and interpreting the interaction between these polysaccharides, this research presents a numerical model based on coarse-grained molecular dynamics that evaluates the mechanical properties of fiber composites. To validate the model and explain the structural and mechanical role of hemicelluloses, bacterial cellulose (BC) was synthesized in the presence of different concentrations of xylan, arabinoxylan, xyloglucan, or glucomannan and subjected to nano- and macroscale structural and mechanical characterization. The data obtained were used to interpret the effects of each hemicellulose on the mechanics of the BC–hemicellulose composite based on the sensitivity of the model. The mechanical properties of the resulting simulated networks agreed well with the experimental observations of the BC–hemicellulose composites. Increased xylan and arabinoxylan contents increased the macroscale mechanical properties, fiber modulus (xylan), and fiber width (arabinoxylan). The addition of xyloglucan increased the mechanical properties of the composites in the elastic deformation phase, associated with an increase in the fiber modulus. Adding glucomannan to the culture medium decreased all the mechanical properties studied while the fiber width increased.

1. Introduction

The primary plant cell wall (PCW) is a complex structure composed predominantly of cellulose, hemicelluloses, and pectins, which largely determine its morphogenesis, architecture, and mechanical properties (Zhang, Gao, et al., 2021). Because it is probably the most complex fiber network in nature, there are still inconsistencies regarding the relationships between the structure and the properties of cellulose–hemicellulose fiber networks in PCW, which have been debated since the late 1960^{s} (Carpita & Gibeaut, 1993; Keegstra et al., 1973; Park, Cosgrove, 2012a, 2012b; Talbott & Ray, 1992). Presently, it is thought that cellulose is the main load-bearing component of cellulose–hemicellulose fiber networks, while the key component of their mechanical performance, interfiber adhesion, is determined by hemicellulose-mediated interactions (Dolan et al., 2019; Park, Cosgrove, 2012b).

The evaluation of cellulose–hemicellulose interaction patterns has been severely limited by the experimental techniques used, which make results variable- and context-dependent (Bidhendi & Geitmann, 2019). Sample processing is also challenging in nanoscale studies, and even when processing is successful, the results are mainly site-dependent (Yakubov et al., 2016). The development of composites of interconnected bacterial cellulose (BC) and PCW hemicelluloses can serve as a tool to achieve a simplified macroscale representation of PCW-like cellulose–hemicellulose fiber networks that have a homogeneous structure and are reproducible (S. Q. Chen et al., 2017). Numerous BC–hemicellulose composites have been investigated, such as BC–xyloglucan, BC–xylan, and BC–xyloglucan–pectin (Cybulska et al., 2010; Dammström et al., 2009; Szymańska-Chargot et al., 2017). This approach allowed to catalog the effects of the main PCW constituents on the structure and mechanical properties of the abovementioned hemicelluloses and define the mechanisms of their interaction with cellulose (Chibrikov et al., 2022; Zhang et al., 2023). Recent studies have reported the tunable elasto-plastic properties of BC–hemicellulose fiber networks, depending on the specific type and amount of the hemicellulose additive (Chibrikov et al., 2023).

Despite the promising results, conventional laboratory techniques cannot explain the phenomenon of the formation of

---

* Corresponding author.

E-mail addresses: v.chibrikov@ipan.lublin.pl (V. Chibrikov), p.pieczywek@ipan.lublin.pl (P.M. Pieczywek), j.cybulska@ipan.lublin.pl (J. Cybulska), a.zdunek@ipan.lublin.pl (A. Zdunek).

https://doi.org/10.1016/j.carbpol.2024.121827
Received 13 November 2023; Received in revised form 29 December 2023; Accepted 12 January 2024

cellulose–hemicellulose interactions or determine their localization, density, and strength trends. Here, *in silico* numerical modeling allows the approximation of the structure and mechanical properties of cellulose–hemicellulose fiber networks with respect to selected parameters (Pieczywek et al., 2023). Recent data on the simulation of cellulose–hemicellulose and cellulose–hemicellulose–pectin fiber networks have allowed the evaluation of the effect of fiber orientation on network stiffness (Kha et al., 2008) and the role of cellulose–hemicellulose interactions (Yi & Puri, 2012, 2014) and hydrogen bonding (Jin et al., 2015; Nili et al., 2015) on the mechanical properties of the network. Most recent studies in this field have focused on exploring the effects of the physicochemical properties of cellulose and hemicellulose (Mani et al., 2020; Zhang et al., 2021) and the role of structural order (Nili et al., 2015; Zhang et al., 2021) on the mechanobiology of the fiber network. It allowed us to consider that understanding of the effects of interfiber adhesion and the nature of cellulose–hemicellulose interactions on the overall mechanical properties of cellulose–hemicellulose fiber networks should be possible with a simple but comprehensive model, which was a hypothesis of the current study.

Inspired by PCW cellulose–hemicellulose fiber networks, we present a new numerical model to evaluate their mechanical properties here. The effects of hemicellulose in BC on the mechanical properties of the network are simulated by changing the structural (length, diameter) and mechanical (force constant, modulus) parameters of the individual fibers in the networks. The mechanical properties of the simulated fiber networks are validated against the nano- and macroscale structural and mechanical properties of BC–hemicellulose composites, depending on the specific type and amount of added hemicellulose. Good agreement between simulations and experiments allowed an indication of the structure- and property-dependent mechanisms of the mechanical response of cellulose–hemicellulose fiber networks, suggesting the specific role of the hemicellulose. To the best of our knowledge, this is the only study that combines experimental data with numerical modeling to investigate the explicit role of hemicelluloses on the mechanical properties of BC-hemicellulose composites.

2. Materials and methods

2.1. Numerical modeling

Numerical models were built following the principles of coarse-grained molecular dynamics, with fibers modeled using the bead–spring approach (Joshi & Deshmukh, 2021). The fibers were modeled as chains of interconnected rigid spheres, that is, the beads. The harmonic bonds and angular potentials formed between adjacent beads were used to simulate the axial and bending stiffness of the fibers. Torsional stiffness was not considered in the present model. The harmonic potentials were set according to the mechanical and geometrical properties of the fiber (fiber diameter, length of the fiber segment between two beads, and Young's modulus). All fibers had the same Young's modulus and diameter. The interfiber non-bonded interactions were modeled with simple two-stage truncated harmonic potentials, which included an adhesion phase for fibers in close proximity (at a distance of less than −1.5 nm) and a repulsion phase resulting from the physical contact of the fibers. The introduced interaction model allowed fibers to slide, adhere to each other, and detach under applied stress. The interfiber interactions were used to indirectly simulate the presence of hemicelluloses in the system, which alter the interfiber adhesive forces (Dolan et al., 2019; Neuman et al., 1993). A narrow range of inter-fiber non-bonded interactions was chosen to mimic the interactions of the biomechanical hotspot model, in which the extensibility of the fiber network is defined by hemicellulose-mediated load-bearing junctions (Park, Cosgrove, 2012a).

The fiber network model was created using a stochastic process in which a specific set of fibers was generated under a set of constraints that forced the fibers to lie in specific directions or occupy a specific volume of space. The fibers were generated to fill 20 % of the volume of a cuboidal space with predefined dimensions of $4\ \mu m \times 8\ \mu m \times 1\ \mu m$, and no treatment of the solvent was introduced to the current model. Initially, the fibers were allowed to overlap. The final geometry was determined in the energy equilibration phase of the simulation, where the model was not deformed, and the fibers were allowed to move freely. An equilibration scheme allowed overlapping fibers to move apart and maintain a stable low-energy model geometry (Fig. 1). The code repository of the stochastic generator is available online (Pieczywek, 2023a).

Finally, the equilibrated models were used to simulate a uniaxial tensile test at a strain up to 5 % of the initial value (Fig. 1,E). The simulations were designed to ensure the comparability of the conditions of a laboratory test. Therefore, all the beads near the edges (0.5 μm each) of the model parallel to the X-axis were fixed. The velocity of the beads on the opposite side of the model was set to a constant value along the Y-axis to simulate the motion of the tensile testing machine clamps. The velocity was set to simulate sample deformation at a strain rate of $-1.5 \times 10^5\ s^{-1}$, and the time step of simulation was set as −0.1 ps. The code repository for the model is available online (Pieczywek, 2023b).

Sensitivity analysis was performed with respect to the four input parameters considered to have a significant effect on the tensile response of the cellulose-based networks (Zhang et al., 2021): fiber diameter (45–55 nm), fiber length (1.5–3.5 μm), fiber modulus (95–155 GPa) as a descriptor of fiber stiffness, and the force constant of interfiber interaction (82–411 N/m). The input parameters of fiber diameter, fiber length, and fiber modulus were chosen as the one commonly reported for cellulose and bacterial cellulose (Cheng et al., 2009; Chibrikov et al., 2022; Guhados et al., 2005).

The final stress–strain curves (Fig. 1,A) were used to determine the Young's modulus, strain hardening modulus, strain at elastic limit, stress at elastic limit, and maximum stress of the simulated network.

The mechanical properties obtained for the simulated network were used to interpret the influence of hemicelluloses on the mechanical properties of BC–hemicellulose composites. For more information on the construction of the numerical model, see the section "Definition of fiber network model" in the Supplementary Materials.

2.2. Sample material

2.2.1. Bacterial cellulose–hemicellulose composites

Bacterial cellulose–hemicellulose composites were prepared in Hestrin–Schramm (HS) medium (Hestrin & Schramm, 1954) modified according to Cybulska et al. (Cybulska et al., 2010). Pure BC was prepared in HS medium, containing 2 % mass glucose (Sigma-Aldrich, St. Louis, Missouri, USA), 0.5 % mass casein peptone (Sigma-Aldrich, St. Louis, Missouri, USA), 0.5 % mass yeast extract (Thermo Fisher Scientific, Waltham, Massachusetts, USA), 0.27 % mass anhydrous disodium phosphate (Sigma-Aldrich, St. Louis, Missouri, USA), and 0.115 % mass citric acid monohydrate (Chempur, Piekary Śląskie, Poland), dissolved in deionized water. The pH of the culture medium was then adjusted to 5.0 by adding 1 M NaOH/HCl. For the preparation of BC–hemicellulose composites, the HS medium was modified by adding four different hemicelluloses: tamarind xyloglucan (P-XYGLN, > 95 % purity, Megazyme, Bray, Ireland), beechwood xylan (P-XYLNBE-10G, > 95 % purity, Megazyme, Bray, Ireland), medium-viscosity wheat flour arabinoxylan (P-WAXYL, > 95 % purity, Megazyme, Bray, Ireland), and low-viscosity konjac glucomannan (P-GLCML, > 98 % purity, Megazyme, Bray, Ireland) at three different concentrations, 0.25 %, 0.50 %, and 1.00 % by mass. The monosaccharide composition and the weight average molecular weight of the hemicelluloses used in this study is shown in Table 1.

The HS and hemicellulose-modified media were autoclaved at 121 °C for 11 min and then brought to room temperature (Mikkelsen & Gidley, 2010). The inoculum was prepared by seeding 2 mg of a two-day fresh

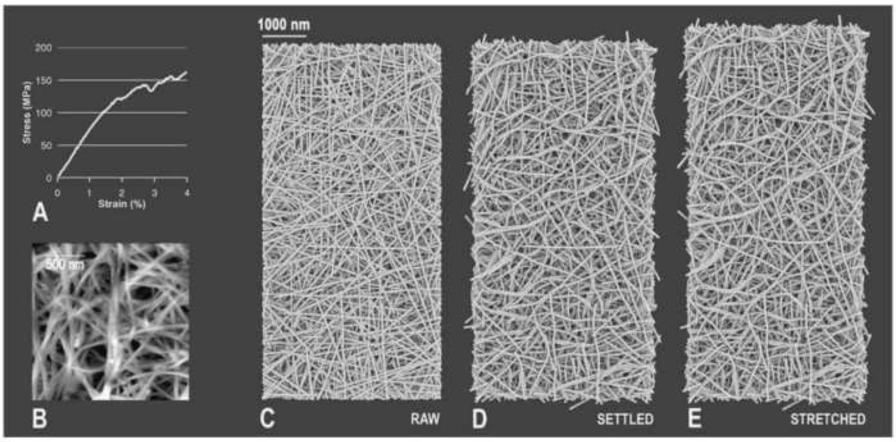

Fig. 1. Stages of fiber network modeling: a) stress–strain curve from simulation, b) atomic force microscopy surface topography image of pure BC, c) raw model of BC generated based on atomic force microscopy (AFM) data, d) model of BC after energy equilibration procedure, and e) model of BC subjected to uniaxial tensile test at constant strain rate.

Table 1
Monosaccharide composition and molecular weight of hemicelluloses, used in current study. Abbreviation of *Araf* stands for arabinose, *Gal* – galactose, *Glc* – glucose, *GlcA* – glucuronic acid, *Man* – mannose, *Xyl* – xylose. Weight average molecular weight was determined by gel permeation chromatography. Asterisk * refers to data from (Franková & Fry, 2021).

Type of hemicellulose	Monosaccharide composition (% mass)							*Weight average molecular weight (kDa)*
	Araf	*Gal*	*Glc*	*GlcA*	*Man*	*Xyl*	*Other*	
Xylan				11.3		86.1	2.6	158.3
Arabinoxylan	37.8					61.7	0.5	323.0
Xyloglucan	2.0	17.0	45.0			34.0	2.0	802.5
Glucomannan			40.0		60.0			950.0*

colony of *Komataeibacter xylinum* ATCC-53524 (LGC Standards, Teddington, UK) bacteria strain in 50 mL of the medium. The BC–hemicellulose composites were produced statically at 30 ± 1 °C for 240 h to obtain flat sheets. Subsequently, the BC–hemicellulose composites were washed in deionized water for 96 h to ensure the removal of the medium, as well as any loosely attached hemicelluloses (Whitney et al., 2006). After washing, the BC–hemicellulose composites were dried in an oven at 40 ± 1 °C to constant mass. The dried BC–hemicellulose composites were stored in the dark at 20 ± 1 °C and 33 % ± 2 % relative humidity before further analysis.

2.2.2. Cellulose fibers

To obtain single cellulose fibers, a piece of never-dried BC–hemicellulose composites with a mass of 0.05 ± 0.01 g was placed in 5 mL of high-performance liquid chromatography (HPLC) -grade water (Chempur, Piekary Śląskie, Poland). Subsequently, the samples were treated with a high-intensity ultrasonic processor (Sonics & Materials, Newtown, Connecticut, USA) for 30 min. The resulting aqueous suspension of the individual cellulose fibers of each composite was spin-coated onto freshly cleaved muscovite mica (Electron Microscopy Sciences, Hatfield, Pennsylvania, USA) in a volume of 5 μL. The prepared samples were stored in a desiccator for 16 h before further analysis.

2.3. Atomic force microscopy (AFM) surface topography imaging

Atomic force microscopy (AFM) surface topography imaging allowed the evaluation of the structural properties of individual fibers at the nanoscale. Images were acquired using a MultiMode 8-HR atomic force microscope (Bruker, Billerica, Massachusetts, USA) in ScanAsyst™ in Air mode. A silicon nitride cantilever with a nominal tip radius of 2 nm and a nominal frequency of 70 kHz was used. The total captured area for a single image was set to 2 × 2 μm with an image resolution of 1.95 nm per pixel. At least 30 images were acquired for each sample to obtain a representative number of data. The images were then subjected to procedure for automatic fiber tracking and measuring its structural parameters. Data from these measurements are provided in Fig. S1.

2.4. Nanoscale mechanical properties of single cellulose fibers

The mechanical properties of the single cellulose fibers of the BC–hemicellulose composites were determined by evaluating the fiber modulus as a Young's modulus of a single fiber with AFM nanoindentation tests using a MultiMode 8-HR atomic force microscope (Bruker, Billerica, Massachusetts, USA) in ScanAsyst™ in Air mode. A high-stiffness antimony-doped silicon cantilever with a nominal tip radius of 8 nm and a nominal frequency of 525 kHz was used. Before the nanoindentation tests, the cantilevers were pre-calibrated using the thermal tune method (Serry, 2005). The nanoindentation test included initial fiber mapping. Then, a set of indentation points was selected for the nanoindentation test. All indentation points tested were located in the center of the fiber lying directly on the mica. The minimum distance required from the fiber intersection or cap to the indentation point was at least 100 nm, as was the distance between two adjacent indentation points (Fig. 2a).

Data from at least 30 fibers were obtained for each sample. Indentation–force curves were extracted using the *NanoPlot* software

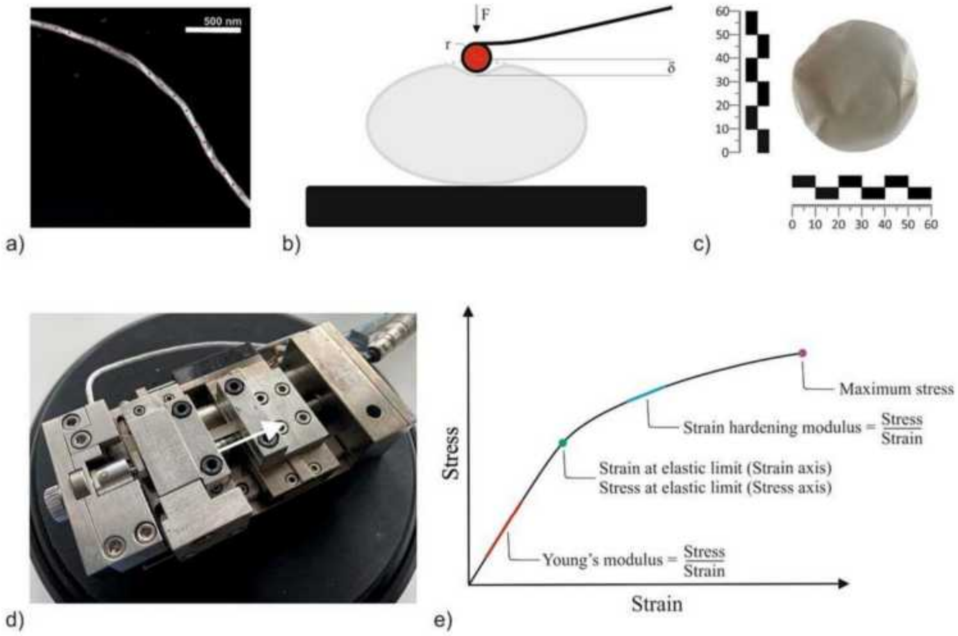

Fig. 2. Structural and mechanical properties of BC–hemicellulose composites on nano- and macroscale: a) AFM surface topography image of an individual cellulose fiber with indentation points (red) for the determination of the fiber modulus, b) cross-sectional graphical representation of the indenter–fiber interaction used to determine fiber modulus according to the Hertz model; cellulose fiber is represented in gray, AFM indenter in red, and the black quadrangle represents the mica surface, c) photograph of dried BC–hemicellulose composite on a millimeter-precision scale, d) photograph of tensile stage microtester for the evaluation of the macroscale mechanical properties of BC–hemicellulose composites with a mounted sample; arrow indicates the direction of sample stretching, and e) schematic stress–strain curve of BC–hemicellulose composites during uniaxial tensile test with constant strain rate; the colored lines and points define mechanical properties evaluated.

(Pieczywek, 2022a). Experimental data was fitted according to the Hertz model of the interaction between a parabolic indenter and an elastic half-space (Kontomaris, 2018), allowing to obtain the fiber modulus as the Young's modulus of a single fiber according to Eq. (1):

$$E = \frac{3 \times F}{4 \times \sqrt{r \times \delta} \times \delta \times (1 - \upsilon^2)}, \tag{1}$$

where E is Young's modulus, δ is the indentation depth (Fig. 2b), F is the force at indentation depth δ, r is the radius of the indenter, and υ is the Poisson's ratio (0.3 for microcrystalline cellulose). In this study, we defined E as the fiber modulus, assuming that in AFM nanoindentation, a hard sphere (cantilever) indents a thick plane (fiber) that is linearly elastic, homogeneous, and isotropic, allowing us to assume qualitative changes of the fiber modulus within the context of the laboratory experiment (Lekka, 2016; Zhou et al., 2021). For all measurements, the indentation depth δ was fixed as 1 nm to avoid the effects of the stiffness of the underlying mica substrate (Persch et al., 1994). Data from the corresponding measurements are shown in Fig. S2.

2.5. *Macroscale mechanical properties of BC–hemicellulose composites*

The macroscale mechanical properties of BC–hemicellulose composites were determined using a uniaxial tensile test with a constant strain rate. The composites (Fig. 2c) were cut into strips with an approximate width of 3 mm and length of 20 mm. The strip width was measured using an Olympus SZX16 microscope (Olympus Corporation, Tokyo, Japan) equipped with an SDF PLAPO 0.5XPF objective and a DMK 21 AU04 AS camera (The Imaging Source, Charlotte, North Carolina, USA). The thickness of each strip was measured using a BAKER IP54 digital micrometer (Baker Gauges Private Limited, Maharashtra, India). The uniaxial tensile tests with constant strain rate were performed using a tensile stage microtester (Deben Microtest, Suffolk, UK) equipped with a 200 N load cell (Fig. 2d). In a laboratory tests, 5 mm edges of each stripe parallel to the X-axis were fixed, giving 10 mm as an effective length of the stripe, capable for stretching.

The specimens were subjected to a uniaxial tensile test with a constant deformation rate of 1.67×10^{-6} m/s until failure, with 25 repetitions for each composite type. The Young's modulus of the fiber network, strain hardening modulus, stress and strain at elastic limit, and maximum stress were extracted using the Python procedure *TDA* (Pieczywek, 2022b). The experimental stress–strain curve of pure BC obtained using a uniaxial tensile test with a constant strain rate can be found in Fig. S3 of the Supplementary Materials. A schematic stress–strain curve with a graphical representation of the evaluated mechanical properties can be found in Fig. 2e.

2.6. *Data analysis*

Data analysis was performed using *RStudio v.4.1.1.* (Posit Software, Boston, Massachusetts, USA). The differences between the mechanical properties of the medium-cultured BC–hemicellulose composites and the fiber network models were analyzed using one-way analysis of variance (ANOVA) and the Tukey test for honestly significant differences at a significance level of $p = 0.05$.

3. Results and discussion

3.1. Models of BC–hemicellulose composites - sensitivity analysis

3.1.1. Effects of fiber modulus

An increase in fiber modulus led to an increase in the Young's modulus of the simulated network of fibers (Fig. 3). Similar to other models that consider realistic fiber geometry, the current model showed that the fibers undergo a series of movements during network deformation, including angular reorientation, straightening, curving, and sliding past each other (Mani et al., 2020; Zhang et al., 2021). Each of these deformations or displacements requires an additional force to be applied in the direction of the network deformation. Because stiffer fibers provide more resistance during deformation, the resulting Young's modulus of the network increases as the fiber modulus increases. Different conclusions have been reached by Yi and Puri, who observed a limited effect of fiber stiffness on the moduli of the network and assumed that the stiffness of the network is determined by its weakest component, hemicellulose cross-links (Yi & Puri, 2014). However, this model simulated fiber geometry as a linear beam and could not simulate fiber deformation, reorientation, or direct interactions. In addition, all fibers in the model were separated from each other and connected by hemicellulose cross-links. As more advanced models based on molecular dynamics show, overlooking these aspects can significantly affect the results obtained and lead to unrealistic estimates.

The strain hardening modulus and strain at elastic limit decreased with increasing fiber modulus (Fig. 3b,c), while the stress at elastic limit showed a moderate increase (Fig. 3d). What is of specific interest within the current study, is that transition to the plastic deformation phase requires reaching a tensile force that exceeds the interfiber attraction forces. Fiber slippage occurs once these attraction forces are exceeded, and the fibers slide past each other. Therefore, in this study, while fibers and, thus, the entire network became stiffer, the transition force was reached at lower strains compared to softer networks (Fig. 3c). Because the interfiber interactions mainly govern the tensile force at the transition to plastic deformation, the stress at elastic limit of the network changed little with increased fiber modulus (Fig. 3d). The tensile forces of fiber networks in the plastic deformation phase are mainly governed by interfiber interactions (Adler & Buehler, 2013; Zhang et al., 2021). Therefore, the observed decrease in strain hardening modulus could be due to the higher bending resistance of fibers, resulting in less entangled structures with fewer interactions with neighboring fibers in the plastic deformation phase. The increase in the Young's modulus of the network was compensated for by a decreased strain hardening modulus resulting fiber stiffening had no statistically significant effect on maximum stress of the network (Fig. 3e).

3.1.2. Effect of fiber diameter

In general, cellulose-based films and composites show increased mechanical properties in terms of stiffness and strength when composed of thinner fibers. This is mainly due to the larger surface area of thin fibers compared to thick fibers (Adusumali et al., 2006). In the present study, several models were built with fibers of different diameters, while the ratio between the volume occupied by the fibers and the total volume of the network was held constant. The range of tested diameters was chosen to correspond to the fiber diameters measured by AFM (Fig. S1).

The simulations showed that the fiber diameter had only a partial effect on the mechanical properties of the network (Fig. 4). An increase in fiber diameter resulted in a statistically significant decrease in the strain hardening modulus (Fig. 4b) of the network and a consequent decrease in the maximum stress (Fig. 4e). It was defined by the different structures of the established networks. Networks with lower average fiber diameters had a higher average number of contacts with adjacent fibers (20 contacts per fiber compared to 23 for fibers of 55- and 45-nm diameters, respectively). Another significant point for a fiber thinning in model is that the networks with thinner fibers were also more intertwined and contained more fibers. In addition, thicker fibers were less susceptible to bending and caused fewer interactions with adjacent fibers in the plastic deformation phase. All this resulted in a decreased strain hardening modulus with increased fiber diameter in the plastic deformation phase, in which the number of contacts between fibers and the interfiber interaction force is particularly important.

3.1.3. Effect of fiber length

An increase in the fiber length increased the evaluated values of all mechanical properties of the simulated fiber networks (Fig. 5). Longer fibers were able to interact with a greater number of adjacent fibers (an average of 17 contacts per fiber compared to 25 for 1.5- and 3.5-μm-long fibers, respectively). Hence, the trends in changes in mechanical properties were likely to reflect an increase in the force constant of interfiber interaction. A higher number of interactions between adjacent fibers led to an increase in Young's modulus (Fig. 5a) and strain hardening modulus (Fig. 5b). For the same reason, the stress at elastic limit also increased with an increasing fiber length (Fig. 5d).

During network reorganization, changes in angular orientation and fiber straightening were prolonged for longer fibers compared to shorter ones. Similar conclusions have been drawn by Zhang et al. based on studies of the distinctive movements of cellulose microfibers during uniaxial stretching of single lamellae of numerically generated cell wall-like structures (Zhang et al., 2021). This effect, coupled with the increased force constant of interfiber interaction, increased strain at elastic limit with increasing fiber length (Fig. 5c).

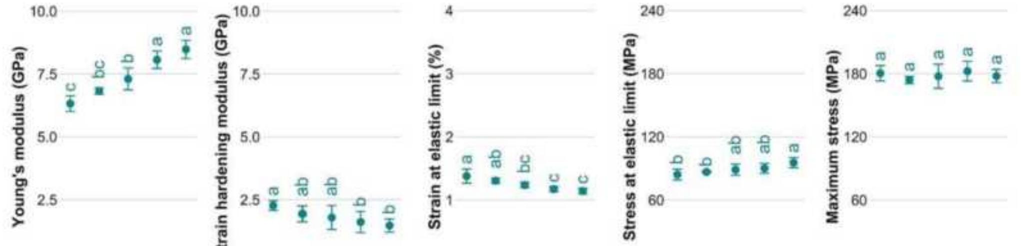

Fig. 3. Effect of fiber modulus on model mechanical properties: a) Young's modulus, b) strain hardening modulus, c) strain at elastic limit, d) stress at elastic limit, and e) maximum stress. Data points and bars refer to mean values and standard deviation, respectively. The same letter shows the lack of statistically significant differences.

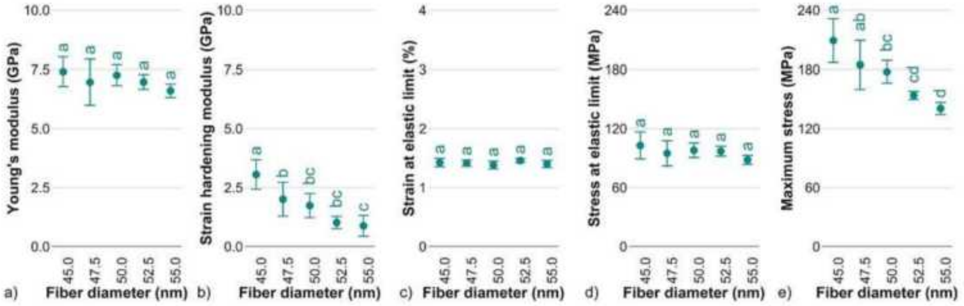

Fig. 4. Effect of fiber diameter on model mechanical properties: a) Young's modulus, b) strain hardening modulus, c) strain at elastic limit, d) stress at elastic limit, and e) maximum stress. Data points and bars refer to mean values and standard deviation, respectively. The same letters show a lack of statistically significant differences.

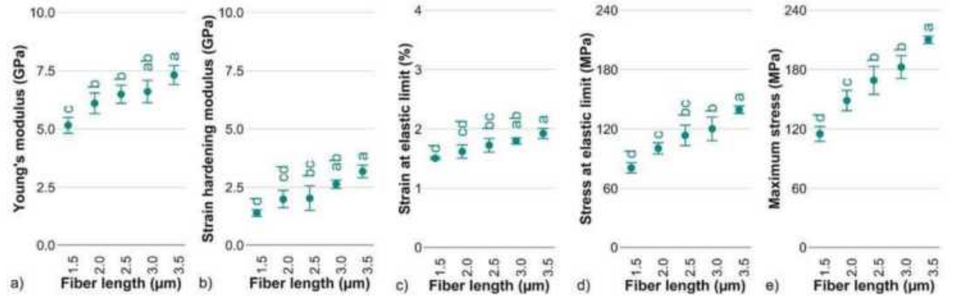

Fig. 5. Effect of fiber length on model mechanical properties: a) Young's modulus, b) strain hardening modulus, c) strain at elastic limit, d) stress at elastic limit, and e) maximum stress. Data points and bars refer to mean values and standard deviation, respectively. The same letter shows lack of statistically significant differences.

3.1.4. *Effect of interfiber interactions*

Direct modification of the force constant of interfiber interaction showed the highest impact on the mechanical properties of the studied fiber networks. An increase in the force constant of interfiber interaction increased all of the evaluated mechanical properties (Fig. 6). The cellulose–hemicellulose interaction force has previously been reported to have a similar effect on the stiffness of the numerically simulated cell wall model (Yi et al., 2013; Yi & Puri, 2014).

A non-linear increase was observed for both Young's modulus (Fig. 6a) and the strain hardening modulus (Fig. 6b) of the network with increasing force constant of interfiber interaction. While Young's modulus increased rapidly at lower force constants of interfiber interaction, the increase in strain hardening modulus was steep at higher force constants of interfiber interaction. This effect is due to the influence of the force constants of interfiber interaction on the structure of the model during its formation (settling phase, see Supplementary Materials). At low force constants of interfiber interaction, the network structure is relatively loose and has a low number of contacts per fiber.

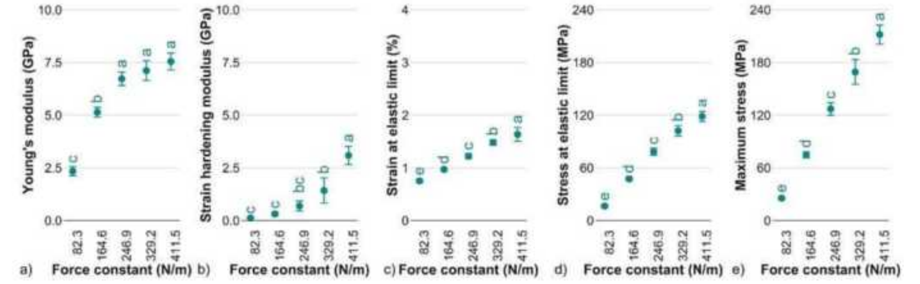

Fig. 6. Effects of force constant of interfiber interaction (force constant) on model mechanical properties: a) Young's modulus, b) strain hardening modulus, c) strain at elastic limit, d) stress at elastic limit, and e) maximum stress. Data points and bars refer to mean values and standard deviation, respectively. The same letters show lack of statistically significant differences. The values of the force constant, provided here, refers to the binding energy constants for adhesive interactions, defined as a parameter a in Eq. S4.

The increase in force constant of interfiber interaction not only causes the fibers to adhere more strongly to each other but also increases the initial number of interfiber contacts, resulting in a rapid increase in Young's modulus at low force constant of interfiber interaction. With further increases of the force constant of interfiber interaction, the limit of possible interfiber contacts for a given network is reached. Because the number of interfiber contacts no longer increases, further increases in Young's modulus are defined solely by an increase in the force constant of interfiber interaction. A faster increase in the strain hardening modulus, compared to Young's modulus, indicated a greater sensitivity to changes in the force constant of interfiber interaction, especially for highly cross-linked structures (with several interfiber contacts close to the threshold). Similar observations have been made in molecular models where the number of fiber interactions defines the strain in the plastic deformation phase (W. Chen et al., 2004).

The overall increase in force constant of interfiber interaction in the elastic and plastic deformation phases resulted in a linear increase in the maximum stress of the network (Fig. 6e). A similar effect has been observed by Zhang et al., who reported that an increase in the force of cellulose–cellulose interactions increases the stresses in both the elastic and plastic deformation phases of the cellulose–hemicellulose–pectin network (Zhang et al., 2021).

Overall, increasing the force constant of interfiber interaction resulted in a prolonged elastic deformation phase, as evidenced by increased strain and stress at the elastic limit (Fig. 6c,d). At higher force constants of interfiber interaction, the fibers in the elastic deformation phase can stretch and reorient more than the fibers under a lower force constant of interfiber interaction. As a result, the elastic deformation phase is prolonged, and the transmitted loads are higher prior to interfiber slippage. Previous observations on the role of the force constant of interfiber interaction in atomistic models of fiber networks align with our results, assuming interfiber interactions are used to define network rigidity (N. Zhang et al., 2015).

3.2. *Mechanical properties of BC–hemicellulose composites: Explanatory analysis with numerical model*

Adding hemicelluloses to the BC culture medium affected the structural and mechanical properties of the resulting BC–hemicellulose composites at both nano- and macroscales (Fig. 7, S1, S2). In this section, the obtained data on the mechanical properties of BC–hemicellulose composites are interpreted in terms of the sensitivity of the numerical model to the structural (length, diameter) and mechanical (force constant of interfiber interaction, modulus) parameters of the individual fibers in the network.

3.2.1. *BC–xylan composites*

Increasing the concentration of xylan in the culture medium resulted in statistically significant increases in the Young's modulus (Fig. 7a), strain hardening modulus (Fig. 7b), and maximum stress (Fig. 7e) of the BC–xylan composites. The width of individual fibers tended to decrease with increasing xylan content in the medium (Fig. S1), while the fiber modulus increased moderately compared to results obtained for pure BC (Fig. S2).

The formation of thinner fibers with increasing xylan concentration is probably due to the use of xylose for bacteria replication (Uraki et al., 2002). The thinning of fibers allows us to assume that for an increasing number of thin fibers within the composite, the number of interfiber contacts and the force constant of interfiber interaction are higher. This finding is of particular importance in terms of the model response to applied load, supposing the mechanical properties of BC–xylan composites are determined not only by the effect of decreasing fiber diameter but also by the effect of increased interfiber interaction.

The data on the fiber modulus extracted from the BC–xylan composites are also consistent with the model output. Based on the model output, increases in the Young's modulus (Fig. 7a), strain at elastic limit (Fig. 7c), and stress at elastic limit (Fig. 7d) result from the increased fiber modulus in the BC–xylan composites (Fig. S2). In BC–xylan composites, the shift in the elastic deformation phase toward higher values may be related to the resistance of the stiffer fibers to rearrangement. The increasing stiffness of individual fibers of BC–xylan composites with increasing xylan concentration in the medium could be due to the ability of xylan to promote the recrystallization of cellulose, as reported by Long et al. for dried casted cellulose–xylan composites (Long et al., 2019).

3.2.2. *BC–arabinoxylan composites*

Similar to the BC–xylan composites, an increase in arabinoxylan content resulted in a statistically significant increase in the Young's modulus (Fig. 8a), strain hardening modulus (Fig. 8b), and maximum stress (Fig. 8e) of the BC–arabinoxylan composites, as well as the fiber width (Fig. S1). As shown by the model, increasing the fiber diameter does not show statistically significant changes in the strain at elastic limit (Fig. 4c), which may explain why arabinoxylan concentration does not affect the elastic limit conditions (Fig. 8c and d). In contrast to that, the change in the Young's modulus (Fig. 8a) and maximum stresses (Fig. 8e) suggest that the mechanical properties of BC–arabinoxylan composites are not determined by the fiber diameter but rather by the force constant of interfiber interaction. This hypothesis is supported by the work of Dolan et al., which showed that arabinoxylan increases interfiber adhesion in BC–arabinoxylan composites (Dolan et al., 2019). In context of current study, this effect may cause a statistically significant increase in the Young's modulus and maximum stress.

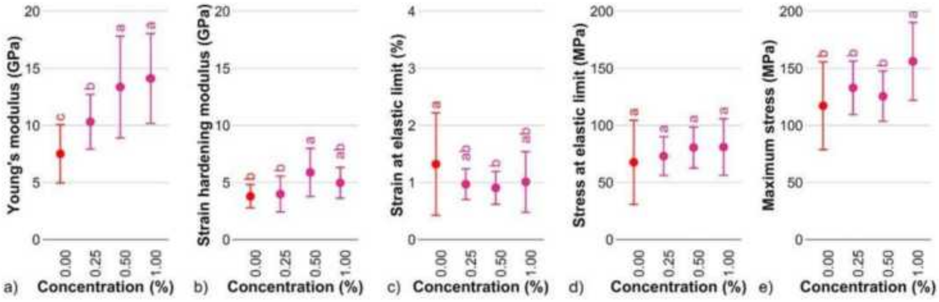

Fig. 7. Mechanical properties of BC–xylan composites: a) Young's modulus, b) strain hardening modulus, c) strain at elastic limit, d) stress at elastic limit, and e) maximum stress. The control sample (BC without hemicellulose additives) is marked in red. The data points and bars refer to mean values and standard deviation, respectively. The same letters show lack of statistically significant differences.

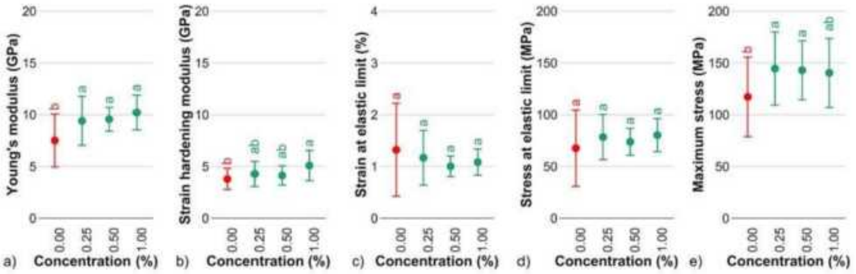

Fig. 8. Mechanical properties of BC–arabinoxylan composites: a) Young's modulus, b) strain hardening modulus, c) strain at elastic limit, d) stress at elastic limit, and e) maximum stress. The control sample (BC without hemicellulose additives) is marked in red. Data points and bars refer to mean values and standard deviation, respectively. The same letters show lack of statistically significant difference.

Arabinoxylan has been reported to form microscale grains closely associated with cellulose (Lopez-Sanchez et al., 2015). This led to the additional assumption that increases in these two mechanical parameters of BC–arabinoxylan composites are related to the occurrence of cellulose–arabinoxylan–cellulose linkages, in addition to the existing cellulose–cellulose interactions. Such linkages increase interfiber adhesion and the number of interfiber contacts, which may support the increased Young's moduli of BC–arabinoxylan composites compared to pure BC. Such linkages may also reduce the lamellar separation within the composite and lead to a more uniform stress distribution, as observed by Stevanic et al. for dried casted cellulose–arabinoxylan composites (Stevanic et al., 2012). Supporting the above explanation, an *in silico* atomistic cellulose–hemicellulose fiber network model has shown that the arabinose sidechains strengthen interfiber interactions (Silveira et al., 2013).

3.2.3. BC–xyloglucan composites

Increasing the xyloglucan content in the culture medium resulted in less pronounced increases in the Young's modulus (Fig. 9a) and stress at elastic limit (Fig. 9d), while the value of the maximum stress decreased (Fig. 9e), compared to pure BC. Because BC–xyloglucan composites break easily (at stresses <100 MPa), determining the strain hardening modulus (Fig. 9b) was difficult or impossible, especially for composites with high xyloglucan content. Both the fiber width (Fig. S1) and fiber modulus (Fig. S2) showed statistically significant increases with increasing xyloglucan concentration, especially when compared to pure BC. According to the model outputs, these changes to the individual fiber parameters explain the increased Young's modulus (Fig. 3a; Fig. 9a) and stress at elastic limit (Fig. 3d; Fig. 9d), and the decreased strain hardening modulus (Fig. 3b; Fig. 9b). The increased fiber modulus of the BC–xyloglucan composites could be due to the reinforcing effect of xyloglucan (Bendaoud et al., 2017), which supports the alignment of cellulose microfibers, increasing the adhesion of microfibers within the fiber. Our model data on the effect of the force constant of interfiber interaction on the mechanical properties of the fiber network are also consistent with the work of Dolan et al. (Dolan et al., 2019), which reported a fourfold increase in the interfiber adhesion of cellulose in the presence of xyloglucan. De Souza et al. have reported a similar effect of xyloglucan on interfiber adhesion in dried casted reconstituted BC–xyloglucan composites (De Souza et al., 2013). In addition, the increased mechanical properties of individual fibers of BC–xyloglucan composites have been attributed to an increase in the length of the cellulose nanocrystals, as reported by Chi and Catchmark for BC cultured in the presence of xyloglucan (Chi & Catchmark, 2017).

3.2.4. BC–glucomannan composites

Adding higher concentrations of glucomannan decreased the Young's modulus (Fig. 10a), strain hardening modulus (Fig. 10b), stress at elastic limit (Fig. 10d), and maximum stress (Fig. 10e) of BC–glucomannan composites. In addition, a statistically significant increase in fiber width (Fig. S1) and a decrease in fiber modulus (Fig. S2) were observed compared to pure BC. Comparably to the effect of xyloglucan, BC–glucomannan composites with high glucomannan content showed decreasing plastic deformation conditions compared to pure BC and a sudden drop in maximum stress when glucomannan concentration exceeded 0.5 %; thus, further evaluation of the strain hardening modulus had larger error bars.

Similarly to the modeling study, decreased fiber modulus led to

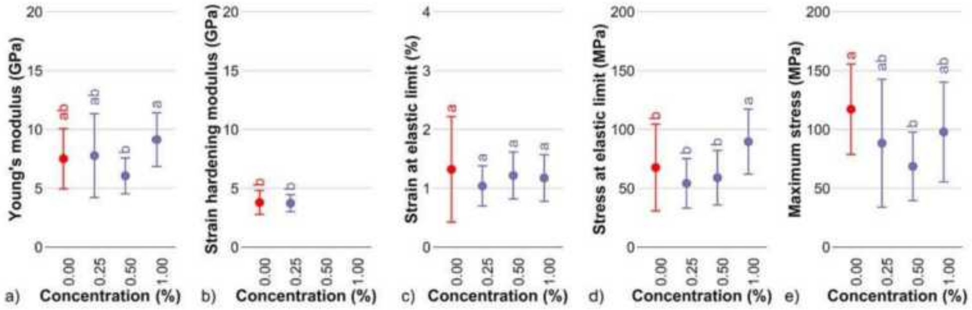

Fig. 9. Mechanical properties of BC–xyloglucan composites: a) Young's modulus, b) strain hardening modulus, c) strain at elastic limit, d) stress at elastic limit, and e) maximum stress. The control sample (BC without hemicellulose additives) is marked in red. Data points and bars refer to mean values and standard deviation, respectively. The same letters show lack of statistically significant difference.

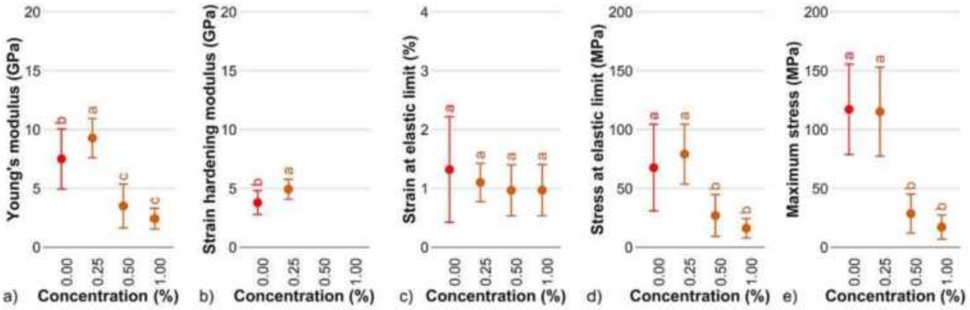

Fig. 10. Mechanical properties of BC–glucomannan composites: a) Young's modulus, b) strain hardening modulus, c) strain at elastic limit, d) stress at elastic limit, and e) maximum stress. The control sample (BC without hemicellulose additives) is marked in red. Data points and bars refer to mean values and standard deviation, respectively. The same letters show lack of statistically significant difference.

decrease in the Young's modulus and stress at elastic limit observed for BC–glucomannan composites. Because glucomannan is structurally similar to cellulose, it has a good binding affinity to the cellulose surface (Chanzy et al., 1982). Thus, glucomannan deposition on the cellulose surface can prevent fiber assembly (Berglund, 2018), forming softer fibers compared to pure BC (Fig. S2). Thus, in the elastic deformation phase, the softer fibers require lower strain and stress to reorganize the network. Softer fibers may also result from disrupting cellulose chain packing by the presence of glucomannan, as previously demonstrated for BC (Atalla et al., 1994; Basu et al., 2017).

The increase in fiber width (Fig. S1) is thought to be due to glucomannan deposition on the cellulose surface, as has been demonstrated for microfibrillar cellulose of apple parenchyma (Szymańska-Chargot et al., 2023). As a consequence, crucial for the mechanical response of the BC-glucomannan composite, surface deposition of glucomannan reduce interfiber adhesion so that the force constant of interfiber interaction decreases with increasing glucomannan content. This is evidenced by the decreasing values of the mechanical properties of the network observed in the simulation study with decreasing force constant of interfiber interaction (Fig. 6). In this case, we assume that the mechanical properties of BC–glucomannan composites with increasing glucomannan content were mainly determined by the force constant of interfiber interaction, rather than the mechanical properties of individual fibers. The effect of the force constant of interfiber interaction on the mechanical properties of BC–glucomannan composites with an increasing glucomannan content is consistent with the previously reported lubricating effect of glucomannan in BC–glucomannan composites (Tokoh et al., 1998; Whitney et al., 1998).

4. Conclusions

Robust laboratory experiments and coarse-grained molecular dynamics simulations of fiber networks allowed us to explain the effects of the structural (length, diameter) and mechanical (force constant of interfiber interaction, modulus) parameters of individual fibers on the overall performance of BC–hemicellulose composites.

To summarize the results of the model, the simulations showed that the transition from elastic to plastic deformation is the result of the reorganization of the fiber network structure and depends on the force constant of interfiber interaction. A direct or indirect change in the force constant of interfiber interaction (tuning the force constant or the number of interfiber contacts) resulted in statistically significant changes in all mechanical parameters evaluated. The stronger the interfiber interactions, the higher the stiffness of the network and the longer the duration of the elastic deformation phase. The effect of the fiber modulus and fiber diameter on the transition from elastic to plastic deformation was relatively small. The stiffness of the network was proportional to the fiber modulus in the elastic deformation phase. After the transition to plastic deformation, an increase in fiber modulus decreased the network stiffness.

The mechanical properties of the simulated networks were in good agreement with the mechanical properties obtained in the experiments with BC–hemicellulose composites and explain the changed mechanics of this system. As a general conclusion, the changes in the structural and mechanical parameters of the individual fibers in BC–hemicellulose composites are relatively small when the concentration of hemicellulose changes. Therefore, according to the simulations, the force constant of interfiber interaction caused by the presence of hemicelluloses should be considered the main factor affecting the mechanical properties of the real BC–hemicellulose composites. However, in certain cases (*e.g.*, BC composites with xyloglucan and glucomannan), the mechanical properties are influenced by the diameter or the modulus of the fibers.

The results show that numerical simulation effectively contributes to understanding the mechanics of cellulose–hemicellulose composites. Our results reveal the structure- and property-dependent mechanisms of the mechanical response of cellulose–hemicellulose fiber networks and indicate the specific role of hemicelluloses. This work demonstrates the agreement between laboratory and modeling studies on the mechanobiology of cellulose–hemicellulose fiber networks; thus, the applicability of a combined approach for studying the structural and mechanical properties of these bioinspired fiber-based biomaterials can be predicted. Although the current combined approach to studying the biomechanics of fiber-based systems can be considered sophisticated, there are still challenges that need to be addressed. Here, top-notch models require the consideration of the direct presence of hemicellulose fibers, the nature of their interaction with cellulose fibers, the spatio-temporal distribution and reorganization within the cellulose fiber network during its deformation, *etc.* Technical limitations, such as the implementation of multiscale models for the comparability of fiber network deformations at nano- and macroscale and co-interpretation of the results, still need to be addressed.

CRediT authorship contribution statement

Vadym Chibrikov: Data curation, Formal analysis, Investigation, Methodology, Software, Validation, Visualization, Writing – original draft. **Piotr Mariusz Pieczywek:** Conceptualization, Data curation, Formal analysis, Funding acquisition, Investigation, Methodology, Project administration, Software, Supervision, Validation, Visualization, Writing – review & editing. **Justyna Cybulska:** Methodology. **Artur Zdunek:** Conceptualization, Writing – review & editing.

Declaration of competing interest

The authors declare the following financial interests/personal relationships which may be considered as potential competing interests: Piotr Mariusz Pieczywek reports financial support was provided by National Science Centre Poland. If there are other authors, they declare that they have no known competing financial interests or personal relationships that could have appeared to influence the work reported in this paper.

Data availability

Data will be made available on request.

Acknowledgments

This work was supported by the National Science Centre, Poland [grant number 2019/35/D/NZ9/00555].

Appendix A. Supplementary data

Supplementary data to this article can be found online at https://doi.org/10.1016/j.carbpol.2024.121827.

References

Adler, D. C., & Buehler, M. J. (2013). Mesoscale mechanics of wood cell walls under axial strain. *Soft Matter, 9*(29), 7138–7144. https://doi.org/10.1039/c3sm50183c

Adusumali, R. B., Reifferscheid, M., Weber, H., Roeder, T., Sixta, H., & Gindl, W. (2006). Mechanical properties of regenerated cellulose fibres for composites. *Macromolecular Symposia, 244*, 119–125. https://doi.org/10.1002/masy.200651211

Atalla, R. H., Vanderhart, D. L., & Hackney.. (1994). Modification of crystallinity and crystalline structure of Acetobacter xylinum cellulose in the presence of polysaccharides : ^{13}C-NMR evidence. *International Journal of Biological Macromolecules, 16*(4), 215–218.

Basu, S., Omadjela, O., Zimmer, J., & Catchmark, J. M. (2017). Impact of plant matrix polysaccharides on cellulose produced by surface-tethered cellulose synthases. *Carbohydrate Polymers, 162*, 93–99. https://doi.org/10.1016/j.carbpol.2017.01.005

Bendaoud, A., Kehrbusch, R., Baranov, A., Duchemin, B., Maigret, J. E., Falourd, X., … Leroy, E. (2017). Nanostructured cellulose-xyloglucan blends via ionic liquid/water processing. *Carbohydrate Polymers, 168*, 163–172. https://doi.org/10.1016/j.carbpol.2017.03.080

Berglund, J. (2018). Wood hemicelluloses - fundamental insights on biological and technical properties [KTH Royal Institute of Technology]. https://www.diva-portal.org/smash/get/diva2:1275732/FULLTEXT01.pdf.

Bidhendi, A. J., & Geitmann, A. (2019). Methods to quantify primary plant cell wall mechanics. *Journal of Experimental Botany, 70*(14), 3615–3648. https://doi.org/10.1093/jxb/erz281

Carpita, N. C., & Gibeaut, D. M. (1993). Structural models of primary cell walls in flowering plants: Consistency of molecular structure with the physical properties of the walls during growth. *Plant Journal, 3*(1), 1–30. https://doi.org/10.1111/j.1365-313X.1993.tb00007.x

Chanzy, H. D., Grosrenaud, A., Joseleau, J. P., Dube, M., & Marchessault, R. H. (1982). Crystallization behavior of Glucomannan. *Biopolymers, 21*(2), 301–319.

Chen, S. Q., Mikkelsen, D., Lopez-Sanchez, P., Wang, D., Martinez-Sanz, M., Gilbert, E. P., … Gidley, M. J. (2017). Characterisation of bacterial cellulose from diverse Komagataeibacter strains and their application to construct plant cell wall analogues. *Cellulose, 24*(3), 1211–1226. https://doi.org/10.1007/s10570-017-1203-3

Chen, W., Lickfield, G. C., & Yang, C. Q. (2004). Molecular modeling of cellulose in amorphous state. Part I: Model building and plastic deformation study. *Polymer, 45*(3), 1063–1071. https://doi.org/10.1016/j.polymer.2003.11.020

Cheng, Q., Wang, S., & Harper, D. P. (2009). Effects of process and source on elastic modulus of single cellulose fibrils evaluated by atomic force microscopy. *Composites Part A: Applied Science and Manufacturing, 40*(5), 583–588. https://doi.org/10.1016/j.compositesa.2009.02.011

Chi, K., & Catchmark, J. M. (2017). The influences of added polysaccharides on the properties of bacterial crystalline nanocellulose. *Nanoscale, 9*(39), 15144–15158. https://doi.org/10.1039/c7nr05615j

Chibrikov, V., Pieczywek, P. M., Cybulska, J., & Zdunek, A. (2023). Evaluation of elasto-plastic properties of bacterial cellulose-hemicellulose composite films. *Industrial Crops and Products, 205*(July), Article 117578. https://doi.org/10.1016/j.indcrop.2023.117578

Chibrikov, V., Pieczywek, P. M., & Zdunek, A. (2022). Tailor-made biosystems - bacterial cellulose-based films with plant cell wall polysaccharides. *Polymer Reviews, 63*(1), 1–27. https://doi.org/10.1080/15583724.2022.2067869

Cybulska, J., Vanstreels, E., Ho, Q. T., Courtin, C. M., Craeyveld, V. V., Nicolaï, B., … Konstankiewicz, K. (2010). Mechanical characteristics of artificial cell walls. *Journal of Food Engineering, 96*(2), 287–294. https://doi.org/10.1016/j.jfoodeng.2009.08.001

Dammström, S., Salmén, L., & Gatenholm, P. (2009). On the interactions between cellulose and xylan, a biomimetic simulation of the hardwood cell wall. *BioResources, 4*(1), 3–14.

De Souza, C. F., Lucyszyn, N., Woehl, M. A., Riegel-Vidotti, I. C., Borsali, R., & Sierakowski, M. R. (2013). Property evaluations of dry-cast reconstituted bacterial cellulose/tamarind xyloglucan biocomposites. *Carbohydrate Polymers, 93*(1), 144–153. https://doi.org/10.1016/j.carbpol.2012.04.062

Dolan, G. K., Cartwright, B., Bonilla, M. R., Gidley, M. J., Stokes, J. R., & Yakubov, G. E. (2019). Probing adhesion between nanoscale cellulose fibres using AFM lateral force spectroscopy: The effect of hemicelluloses on hydrogen bonding. *Carbohydrate Polymers, 208*, 97–107. https://doi.org/10.1016/j.carbpol.2018.12.052

Frankova, L., & Fry, S. C. (2021). Hemicellulose-remodelling transglycanase activities from charophytes: Towards the evolution of the land-plant cell wall. *Plant Journal, 108*(1), 7–28. https://doi.org/10.1111/tpj.15500

Guhados, G., Wan, W., & Hutter, J. L. (2005). Measurement of the elastic modulus of single bacterial cellulose fibers using atomic force microscopy. *Langmuir, 21*(14), 6642–6646. https://doi.org/10.1021/la0504311

Hestrin, S., & Schramm, M. (1954). Synthesis of cellulose by Acetobacter xylinum. II. Preparation of freeze-dried cells capable of polymerizing glucose to cellulose. *The Biochemical Journal, 58*(2), 345–352. https://doi.org/10.1042/bj0580345

Jin, K., Qin, Z., & Buehler, M. J. (2015). Molecular deformation mechanisms of the wood cell wall material. *Journal of the Mechanical Behavior of Biomedical Materials, 42*, 198–206. https://doi.org/10.1016/j.jmbbm.2014.11.010

Joshi, S. Y., & Deshmukh, S. A. (2021). A review of advancements in coarse-grained molecular dynamics simulations. *Molecular Simulation, 47*(10–11), 786–803. https://doi.org/10.1080/08927022.2020.1828583

Keegstra, K., Talmadge, K. W., Bauer, W. D., & Albersheim, P. (1973). The structure of plant cell walls: III. A model of the walls of suspension-cultured sycamore cells based on the interconnections of the macromolecular components. *Plant Physiology, 51*(1), 188–197. https://doi.org/10.1104/pp.51.1.188

Kha, H., Tuble, S., Kalyanasundaram, S., & Williamson, R. E. (2008). Finite element analysis of plant cell wall materials. *Advanced Materials Research, 32*, 197–202. https://doi.org/10.4028/www.scientific.net/amr.32.197

Kontomaris, S.-V. (2018). The hertz model in AFM nanoindentation experiments: Applications in biological samples and biomaterials. *Micro and Nanosystems, 10*(1), 11–22. https://doi.org/10.2174/1876402910666180426114700

Lekka, M. (2016). Discrimination between normal and cancerous cells using AFM. *BioNanoScience, 6*(1), 65–80. https://doi.org/10.1007/s12668-016-0191-3

Long, L., Shen, F., Wang, F., Tian, D., & Hu, J. (2019). Synthesis, characterization and enzymatic surface roughing of cellulose/xylan composite films. *Carbohydrate Polymers, 213*, 121–127. https://doi.org/10.1016/j.carbpol.2019.02.086

Lopez-Sanchez, P., Cersosimo, J., Wang, D., Flanagan, B., Stokes, J. R., & Gidley, M. J. (2015). Poroelastic mechanical effects of hemicelluloses on cellulosic hydrogels under compression. *PLoS One, 10*(3), Article e0122132. https://doi.org/10.1371/journal.pone.0122132

Mani, S., Cosgrove, D. J., & Voth, G. A. (2020). Anisotropic motions of fibrils dictated by their orientations in the lamella: A coarse-grained model of a plant cell wall. *Journal of Physical Chemistry B, 124*(17), 3527–3539. https://doi.org/10.1021/acs.jpcb.0c01697

Mikkelsen, D., & Gidley, M. J. (2010). Formation of cellulose-based composites with hemicelluloses and pectins using gluconacetobacter fermentation. In *The plant cell wall* (pp. 197–208). https://doi.org/10.1007/978-1-61779-008-9

Neuman, R. D., Berg, J. M., & Claesson, P. M. (1993). Direct measurement of surface forces in papermaking and paper coating systems. *Nordic Pulp & Paper Research Journal, 8*(1), 96–104. https://doi.org/10.3183/npprj-1993-08-01-p096-104

Nili, A., Yi, H., Crespi, V. H., & Puri, V. M. (2015). Examination of biological hotspot hypothesis of primary cell wall using a computational cell wall network model. *Cellulose, 22*(2), 1027–1038. https://doi.org/10.1007/s10570-015-0568-4

Park, Y. B., & Cosgrove, D. J. (2012a). A revised architecture of primary cell walls based on biomechanical changes induced by substrate-specific endoglucanases. *Plant Physiology, 158*(4), 1933–1943. https://doi.org/10.1104/pp.111.192880

Park, Y. B., & Cosgrove, D. J. (2012b). Changes in cell wall biomechanical properties in the xyloglucan-deficient xxt1/xxt2 mutant of Arabidopsis. *Plant Physiology, 158*(1), 465–475. https://doi.org/10.1104/pp.111.189779

Persch, G., Born, C., & Utesch, B. (1994). Nano-hardness investigations of thin films by an atomic force microscope. *Microelectronic Engineering, 24*(1–4), 113–121. https://doi.org/10.1016/0167-9317(94)90061-2

Pieczywek, P. M. (2022a). NanoPlot. https://github.com/ppieczywek/NanoPlot.

Pieczywek, P. M. (2022b). TDA. https://github.com/ppieczywek/TDA.

Pieczywek, P. M. (2023a). FibreGen. https://github.com/ppieczywek/FibreGen.

Pieczywek, P. M. (2023b). FibreNet. https://github.com/ppieczywek/FibreNet.

Pieczywek, P. M., Chibrikov, V., & Zdunek, A. (2023). In silico studies of plant primary cell walls – Structure and mechanics. *Biological Reviews, 98*, 887–899. https://doi.org/10.1111/brv.12935

Serry, F. M. (2005). Improving the accuracy of the AFM force measurements: The thermal tune solution to the cantilever spring constant problem. *Veeco Application Notes, 14*, 4. bruker.com.

Silveira, R. L., Stoyanov, S. R., Gusarov, S., Skaf, M. S., & Kovalenko, A. (2013). Plant biomass recalcitrance: Effect of hemicellulose composition on nanoscale forces that control cell wall strength. *Journal of the American Chemical Society, 135*(51), 19048–19051. https://doi.org/10.1021/ja405634k

Stevanic, J. S., Bergström, E. M., Gatenholm, P., Berglund, L., & Salmén, L. (2012). Arabinoxylan/nanofibrillated cellulose composite films. *Journal of Materials Science, 47*(18), 6724–6732. https://doi.org/10.1007/s10853-012-6615-8

Szymańska-Chargot, M., Chylińska, M., Cybulska, J., Kozioł, A., Pieczywek, P. M., & Zdunek, A. (2017). Simultaneous influence of pectin and xyloglucan on structure and mechanical properties of bacterial cellulose composites. *Carbohydrate Polymers, 174*, 970–979. https://doi.org/10.1016/j.carbpol.2017.07.004

Szymańska-Chargot, M., Pękala, P., Myśliwiec, D., Cieśla, J., Pieczywek, P. M., Siemińska-Kuczer, A., & Zdunek, A. (2023). A study of the properties fo hemicelluloses adsorbed onto microfibrillar cellulose isolated from apple parenchyma. *Food Chemistry, 430*(July 2023). https://doi.org/10.1016/j.foodchem.2023.137116

Talbott, L. D., & Ray, P. M. (1992). Molecular size and separability features of pea cell wall polysaccharides: Implications for models of primary wall structure. *Plant Physiology*, 98(1), 357–368. https://doi.org/10.1104/pp.98.1.357

Tokoh, C., Takabe, K., Fujita, M., & Saiki, H. (1998). Cellulose synthesized by Acetobacter xylinum in the presence of acetyl glucomannan. *Cellulose, 5*(4), 249–261. https://doi.org/10.1023/A:1009211927183

Uraki, Y., Morito, M., Kishimoto, T., & Sano, Y. (2002). Bacterial cellulose production using monosaccharides derived from hemicelluloses in water-soluble fraction of waste liquor from atmospheric acetic acid pulping. *Holzforschung, 56*(4), 341–347. https://doi.org/10.1515/HF.2002.054

Whitney, S. E. C., Brigham, J. E., Darke, A. H., Reid, J. S. G., & Gidley, M. J. (1998). Structural aspects of the interaction of mannan-based polysaccharides with bacterial cellulose. *Carbohydrate Research, 307*(3–4), 299–309. https://doi.org/10.1016/S0008-6215(98)00004-4

Whitney, S. E. C., Wilson, E., Webster, J., Bacic, A., Grant Reid, J. S., & Gidley, M. J. (2006). Effects of structural variation in xyloglucan polymers on interactions with bacterial cellulose. *American Journal of Botany, 93*(10), 1402–1414. https://doi.org/10.3732/ajb.93.10.1402

Yakubov, G. E., Bonilla, M. R., Chen, H., Doblin, M. S., Bacic, A., Gidley, M. J., & Stokes, J. R. (2016). Mapping nano-scale mechanical heterogeneity of primary plant cell walls. *Journal of Experimental Botany, 67*(9), 2799–2816. https://doi.org/10.1093/jxb/erw117

Yi, H., & Puri, V. M. (2012). Architecture-based multiscale computational modeling of plant cell wall mechanics to examine the hydrogen-bonding hypothesis of the cell wall network structure model. *Plant Physiology, 160*(3), 1281–1292. https://doi.org/10.1104/pp.112.201228

Yi, H., & Puri, V. M. (2014). Contributions of the mechanical properties of major structural polysaccharides to the stiffness of a cell wall network model. *American Journal of Botany, 101*(2), 244–254. https://doi.org/10.3732/ajb.1300315

Yi, H., Zamil, M. S., & Puri, V. M. (2013). Investigation of the plant cell wall's molecular structure models using the finite element modeling. American Society of Agricultural and Biological Engineers Annual International Meeting 2013, ASABE 2013, 1, 488–493. Doi:10.13031/aim.20131587129.

Zhang, B., Gao, Y., Zhang, L., & Zhou, Y. (2021). The plant cell wall: Biosynthesis, construction, and functions. *Journal of Integrative Plant Biology, 63*(1), 251–272. https://doi.org/10.1111/jipb.13055

Zhang, N., Li, S., Xiong, L., Hong, Y., & Chen, Y. (2015). Cellulose-hemicellulose interaction in wood secondary cell-wall. *Modelling and Simulation in Materials Science and Engineering, 23*(8). https://doi.org/10.1088/0965-0393/23/8/085010

Zhang, W., Yang, J., Lu, Y., Li, M., Peng, F., & Bian, J. (2023). Insights into the contributions of hemicelluloses to assembly and mechanical properties of cellulose networks. *Carbohydrate Polymers, 301*(PA), Article 120292. https://doi.org/10.1016/j.carbpol.2022.120292

Zhang, Y., Yu, J., Wang, X., Durachko, D. M., Zhang, S., & Cosgrove, D. J. (2021). Molecular insights into the complex mechanics of plant epidermal cell walls. *Science, 372*(6543), 706–711. https://doi.org/10.1126/science.abf2824

Zhou, G., Zhang, B., Tang, G., Yu, X. F., & Galluzzi, M. (2021). Cells nanomechanics by atomic force microscopy: Focus on interactions at nanoscale. *Advances in Physics: X, 6*(1). https://doi.org/10.1080/23746149.2020.1866668

6.4.3. Supplementary Materials of the manuscript P4

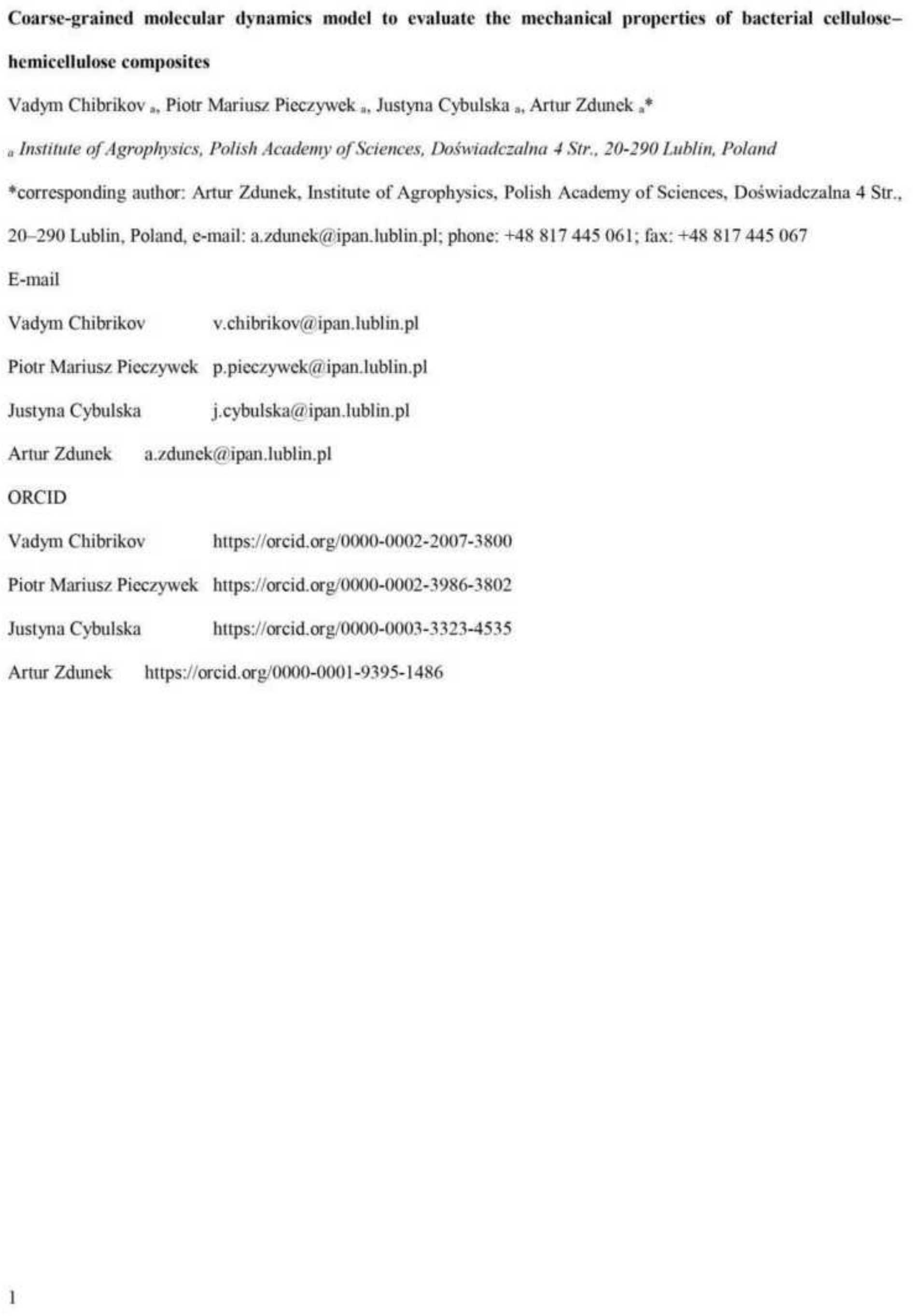

Coarse-grained molecular dynamics model to evaluate the mechanical properties of bacterial cellulose–hemicellulose composites

Vadym Chibrikov [a], Piotr Mariusz Pieczywek [a], Justyna Cybulska [a], Artur Zdunek [a]*

[a] *Institute of Agrophysics, Polish Academy of Sciences, Doświadczalna 4 Str., 20-290 Lublin, Poland*

*corresponding author: Artur Zdunek, Institute of Agrophysics, Polish Academy of Sciences, Doświadczalna 4 Str., 20–290 Lublin, Poland, e-mail: a.zdunek@ipan.lublin.pl; phone: +48 817 445 061; fax: +48 817 445 067

E-mail

Vadym Chibrikov	v.chibrikov@ipan.lublin.pl
Piotr Mariusz Pieczywek	p.pieczywek@ipan.lublin.pl
Justyna Cybulska	j.cybulska@ipan.lublin.pl
Artur Zdunek	a.zdunek@ipan.lublin.pl

ORCID

Vadym Chibrikov	https://orcid.org/0000-0002-2007-3800
Piotr Mariusz Pieczywek	https://orcid.org/0000-0002-3986-3802
Justyna Cybulska	https://orcid.org/0000-0003-3323-4535
Artur Zdunek	https://orcid.org/0000-0001-9395-1486

Supplementary data 1. Fiber nano- and macroscale properties

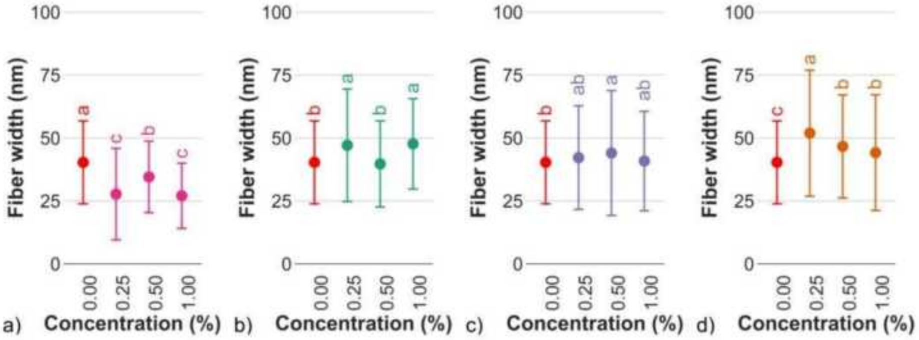

Fig.S1. Width of fibers derived from: a) bacterial cellulose-xylan, b) bacterial cellulose-arabinoxylan, c) bacterial cellulose-xyloglucan, and d) bacterial cellulose-glucomannan composites. The control sample (bacterial cellulose without hemicellulose additives) is marked with red colour. For the estimated parameters, the data points and bars indicate the means and standard deviations, respectively. Treatments with the same letter indicate lack of statistically significant differences.

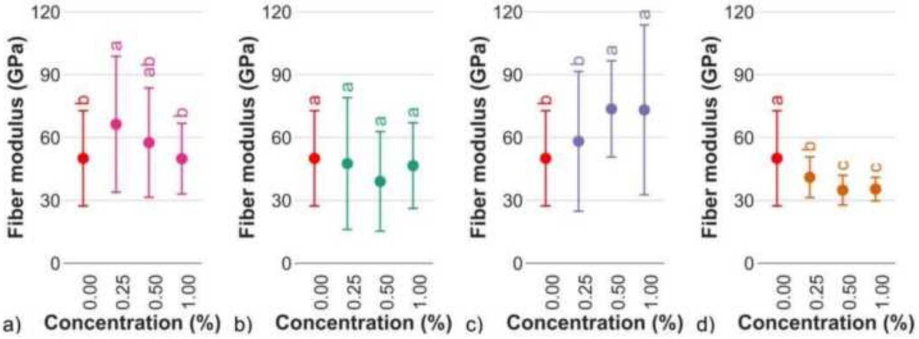

Fig.S2. Hertz modulus of fibers derived from: a) bacterial cellulose-xylan, b) bacterial cellulose-arabinoxylan, c) bacterial cellulose-xyloglucan, and d) bacterial cellulose-glucomannan composites. The control sample (bacterial cellulose without hemicellulose additives) is marked with red colour. For the estimated parameters, the data points and bars indicate the means and standard deviations, respectively. Treatments with the same letter indicate lack of statistically significant differences.

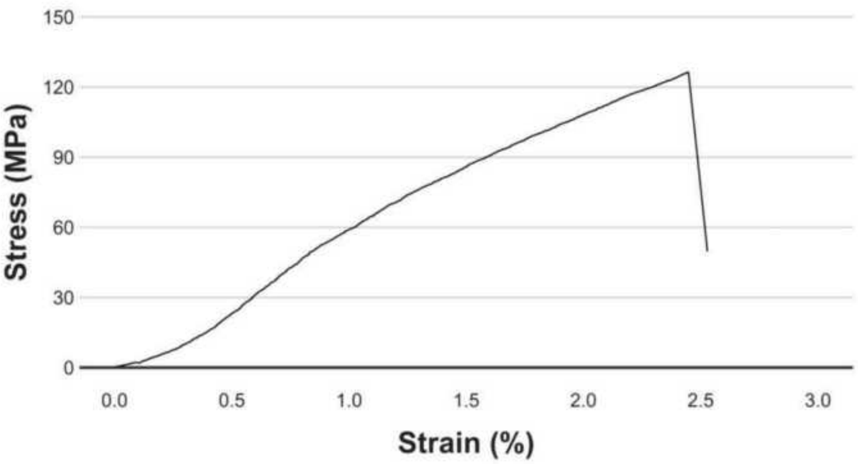

Fig.S3. Experimental stress-strain curve of pure bacterial cellulose, obtained by uniaxial tensile test with constant strain rate. Original curves were captured as force-elongation one, converted to stress-strain curves, following by data smooth with convolution filter. Elongation was repeated up to composite fracture.

Supplementary data 2. Definition of fiber network model

2.1. Single fiber definition

Each fiber was modelled as chain of beads (spheres), with harmonic bonds connecting two adjacent beads and angular potentials connecting three consequtive beads. Each bead was defined by its diameter, which was equal to the diameter of the fiber. Harmonic bonds and angular potentials were used to simulate axial and bending stiffness of the fibers. Torsional stiffness was not considered in the present model. The harmonic bond potential was defined as:

$$U_B = \frac{1}{2}k(l_0 - l)^2 \tag{S1}$$

where k is the stiffness of the fiber, l_0 is the residual length of the bond, and l is the current length of the bond.

The rest length between consecutive beads was equal to the radius of the fiber. The bond stiffness was defined as:

$$k = \frac{AE}{l_0} \tag{S2}$$

where A is the fiber cross-section area and E is the Young's modulus of fiber.

The angular bond potential was defined as:

$$U_A = \frac{EI}{2l_0}(\theta_0 - \theta)^2 \tag{S3}$$

where I is the second moment of area for circular fibers, θ_0 is the rest angle of angle bond potential and θ is the current angle of bond between three beads.

The mass of each bead was equal to the mass of a cylindrical fiber segment, with base diameter and height equal to the diameter of the bead, assuming the cellulose density of 1.5 g/cm^3.

2.2. Inter-fiber interactions

Inter-fiber non-bonded interactions were modeled using simple two-step truncated harmonic potentials (Fig.S3). The introduced potentials allowed the fibers to slide, attach, and detach under the applied load. The interaction between cellulose microfibers was described by:

$$U_I = \begin{cases} \frac{1}{2}a(r_0 - r)^2, & if\ (r_0 - r) < (r_c - r_0) \\ \frac{1}{2}a(r_0 - r)^2 + \frac{1}{2}b(2r_0 - r_c - r)^2, & if\ (r_0 - r) > (r_c - r_0) \end{cases} \tag{S4}$$

where a and b are the binding energy constants for adhesive and repulsive interactions respectively, r is the distance between beads, r_c is the cut-off distance of non-bonding interactions, r_0 is the distance between beads at potential minima.

In all simulations, two cellulose fibers produced attractive-repulsive forces when their surfaces were less than ~1.5 nm apart. A narrow range of inter-fiber non-bonded interactions was chosen to mimic the interactions of the biomechanical hotspot model, in which the extensibility of the fiber network is defined by hemicellulose-mediated load-bearing junctions.

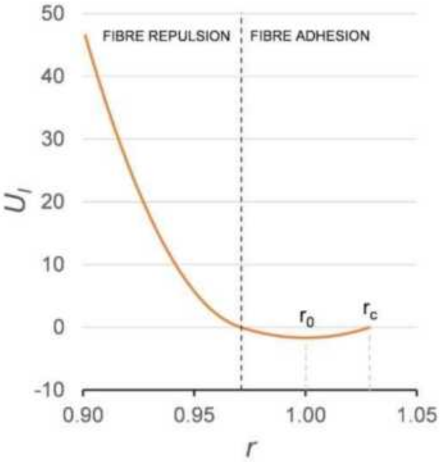

Fig.S4. Example of potential energy of non-bonding interactions (U_I) as a function of bead-to-bead distance (r). Both values are expressed in reduced units.

2.3. Model geometry

The geometry of the numerical models was established using a stochastic generator. Individual fibres were randomly generated in three-dimensional space to create layers of fibers filling a cuboidal space (Fig.S5-S6), that mimics the strips excised from bacterial cellulose pellicles. No treatment of the solvent was introduced to the current model.

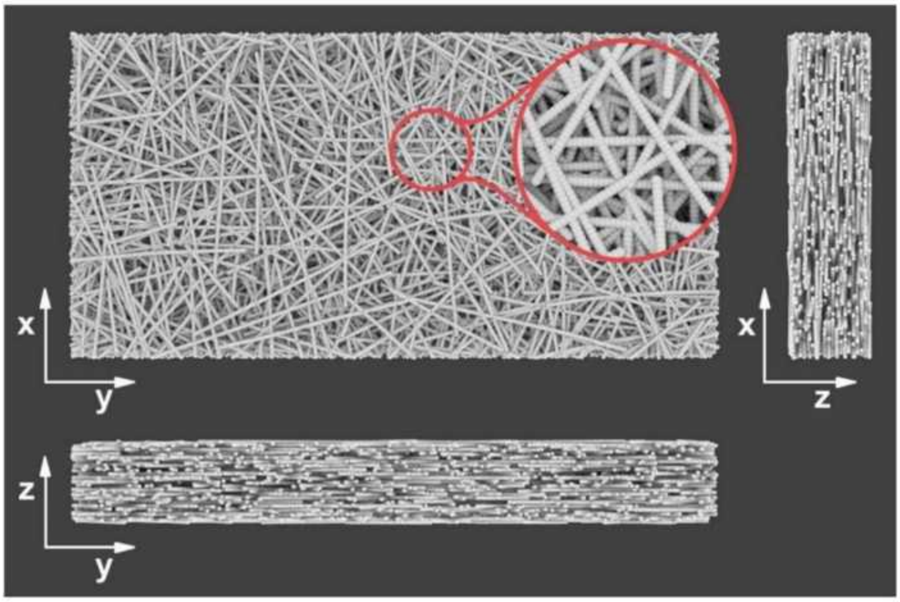

Fig.S5. Three-dimensional model of fiber network built using stochastic generator.

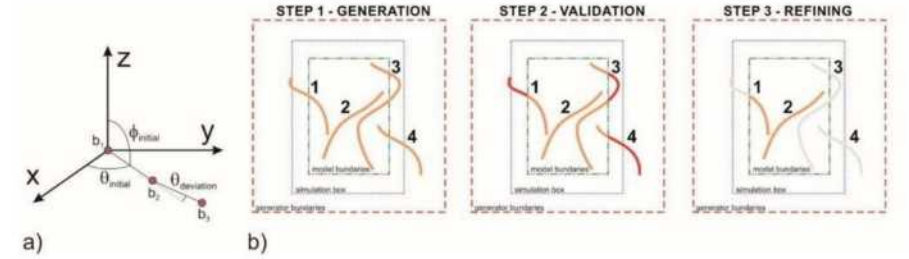

Fig.S6. Schematic representations of the algorithms of the stochastic generator introduced to create a three-dimensional model of fiber network: a) the first three steps (*b1*, *b2*, and *b3*) of generation of single fiber using a spherical coordinate system, and b) the three steps in creating a fibre network – generation of individual fiber, its validation, and model refinement.

The fibers were generated one by one, each fibre in a sequential process, bead by bead. The total length and diameter of the fiber were determined before the process began. Then, the initial position of the first fiber bead was determined (*b1* in Fig.S6a), which had to be within the predefined area of the generator (generator boundaries in

Fig.S5b). The fibers were generated in a much larger space than the actual space defined by the simulation box or the model boundaries. This approach was used to obtain a homogeneous model structure within the target volume (especially near the edges of the model). For the current model, vacuum was considered all around the simulation box, and the surface tension was considered as negligible.

Orientation of the fibers was defined using the spherical coordinate system. The initial values of the polar and azimuthal angles were determined in the following step. The azimuthal angle θ (direction of the fibre in the X-Y plane, see Fig.S6a) was randomly chosen from a range of 0 to 2π. The polar angle φ (with respect to the Z-axis) was set close to $\pi/2$ to initially obtain a fibre oriented parallel with respect to X-Y plane. The next fiber bead was placed at a distance of half the fiber diameter (length of a single fiber segment) along the direction defined by the azimuthal and polar angles (*b2* in Fig.S6a). Then, the newly formed bead was used as the starting point for the next fiber section (*b3* on Fig.S6a). This process was repeated until a fiber with the predetermined length was created. Between each section, the azimuthal and polar angles were allowed to deviate by a certain fraction of their initial value ($\theta_{deviation}$ in Fig.S6a). The magnitude of this deviation was used to create fibers with different curvatures. In this study, the deviations were set to ±0.005 rad and ±0.01 rad for polar and azimuthal angles, respectively. After the fibers were formed, the validation and refinement procedure was started (Fig.S5b). The fiber was removed if the central or larger part of the fiber extended beyond the model range (Fig.S5b, fibres 3 and 4). Otherwise, the fiber was left whole or shortened by a portion that did not fit within the model range (Fig.S6b, fibers 1 and 2). The process was continued until a certain number of fibers was reached in the designated area of the model. All the fibers generated had the same diameter. In this study, the fibers were generated to fill 20% of cuboidal space with predefined dimensions of $4\ \mu m \times 8\ \mu m \times 1\ \mu m$. Initially, all fibers were allowed to partially overlap.

The code of the generator is available in the GitHub repository: *https://github.com/ppieczywek/FibreGen*

2.4. Simulation procedure

The initial model geometry was imported into a simulation framework implemented as a hand-written multi-thread code in the C++ programming language. The architecture of the code was optimized to perform computations using graphics processing units. This was achieved by incorporating the open-source OpenCL library (The Khronos Group Inc., USA). The code was organized and compiled using *Microsoft Visual Studio 16.4.0* (Microsoft Corporation, USA).

The code repository is available for download from the GitHub repository: *https://github.com/ppieczywek/FibreNet*

All models were initiated with 400000 simulation steps of the energy equilibration scheme. The equations of motion of the beads were integrated with a modified Velocity Verlet scheme. During this phase, the bead velocities and forces of the beads were reset to zero every 1000 steps. The models were not subjected to external loads and the fibers were allowed to move freely. The equilibration scheme was used to allow overlapping fibers to move apart and obtain a stable low-energy model geometry.

Finally, the equilibrated models were used to simulate a uniaxial tensile test with strain up to 5% of its initial value. The positions of all beads along Y-axis at a distance of less than 0.5 μm from the edge of the model parallel to the X-axis were fixed. The velocity of beads on the opposite side of the model was set to a constant value along the Y-axis, to simulate the motion of the clamps of the tensile testing machine. The velocity was set to simulate sample deformation at a strain rate of ~$1.5 \times 10^5\ s^{-1}$, and the time step of simulation was set as ~0.1 ps. Global damping was implemented to numerically stabilize the entire system. Non-equilibrium effects were not considered in current study.

Sensitivity analysis was performed with respect to four input parameters: fiber diameter, fiber length, fiber modulus as a descriptor of fiber stiffness and force constant of interfiber interaction.

The complete set of input parameters is listed in Table S1. For each set of parameters, five separate models were generated.

During the simulation, the sum of the tensile forces along the stretching direction from all fixed beads along with sample strain was recorded. For each measurement point, the thickness and width of the model were determined at a point equidistant between the virtual clamps. Both values were used to calculate the rectangular cross-sectional area of the model. Tensile force of the specimen and the cross-sectional area were used to calculate tensile stress.

The final stress-strain curves were used to determine Young's modulus, strain hardening modulus, strain at elastic limit, stress at elastic limit and maximum stress of the sample.

Table S1. Sets of input parameters of the model, tested during the sensitivity analysis.

Parameter	Network density	Fiber radius	Fiber modulus	Fiber length	Force constant of interfiber interaction
	%	nm	GPa	μm	N/m
Fiber radius	20	45	125	2.5	246 - 987
		47.5			
		50			
		52.5			
		55			
Fiber modulus	20	50	95	2.5	246 - 987
			110		
			125		
			140		
			155		
Fiber length	20	50	125	1.5	246 - 987
				2	
				2.5	
				3	
				3.5	
Force constant of interfiber interaction	20	50	125	2.5	82 - 329
					164 - 658
					246 - 987
					329 - 1316
					411 - 1645

6.5. Supplementary research P5

6.5.1. Graphical abstract of the Supplementary research P5

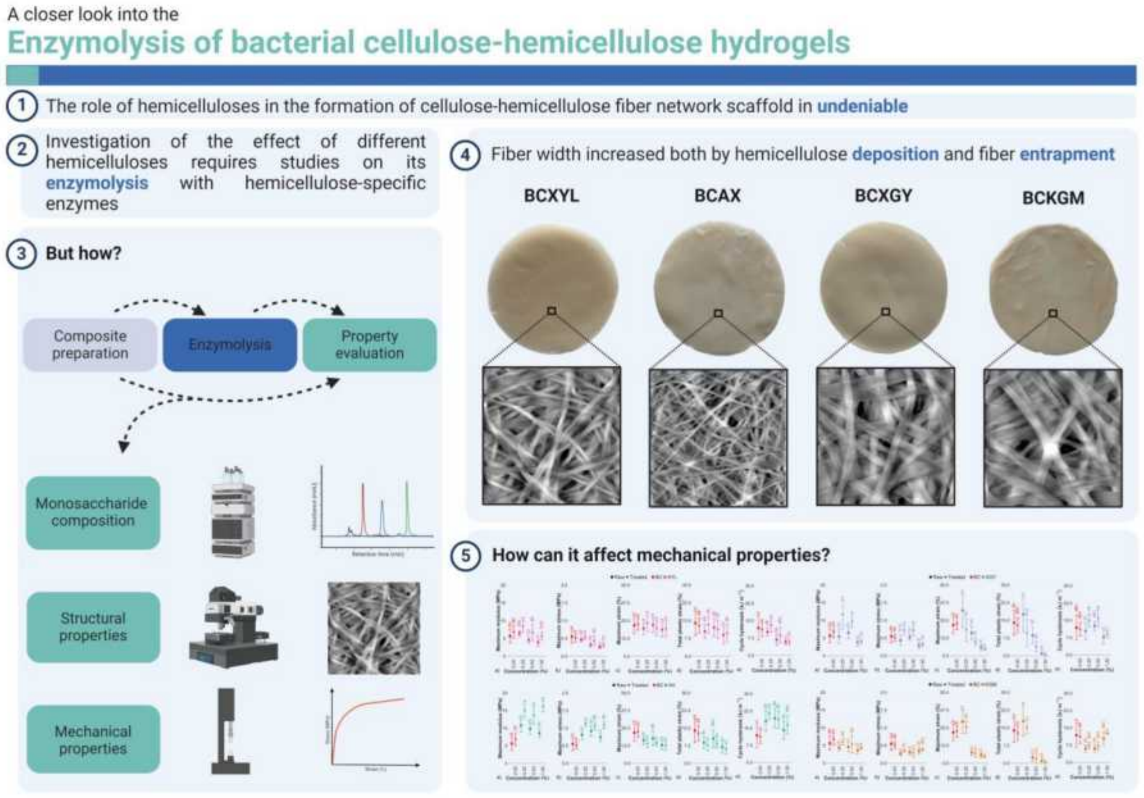

A closer look into the

Enzymolysis of bacterial cellulose-hemicellulose hydrogels

① The role of hemicelluloses in the formation of cellulose-hemicellulose fiber network scaffold in **undeniable**

② Investigation of the effect of different hemicelluloses requires studies on its **enzymolysis** with hemicellulose-specific enzymes

③ **But how?**

④ Fiber width increased both by hemicellulose **deposition** and fiber **entrapment**

⑤ **How can it affect mechanical properties?**

6.5.2. Content of the Supplementary research P5

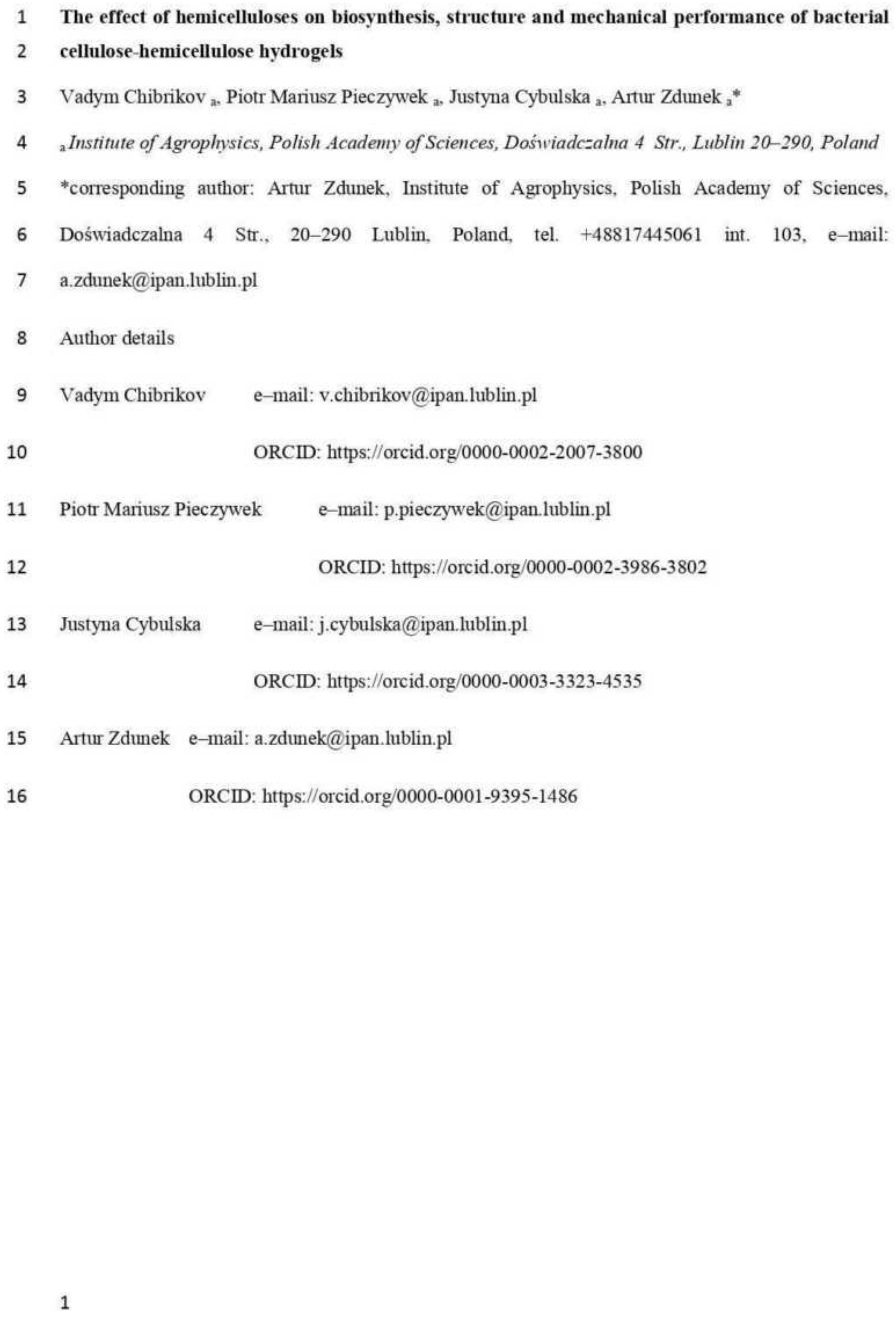

The effect of hemicelluloses on biosynthesis, structure and mechanical performance of bacterial cellulose-hemicellulose hydrogels

Vadym Chibrikov [a], Piotr Mariusz Pieczywek [a], Justyna Cybulska [a], Artur Zdunek [a]*

[a] *Institute of Agrophysics, Polish Academy of Sciences, Doświadczalna 4 Str., Lublin 20–290, Poland*

*corresponding author: Artur Zdunek, Institute of Agrophysics, Polish Academy of Sciences, Doświadczalna 4 Str., 20–290 Lublin, Poland, tel. +48817445061 int. 103, e–mail: a.zdunek@ipan.lublin.pl

Author details

Vadym Chibrikov e–mail: v.chibrikov@ipan.lublin.pl
ORCID: https://orcid.org/0000-0002-2007-3800

Piotr Mariusz Pieczywek e–mail: p.pieczywek@ipan.lublin.pl
ORCID: https://orcid.org/0000-0002-3986-3802

Justyna Cybulska e–mail: j.cybulska@ipan.lublin.pl
ORCID: https://orcid.org/0000-0003-3323-4535

Artur Zdunek e–mail: a.zdunek@ipan.lublin.pl
ORCID: https://orcid.org/0000-0001-9395-1486

Abstract

The primary plant cell wall (PCW) is a specialized structure composed predominantly of cellulose, hemicelluloses and pectin. While the role of cellulose and hemicelluloses in the formation of the PCW scaffold is undeniable, the mechanisms of how hemicelluloses determine the mechanical properties of PCW remain debatable. Thus, we produced bacterial cellulose–hemicellulose hydrogels as PCW analogues, incorporated with hemicelluloses. Next, we treated samples with hemicellulose degrading enzymes, and explored its structural and mechanical properties. As suggested, difference of hemicelluloses in structure and chemical composition resulted in a variety of the properties studied. By analyzing all the direct and indirect evidences we have found that glucomannan, xyloglucan and arabinoxylan increased the width of cellulose fibers both by hemicellulose surface deposition and fiber entrapment. Arabinoxylan increased stresses and moduli of the hydrogel by its reinforcing effect, while for xylan, increase in mechanical properties was determined by establishment of stiff cellulose–cellulose junctions. In contrast, increasing content of xyloglucan decreased stresses and moduli of hydrogel by its weak interactions with cellulose, while glucomannan altered cellulose network formation via surface deposition, decreasing its strength. The current results provide evidence for structure–dependent mechanisms of cellulose–hemicellulose interactions, suggesting the specific structural role of the latter.

Keywords

Bacterial cellulose; hemicellulose; hydrogels; enzymolysis; structure; mechanical properties.

1. Introduction

The primary plant cell wall (PCW) is a highly specialized structure composed primarily of water and polysaccharides, while glycoproteins, phenols, minerals, and enzymes serve as minor components. Cellulose, hemicelluloses and pectins are the three main types of PCW polysaccharides with mass fractions of 20-40%, 20-30% and 30-50% of dry mass, respectively [1]. Cellulose is a linear polysaccharide of β-D-glucose linked by 1→4 glycosidic bonds, which is considered to be the major load-bearing component of PCW [2]. Hemicelluloses consist predominantly of 1→4-linked monosaccharides of β-D-glucose, β-D-glucuronic acid, D-xylose, β-D-mannose, β-D-galactose, α-L-fucose, and α-L-arabinose [3]. Due to structural similarity to cellulose, hemicelluloses are thought to enable the formation of a broad hydrogen bonding network that determines the mechanical properties of PCW [4]. And for the last 60 years, it allowed the scientific community to evolve through the various concepts of primary plant cell wall structure [5–10]. The very first PCW models considered cellulose as an organized network, immersed in amorphous matrix of PCW components [5]. However, the following PCW models suggested there is an option PCW matrix polysaccharides (hemicellulose, pectin) to define intefiber interactions by covalent linkages [6,11], direct fiber coating [7], formation of interfiber tethers [8], as well as forming polysaccharide-linking amalgam in close proximity to fiber surface [9,10]. To the best of our knowledge, all the PCW models reported have declared undeniable role of hemicelluloses in the integrity of the PCW scaffold. So do the modern theory, supporting the notion that cellulose is the main load-bearing component of PCW, while the key component of PCW mechanical properties - interfiber adhesion - is determined by the hemicellulose-mediated interactions.

The main insights into the structure and mechanical properties of PCW can be reached by the decomposition of PCW constituents *in muro* [12], inhibition of its biosynthesis [10], *in vitro* solubilisation [13], or chemical modification [14]. Beside of that, fiber networks such as those of bacterial cellulose (BC) mimic PCW fiber networks on a macroscale, being homogeneous, repeatable, modifiable, and easy to handle. The homogeneous fiber distribution and its layered structure are the key factors for the stiffness of the BC fiber network, similar to those of PCW.

Despite the most common BC-hemicellulose fiber networks, such as BC-xyloglucan, BC-pectin, and BC-xyloglucan-pectin have already been studied [15–17], there is still a lack of understanding on the role of other hemicelluloses and their content on structure and mechanical properties of cellulose-hemicellulose fiber networks. Moreover, previous explorations of mechanical properties of cellulose‑ hemicellulose fiber networks were limited to their study in the dry state, while its description and exploration as a water‑ swollen network, analogous to in vivo PCW, was barely revealed [18].

This study aimed to investigate the effect of different hemicelluloses on the process of biosynthesis, composition, structure and mechanical properties of cellulose-hemicellulose hydrogels, that mimic PCW. The study was particularly focused on the effect of post-biosynthetic enzymolysis of hemicelluloses. Current approach aimed to define the structure-dependent interaction of hemicelluloses with cellulose and to evaluate its consequences for the structure and mechanical properties of cellulose-hemicellulose hydrogels. Since the hemicelluloses differ in chemical composition (molecular weight, monosaccharide composition), their incorporation in cellulose fiber network and enzymatic degradation affect the load bearing junctions in cellulose-hemicellulose hydrogels, so that affecting its mechanical properties. Because the hemicelluloses, used in the study, represent the most common in monocots and dicots, the results obtained can serve as a reference for a wide range of PCW, their models, as well as get across the possible commercial use of respected biomaterials. To our knowledge, this study is the only integrated analysis of the role of hemicelluloses and its enzymolysis on the mechanical properties of cellulose-hemicellulose hydrogels, combined with structural studies, and exploration of its chemical composition.

2. Materials and methods

2.1. Sample preparation

2.1.1. Biosynthesis of BC-hemicellulose hydrogels

Pure BC was produced in Hestrin-Schramm (HS) culturing medium with no hemicelluloses [19]. The culturing medium was autoclaved at 121 °C for 11 min, and then brought to reach room temperature. Then, 100 mL of culturing medium was transferred to sterile 250 mL Erlenmeyer flasks followed by 2 mg of two‑ day fresh colonies of *Komagataiebacter xylinum* ATCC‑ 53524 (LGC Standards, UK) bacteria strain. To obtain flat sheets, BC hydrogels were produced statically at

30±1 °C for 10 days. After production, samples were stirred with deionized water for 4 days to remove debris from culturing medium, bacteria trapped, proteins, as well as loosely attached hemicelluloses. BC-hemicellulose hydrogels were stored in a 0.02% mass sodium azide solution at 4±1 °C before further use [20]. The dry yield of biosynthesis of raw samples was calculated in triplicate as a dry mass of BC synthesized per 1 litre of culturing medium.

In contrast, BC- hemicellulose hydrogels were prepared in a HS medium with an addition of respected hemicelluloses [17]. The medium was prepared by dissolving 2% mass glucose (Sigma-Aldrich, USA), 0.5% mass casein peptone (Sigma-Aldrich, USA), 0.5% mass yeast extract (Thermo Fisher Scientific, USA), 0.27% mass anhydrous disodium phosphate (Chempur, Poland), and 0.115% mass citric acid monohydrate (Chempur, Poland) in deionized water. The pH of the culturing medium was then adjusted to 5.0 with 1M NaOH/HCl. One of the four hemicelluloses - tamarind xyloglucan (P-XYGLN, > 95% purity, Megazyme, Bray, Ireland), beechwood xylan (P-XYLNBE-10G, > 95% purity, Megazyme, Bray, Ireland), medium-viscosity wheat flour arabinoxylan (P-WAXYL, > 95% purity, Megazyme, Bray, Ireland), and low-viscosity konjac glucomannan (P-GLCML, > 98% purity, Megazyme, Bray, Ireland) was added to culturing media. Monosaccharide composition and the weight average molecular weight of hemicelluloses used in current study is provided in Table 1 [21].

Hemicellulose	Monosaccharide composition (% dry polysaccharide mass)							Weight average molecular weight (kDa)
	Araf	*Gal*	*Glc*	*GlcA*	*Man*	*Xyl*	Other	
Xylan				11.3		86.1	2.6	158.3
Arabinoxylan	37.8					61.7	0.5	323.0
Xyloglucan	2.0	17.0	45.0			34.0	2.0	802.5
Glucomannan			40.0		60.0			950.0*

Table 1. Monosaccharide composition and weight average molecular weight of hemicelluloses, used in current study. Abbreviation of *Araf* stands for arabinose, *Gal* – galactose, *Glc* – glucose, *GlcA* – glucuronic acid, *Man* – mannose, *Xyl* – xylose. Data on monosaccharide composition and weight average molecular weight was provided by a manufacturer. Asterisk sign * refers to data from [22].

The mass fractions of hemicelluloses in the culturing medium of respected hydrogels are presented in Table 2.

Type of hemicellulose	Mass fraction in culturing medium (% w/v)			
	0.00	0.25	0.50	1.00
Arabinoxylan	BC	AX0.25	AX0.50	AX1.00
Glucomannan		KGM0.25	KGM0.50	KGM1.00
Xyloglucan		XGY0.25	XGY0.50	XGY1.00
Xylan		XYL0.25	XYL0.50	XYL1.00

Table 2 Samples studied, code names, and mass fractions of hemicelluloses in culturing medium. BC stands for pure bacterial cellulose, other abbreviations stand for the specific hemicelluloses used.

At the beginning of the preparation of BC-hemicellulose hydrogels, an increasing turbidity of the culturing medium was observed, corresponding to the initiation of BC biosynthesis [23], followed by the formation of a hydrogel pellicle on medium-air interphase. After terminating of cultivation and washing, BC- hemicellulose hydrogels appeared as a round pellicles with an approximate diameter of 55±2 mm, and highly hydrated (~98% mass of water; Fig.1a). In the following sections, current samples were defined as *raw*.

2.1.2. *Alkali treatment and enzymolysis*

Alkali treatment and enzymolysis were performed to ensure depolymerization and removal of hemicelluloses of BC-hemicellulose hydrogels. Initially, samples were washed with deionized water to remove excess sodium azide. Then, samples were treated with 0.1M NaOH at 80±1 °C for 30 min in triplicate, to remove proteins. Subsequently, the samples were washed in deionized water at 100±1 °C for 60 min, which is supposed not to affect hemicellulose composition, and not to change the structure and properties of BC [15,24]. Commercial enzymes (all - Megazyme, Ireland), specific to hemicelluloses used in current study, were chosen for enzymolyses. Enzyme solutions were prepared according to the manufacturer's recommendations, and the following data are presented in Table 3.

Hemicellulose	Enzyme	Solution composition	Reaction catalyzed
Arabinoxylan	Endo-β-1→4-xylanase (EC 3.2.1.8)	0.1M sodium phosphate buffer (pH=6), 0.5 mg/mL BSA	Enzymolysis of xylan to oligosaccharides
	α-L-arabinofuranosidase (EC 3.2.1.55)	0.1M sodium acetate buffer (pH=4)	Enzymolysis of α-1→2- and α-1→3-linked L-arabinofuranose sidechains of arabinoxylan
Glucomannan	Endo-1→4-β-mannanase (EC 3.2.1.78)	0.1M sodium acetate buffer (pH=4)	Enzymolysis of β-1→4-D-mannosidic linkages of glucomannan
Xyloglucan	Xyloglucan-specific endo-β-1→4-glucanase (EC 3.2.1.151)	0.1M sodium acetate buffer (pH=5.5), 1 mg/mL BSA	Enzymolysis of β-1→4-D-glycosidic linkages of xyloglucan
Xylan	Endo-β-1→4-xylanase (EC 3.2.1.8)	0.1M sodium phosphate buffer (pH=6), 0.5 mg/mL BSA	Enzymolysis of xylan to oligosaccharides

Table 3 Hemicelluloses, hemicellulose-specific enzymes used, the composition of the enzyme solutions, and the reactions catalysed by enzymes. EC – Enzyme Commission number, BSA – bovine serum albumin.

Enzymatic treatment of BC-hemicellulose hydrogels was conducted by immersing hydrogels in 10 U/mL enzyme solutions up to $6.67 \times 10^{-3} \frac{g\ of\ hydrogel\ dry\ mass}{mL\ of\ enzyme\ solution}$ concentration. Thus, approximately 5 g of BC-hemicellulose hydrogels were immersed in 15 mL of enzyme solutions with an enzyme activity of 10 U/mL, where 1 U stands for conversion of 1 μmol of substrate per minute. The enzyme solutions were left diffusing within the samples for 3 h at 21±1 °C, followed by 5 h at 40±1 °C [25]. In the case of BC-arabinoxylan hydrogels, two successive enzymolyses were performed - first with endo-β-1→4-xylanase, followed by α-L-arabinofuranosidase. Pure BC was treated with 0.1M sodium phosphate buffer (pH=6) under the same conditions. Each treatment was terminated by washing hydrogels first in respected buffers, followed by deionized water. Finally, hydrogels were stored in a 0.02% mass sodium azide solution at 4 °C prior to further use. In the following sections, the samples were defined as *treated*.

2.2. Monosaccharide composition

Monosaccharide composition of both raw and treated BC-hemicellulose hydrogels was conducted according to [26] with slight modifications. Oven-dried and milled samples with a mass of appr. 0.1 g were first incubated at 80 °C for 72 h in 2M hydrochloric acid in methanol (Sigma-Aldrich, USA), followed by hydrolysis with 2 mL of 3M trifluoroacetic acid (Merck, Germany) at 100 ºC for 7 h. Hydrolyzed samples were incubated at 70 ºC for 1 h in a mixture of 1 mL of high-performance liquid chromatography (HPLC) water (Chempur, Poland), 0.05 mL of 0.3M aqueous sodium hydroxide and 0.05 mL of 0.5M 1-phenyl-3-methyl-5-pyrazolone (Thermo Scientific Chemicals, USA) solution in methanol. After that, samples were neutralized with 0.05 mL of 0.3M aqueous hydrochloric acid (Chempur, Poland), and sample monosaccharides were extracted threefold with chloroform (Merck, Germany). Reference samples of monosaccharides and uronic acids (arabinose, galactose, galacturonic acid, glucose, glucuronic acid, mannose, rhamnose, and xylose; all – Sigma-Aldrich, Germany) were processed the same way.

Samples were analysed using a HPLC system of S1130 pump, S5300 sample injector, S4120 column oven, and S3350 photodiode array detector at 246 nm wavelength (all – Sykam GmbH, Germany). For HPLC analysis, the ZORBAX Eclipse XDB analytical column, and Eclipse XDB–C18 guard column (all - Agilent Technologies, USA) were used. For each sample, monosaccharide analysis was performed in triplicate.

2.3. Surface topography

Surface topography imaging was performed with an atomic force microscope (MultiMode 8-HR, Bruker, USA) in ScanAsyst in Air™ tapping mode on samples oven-dried at 45±1 ºC up to constant mass. Two randomly chosen pieces of an approximate area of 15 mm^2 were cut out and stuck to atomic force microscope (AFM) metal specimen disks. A SCANASYST-AIR AFM cantilever (Bruker, USA) was used for imaging. Overall captured area for single image was set to 2×2 μm with an image resolution of 1.95 nm per pixel. Images were processed with *Gwyddion 2.48* software [27] for correction of data artefacts. For each sample, 10 images were captured to obtain a representative number of data. Surface topography imaging of samples was performed at a temperature of 19±1 ºC, and a relative humidity of 33±2% Then, the average width was evaluated for 100 random cellulose fibers. In the current paper, the term *microfiber* characterizes a structural unit of cellulose chains of identical dimensional configuration, gathered in crystalline/semi-crystalline/amorphous domains. The term *fiber* refers to a group of microfibers, interacting with each other by weak forces, which structurally appear as a single unit, and in terms of applied load provide a similar response. For 10 random surface topography images of each type of bacterial cellulose-hemicellulose hydrogels, root mean square toughness was calculated according to the following equation:

$$Rq = \sqrt{\frac{1}{n}\sum_{i=1}^{n} y_i^2} \qquad \textbf{(1)},$$

where Rq is root mean square roughness, n is a value of points measured, and y is surface profile deviation value.

2.4. Uniaxial tensile test with cyclic load

The mechanical properties of both raw and treated BC-hemicellulose hydrogels were evaluated using uniaxial tensile test with cyclic load. Pellicles (Fig.1a) were cut into rectangular strips with an approximate length of 20 mm and width of 3 mm (Fig.1b, I). The width of strips was defined as an average of three along the sample. The thickness of each specimen was measured using a BAKER IP54 digital micrometer (Baker Gauges India Private Limited, India). A tensile stage microtester (Deben Microtest, UK) with a 200N load cell was used for mechanical testing (Fig.1b).

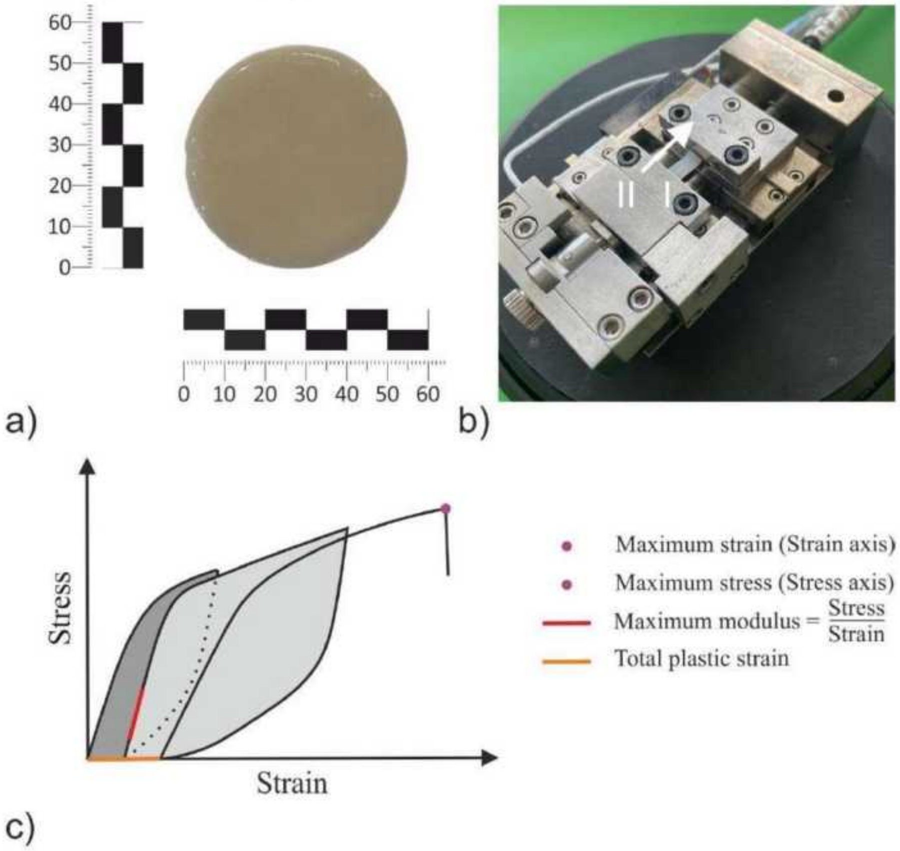

Fig.1. Uniaxial tensile test with cyclic load of BC-hemicellulose hydrogels: a) BC-hemicellulose hydrogel on a millimeter-precision scale; b) tensile stage microtester with marked: I) strip of BC-hemicellulose hydrogel, II) direction of loading; c) schematic three-cycle stress-strain curve. The colored lines, points and areas define mechanical properties evaluated, while the annotation on the right provides the definition.

Samples were subjected to uniaxial tensile test with cyclic load at a strain rate of 500 μm/min, with the tensile strain increase of 500 μm per cycle. Prior to the initial loading of the first cycle, the sample was pre-loaded with a force of 0.05N to ensure fiber uncrimping. A dwelling time of 10 s was applied for stress relaxation within the sample between consecutive cycles. During the dwelling time of each consecutive cycle, sample was rehydrated by drop-deposition of 10 µL of deionized water to ensure sample hydration. Cyclic tension was performed up to the sample fracture. The tests were performed in 10 replicates at a temperature of 19±1 °C, and a relative humidity of 33±2%. Schematic stress-strain curve with a graphical representation of the evaluated mechanical properties are given in Fig.1c. Experimental stress-strain curve of raw BC, obtained by the uniaxial tensile test with cyclic load is provided in Supplementary Materials as Fig.S1.

Data from stress-strain curves were extracted using Python procedure [28]. The maximum stress and maximum strain were defined at the cycle with the highest force. Maximum modulus was defined as the maximum value of the slope of the linear part of the stress-strain curve in a single test. The total plastic strain was given as a sum of the irreversible strains in each cycle.

2.5. Statistical analysis

Statistical analysis of experimental data was performed using *RStudio v.4.1.1* software (Posit Software, USA). Differences between monosaccharide composition, and structural and mechanical properties were analyzed using one-way analysis of variance and Tukey test at a significance level of p=0.05.

3. Results and discussion

3.1. Dry yield of biosynthesis

Produced BC-hemicellulose hydrogels (Fig.1a) appeared as smooth layered pellicles. The dry yield of biosynthesis of pure BC was 2.8±0.4 g/L (Fig.2), being consistent with data, reported previously [16,29].

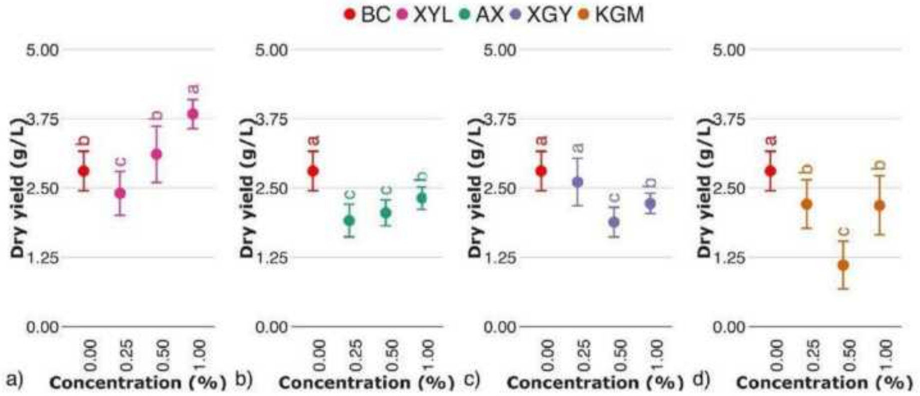

Fig.2. Dry yield of biosynthesis of BC-hemicellulose hydrogels in relation to the presence of a) xylan (XYL), b) arabinoxylan (AX), c) xyloglucan (XGY), and d) glucomannan (KGM) in culturing medium. The control sample (BC) is marked with red colour. For the estimated parameters, the data points and bars refer to the mean values and standard deviation, respectively. Treatments with the same letter show a lack of statistically significant differences.

The presence of hemicelluloses in the culturing medium resulted in a change of the dry yield of biosynthesis of respected hydrogels. An increase in dry yield of biosynthesis of BC with xylan presence was obtained compared to the pure BC (Fig.2a). Despite the presence of glucose in the culturing medium, *K.xylinum* has also been reported to metabolise xylose [30], being involved in bacterial growth rather than BC biosynthesis. In contrast to xylan, the addition of arabinoxylan resulted in a decrease in the dry yield of biosynthesis (Fig.2b), showing poor ability to be utilized by *K.xylinum* [29]. Compared to unsubstituted xylan, arabinose sidechains stabilize the arabinoxylan backbone, so that the degradation of arabinoxylan backbone to xylose should be considered minor.

The presence of xyloglucan in the culturing medium resulted in a decrease in dry yield of biosynthesis (Fig.2c), which correlates with limited water solubility of xyloglucan, restricting the mobility of bacteria and nutrients. Statistically significant higher dry yield of BC biosynthesis in xyloglucan-enriched medium was previously reported for agitated culturing [31]. Since agitated culturing conditions provide a homogeneous distribution of bacteria and nutrients within the medium, xyloglucan may act as a stabilizer of solution, while for static culturing conditions, limited solubility and possible aggregation of xyloglucan may limit BC biosynthesis. Biosynthesis of BC in the presence of glucomannan resulted in a decrease of dry yield of biosynthesis, compared to control (Fig.2d). A similar phenomenon has been reported for other culturing media [31,32] and is related to its limited solubility and polysaccharide over supplementation of culturing medium.

3.2. Monosaccharide composition

Monosaccharide composition of both raw and treated BC-hemicellulose hydrogels is provided in Fig.3. Apart from glucose, both raw and treated BC contained trace amounts of arabinose and xylose, originating from an entrapped medium components. Raw hydrogels, cultured in the medium with specific hemicellulose additives resulted in the presence of the respected monosaccharides – glucuronic acid and xylose – for BC–xylan hydrogels; arabinose, galactose, galacturonic acid, and xylose – for BC–arabinoxylan hydrogels; galactose, galacturonic acid and xylose – for BC–xyloglucan hydrogels; mannose – for BC–glucomannan hydrogels. What is of specific interest, is that the traces of galacturonic acid were observed in BC–hemicellulose hydrogels, possible as a backbone β-D-GalpA-(1→2)-α-D-Xylp inclusions [33,34]. Another monosaccharide, common for pectin – rhamnose – was also reported in current samples, suggesting its appearance as a co-product of hemicellulose extraction, also being reported in reducing ends of some hemicelluloses [35–37]. Statistically significant increase of the content of hemicellulose monosaccharides in hydrogels with an increasing hemicellulose content in culturing medium allowed us to assume that hemicelluloses incorporated within respected hydrogels in a concentration–dependent manner.

For the treated BC–hemicellulose hydrogels, a statistically significant increase in glucose content was found, in addition to the reduction of the amount of hemicellulose monosaccharides. It allowed us to assume enzymolysis of hemicelluloses in respected hydrogels took place. However, enzymolysis was not complete in terms of entire hemicellulose removal, as from half to two–thirds of its initial content were still present within treated hydrogels. We suppose that incomplete enzymolysis occur since hemicelluloses are partially trapped in/within cellulose fibers, so that can only be released by cellulase treatment [9]. Thus, in this study, we assume enzyme–inaccessible hemicelluloses as an integral component of BC–hemicellulose hydrogels. Another crucial point is that despite culturing at various hemicellulose concentrations, no predominant mechanism (fiber entrapment, irreversible adsorption, etc.) of cellulose–hemicellulose binding was observed, since with an increasing hemicellulose content, both amounts of enzyme–accessible and enzyme–inaccessible hemicelluloses were increasing.

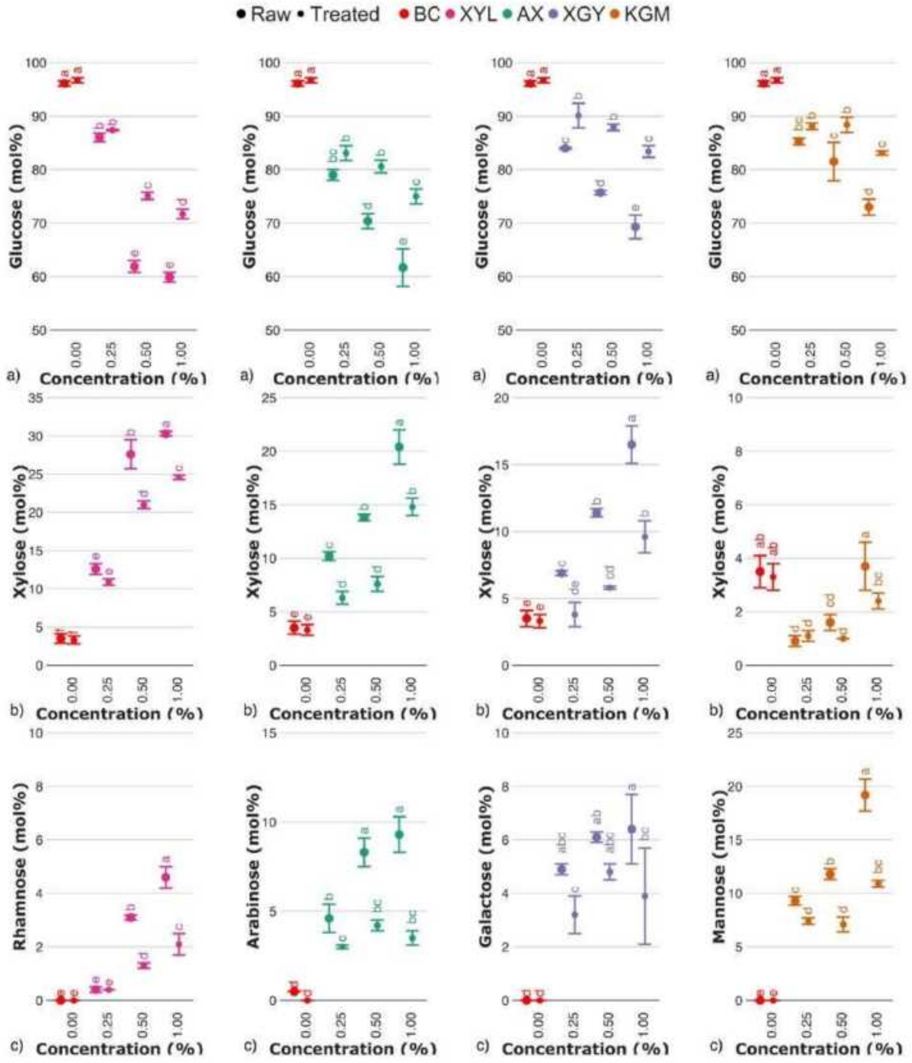

Fig.3. Monosaccharide composition of raw and treated BC–hemicellulose hydrogels in relation to the presence of xylan (XYL), arabinoxylan (AX), xyloglucan (XGY), and glucomannan (KGM) in culturing medium. Subsequent figures represent the content of a) glucose, b) xylose, and c) rhamnose (for bacterial cellulose-xylan hydrogels); arabinose (for bacterial cellulose-arabinoxylan hydrogels); galactose (for bacterial cellulose-xyloglucan hydrogels) mannose (for bacterial cellulose-glucomannan hydrogels). Raw and treated samples are indicated by the bullet points of different sizes. The control sample (BC) is marked with red colour. For the estimated parameters, the data points and bars refer to the mean values and standard deviation, respectively. Treatments with the same letter show a lack of statistically significant differences. Complete data on monosaccharide composition of bacterial cellulose-hemicellulose hydrogels is provided in Fig.S2 of Supplementary Materials.

3.3. Surface topography

AFM surface topography revealed that both raw and treated samples appeared as a network of randomly distributed fibers (Fig.4-5). No detectable differences in thicknesses of raw and treated BC-hemicellulose hydrogels were observed.

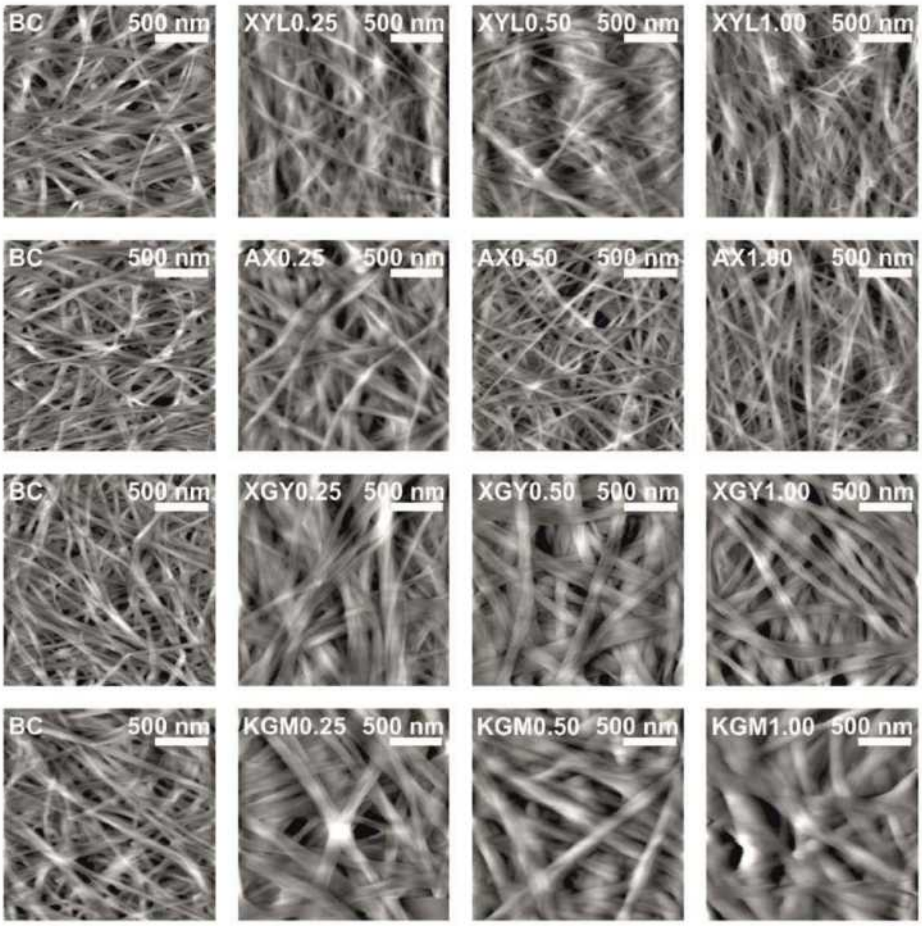

Fig.4. Atomic force microscopy surface topography images of raw BC-hemicellulose hydrogels in a dry state. Images are divided into rows according to the type of hemicellulose additive, while column indicate the amount of hemicellulose additive (% mass) in culturing medium. For each image, abbreviation and scale are provided.

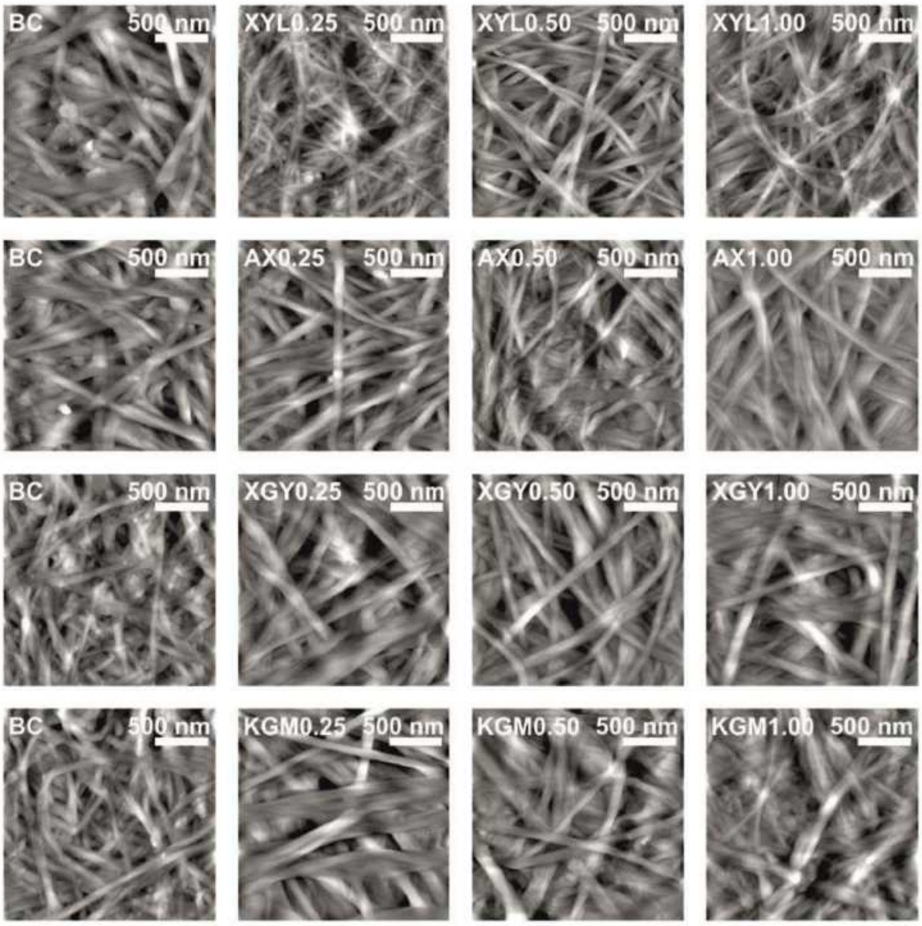

Fig.5. Atomic force microscopy surface topography images of treated BC-hemicellulose hydrogels in a dry state. Images are divided into rows according to the type of hemicellulose additive, while column indicate the amount of hemicellulose additive (% mass) in culturing medium. For each image, abbreviation and scale are provided.

In the case of pure BC, an average fiber width of 53±13 nm (Fig.6) was observed on AFM images. In terms of length, no cellulose fiber caps were observed on either the 2×2 μm capturing area or the larger area tested.

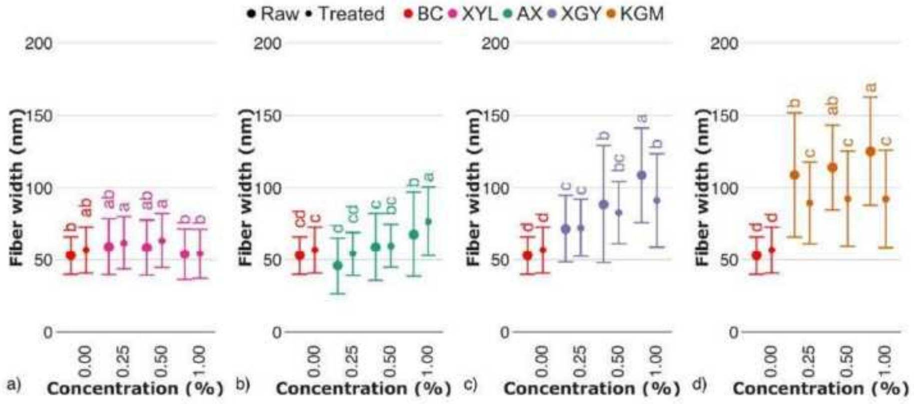

Fig.6. Cellulose fiber width of raw and treated BC–hemicellulose hydrogels with a) xylan (XYL), b) arabinoxylan (AX), c) xyloglucan (XGY), and d) glucomannan (KGM) in the dry state. Raw and treated samples are indicated by the bullet points of different sizes. The control sample (BC) is marked with red color. For the estimated parameters, the data points and bars refer to mean values and standard deviation, respectively. Treatments with the same letter show a lack of statistically significant differences.

With increasing xylan concentration, the fiber width of the treated samples have not changed, compared to the raw samples and pure BC (Fig.6a). Lack of data change may be related to the xylan entrapment within cellulose fibers, or in close proximity to interfiber crosslinks, making it enzyme–inaccessible. Contrary to xylan, the addition of arabinoxylan to the culturing medium increased fiber width (Fig.6b). We consider it to be a matter of nonspecific irreversible adsorption of arabinoxylan on the cellulose [38], since arabinoxylan has been reported to interact with cellulose fibers by surface deposition. Fiber width has not decreased after enzymolysis, compared to raw samples. We suppose that the endo–β–1→4–xylanase treatment of arabinoxylan could be hindered sterically by arabinose substitutes, and as far as the removal of arabinose sidechains increases arabinoxylan adsorption affinity to cellulose [39], the resulting change in fiber width was within the standard deviation. Another point may suggest substitution pattern define statistically significant differences in fiber width of both xylan and arabinoxylan, since it was reported to define interactions of hemicelluloses with cellulose [40].

Fiber width increased almost twofold for the XGY1.00 sample, compared to pure BC (Fig.6c). Fiber thickening may occur due to the adsorption of xyloglucan on the microfiber, which precedes fiber formation [41]. In addition to some entrapped xyloglucan fraction, partial xyloglucan deposition on fiber can be confirmed by the decrease in fiber width of the treated samples compared to raw.

Increasing concentration of glucomannan in the culturing medium resulted in a two– to threefold increase in fiber width in the case of the KGM1.00 sample, compared to pure BC (Fig.6d). Heterogeneous surface structure, in which cellulose bands are hardly distinguished, was the one, specific for BC–glucomannan fiber network. It matches with the research of Szymańska–Chargot et al., who reported higher affinity of glucomannan to adsorb on apple parenchyma cellulose, compared to other hemicelluloses (Szymańska–Chargot et al., 2024). Treatment of BC–glucomannan hydrogels with dilute alkali and endo–1→4–β–mannanase resulted in a decrease of cellulose fiber width (Fig.4d), reaching a plateau of about 90±30 nm of fiber width. It allowed us to assume that enzymolysis enabled complete removal of enzyme–accessible glucomannan, reaching the minimum values of fiber width, determined by enzyme–inaccessible glucomannan.

Data of fiber width is somehow correlated with one of surface roughness, which, despite moderacy of statistical differences, was on average lower for treated samples, compared to raw (Fig.7; Fig. S3-S4). Together with a lower data deviation for treated sampled, current data may provide to a conclusion that smoother surface of oven-dried bacterial cellulose-hemicellulose hydrogels may be a matter of the removal of enzyme-accessible hemicelluloses.

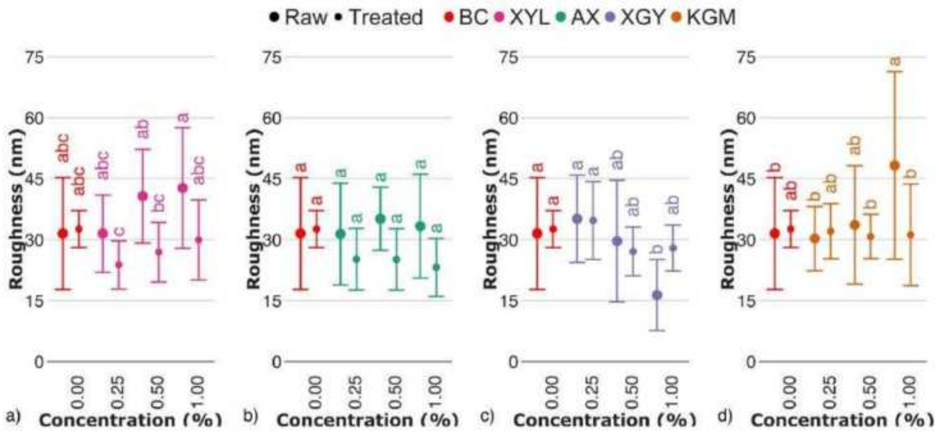

Fig.7. Root mean square roughness of raw and treated bacterial cellulose-hemicellulose hydrogels in relation to the presence of xylan (XYL), arabinoxylan (AX), xyloglucan (XGY), and glucomannan (KGM) in culturing medium. Subsequent figures represent the content of a) arabinose, b) fucose, c) galactose, d) galacturonic acid, e) glucose, f) glucuronic acid, g) mannose, h) rhamnose, and i) xylose in samples studied. Raw and treated samples are indicated by the bullet points rectangles, respectively. The control sample (BC) is marked with red colour. For the estimated parameters, the data points and bars refer to the mean values and standard deviation, respectively. Treatments with the same letter show a lack of statistically significant differences.

3.3. Mechanical properties of BC–hemicellulose hydrogels

As the concentration of xylan in the culturing medium increased, the values of the mechanical parameters decreased statistically significant for both raw and treated samples (Fig.8). Decreasing maximum modulus (Fig.8a) of BC–xylan hydrogels with increasing xylan content was observed. It allowed us to suggest the mechanism, according to which xylan, entrapped within cellulose fiber, affected packaging of cellulose microfibers, and promoting the formation of an amorphous cellulose. In addition, water within hydrogel may contribute to polysaccharide chains pushing away, forcing water–induced phase separation [43]. This is consistent with our data on the decreasing maximum modulus (Fig.8a) of BC–xylan hydrogels with increasing xylan content, suggesting that adsorbed water reduced the friction between fibers during cyclic loading and unloading. Phase separation phenomenon was also reported for other hemicelluloses studied, with the most prominent effect reported for xylan [44–46]. No statistically significant changes on maximum strain of BC-xylan hydrogels were observed (Fig.8c), while the one of total plastic strain (Fig.8d) were moderate.

For treated BC–xylan hydrogels, values of mechanical properties increased compared to raw samples (Fig.8). Mechanical properties of BC–xylan hydrogels were previously shown to be determined by the conformation of the xylan chain [47], with patterned rigid domains of the xylan chain tightly adsorbed to cellulose [48], and non–patterned irregularly substituted domains forming flexible loops and tails between the cellulose fibers. In addition, regularity/irregularity of xylose acetylation degree may facilitate tighter binding to cellulose, defining rigidity of bacterial cellulose-xylan fiber network [49]. It allows us to suggest a mechanism, in which enzymolysis of flexible or both rigid and flexible domains of the xylan lead to direct interactions between cellulose fibers, resulting in higher moduli and stresses (Fig.8b) in the treated samples, compared to raw. Moderate decrease in xylose content in treated BC–xylan hydrogels (Fig.3b) somehow confirm suggested mechanism.

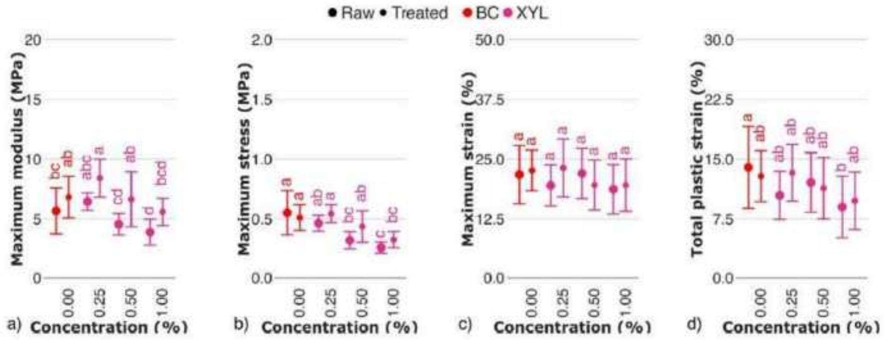

Fig.8. Mechanical properties of raw and treated BC–xylan hydrogels evaluated by cyclic tests: a) maximum modulus, b) maximum stress, c) maximum strain, d) total plastic strain. The control sample (BC) is marked in red. Raw and treated samples are indicated by bullet points and rectangles, respectively. For the estimated parameters, data points and bars refer to the mean and standard deviation, respectively. Treatments with the same letter show no statistically significant differences.

The mechanical properties of raw BC–arabinoxylan hydrogels showed statistically significant increase in terms of maximum modulus (Fig.9a), and maximum stress (Fig.9b), compared to pure BC. The dominant idea that may be considered here is that increasing maximum stress of BC–arabinoxylan hydrogels with an increasing arabinoxylan content can be attributed to its reinforcing effect [50], with unsubstituted regions of arabinoxylan chains interacting during the plastic deformation of the sample, so that enhancing the effect of fiber realignment. In addition, arabinoxylan was not reported to incorporate into cellulose fiber as xylan [51], affecting the packaging of cellulose chains, but mainly adsorb nonspecifically on cellulose surface [38]. The same effect was also observed in BC–arabinogalactan networks [52], suggesting a key role of arabinose sidechains in arabinoxylan–cellulose interactions.

The values of moduli and stresses of treated BC-arabinoxylan hydrogels showed statistically significant increase, compared to raw hydrogels, contrasting with other BC-hemicellulose hydrogels by trends on data change. Low–arabinosylated arabinoxylan with a decreased degree of polymerization were shown to exhibit lower moisture uptake compared to native arabinoxylan [53], being a matter of its higher crystallinity [54]. It is consistent with our study and suggests that increase in moduli and stresses (Fig.9a,b), and decrease in strains (Fig.9c,d) of BC–arabinoxylan hydrogels were defined by both the increase in polysaccharide crystallinity within the network and reduced moisture–induced plastic deformation. In addition, the removal of the arabinose sidechains increases the flexibility of the xylan chain, as well as the number of hydroxyl groups, resulting in a reinforcing effect of the flexible, low–substituted arabinoxylan.

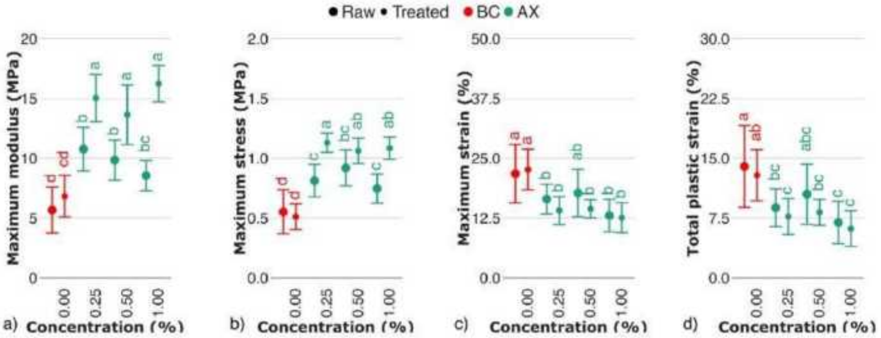

Fig.9. Mechanical properties of raw and treated BC–arabinoxylan hydrogels evaluated by cyclic tests: a) maximum modulus, b) maximum stress, c) maximum strain, d) total plastic strain. The control sample (BC) is marked in red. Raw and treated samples are indicated by bullet points and rectangles, respectively. For the estimated parameters, data points and bars refer to the mean and standard deviation, respectively. Treatments with the same letter show no statistically significant differences.

Contrary to both xylan and arabinoxylan, the presence of xyloglucan and glucomannan in culturing medium decreased the mechanical properties of the respective hydrogels. With increasing xyloglucan content, the values of maximum modulus, maximum stress, maximum strain, and total plastic strain decreased with a treatment–dependent trend (Fig.10). Xyloglucan was observed to deposit on cellulose surface during fiber extrusion by bacteria [55]. With a sequential increase of xyloglucan content in culturing medium, its deposition within the cellulose fibers also increases, reducing a number of stiff cellulose–cellulose junctions. In that case, we consider mechanical properties of BC–xyloglucan hydrogels are predominantly determined by weaker xyloglucan–

cellulose interactions, occurring both on surface of cellulose fiber and between cellulose microfibers forming fiber [42], which conceptually similar to PCW biomechanical hotspots [9] rather than stronger cellulose–cellulose interactions. Such a xyloglucan fraction is enzyme–inaccessible, acts as a mediate of both microfibers and fibers, and determines the trends of data change. At the same time, the presence (adsorption, adhesion, entrapment) or absence (solubilisation, enzymolysis) of enzyme–accessible xyloglucan determines data fluctuation.

Suggested role of enzyme–accessible xyloglucan correlates with a statistically significant increase of moduli (Fig.10a), and stresses (Fig.10b) of treated samples compared to raw. As xyloglucan content in hydrogel increases, the maximum stress is determined more by enzyme–inaccessible xyloglucan–mediated interfiber interactions, so that the effect of xyloglucan enzymolysis is limited.

In contrast to the moduli and stresses, the maximum strain (Fig.10c) was higher for raw samples, compared to treated. The total plastic strain of BC-xyloglucan hydrogels decreased (Fig.10d) with an increasing xyloglucan content, being governed by a reduction of interfiber friction by an amorphous xyloglucan.

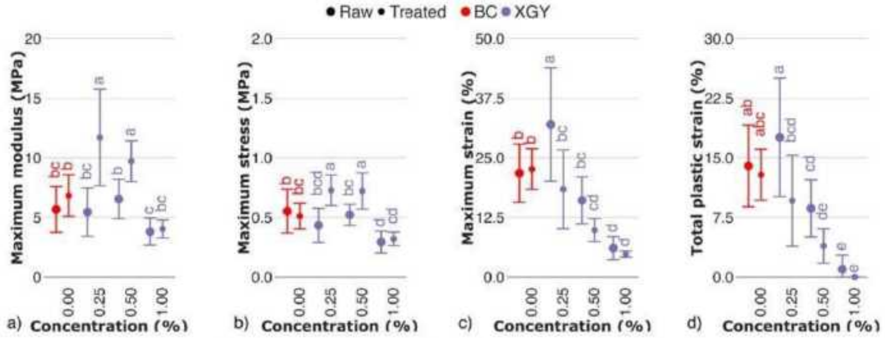

Fig.10. Mechanical properties of raw and treated BC–xyloglucan hydrogels evaluated by cyclic tests: a) maximum modulus, b) maximum stress, c) maximum strain, d) total plastic strain. The control sample (BC) is marked in red. Raw and treated samples are indicated by bullet points and rectangles, respectively. For the estimated parameters, data points and bars refer to the mean and standard deviation, respectively. Treatments with the same letter show no statistically significant differences.

The decrease of the mechanical properties of BC–glucomannan hydrogels was more prominent, compared to xyloglucan (Fig.11). An increase in glucomannan content resulted in a moderate decrease in moduli (Fig.11a), and stresses (Fig.11b). However, the change in maximum strain of the BC–glucomannan hydrogels was steep, decreasing from 22.6±4.3% to 4.7±0.2% for BC and KGM1.00, respectively (Fig.11c). At low glucomannan content, increase in mechanical properties is hypothesized to occur due to co–crystallization of low amounts of semi–crystalline glucomannan with BC [56], while with an increasing glucomannan content, decrease in mechanical properties is determined by an increasing glucomannan deposition on cellulose [57]. Due to the structural similarity of cellulose and glucomannan, it not only exhibits good binding affinity to cellulose, but also prevents direct assembly of microfibers and/or fibers [56]. The *in situ* interaction between glucomannan and bacteria–extruded microfibers can lead to the disruption of cellulose chain packaging [58], resulting in a formation of fragile fibers and fiber network, compared to pure BC.

In terms of mechanical properties, enzymolysis of the BC–glucomannan hydrogels resulted in moderate data change. The higher maximum strain for raw samples (Fig.11c), compared to treated, might indicate the role of glucomannan in resisting load at high strain, with a less pronounced effect compared to BC–xyloglucan hydrogels. Despite the decrease in fiber width for the treated BC–glucomannan hydrogels, the values were still higher compared to the control, suggesting that a part of glucomannan is enzyme–inaccessible. Therefore, the thicker fibers of raw samples resulted in limited entanglement and interfiber interactions within the network, leading to a lower maximum modulus, compared to the treated samples.

Similar to other hemicelluloses studied, glucomannan decreased the total plastic strain of BC–glucomannan hydrogels (Fig.11d). At low glucomannan content in culturing medium, its deposition on cellulose is lower, compared to water, so irreversible deformations are likely defined by a weakened hydrogen bonding network of water–mediated cellulose–cellulose and cellulose–glucomannan slip–stick interactions [59]. With increasing content, glucomannan predominantly deposits on cellulose, forming a strong hydrogen bonding network. The data obtained are consistent with the predominantly reversible deformation of cellulose–glucomannan hydrogels to cyclic compression, observed previously [18]. Moreover, observations on fiber width allowed to hypothesize that the decrease of irreversible deformation of BC–glucomannan hydrogels was governed by the limited formation of loops of thick fibers, so that interfiber friction define irreversibility of deformation was governed by interfiber friction.

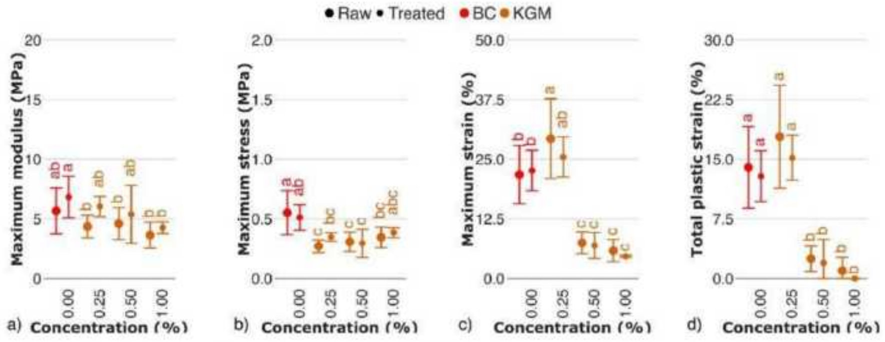

Fig.11. Mechanical properties of raw and treated BC–glucomannan hydrogels evaluated by cyclic tests: a) maximum modulus, b) maximum stress, c) maximum strain, d) total plastic strain. The control sample (BC) is marked in red. Raw and treated samples are indicated by bullet points and rectangles, respectively. For the estimated parameters, data points and bars refer to the mean and standard deviation, respectively. Treatments with the same letter show no statistically significant differences.

4. Conclusion

In current study we have investigated the interactions between bacterial cellulose (BC) and four hemicelluloses—arabinoxylan, xylan, xyloglucan, and glucomannan—in hydrogels. By examining the effects of these hemicelluloses on the structure, mechanical properties, and biosynthesis of BC-hemicellulose hydrogels, we were able to identify how the distinct structures and compositions of each hemicellulose influence these interactions.

Low-molecular-weight xylan and arabinoxylan had minimal impact on BC biosynthesis. In contrast, high-molecular-weight xyloglucan and glucomannan altered hydrogel formation due to increased medium viscosity and limited nutrient mobility. Removal of enzyme-accessible hemicelluloses, particularly xylan and xyloglucan, generally improved the mechanical properties of the hydrogels by enhancing cellulose-cellulose interactions.

The study also found that increasing xyloglucan content weakened the mechanical properties of BC–xyloglucan hydrogels due to weaker xyloglucan–cellulose interactions, while higher arabinoxylan content led to stronger hydrogels due to reinforced cellulose fibers. Glucomannan's impact on mechanical properties was less pronounced but similar to xyloglucan, with fiber network formation being altered by glucomannan deposition on and within the cellulose fibers.

These findings demonstrate the structure-dependent mechanisms of cellulose–hemicellulose interactions and suggest specific structural roles for each hemicellulose in determining the properties of BC–hemicellulose hydrogels. The results have potential applications in developing composite biomaterials for scientific and commercial use.

CRediT authorship contribution statement

Vadym Chibrikov: Methodology, Software, Formal Analysis, Investigation, Data Curation, Visualization, Writing – Original Draft; **Piotr Mariusz Pieczywek:** Conceptualization, Software, Formal Analysis, Data Curation, Writing – Review & Editing, Visualization, Supervision, Project Administration, Funding Acquisition; **Justyna Cybulska**: Methodology; Writing – Review & Editing; Formal analysis, Funding Acquisition; **Artur Zdunek:** Conceptualization, Writing – Review & Editing. All authors have read and agreed to the published version of the manuscript.

Declaration of competing interest

No potential conflict of interest was reported by the authors.

Data availability

Data will be made available on request. For data request, please contact v.chibrikov@ipan.lublin.pl

Acknowledgements

This work was supported by the National Science Centre, Poland [grant numbers 2019/35/D/NZ9/00555, 2020/37/B/NZ9/03159].

References

1. Cosgrove, D. J. & Jarvis, M. C. Comparative structure and biomechanics of plant primary and

secondary cell walls. *Front. Plant Sci.* **3**, 1–6 (2012).

2. Carpita, N. C. Update on mechanisms of plant cell wall biosynthesis: How plants make cellulose and other (1→4)-β-D-Glycans. *Plant Physiol.* **155**, 171–184 (2011).
3. Scheller, H. V. & Ulvskov, P. Hemicelluloses. *Annu. Rev. Plant Biol.* **61**, 263–289 (2010).
4. Khodayari, A., Thielemans, W., Hirn, U., Van Vuure, A. W. & Seveno, D. Cellulose-hemicellulose interactions - A nanoscale view. *Carbohydr. Polym.* **270**, 118364 (2021).
5. Probine, M. C. & Barber, N. F. The Structure and Plastic Properties of the Cell Wall of Nitella in Relation to Extension Growth. *Aust. J. Biol. Sci.* **19**, 439 (1966).
6. Keegstra, K., Talmadge, K. W., Bauer, W. D. & Albersheim, P. The Structure of Plant Cell Walls: III. A Model of the Walls of Suspension-cultured Sycamore Cells Based on the Interconnections of the Macromolecular Components. *Plant Physiol.* **51**, 188–97 (1973).
7. Talbott, L. D. & Ray, P. M. Molecular size and separability features of pea cell wall polysaccharides: Implications for models of primary wall structure. *Plant Physiol.* **98**, 357–368 (1992).
8. Carpita, N. C. & Gibeaut, D. M. Structural models of primary cell walls in flowering plants: Consistency of molecular structure with the physical properties of the walls during growth. *Plant J.* **3**, 1–30 (1993).
9. Park, Y. B. & Cosgrove, D. J. A revised architecture of primary cell walls based on biomechanical changes induced by substrate-specific endoglucanases. *Plant Physiol.* **158**, 1933–1943 (2012).
10. Park, Y. B. & Cosgrove, D. J. Changes in cell wall biomechanical properties in the xyloglucan-deficient xxt1/xxt2 mutant of Arabidopsis. *Plant Physiol.* **158**, 465–475 (2012).
11. Albersheim, P., Darvill, A., Roberts, K., Sederoff, R. & Staehelin, A. *Plant Cell Walls: A Renewable Material Resource.* (Garland Science, Taylo & Francis Group, 2011).
12. Hervé, C., Rogowski, A., Gilbert, H. J. & Knox, J. P. Enzymatic treatments reveal differential capacities for xylan recognition and degradation in primary and secondary plant cell walls. *Plant J.* **58**, 413–422 (2009).
13. Goulao, L. F. & Oliveira, C. M. Cell wall modifications during fruit ripening: when a fruit is not the fruit. *Trends Food Sci. Technol.* **19**, 4–25 (2008).
14. Kozioł, A., Cybulska, J., Pieczywek, P. M. & Zdunek, A. Changes of pectin nanostructure and cell wall stiffness induced in vitro by pectinase. *Carbohydr. Polym.* **161**, 197–207 (2017).
15. Szymańska-Chargot, M. *et al.* Simultaneous influence of pectin and xyloglucan on structure and mechanical properties of bacterial cellulose composites. *Carbohydr. Polym.* **174**, 970–979 (2017).
16. Chen, S. Q. *et al.* Characterisation of bacterial cellulose from diverse Komagataeibacter strains and their application to construct plant cell wall analogues. *Cellulose* **24**, 1211–1226 (2017).
17. Cybulska, J. *et al.* Mechanical characteristics of artificial cell walls. *J. Food Eng.* **96**, 287–294

(2010).

18. Berglund, J. *et al.* Wood hemicelluloses exert distinct biomechanical contributions to cellulose fibrillar networks. *Nat. Commun.* **11**, 1–16 (2020).

19. Hestrin, S. & Schramm, M. Synthesis of cellulose by Acetobacter xylinum. II. Preparation of freeze-dried cells capable of polymerizing glucose to cellulose. *Biochem. J.* **58**, 345–352 (1954).

20. Astley, O. M., Chanliaud, E., Donald, A. M. & Gidley, M. J. Tensile deformation of bacterial cellulose composites. *Int. J. Biol. Macromol.* **32**, 28–35 (2003).

21. Chibrikov, V., Pieczywek, P. M., Cybulska, J. & Zdunek, A. Coarse-grained molecular dynamics model to evaluate the mechanical properties of bacterial cellulose–hemicellulose composites. *Carbohydr. Polym.* **330**, 121827 (2024).

22. Franková, L. & Fry, S. C. Hemicellulose-remodelling transglycanase activities from charophytes: towards the evolution of the land-plant cell wall. *Plant J.* **108**, 7–28 (2021).

23. Avcioglu, N. H., Birben, M. & Seyis Bilkay, I. Optimization and physicochemical characterization of enhanced microbial cellulose production with a new Kombucha consortium. *Process Biochem.* **108**, 60–68 (2021).

24. Wolf, M. *et al.* Hot-Water Hemicellulose Extraction from Fruit Processing Residues. *ACS Omega* **7**, 13436–13447 (2022).

25. Chanliaud, E., De Silva, J., Strongitharm, B., Jeronimidis, G. & Gidley, M. J. Mechanical effects of plant cell wall enzymes on cellulose/xyloglucan composites. *Plant J.* **38**, 27–37 (2004).

26. Zhang, S., Hu, H., Wang, L., Liu, F. & Pan, S. Preparation and prebiotic potential of pectin oligosaccharides obtained from citrus peel pectin. *Food Chem.* **244**, 232–237 (2018).

27. Nečas, D. & Klapetek, P. Gwyddion: An open-source software for SPM data analysis. *Cent. Eur. J. Phys.* **10**, 181–188 (2012).

28. Pieczywek, P. M. TDA. https://github.com/ppieczywek/TDA (2022).

29. Fang, L. & Catchmark, J. M. Characterization of cellulose and other exopolysaccharides produced from Gluconacetobacter strains. *Carbohydr. Polym.* **115**, 663–669 (2015).

30. Cavka, A. *et al.* Production of bacterial cellulose and enzyme from waste fiber sludge. *Biotechnol. Biofuels* **6**, 1–10 (2013).

31. Gu, J. & Catchmark, J. M. Impact of hemicelluloses and pectin on sphere-like bacterial cellulose assembly. *Carbohydr. Polym.* **88**, 547–557 (2012).

32. Hu, Y., Catchmark, M. & Vogler, E. A. Factors Impacting the Formation of Sphere-Like Bacterial Cellulose Particles and Their Biocompatibility for Human Osteoblast Growth. *Biomacromolecules* **14**, 3444–3452 (2013).

33. Kong, Y. & York, W. S. A Galacturonic Acid – Containing Xyloglucan Is Involved in Arabidopsis Root Hair Tip Growth. *Plant Cell* **24**, 4511–4524 (2012).

34. Kaur, A. *et al.* Isolation and characterization of arabinoxylans from wheat bran and study of their contribution to wheat flour dough rheology. *Carbohydr. Polym.* **221**, 166–173 (2019).

35. Ray, B. *et al.* Structural investigation of hemicellulosic polysaccharides from Argania spinosa: Characterisation of a novel xyloglucan motif. *Carbohydr. Res.* **339**, 201–208 (2004).

36. Qaisrani, T. B., Qaisrani, M. M. & Qaisrani, T. M. Arabinoxylans from psyllium husk: A review. *J. Environ. Agric. Sci.* **6**, 33–39 (2016).

37. Huang, Y. *et al.* Relationships between Hemicellulose Composition and Lignin Structure in Woods. *J. Wood Chem. Technol.* **36**, 9–15 (2016).

38. Martinez-Sanz, M., Gidley, M. J. & Gilbert, E. P. Hierarchical architecture of bacterial cellulose and composite plant cell wall polysaccharide hydrogels using small angle neutron scattering. *Soft Matter* **12**, 1534–1549 (2016).

39. Mikkonen, K. S. *et al.* Arabinoxylan structure affects the reinforcement of films by microfibrillated cellulose. *Cellulose* **19**, 467–480 (2012).

40. Grantham, N. J. *et al.* An even pattern of xylan substitution is critical for interaction with cellulose in plant cell walls. *Nat. Plants* **3**, 859–865 (2017).

41. Martinez-Sanz, M., Lopez-Sanchez, P., Gidley, M. J. & Gilbert, E. P. Evidence for differential interaction mechanism of plant cell wall matrix polysaccharides in hierarchically-structured bacterial cellulose. *Cellulose* **22**, 1541–1563 (2015).

42. Szymańska-Chargot, M. *et al.* A study of the properties fo hemicelluloses adsorbed onto microfibrillar cellulose isolated from apple parenchyma. *Food Chem.* **1**, 137116 (2024).

43. Kulasinski, K., Guyer, R., Derome, D. & Carmeliet, J. Water Adsorption in Wood Microfibril-Hemicellulose System: Role of the Crystalline-Amorphous Interface. *Biomacromolecules* **16**, 2972–2978 (2015).

44. Berglund, J. *et al.* Acetylation and Sugar Composition Influence the (In)Solubility of Plant β-Mannans and Their Interaction with Cellulose Surfaces. *ACS Sustain. Chem. Eng.* **8**, 10027–10040 (2020).

45. Kishani, S., Vilaplana, F., Ruda, M., Hansson, P. & Wågberg, L. Influence of Solubility on the Adsorption of Different Xyloglucan Fractions at Cellulose-Water Interfaces. *Biomacromolecules* **21**, 772–782 (2020).

46. Sundberg, J., Toriz, G. & Gatenholm, P. Effect of xylan content on mechanical properties in regenerated cellulose/xylan blend films from ionic liquid. *Cellulose* **22**, 1943–1953 (2015).

47. Berglund, J. *et al.* Wood hemicelluloses exert distinct biomechanical contributions to cellulose fibrillar networks. *Nat. Commun.* **11**, 1–16 (2020).

48. Cosgrove, D. J. Nanoscale structure, mechanics and growth of epidermal cell walls. *Curr. Opin. Plant Biol.* **46**, 77–86 (2018).

49. Busse-Wicher, M. *et al.* The pattern of xylan acetylation suggests xylan may interact with cellulose microfibrils as a twofold helical screw in the secondary plant cell wall of Arabidopsis

thaliana. *Plant J.* **79**, 492–506 (2014).

50. Hoije, A., Stememalm, E., Heikkinen, S., Tenkanen, M. & Gatenholm, P. Material properties of films from enzymatically tailored arabinoxylans. *Biomacromolecules* **9**, 2042–2047 (2008).

51. Martinez-Sanz, M., Mikkelsen, D., Flanagan, B. M., Gidley, M. J. & Gilbert, E. P. Multi-scale characterisation of deuterated cellulose composite hydrogels reveals evidence for different interaction mechanisms with arabinoxylan, mixed-linkage glucan and xyloglucan. *Polymer (Guildf).* **124**, 1–11 (2017).

52. Lin, D., Lopez-Sanchez, P. & Gidley, M. J. Interactions of arabinogalactans with bacterial cellulose during its synthesis: Structure and physical properties. *Food Hydrocoll.* **96**, 644–652 (2019).

53. Sternemalm, E., Höije, A. & Gatenholm, P. Effect of arabinose substitution on the material properties of arabinoxylan films. *Carbohydr. Res.* **343**, 753–757 (2008).

54. Mikkonen, K. S. *et al.* Arabinoxylan structure affects the reinforcement of films by microfibrillated cellulose. *Cellulose* **19**, 467–480 (2012).

55. Whitney, S. E. C. *The interaction of cellulose with xyloglucan and other glucan-binding polymers*. (1996).

56. Berglund, J. Wood Hemicelluloses - Fundamental Insights on Biological and Technical Properties. (KTH Royal Institute of Technology, 2018).

57. Tokoh, C., Takabe, K., Fujita, M. & Saiki, H. Cellulose synthesized by Acetobacter xylinum in the presence of acetyl glucomannan. *Cellulose* **5**, 249–261 (1998).

58. Whitney, S. E. C., Brigham, J. E., Darke, A. H., Reid, J. S. G. & Gidley, M. J. Structural aspects of the interaction of mannan-based polysaccharides with bacterial cellulose. *Carbohydr. Res.* **307**, 299–309 (1998).

59. Hill, S. J., Franich, R. A., Callaghan, P. T. & Newman, R. H. Nature's nanocomposites: A new look at molecular architecture in wood cell walls. *New Zeal. J. For. Sci.* **39**, 251–257 (2009).

6.5.3. Supplementary Materials of the Supplementary research P5

The effect of hemicelluloses on biosynthesis, structure and mechanical performance of bacterial cellulose-hemicellulose hydrogels

Vadym Chibrikov [a], Piotr Mariusz Pieczywek [a], Justyna Cybulska [a], Artur Zdunek [a]*

[a] *Institute of Agrophysics, Polish Academy of Sciences, Doświadczalna 4 Str., Lublin 20–290, Poland*

*corresponding author: Artur Zdunek, Institute of Agrophysics, Polish Academy of Sciences, Doświadczalna 4 Str., 20–290 Lublin, Poland, tel. +48817445061 int. 103, e–mail: a.zdunek@ipan.lublin.pl

Author details

Vadym Chibrikov e–mail: v.chibrikov@ipan.lublin.pl
ORCID: https://orcid.org/0000-0002-2007-3800

Piotr Mariusz Pieczywek e–mail: p.pieczywek@ipan.lublin.pl
ORCID: https://orcid.org/0000-0002-3986-3802

Justyna Cybulska e–mail: j.cybulska@ipan.lublin.pl
ORCID: https://orcid.org/0000-0003-3323-4535

Artur Zdunek e–mail: a.zdunek@ipan.lublin.pl
ORCID: https://orcid.org/0000-0001-9395-1486

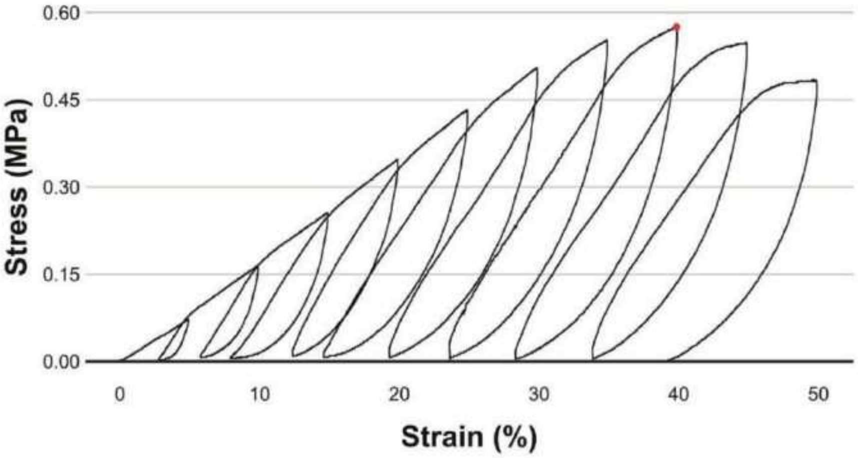

Fig.S1. Experimental stress-strain curve of raw BC, obtained by uniaxial tensile test with cyclic load. Original curves were captured as elongation-force one, converted to stress-strain curves, following by data smooth with convolution filter. The single deformation cycle was divided into a loading (up to a maximum stress reached within the applied strain increment), and an unloading (up to zero stress reached) stages. Deformation cycles were repeated with the constant tensile strain increments up to decrease of maximum force within two consecutive cycles. The maximum stress and maximum strain were defined as that, reached at the cycle with the highest stress value (marked with red point).

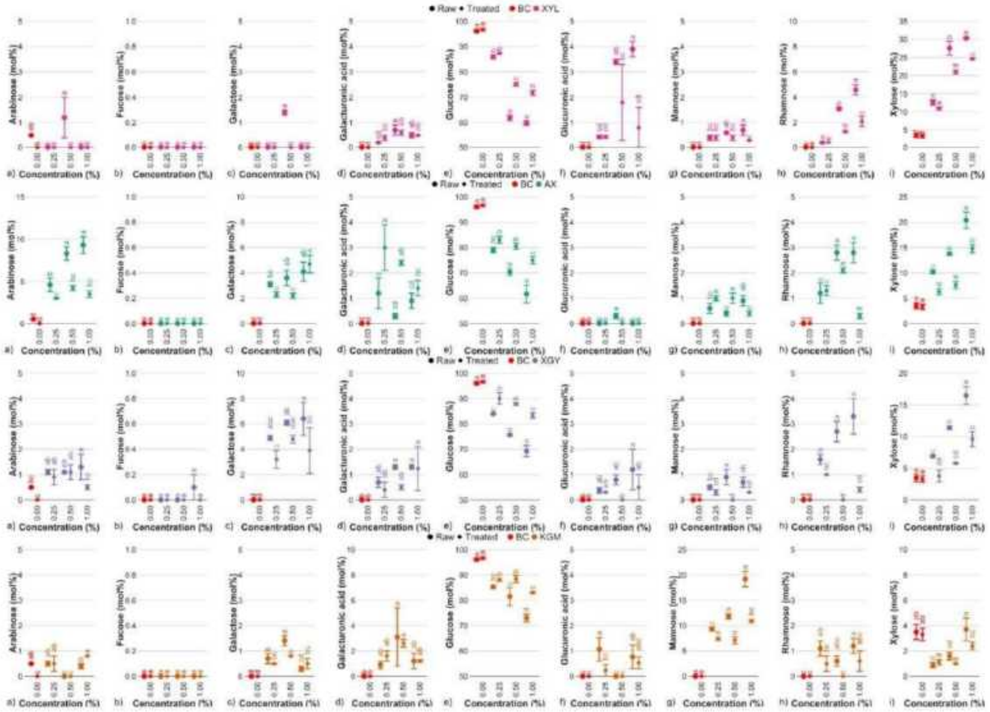

Fig.S2. Monosaccharide composition of raw and treated BC–hemicellulose hydrogels in relation to the presence of xylan (XYL), arabinoxylan (AX), xyloglucan (XGY), and glucomannan (KGM) in culturing medium. Subsequent figures represent the content of a) arabinose, b) fucose, c) galactose, d) galacturonic acid, e) glucose, f) glucuronic acid, g) mannose, h) rhamnose, and i) xylose in samples studied. Raw and treated samples are indicated by the bullet points rectangles, respectively. The control sample (BC) is marked with red colour. For the estimated parameters, the data points and bars refer to the mean values and standard deviation, respectively. Treatments with the same letter show a lack of statistically significant differences.

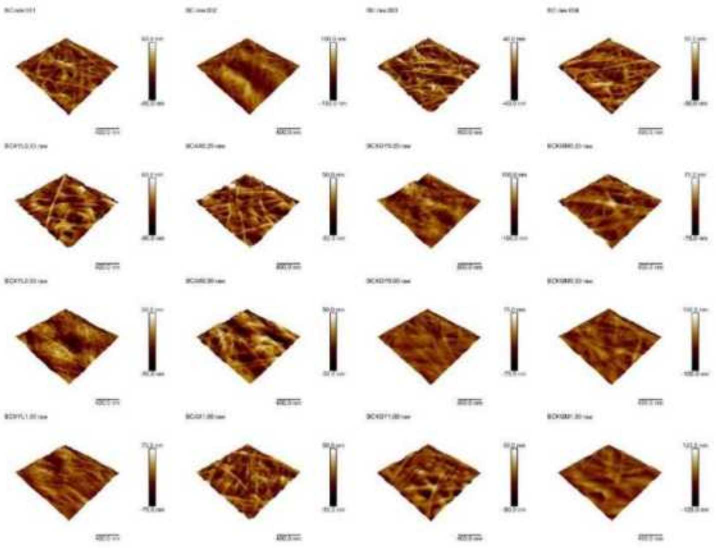

Fig.S3. Three-dimensional surface representation of raw bacterial cellulose-hemicellulose hydrogels in relation to the presence of xylan, arabinoxylan, xyloglucan, and glucomannan in culturing medium. Sample naming convention includes bacterial cellulose (BC), presence of hemicelluloses (XYL for xylan, AX for arabinoxylan, XGY for xyloglucan, and KGM for glucomannan), and concentration of hemicelluloses in culturing medium (% w/v). Colorbar of each image encodes values in Z axis.

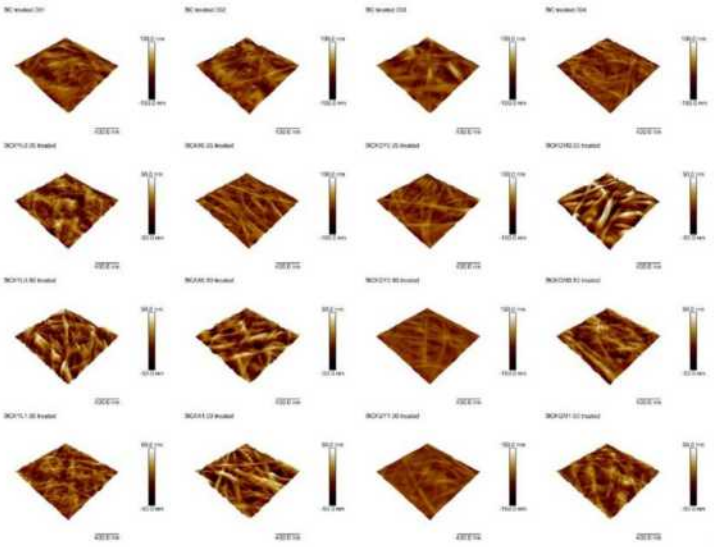

Fig.S4. Three-dimensional surface representation of treated bacterial cellulose-hemicellulose hydrogels in relation to the presence of xylan, arabinoxylan, xyloglucan, and glucomannan in culturing medium. Sample naming convention includes bacterial cellulose (BC), presence of hemicelluloses (XYL for xylan, AX for arabinoxylan, XGY for xyloglucan, and KGM for glucomannan), and concentration of hemicelluloses in culturing medium (% w/v). Colorbar of each image encodes values in Z axis.

7. References

Albersheim, P., Darvill, A., Roberts, K., Sederoff, R., & Staehelin, A. (2011). *Plant Cell Walls: A Renewable Material Resource*. Garland Science, Taylo & Francis Group.

Allison, G. G., Morris, C., Clifton-Brown, J., Lister, S. J., & Donnison, I. S. (2011). Genotypic variation in cell wall composition in a diverse set of 244 accessions of Miscanthus. *Biomass and Bioenergy*, *35*(11), 4740–4747. https://doi.org/10.1016/j.biombioe.2011.10.008

Altaner, C. M., Thomas, L. H., Fernandes, A. N., & Jarvis, M. C. (2014). How cellulose stretches: Synergism between covalent and hydrogen bonding. *Biomacromolecules*, *15*(3), 791–798. https://doi.org/10.1021/bm401616n

Andrade, F. K., Dourado, F., & Gama, F. M. (2010). Bacterial Cellulose: properties, production and applications. In *Cellulose: Structure and Properties, Derivatives and Industrial Uses* (pp. 427–458). http://repositorium.sdum.uminho.pt/bitstream/1822/57017/1/document_2909_1.pdf

Åström, J., & Niskanen, K. (1993). Symmetry-Breaking Fracture in Random Fibre Networks. *Europhysics Letters*, *21*(5), 557. https://doi.org/10.1088/1126-6708/2009/04/129

Berglund, J. (2018). *Wood Hemicelluloses - Fundamental Insights on Biological and Technical Properties* [KTH Royal Institute of Technology]. https://www.diva-portal.org/smash/get/diva2:1275732/FULLTEXT01.pdf

Berglund, J., Angles d'Ortoli, T., Vilaplana, F., Widmalm, G., Bergenstråhle-Wohlert, M., Lawoko, M., Henriksson, G., Lindström, M., & Wohlert, J. (2016). A molecular dynamics study of the effect of glycosidic linkage type in the hemicellulose backbone on the molecular chain flexibility. *Plant Journal*, *88*(1), 56–70. https://doi.org/10.1111/tpj.13259

Berglund, J., Azhar, S., Lawoko, M., Lindström, M., Vilaplana, F., Wohlert, J., & Henriksson, G. (2019). The structure of galactoglucomannan impacts the degradation under alkaline conditions. *Cellulose*, *26*(3), 2155–2175. https://doi.org/10.1007/s10570-018-1737-z

Besombes, S., & Mazeau, K. (2005). The cellulose/lignin assembly assessed by molecular modeling. Part 1: Adsorption of a threo guaiacyl β-O-4 dimer onto a Iβ cellulose whisker. *Plant Physiology and Biochemistry*, *43*(3), 299–308. https://doi.org/10.1016/j.plaphy.2005.02.005

Bhatia, R., Gallagher, J. A., Gomez, L. D., & Bosch, M. (2017). Genetic engineering of grass cell wall polysaccharides for biorefining. *Plant Biotechnology Journal*, *15*(9), 1071–1092. https://doi.org/10.1111/pbi.12764

Bichot, A., Delgenès, J. P., Méchin, V., Carrère, H., Bernet, N., & García-Bernet, D. (2018). Understanding biomass recalcitrance in grasses for their efficient utilization as biorefinery feedstock. In *Reviews in Environmental Science and Biotechnology* (Vol. 17, Issue 4). https://doi.org/10.1007/s11157-018-9485-y

Braidwood, L., Breuer, C., & Sugimoto, K. (2014). My body is a cage: Mechanisms and modulation of plant cell growth. *New Phytologist*, *201*(2), 388–402. https://doi.org/10.1111/nph.12473

Brillouet, J. M., Rouau, X., Lorta, E., Hoebler, C., Barry, J. L., & Carré, B. (1988). A new method for determination of insoluble cell walls and soluble nonstarchy polysaccharides from plant materials. *Journal of Agricultural and Food Chemistry*, *36*(5), 969–979. https://doi.org/10.1021/jf00083a018

Brown, R. M. J. (1982). *Cellulose and Other Natural Polymer Systems. Biogenesis,* *Structure, and Degradation* (1st ed.). Springer.

Broxterman, S. E., & Schols, H. A. (2018). Interactions between pectin and cellulose in primary plant cell walls. *Carbohydrate Polymers*, *192*(March), 263–272. https://doi.org/10.1016/j.carbpol.2018.03.070

Burton, R. A., Gidley, M. J., & Fincher, G. B. (2010). Heterogeneity in the chemistry, structure and function of plant cell walls. *Nature Chemical Biology*, *6*(10), 724–732. https://doi.org/10.1038/nchembio.439

Carpita, N. C. (1996). Structure and biogenesis of the cell walls of grasses. *Annual Review of Plant Physiology and Plant Molecular Biology*, *47*(1), 445–476. https://doi.org/10.1146/annurev.arplant.47.1.445

Carpita, N. C. (2011). Update on mechanisms of plant cell wall biosynthesis: How plants make cellulose and other (1→4)-β-D-Glycans. *Plant Physiology*, *155*(1), 171–184. https://doi.org/10.1104/pp.110.163360

Carpita, N. C., & Gibeaut, D. M. (1993). Structural models of primary cell walls in flowering plants: Consistency of molecular structure with the physical properties of the walls during growth. *Plant Journal*, *3*(1), 1–30. https://doi.org/10.1111/j.1365-313X.1993.tb00007.x

Carpita, N. C., & McCann, M. C. (2020). Redesigning plant cell walls for the biomass-based bioeconomy. *Journal of Biological Chemistry*, *295*(44), 15144–15157. https://doi.org/10.1074/jbc.REV120.014561

Cavalier, D. M., Lerouxel, O., Neumetzler, L., Yamauchi, K., Reinecke, A., Freshour, G., Zabotina, O. A., Hahn, M. G., Burgert, I., Pauly, M., Raikhel, N. V., & Keegstra, K. (2008). Disrupting two Arabidopsis thaliana xylosyltransferase genes results in plants deficient in xyloglucan, a major primary cell wall component. *Plant Cell*, *20*(6), 1519–1537. https://doi.org/10.1105/tpc.108.059873

Cavka, A., Guo, X., Tang, S. J., Winestrand, S., Jönsson, L. J., & Hong, F. (2013). Production of bacterial cellulose and enzyme from waste fiber sludge. *Biotechnology for Biofuels*, *6*(1), 1–10. https://doi.org/10.1186/1754-6834-6-25

Chanliaud, E., Burrows, K. M., Jeronimidis, G., & Gidley, M. J. (2002). Mechanical properties of primary plant cell wall analogues. *Planta*, *215*(6), 989–996. https://doi.org/10.1007/s00425-002-0783-8

Chen, S. Q., Lopez-Sanchez, P., Wang, D., Mikkelsen, D., & Gidley, M. J. (2018). Mechanical properties of bacterial cellulose synthesised by diverse strains of the genus Komagataeibacter. *Food Hydrocolloids*, *81*, 87–95. https://doi.org/10.1016/j.foodhyd.2018.02.031

Chen, W., Lickfield, G. C., & Yang, C. Q. (2004). Molecular modeling of cellulose in amorphous state. Part I: Model building and plastic deformation study. *Polymer*, *45*(3), 1063–1071. https://doi.org/10.1016/j.polymer.2003.11.020

Chi, K., & Catchmark, J. M. (2017). The influences of added polysaccharides on the properties of bacterial crystalline nanocellulose. *Nanoscale*, *9*(39), 15144–15158. https://doi.org/10.1039/c7nr05615j

Chibrikov, V., Pieczywek, P. M., Cybulska, J., & Zdunek, A. (2023). Evaluation of elasto-plastic properties of bacterial cellulose-hemicellulose composite films. *Industrial Crops & Products*, *205*(December), 117578. https://doi.org/10.1016/j.indcrop.2023.117578

Chibrikov, V., Pieczywek, P. M., Cybulska, J., & Zdunek, A. (2024). Coarse-grained molecular dynamics model to evaluate the mechanical properties of bacterial cellulose–hemicellulose composites. *Carbohydrate Polymers*, *330*(January), 121827. https://doi.org/10.1016/j.carbpol.2024.121827

Cone, J. W., & Engels, F. M. (1993). The influence of ageing on cell wall composition and degradability of three maize genotypes. *Animal Feed Science and Technology*, *40*(4), 331–342. https://doi.org/10.1016/0377-8401(93)90062-O

Cosgrove, D. J. (2000). Expansive growth of plant cell walls. *Plant Physiology and Biochemistry*, *38*(1–2), 109–124. https://doi.org/10.1016/S0981-9428(00)00164-9

Cosgrove, D. J., & Jarvis, M. C. (2012). Comparative structure and biomechanics of plant primary and secondary cell walls. *Frontiers in Plant Science*, *3*(AUG), 1–6. https://doi.org/10.3389/fpls.2012.00204

Cybulska, J., Cieśla, J., Kurzyna-Szklarek, M., Szymańska-Chargot, M., Pieczywek, P. M., & Zdunek, A. (2023). Influence of pectin and hemicelluloses on physical properties of bacterial cellulose. *Food Chemistry*, *429*(July), 1–10. https://doi.org/10.1016/j.foodchem.2023.136996

Cybulska, J., Vanstreels, E., Ho, Q. T., Courtin, C. M., Craeyveld, V. V., Nicolaï, B., Zdunek, A., & Konstankiewicz, K. (2010). Mechanical characteristics of artificial cell walls. *Journal of Food Engineering*, *96*(2), 287–294. https://doi.org/10.1016/j.jfoodeng.2009.08.001

Cybulska, J., Zdunek, A., & Konstankiewicz, K. (2011). Calcium effect on mechanical properties of model cell walls and apple tissue. *Journal of Food Engineering*, *102*(3), 217–223. https://doi.org/10.1016/j.jfoodeng.2010.08.019

Djahedi, C., Bergenstråhle-Wohlert, M., Berglund, L. A., & Wohlert, J. (2016). Role of hydrogen bonding in cellulose deformation: the leverage effect analyzed by molecular modeling. *Cellulose*, *23*(4), 2315–2323. https://doi.org/10.1007/s10570-016-0968-0

Djahedi, C., Berglund, L. A., & Wohlert, J. (2015). Molecular deformation mechanisms in cellulose allomorphs and the role of hydrogen bonds. *Carbohydrate Polymers*, *130*, 175–182. https://doi.org/10.1016/j.carbpol.2015.04.073

Doineau, E., Bauer, G., Ensenlaz, L., Novales, B., Sillard, C., Bénézet, J. C., Bras, J., Cathala, B., & Le Moigne, N. (2020). Adsorption of xyloglucan and cellulose nanocrystals on natural fibres for the creation of hierarchically structured fibres. *Carbohydrate Polymers*, *248*(June). https://doi.org/10.1016/j.carbpol.2020.116713

Douglass, E. F. (2010). *The Development of Cellulose Blend Membranes using Cellulose and other Natural Biopolymers using a Novel Solvent System* (Issue November) [North Carolina State University]. https://doi.org/10.13140/RG.2.1.3425.4162

Eichhorn, S. J., & Davies, G. R. (2006). Modelling the crystalline deformation of native and regenerated cellulose. *Cellulose*, *13*(3), 291–307. https://doi.org/10.1007/s10570-006-9046-3

Eklöf, J. M., & Brumer, H. (2010). The XTH gene family: An update on enzyme structure, function, and phylogeny in xyloglucan remodeling. *Plant Physiology*, *153*(2), 456–466. https://doi.org/10.1104/pp.110.156844

Endler, A., & Persson, S. (2011). Cellulose synthases and synthesis in arabidopsis. *Molecular Plant*, *4*(2), 199–211. https://doi.org/10.1093/mp/ssq079

Fan, B., & Maranas, J. K. (2015). Coarse-grained simulation of cellulose Iβ with application to long fibrils. *Cellulose*, *22*(1), 31–44. https://doi.org/10.1007/s10570-014-0481-2

Fang, L., & Catchmark, J. M. (2015). Characterization of cellulose and other exopolysaccharides produced from Gluconacetobacter strains. *Carbohydrate Polymers*, *115*, 663–669. https://doi.org/10.1016/j.carbpol.2014.09.028

Farkas, V., Sulova, Z., Stratilova, E., Hanna, R., & Maclachlan, G. (1992). Cleavage of xyloglucan by nasturtium seed xyloglucanase and transglycosylation to xyloglucan subunit oligosaccharides. *Archives of Biochemistry and Biophysics*, *298*(2), 365–370. https://doi.org/10.1016/0003-9861(92)90423-T

Fernandes, A. N., Thomas, L. H., Altaner, C. M., Callow, P., Forsyth, V. T., Apperley, D. C., Kennedy, C. J., & Jarvis, M. C. (2011). Nanostructure of cellulose microfibrils in spruce wood. *Proceedings of the National Academy of Sciences of the United States of America*, *108*(47). https://doi.org/10.1073/pnas.1108942108

Franková, L., & Fry, S. C. (2021). Hemicellulose-remodelling transglycanase activities from charophytes: towards the evolution of the land-plant cell wall. *Plant Journal*, *108*(1), 7–28. https://doi.org/10.1111/tpj.15500

Geitmann, A. (2010). Mechanical modeling and structural analysis of the primary plant cell wall. *Current Opinion in Plant Biology*, *13*(6), 693–699. https://doi.org/10.1016/j.pbi.2010.09.017

Gibson, L. J. (2012). The hierarchical structure and mechanics of plant materials. *Journal of the Royal Society Interface*, *9*(76), 2749–2766. https://doi.org/10.1098/rsif.2012.0341

Glass, D. C., Moritsugu, K., Cheng, X., & Smith, J. C. (2012). REACH coarse-grained simulation of a cellulose fiber. *Biomacromolecules*, *13*(9), 2634–2644. https://doi.org/10.1021/bm300460f

Goto, M., Gordon, A. H., & Chesson, A. (1991). Changes in cell-wall composition and degradability of sorghum during growth and maturation. *Journal of the Science of Food and Agriculture*, *54*(1), 47–60. https://doi.org/10.1002/jsfa.2740540107

Goubet, F., Misrahi, A., Park, S. K., Zhang, Z., Twell, D., & Dupree, P. (2003). AtCSLA7, a cellulose synthase-like putative glycosyltransferase, is important for pollen tube growth and embryogenesis in Arabidopsis. *Plant Physiology*, *131*(2), 547–557. https://doi.org/10.1104/pp.014555

Goulao, L. F., & Oliveira, C. M. (2008). Cell wall modifications during fruit ripening: when a fruit is not the fruit. *Trends in Food Science and Technology*, *19*(1), 4–25. https://doi.org/10.1016/j.tifs.2007.07.002

Gu, J., & Catchmark, J. M. (2012). Impact of hemicelluloses and pectin on sphere-like bacterial cellulose assembly. *Carbohydrate Polymers*, *88*(2), 547–557. https://doi.org/10.1016/j.carbpol.2011.12.040

Habibi, Y., Lucia, L. A., & Rojas, O. J. (2010). Cellulose nanocrystals: Chemistry, self-assembly, and applications. *Chemical Reviews*, *110*(6), 3479–3500. https://doi.org/10.1021/cr900339w

Haigler, C. H., White, A. R., Malcolm Brown, R., & Cooper, K. M. (1982). Alteration of in vivo cellulose ribbon assembly by carboxymethylcellulose and other cellulose derivatives. *Journal of Cell Biology*, *94*(1), 64–69. https://doi.org/10.1083/jcb.94.1.64

Hamlen, R. C. (1991). *Paper structure, mechanics and permeability: computer-aided* *modeling* [University of Minnesota]. http://dx.doi.org/10.1016/j.jaci.2012.05.050

Hanus, J., & Mazeau, K. (2006). The Xyloglucan-Cellulose Assembly at the Atomic Scale. In *Biopolymers* (Vol. 85, Issue 4, pp. 392–406). https://doi.org/https://doi.org/10.1002/bip.20460

Hartley, R. D., Morrison, W. H., Himmelsbach, D. S., & Borneman, W. S. (1990). Cross-linking of cell wall phenolic arabinoxylans in graminaceous plants. *Phytochemistry*, *29*(12), 3705–3709. https://doi.org/10.1016/0031-9422(90)85317-9

Hervé, C., Rogowski, A., Gilbert, H. J., & Knox, J. P. (2009). Enzymatic treatments reveal differential capacities for xylan recognition and degradation in primary and secondary plant cell walls. *Plant Journal*, *58*(3), 413–422. https://doi.org/10.1111/j.1365-313X.2009.03785.x

Heyden, S. (2000). Network Modelling for the Evaluation of Mechanical Properties of Cellulose Fluff. In *Department of Mechanics and Materials: Vol. PhD*.

Himmel, M. E. (2008). *Biomass recalcitrance: deconstructing the plant cell wall for bioenergy*. Wiley-Blackwell.

Hirai, A., Tsuji, M., Yamamoto, H., & Horii, F. (1998). In situ crystallization of bacterial cellulose III. Influences of different polymeric additives on the formation of microfibrils as revealed by transmission electron microscopy. *Cellulose*, *5*(3), 201–213. https://doi.org/10.1023/A:1009233323237

Hoije, A., Stememalm, E., Heikkinen, S., Tenkanen, M., & Gatenholm, P. (2008). Material properties of films from enzymatically tailored arabinoxylans. *Biomacromolecules*, *9*(7), 2042–2047. https://doi.org/10.1021/bm800290m

Hori, C., Yu, X., Mortimer, J. C., Sano, R., Matsumoto, T., Kikuchi, J., Demura, T., & Ohtani, M. (2020). Impact of abiotic stress on the regulation of cell wall biosynthesis in populus trichocarpa. *Plant Biotechnology*, *37*(3), 1–11. https://doi.org/10.5511/plantbiotechnology.20.0326a

Houston, K., Tucker, M. R., Chowdhury, J., Shirley, N., & Little, A. (2016). The plant cell wall: A complex and dynamic structure as revealed by the responses of genes under stress conditions. *Frontiers in Plant Science*, *7*(AUG2016), 1–18. https://doi.org/10.3389/fpls.2016.00984

Hu, Y., Catchmark, M., & Vogler, E. A. (2013). Factors Impacting the Formation of Sphere-Like Bacterial Cellulose Particles and Their Biocompatibility for Human Osteoblast Growth. *Biomacromolecules*, *14*, 3444–3452. https://doi.org/https://doi.org/10.1021/bm400744a

Itoh, T., & Ogawa, T. (1993). Molecular architecture of the cell wall of poplar cells in suspension culture, as revealed by rapid-freezing and deep-etching techniques. *Plant and Cell Physiology*, *34*(8), 1187–1196. https://doi.org/10.1093/oxfordjournals.pcp.a078540

Iwata, T., Indrarti, L., & Azuma, J. I. (1998). Affinity of hemicellulose for cellulose produced by Acetobacter xylinum. *Cellulose*, *5*(3), 215–228. https://doi.org/10.1023/A:1009237401548

Jarvis, M. C. (2000). Interconversion of the Iα and Iβ crystalline forms of cellulose by bending. *Carbohydrate Research*, *325*(2), 150–154. https://doi.org/10.1016/S0008-6215(99)00316-X

Kabel, M. A., van den Borne, H., Vincken, J. P., Voragen, A. G. J., & Schols, H. A. (2007). Structural differences of xylans affect their interaction with cellulose. *Carbohydrate*

Polymers, *69*(1), 94–105. https://doi.org/10.1016/j.carbpol.2006.09.006

Keegstra, K., Talmadge, K. W., Bauer, W. D., & Albersheim, P. (1973). The Structure of Plant Cell Walls: III. A Model of the Walls of Suspension-cultured Sycamore Cells Based on the Interconnections of the Macromolecular Components. *Plant Physiology*, *51*(1), 188–197. https://doi.org/10.1104/pp.51.1.188

Kha, H., Tuble, S. C., Kalyanasundaram, S., & Williamson, R. E. (2010). WallGen, software to construct layered cellulose-hemicellulose networks and predict their small deformation mechanics. *Plant Physiology*, *152*(2), 774–786. https://doi.org/10.1104/pp.109.146936

Kha, H., Tuble, S., Kalyanasundaram, S., & Williamson, R. E. (2008). Finite Element Analysis of Plant Cell Wall Materials. *Advanced Materials Research*, *32*, 197–202. https://doi.org/10.4028/www.scientific.net/amr.32.197

Khodayari, A., Thielemans, W., Hirn, U., Van Vuure, A. W., & Seveno, D. (2021). Cellulose-hemicellulose interactions - A nanoscale view. *Carbohydrate Polymers*, *270*(April), 118364. https://doi.org/10.1016/j.carbpol.2021.118364

Kishani, S., Vilaplana, F., Ruda, M., Hansson, P., & Wågberg, L. (2020). Influence of Solubility on the Adsorption of Different Xyloglucan Fractions at Cellulose-Water Interfaces. *Biomacromolecules*, *21*(2), 772–782. https://doi.org/10.1021/acs.biomac.9b01465

Kiziltas, E. E., Kiziltas, A., & Gardner, D. J. (2015). Synthesis of bacterial cellulose using hot water extracted wood sugars. *Carbohydrate Polymers*, *124*, 131–138. https://doi.org/10.1016/j.carbpol.2015.01.036

Kozioł, A., Cybulska, J., Pieczywek, P. M., & Zdunek, A. (2017). Changes of pectin nanostructure and cell wall stiffness induced in vitro by pectinase. *Carbohydrate Polymers*, *161*, 197–207. https://doi.org/10.1016/j.carbpol.2017.01.014

Lau, D., Jian, W., Yu, Z., & Hui, D. (2018). Nano-engineering of construction materials using molecular dynamics simulations: Prospects and challenges. *Composites Part B: Engineering*, *143*(January), 282–291. https://doi.org/10.1016/j.compositesb.2018.01.014

Le Gall, H., Philippe, F., Domon, J. M., Gillet, F., Pelloux, J., & Rayon, C. (2015). Cell wall metabolism in response to abiotic stress. *Plants*, *4*(1), 112–166. https://doi.org/10.3390/plants4010112

Lerouxel, O., Cavalier, D. M., Liepman, A. H., & Keegstra, K. (2006). Biosynthesis of plant cell wall polysaccharides - a complex process. *Current Opinion in Plant Biology*, *9*(6), 621–630. https://doi.org/10.1016/j.pbi.2006.09.009

Levy, S., Maclachlan, G., & Staehelin, L. A. (1997). Xyloglucan sidechains modulate binding to cellulose during in vitro binding assays as predicted by conformational dynamics simulations. *The Plant Journal*, *11*(3), 373–386.

Li, L., Pérré, P., Frank, X., & Mazeau, K. (2015). A coarse-grain force-field for xylan and its interaction with cellulose. *Carbohydrate Polymers*, *127*, 438–450. https://doi.org/10.1016/j.carbpol.2015.04.003

Lima, D. U., Loh, W., & Buckeridge, M. S. (2004). Xyloglucan-cellulose interaction depends on the sidechains and molecular weight of xyloglucan. *Plant Physiology and Biochemistry*, *42*(5), 389–394. https://doi.org/10.1016/j.plaphy.2004.03.003

Lin, S. P., Loira Calvar, I., Catchmark, J. M., Liu, J. R., Demirci, A., & Cheng, K. C. (2013). Biosynthesis, production and applications of bacterial cellulose. *Cellulose*, *20*(5), 2191–2219. https://doi.org/10.1007/s10570-013-9994-3

Lopez-Sanchez, P., Cersosimo, J., Wang, D., Flanagan, B., Stokes, J. R., & Gidley, M. J. (2015). Poroelastic Mechanical Effects of Hemicelluloses on Cellulosic Hydrogels under Compression. *PLOS ONE*, *10*(3), e0122132. https://doi.org/10.1371/journal.pone.0122132

Lopez, M., Bizot, H., Chambat, G., Marais, M. F., Zykwinska, A., Ralet, M. C., Driguez, H., & Buléon, A. (2010). Enthalpic studies of xyloglucan-cellulose interactions. *Biomacromolecules*, *11*(6), 1417–1428. https://doi.org/10.1021/bm1002762

Mani, S., Cosgrove, D. J., & Voth, G. A. (2020). Anisotropic Motions of Fibrils Dictated by Their Orientations in the Lamella: A Coarse-Grained Model of a Plant Cell Wall. *Journal of Physical Chemistry B*, *124*(17), 3527–3539. https://doi.org/10.1021/acs.jpcb.0c01697

Mao, R., Goutianos, S., Tu, W., Meng, N., Chen, S., & Peijs, T. (2017). Modelling the elastic properties of cellulose nanopaper. *Materials and Design*, *126*(April), 183–189. https://doi.org/10.1016/j.matdes.2017.04.050

Martínez-Abad, A., Berglund, J., Toriz, G., Gatenholm, P., Henriksson, G., Lindström, M., Wohlert, J., & Vilaplana, F. (2017). Regular motifs in xylan modulate molecular flexibility and interactions with cellulose surfaces. *Plant Physiology*, *175*(4), 1579–1592. https://doi.org/10.1104/pp.17.01184

Martinez-Sanz, M., Gidley, M. J., & Gilbert, E. P. (2016). Hierarchical architecture of bacterial cellulose and composite plant cell wall polysaccharide hydrogels using small angle neutron scattering. *Soft Matter*, *12*(5), 1534–1549. https://doi.org/10.1039/c5sm02085a

Martinez-Sanz, M., Mikkelsen, D., Flanagan, B. M., Gidley, M. J., & Gilbert, E. P. (2017). Multi-scale characterisation of deuterated cellulose composite hydrogels reveals evidence for different interaction mechanisms with arabinoxylan, mixed-linkage glucan and xyloglucan. *Polymer*, *124*, 1–11. https://doi.org/10.1016/j.polymer.2017.07.036

Martinez-Sanz, M., Pettolino, F., Flanagan, B., Gidley, M. J., & Gilbert, E. P. (2017). Structure of cellulose microfibrils in mature cotton fibres. *Carbohydrate Polymers*, *175*, 450–463. https://doi.org/10.1016/j.carbpol.2017.07.090

Matthews, J. F., Skopec, C. E., Mason, P. E., Zuccato, P., Torget, R. W., Sugiyama, J., Himmel, M. E., & Brady, J. W. (2006). Computer simulation studies of microcrystalline cellulose Iβ. *Carbohydrate Research*, *341*(1), 138–152. https://doi.org/10.1016/j.carres.2005.09.028

Mazeau, K. (2005). Structural micro-heterogeneities of crystalline Iβ-cellulose. *Cellulose*, *12*(4), 339–349. https://doi.org/10.1007/s10570-005-2200-5

McDougall, G. J., & Fry, S. C. (1989). Structure-Activity Relationships for Xyloglucan Oligosaccharides with Antiauxin Activity. *Plant Physiology*, *89*(3), 883–887. https://doi.org/10.1104/pp.89.3.883

McFarlane, H. E., Döring, A., & Persson, S. (2014). The cell biology of cellulose synthesis. *Annual Review of Plant Biology*, *65*, 69–94. https://doi.org/10.1146/annurev-arplant-050213-040240

Mestechkina, N. M., Anulov, O. V., Smirnova, N. I., & Shcherbukhin, V. D. (2000). Composition and structure of a galactomannan macromolecule from seeds of Astragalus lehmannianus bunge. *Applied Biochemistry and Microbiology*, *36*(5), 502–506. https://doi.org/10.1007/BF02731898

Miedes, E., Herbers, K., Sonnewald, U., & Lorences, E. P. (2010). Overexpression of a cell wall enzyme reduces xyloglucan depolymerization and softening of transgenic tomato fruits. *Journal of Agricultural and Food Chemistry*, *58*(9), 5708–5713. https://doi.org/10.1021/jf100242z

Mikkelsen, D., & Gidley, M. J. (2010). Formation of Cellulose-Based Composites with Hemicelluloses and Pectins Using Gluconacetobacter Fermentation. In *The Plant Cell Wall* (pp. 197–208). https://doi.org/10.1007/978-1-61779-008-9

Mikkonen, K. S., Pitkänen, L., Liljeström, V., Mabasa Bergström, E., Serimaa, R., Salmén, L., & Tenkanen, M. (2012). Arabinoxylan structure affects the reinforcement of films by microfibrillated cellulose. *Cellulose*, *19*(2), 467–480. https://doi.org/10.1007/s10570-012-9655-y

Mora-Montes, H. M., Bates, S., Netea, M. G., Díaz-Jiménez, D. F., López-Romero, E., Zinker, S., Ponce-Noyola, P., Kullberg, B. J., Brown, A. J. P., Odds, F. C., Flores-Carreón, A., & Gow, N. A. R. (2007). Endoplasmic reticulum α-glycosidases of Candida albicans are required for N glycosylation, cell wall integrity, and normal host-fungus interaction. *Eukaryotic Cell*, *6*(12), 2184–2193. https://doi.org/10.1128/EC.00350-07

Newman, R. H., Hill, S. J., & Harris, P. J. (2013). Wide-angle x-ray scattering and solid-state nuclear magnetic resonance data combined to test models for cellulose microfibrils in mung bean cell walls. *Plant Physiology*, *163*(4), 1558–1567. https://doi.org/10.1104/pp.113.228262

Nili, A., Yi, H., Crespi, V. H., & Puri, V. M. (2015). Examination of biological hotspot hypothesis of primary cell wall using a computational cell wall network model. *Cellulose*, *22*(2), 1027–1038. https://doi.org/10.1007/s10570-015-0568-4

Nishinari, K., Takemasa, M., Zhang, H., & Takahashi, R. (2007). Storage Plant Polysaccharides: Xyloglucans, Galactomannans, Glucomannans. In *Comprehensive Glycoscience* (pp. 613–623).

Ochoa-Villarreal, M., Aispuro-Hernndez, E., Vargas-Arispuro, I., & ngel, M. (2012). Plant Cell Wall Polymers: Function, Structure and Biological Activity of Their Derivatives. *Polymerization*, *May 2014*. https://doi.org/10.5772/46094

Park, Y. B., & Cosgrove, D. J. (2012a). A revised architecture of primary cell walls based on biomechanical changes induced by substrate-specific endoglucanases. *Plant Physiology*, *158*(4), 1933–1943. https://doi.org/10.1104/pp.111.192880

Park, Y. B., & Cosgrove, D. J. (2012b). Changes in cell wall biomechanical properties in the xyloglucan-deficient xxt1/xxt2 mutant of Arabidopsis. *Plant Physiology*, *158*(1), 465–475. https://doi.org/10.1104/pp.111.189779

Park, Y. B., & Cosgrove, D. J. (2015). Xyloglucan and its Interactions with Other Components of the Growing Cell Wall. *Plant and Cell Physiology*, *56*(2), 180–194. https://doi.org/10.1093/pcp/pcu204

Park, Y. B., Lee, C. M., Kafle, K., Park, S., Cosgrove, D. J., & Kim, S. H. (2014). Effects of plant cell wall matrix polysaccharides on bacterial cellulose structure studied with vibrational sum frequency generation spectroscopy and x-ray diffraction. *Biomacromolecules*, *15*(7), 2718–2724. https://doi.org/10.1021/bm500567v

Pauly, M., Albersheim, P., Darvill, A., & York, W. S. (1999). Molecular domains of the cellulose/xyloglucan network in the cell walls of higher plants. *Plant Journal*, *20*(6), 629–639. https://doi.org/10.1046/j.1365-313X.1999.00630.x

Pauly, M., Gille, S., Liu, L., Mansoori, N., de Souza, A., Schultink, A., & Xiong, G. (2013). Hemicellulose biosynthesis. *Planta*, *238*(4), 627–642. https://doi.org/10.1007/s00425-013-1921-1

Pauly, M., & Keegstra, K. (2016). Biosynthesis of the Plant Cell Wall Matrix Polysaccharide Xyloglucan∗. *Annual Review of Plant Biology*, *67*(February), 235–259. https://doi.org/10.1146/annurev-arplant-043015-112222

Pereira, C. S., Silveira, R. L., Dupree, P., & Skaf, M. S. (2017). Effects of Xylan Side-Chain Substitutions on Xylan-Cellulose Interactions and Implications for Thermal Pretreatment of Cellulosic Biomass. *Biomacromolecules*, *18*(4), 1311–1321. https://doi.org/10.1021/acs.biomac.7b00067

Petkowicz, C. L. O., Schaefer, S., & Reicher, F. (2007). The mannan from Schizolobium parahybae endosperm is not a reserve polysaccharide. *Carbohydrate Polymers*, *69*(4), 659–664. https://doi.org/10.1016/j.carbpol.2007.02.002

Petridis, L., O’Neill, H. M., Johnsen, M., Fan, B., Schulz, R., Mamontov, E., Maranas, J., Langan, P., & Smith, J. C. (2014). Hydration control of the mechanical and dynamical properties of cellulose. *Biomacromolecules*, *15*(11), 4152–4159. https://doi.org/10.1021/bm5011849

Pieczywek, P. M., Chibrikov, V., & Zdunek, A. (2023). In silico studies of plant primary cell walls – structure and mechanics. *Biological Reviews*, *98*, 887–899. https://doi.org/10.1111/brv.12935

Poma, A. B., Chwastyk, M., & Cieplak, M. (2015). Polysaccharide-Protein Complexes in a Coarse-Grained Model. *Journal of Physical Chemistry B*, *119*(36), 12028–12041. https://doi.org/10.1021/acs.jpcb.5b06141

Poma, A. B., Chwastyk, M., & Cieplak, M. (2016). Coarse-grained model of the native cellulose I α and the transformation pathways to the I β allomorph. *Cellulose*, *23*(3), 1573–1591. https://doi.org/10.1007/s10570-016-0903-4

Popper, Z. A., & Fry, S. C. (2008). Xyloglucan-pectin linkages are formed intra-protoplasmically, contribute to wall-assembly, and remain stable in the cell wall. *Planta*, *227*(4), 781–794. https://doi.org/10.1007/s00425-007-0656-2

Probine, M. C., & Barber, N. F. (1966). The Structure and Plastic Properties of the Cell Wall of Nitella in Relation to Extension Growth. *Australian Journal of Biological Sciences*, *19*(3), 439. https://doi.org/10.1071/bi9660439

Reid, G. J. S., & Bewley, D. J. (1979). A dual rôle for the endosperm and its galactomannan reserves in the germinative physiology of fenugreek (Trigonella foenum-graecum L.), an endospermic leguminous seed. *Planta*, *147*(2), 145–150. https://doi.org/10.1007/BF00389515

Rigdahl, M., Westerlind, B., & Hollmark, H. (1984). Analysis of cellulose networks by the finite element method. *Journal of Materials Science*, *19*, 3945–3952.

Rodriquez-Gacio, M. del C., Iglesias-Fernandez, R., Carbonero, P., & Matilla, A. (2012). Softening-up mannan-rich cell walls. *Journal of Experimental Botany*, *63*(11), 3975–3988. https://doi.org/10.1093/jxb/err313

Rose, J. K. C. (2003). The plant cell wall. In J. A. Roberts, H. Imaseki, M. T. McManus, S. D. O’Neill, & D. G. Robinson (Eds.), *Journal of Integrative Plant Biology* (Vol. 8). Blackwell Publishing Ltd. https://doi.org/10.1111/jipb.12351

Sanchavanakit, N., Sangrungraungroj, W., Kaomongkolgit, R., Banaprasert, T., Pavasant, P., & Phisalaphong, M. (2006). Growth of human keratinocytes and fibroblasts on bacterial cellulose film. *Biotechnology Progress*, *22*(4), 1194–1199. https://doi.org/10.1021/bp060035o

Sarkar, P., Bosneaga, E., & Auer, M. (2009). Plant cell walls throughout evolution: Towards a molecular understanding of their design principles. *Journal of Experimental Botany*, *60*(13), 3615–3635. https://doi.org/10.1093/jxb/erp245

Scheller, H. V., & Ulvskov, P. (2010). Hemicelluloses. *Annual Review of Plant Biology*, *61*, 263–289. https://doi.org/10.1146/annurev-arplant-042809-112315

Schultink, A., Liu, L., Zhu, L., & Pauly, M. (2014). Structural diversity and function of xyloglucan sidechain substituents. *Plants*, *3*(4), 526–542. https://doi.org/10.3390/plants3040526

Silva, C. O. G., Vaz, R. P., & Filho, E. X. F. (2018). Bringing plant cell wall-degrading enzymes into the lignocellulosic biorefinery concept. *Biofuels, Bioproducts and Biorefining*, *12*(2), 277–289. https://doi.org/10.1002/bbb.1832

Silva, G. B., Ionashiro, M., Carrara, T. B., Crivellari, A. C., Tiné, M. A. S., Prado, J., Carpita, N. C., & Buckeridge, M. S. (2011). Cell wall polysaccharides from fern leaves: Evidence for a mannan-rich Type III cell wall in Adiantum raddianum. *Phytochemistry*, *72*(18), 2352–2360. https://doi.org/10.1016/j.phytochem.2011.08.020

Sternemalm, E., Höije, A., & Gatenholm, P. (2008). Effect of arabinose substitution on the material properties of arabinoxylan films. *Carbohydrate Research*, *343*(4), 753–757. https://doi.org/10.1016/j.carres.2007.11.027

Szymańska-Chargot, M., Chylińska, M., Cybulska, J., Kozioł, A., Pieczywek, P. M., & Zdunek, A. (2017). Simultaneous influence of pectin and xyloglucan on structure and mechanical properties of bacterial cellulose composites. *Carbohydrate Polymers*, *174*, 970–979. https://doi.org/10.1016/j.carbpol.2017.07.004

Szymańska-Chargot, M., Cybulska, J., & Zdunek, A. (2011). Sensing the structural differences in cellulose from apple and bacterial cell wall materials by Raman and FT-IR Spectroscopy. *Sensors*, *11*(6), 5543–5560. https://doi.org/10.3390/s110605543

Talbott, L. D., & Ray, P. M. (1992). Molecular size and separability features of pea cell wall polysaccharides: Implications for models of primary wall structure. *Plant Physiology*, *98*(1), 357–368. https://doi.org/10.1104/pp.98.1.357

Tan, M. S. F., Rahman, S., & Dykes, G. A. (2016). Pectin and xyloglucan influence the attachment of Salmonella enterica and Listeria monocytogenes to bacterial cellulose-derived plant cell wall models. *Applied and Environmental Microbiology*, *82*(2), 680–688. https://doi.org/10.1128/AEM.02609-15

Tenhaken, R. (2015). Cell wall remodeling under abiotic stress. *Frontiers in Plant Science*, *5*(JAN), 1–9. https://doi.org/10.3389/fpls.2014.00771

Teramoto, A., & Fuchigami, M. (2000). Changes in temperature, texture, and structure of konnyaku (Konjac glucomannan gel) during high-pressure-freezing. *Journal of Food Science*, *65*(3), 491–497. https://doi.org/10.1111/j.1365-2621.2000.tb16034.x

Thomas, L. H., Trevor Forsyth, V., Šturcová, A., Kennedy, C. J., May, R. P., Altaner, C. M., Apperley, D. C., Wess, T. J., & Jarvis, M. C. (2013). Structure of cellulose microfibrils in primary cell walls from collenchyma. *Plant Physiology*, *161*(1), 465–476. https://doi.org/10.1104/pp.112.206359

Thompson, D. S. (2005). How do cell walls regulate plant growth? *Journal of Experimental Botany*, *56*(419), 2275–2285. https://doi.org/10.1093/jxb/eri247

Thompson, J. E., & Fry, S. C. (1997). Trimming and solubilization of xyloglucan after deposition in the walls of cultured rose cells. *Journal of Experimental Botany*, *48*(307), 297–305. https://doi.org/10.1093/jxb/48.2.297

Tokoh, C., Takabe, K., Fujita, M., & Saiki, H. (1998). Cellulose synthesized by Acetobacter xylinum in the presence of acetyl glucomannan. *Cellulose*, *5*(4), 249–261. https://doi.org/10.1023/A:1009211927183

Tokoh, C., Takabe, K., Sugiyama, J., & Fujita, M. (2002). CP/MAS 13C NMR and electron diffraction study of bacterial cellulose structure affected by cell wall polysaccharides. *Cellulose*, *9*(3–4), 351–360. https://doi.org/10.1023/A:1021150520953

Tuomivaara, S. T., Yaoi, K., O'Neill, M. A., & York, W. S. (2015). Generation and structural validation of a library of diverse xyloglucan-derived oligosaccharides, including an update on xyloglucan nomenclature. *Carbohydrate Research*, *402*, 56–66. https://doi.org/10.1016/j.carres.2014.06.031

Uhlin, K. (1990). *The influence of hemicelluloses on the structure of bacterial cellulose*. https://smartech.gatech.edu/handle/1853/5454

Uhlin, K. I., Atalla, R. H., & Thompson, N. S. (1995). Influence of hemicelluloses on the aggregation patterns of bacterial cellulose. *Cellulose*, *2*(2), 129–144. https://doi.org/10.1007/BF00816385

Van De Ven, T. G. M., & Sheikhi, A. (2016). Hairy cellulose nanocrystalloids: A novel class of nanocellulose. *Nanoscale*, *8*(33), 15101–15114. https://doi.org/10.1039/c6nr01570k

Vandamme, E. J., De Baets, S., Vanbaelen, A., Joris, K., & De Wulf, P. (1998). Improved production of bacterial cellulose and its application potential. *Polymer Degradation and Stability*, *59*(1–3), 93–99. https://doi.org/10.1016/s0141-3910(97)00185-7

Vrublevskaya, V., Matusevich, V., & Kuznetsova, V. (2017). Substantiation of the Interaction Mechanism of Wood Components and Water. *Bulletin of Higher Educational Institutions. Lesnoi Zhurnal (Forestry Journal)*, *3*, 152–163. https://doi.org/10.17238/issn0536-1036.2017.3.152

Wallsten, J., & Hatfield, R. (2016). Cell wall chemical characteristics of whole-crop cereal silages harvested at three maturity stages. *Journal of the Science of Food and Agriculture*, *96*(10), 3604–3612. https://doi.org/10.1002/jsfa.7736

Whitney, S. E. C., Brigham, J. E., Darke, A. H., Reid, J. S. G., & Gidley, M. J. (1998). Structural aspects of the interaction of mannan-based polysaccharides with bacterial cellulose. *Carbohydrate Research*, *307*(3–4), 299–309. https://doi.org/10.1016/S0008-6215(98)00004-4

Winter, H., Barakat, A., Cathala, B., & Saake, B. (2005). Preparation of arabinoxylan and its sorption on bacterial cellulose during cultivation. *Macromolecular Symposia*, *232*, 74–84. https://doi.org/10.1002/masy.200551409

Wu, X., Moon, R. J., & Martini, A. (2011). Calculation of single chain cellulose elasticity using fully atomistic modeling. *Tappi Journal*, *10*(4), 37–42. https://doi.org/10.32964/tj10.4.37

Xiao, C., Zhang, T., Zheng, Y., Cosgrove, D. J., & Anderson, C. T. (2016). Xyloglucan deficiency disrupts microtubule stability and cellulose biosynthesis in arabidopsis, altering cell growth and morphogenesis1[OPEN]. *Plant Physiology*, *170*(1), 234–249.

https://doi.org/10.1104/pp.15.01395

Yang, C. (1975). *Plane modeling and analysis of fiber system*. University of Washington.

Yi, H., & Puri, V. M. (2012). Architecture-based multiscale computational modeling of plant cell wall mechanics to examine the hydrogen-bonding hypothesis of the cell wall network structure model. *Plant Physiology*, *160*(3), 1281–1292. https://doi.org/10.1104/pp.112.201228

Yi, H., & Puri, V. M. (2014). Finite element approach to examine mechanical consequences of molecular structure of plant cell wall. *American Society of Agricultural and Biological Engineers Annual International Meeting 2014, ASABE 2014*, *2*, 1013–1019. https://doi.org/10.13031/aim.20141894465

Yi, H., Zamil, M. S., & Puri, V. M. (2012). Structure based computational plant cell wall model. *American Society of Agricultural and Biological Engineers Annual International Meeting 2012, ASABE 2012*, *2*(12), 1195–1199. https://doi.org/10.13031/2013.42145

Yi, H., Zamil, M. S., & Puri, V. M. (2013). Investigation of the plant cell wall's molecular structure models using the finite element modeling. *American Society of Agricultural and Biological Engineers Annual International Meeting 2013, ASABE 2013*, *1*, 488–493. https://doi.org/10.13031/aim.20131587129

York, W. S., Darvill, A. G., McNeil, M., Stevenson, T. T., & Albersheim, P. (1986). Isolation and characterization of plant cell walls and cell wall components. In *Methods in Enzymology* (Vol. 118, pp. 3–40). Academic Press. https://doi.org/10.1016/0076-6879(86)18062-1

York, W. S., Harvey, L. K., Guillen, R., Alberhseim, P., & Darvill, A. G. (1993). Structural analysis of tamarind seed xyloglucan oligosaccharides using β-galactosidase digestion and spectroscopic methods. *Carbohydrate Research*, *248*(C), 285–301. https://doi.org/10.1016/0008-6215(93)84135-S

York, W. S., van Halbeek, H., Darvill, A. G., & Albersheim, P. (1990). Structural analysis of xyloglucan oligosaccharides by 1H-NMR spectroscopy and fast-atom-bombardment mass spectrometry. *Carbohydrate Research*, *200*(C), 9–31. https://doi.org/10.1016/0008-6215(90)84179-X

Zhang, B., Gao, Y., Zhang, L., & Zhou, Y. (2021). The plant cell wall: Biosynthesis, construction, and functions. *Journal of Integrative Plant Biology*, *63*(1), 251–272. https://doi.org/10.1111/jipb.13055

Zhang, N., Li, S., Xiong, L., Hong, Y., & Chen, Y. (2015). Cellulose-hemicellulose interaction in wood secondary cell-wall. *Modelling and Simulation in Materials Science and Engineering*, *23*(8). https://doi.org/10.1088/0965-0393/23/8/085010

Zhang, Q., Brumer, H., Ågren, H., & Tu, Y. (2011). The adsorption of xyloglucan on cellulose: Effects of explicit water and side chain variation. *Carbohydrate Research*, *346*(16), 2595–2602. https://doi.org/10.1016/j.carres.2011.09.007

Zhang, S., Hu, H., Wang, L., Liu, F., & Pan, S. (2018). Preparation and prebiotic potential of pectin oligosaccharides obtained from citrus peel pectin. *Food Chemistry*, *244*(1), 232–237. https://doi.org/10.1016/j.foodchem.2017.10.071

Zhang, X. M., Shi, S. Q., & Cao, J. (2013). Elastic properties of cellulose by molecular dynamics simulation. *Applied Mechanics and Materials*, *416–417*, 1726–1730. https://doi.org/10.4028/www.scientific.net/AMM.416-417.1726

Zhang, Y., Yu, J., Wang, X., Durachko, D. M., Zhang, S., & Cosgrove, D. J. (2021). Molecular insights into the complex mechanics of plant epidermal cell walls. *Science*, *372*(6543), 607–711. https://doi.org/10.1126/science.abf2824

Zhao, Z., Crespi, V. H., Kubicki, J. D., Cosgrove, D. J., & Zhong, L. (2014). Molecular dynamics simulation study of xyloglucan adsorption on cellulose surfaces: Effects of surface hydrophobicity and side-chain variation. *Cellulose*, *21*(2), 1025–1039. https://doi.org/10.1007/s10570-013-0041-1

Zheng, Y., Wang, X., Chen, Y., Wagner, E., & Cosgrove, D. J. (2018). Xyloglucan in the primary cell wall: assessment by FESEM, selective enzyme digestions and nanogold affinity tags. *Plant Journal*, *93*(2), 211–226. https://doi.org/10.1111/tpj.13778

Zykwinska, A., Thibault, J. F., & Ralet, M. C. (2008). Competitive binding of pectin and xyloglucan with primary cell wall cellulose. *Carbohydrate Polymers*, *74*(4), 957–961. https://doi.org/10.1016/j.carbpol.2008.05.004

8. Authors declaration

8.1. Vadym Chibrikov

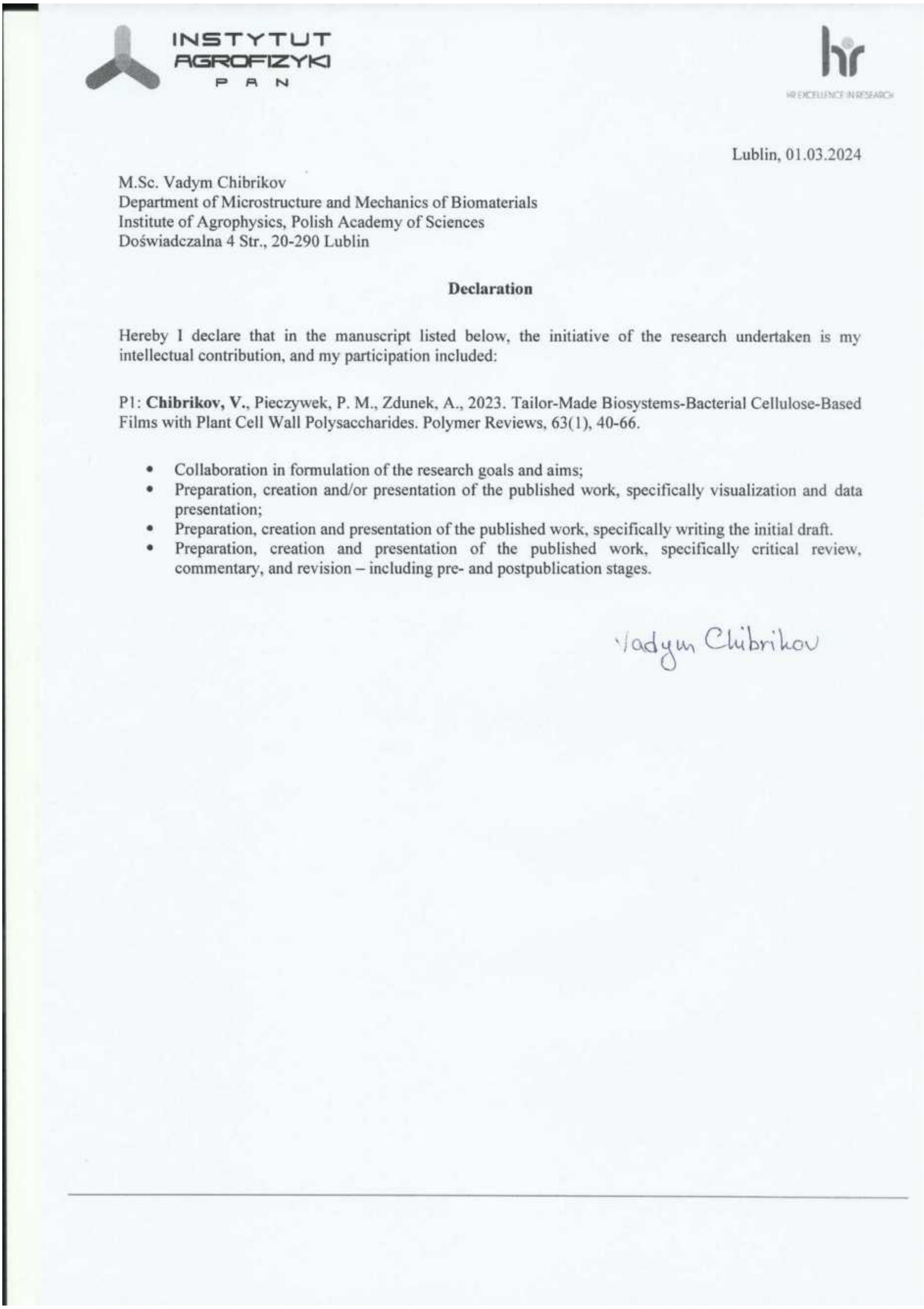

INSTYTUT
AGROFIZYKI
PAN

HR EXCELLENCE IN RESEARCH

Lublin, 01.03.2024

M.Sc. Vadym Chibrikov
Department of Microstructure and Mechanics of Biomaterials
Institute of Agrophysics, Polish Academy of Sciences
Doświadczalna 4 Str., 20-290 Lublin

Declaration

Hereby I declare that in the manuscript listed below, the initiative of the research undertaken is my intellectual contribution, and my participation included:

P1: **Chibrikov, V.**, Pieczywek, P. M., Zdunek, A., 2023. Tailor-Made Biosystems-Bacterial Cellulose-Based Films with Plant Cell Wall Polysaccharides. Polymer Reviews, 63(1), 40-66.

- Collaboration in formulation of the research goals and aims;
- Preparation, creation and/or presentation of the published work, specifically visualization and data presentation;
- Preparation, creation and presentation of the published work, specifically writing the initial draft.
- Preparation, creation and presentation of the published work, specifically critical review, commentary, and revision – including pre- and postpublication stages.

Vadym Chibrikov

INSTYTUT
AGROFIZYKI
PAN

HR EXCELLENCE IN RESEARCH

Lublin, 01.03.2024

M.Sc. Vadym Chibrikov
Department of Microstructure and Mechanics of Biomaterials
Institute of Agrophysics, Polish Academy of Sciences
Doświadczalna 4 Str., 20-290 Lublin

Declaration

Hereby I declare that in the manuscript listed below, the initiative of the research undertaken is my intellectual contribution, and my participation included:

P2: Pieczywek, P. M., **Chibrikov, V.**, Zdunek, A., 2023. *In silico* studies of plant primary cell walls–structure and mechanics. Biological Reviews, 98(3), 887-899.

- Collaboration in formulation of the research goals and aims;
- Preparation, creation and/or presentation of the published work, specifically visualization/data presentation;
- Preparation, creation and presentation of the published work, specifically writing the initial draft;
- Preparation, and creation of the published work, specifically critical review, commentary and revision – including pre- and postpublication stages.

Vadym Chibrikov

INSTYTUT
AGROFIZYKI
PAN

HR EXCELLENCE IN RESEARCH

Lublin, 01.03.2024

M.Sc. Vadym Chibrikov
Department of Microstructure and Mechanics of Biomaterials
Institute of Agrophysics, Polish Academy of Sciences
Doświadczalna 4 Str., 20-290 Lublin

Declaration

Hereby I declare that in the manuscript listed below, the initiative of the research undertaken is my intellectual contribution, and my participation included:

P3: **Chibrikov, V.**, Pieczywek, P. M., Cybulska, J., Zdunek, A., 2023. Evaluation of elasto-plastic properties of bacterial cellulose-hemicellulose composite films. Industrial Crops and Products, 205, 117578.

- Collaboration in formulation of the research goals and aims;
- Development and design of the research methodology, especially for the mechanical testing and Raman spectroscopy studies of bacterial cellulose-hemicellulose composite films;
- Application of statistical, mathematical, and other formal techniques for the analysis or synthesis of the study data;
- Conducting a research and investigation process, specifically performing the experiments of mechanical and molecular characterization of bacterial cellulose-hemicellulose composite films, and data collection;
- Management activities to annotate (produce metadata), scrub data and maintain research data (including software code, necessary for interpreting the data itself) for initial use and later reuse;
- Preparation, creation and presentation of the published work, specifically writing the initial draft;
- Preparation, creation and presentation of the published work, specifically critical review, commentary and revision – including pre- and postpublication stages.
- Preparation, creation and presentation of the published work, specifically visualization/data presentation.

Vadym Chibrikov

INSTYTUT AGROFIZYKI PAN

HR EXCELLENCE IN RESEARCH

Lublin, 01.03.2024

M.Sc. Vadym Chibrikov
Department of Microstructure and Mechanics of Biomaterials
Institute of Agrophysics, Polish Academy of Sciences
Doświadczalna 4 Str., 20-290 Lublin

Declaration

Hereby I declare that in the manuscript listed below, the initiative of the research undertaken is my intellectual contribution, and my participation included:

P4: **Chibrikov, V.**, Pieczywek, P. M., Cybulska, J., Zdunek, A., 2024. Coarse-grained molecular dynamics model to evaluate the mechanical properties of bacterial cellulose–hemicellulose composites. Carbohydrate Polymers, 121827.

- Collaboration in formulation of the research goals and aims;
- Development and design of the research methodology, specifically for the preparation of bacterial cellulose–hemicellulose composites, atomic force microscopy surface topography imaging, nano– and macroscale characterization of the mechanical properties of bacterial cellulose-hemicellulose composites;
- Programming, software development; implementation of the computer code and supporting algorithms; testing of existing code components;
- Application of statistical, mathematical, and other formal techniques for the analysis or synthesis of the study data;
- Conducting a research and investigation process, specifically performing the experiments, and data collection;
- Management activities to annotate (produce metadata), scrub data and maintain research data (including software code, necessary for interpreting the data itself) for initial use and later reuse;
- Verification, whether as a part of the activity or separate, of the overall replication/ reproducibility of results/experiments and other research outputs;
- Preparation, creation and presentation of the published work, specifically writing the initial draft;
- Preparation, creation and presentation of the published work, specifically critical review, commentary and revision – including pre- and postpublication stages;
- Preparation, creation and presentation of the published work, specifically visualization/data presentation.

Vadym Chibrikov

INSTYTUT AGROFIZYKI PAN

HR EXCELLENCE IN RESEARCH

Lublin, 01.03.2024

M.Sc. Vadym Chibrikov
Department of Microstructure and Mechanics of Biomaterials
Institute of Agrophysics, Polish Academy of Sciences
Doświadczalna 4 Str., 20-290 Lublin

Declaration

Hereby I declare that in the manuscript draft listed below, the initiative of the research undertaken is my intellectual contribution, and my participation included:

P5: **Chibrikov, V.**, Pieczywek, P. M., Cybulska, J., Zdunek, A. The effect of hemicellulose-specific enzymes on the structure and mechanical performance of cellulose-hemicellulose hydrogels.

- Collaboration in formulation of the research goals and aims;
- Development and design of the research methodology, specifically for the preparation of bacterial cellulose–hemicellulose hydrogels, its enzymolysis, surface topography imaging by means of atomic force microscopy, and exploration of mechanical properties by means of uniaxial tensile test with cyclic load;
- Programming, software development; implementation of the computer code and supporting algorithms; testing of existing code components;
- Application of statistical, mathematical, and other formal techniques for the analysis or synthesis of the study data;
- Conducting a research and investigation process, specifically performing the experiments, and data collection;
- Management activities to annotate (produce metadata), scrub data and maintain research data (including software code, necessary for interpreting the data itself) for initial use and later reuse;
- Preparation, creation and presentation of the work, specifically writing the initial draft;
- Preparation, creation and presentation of the work, specifically critical reviews, commentary and revision;
- Preparation, creation and presentation of the work, specifically visualization/data presentation.

Vadym Chibrikov

8.2. Piotr Pieczywek

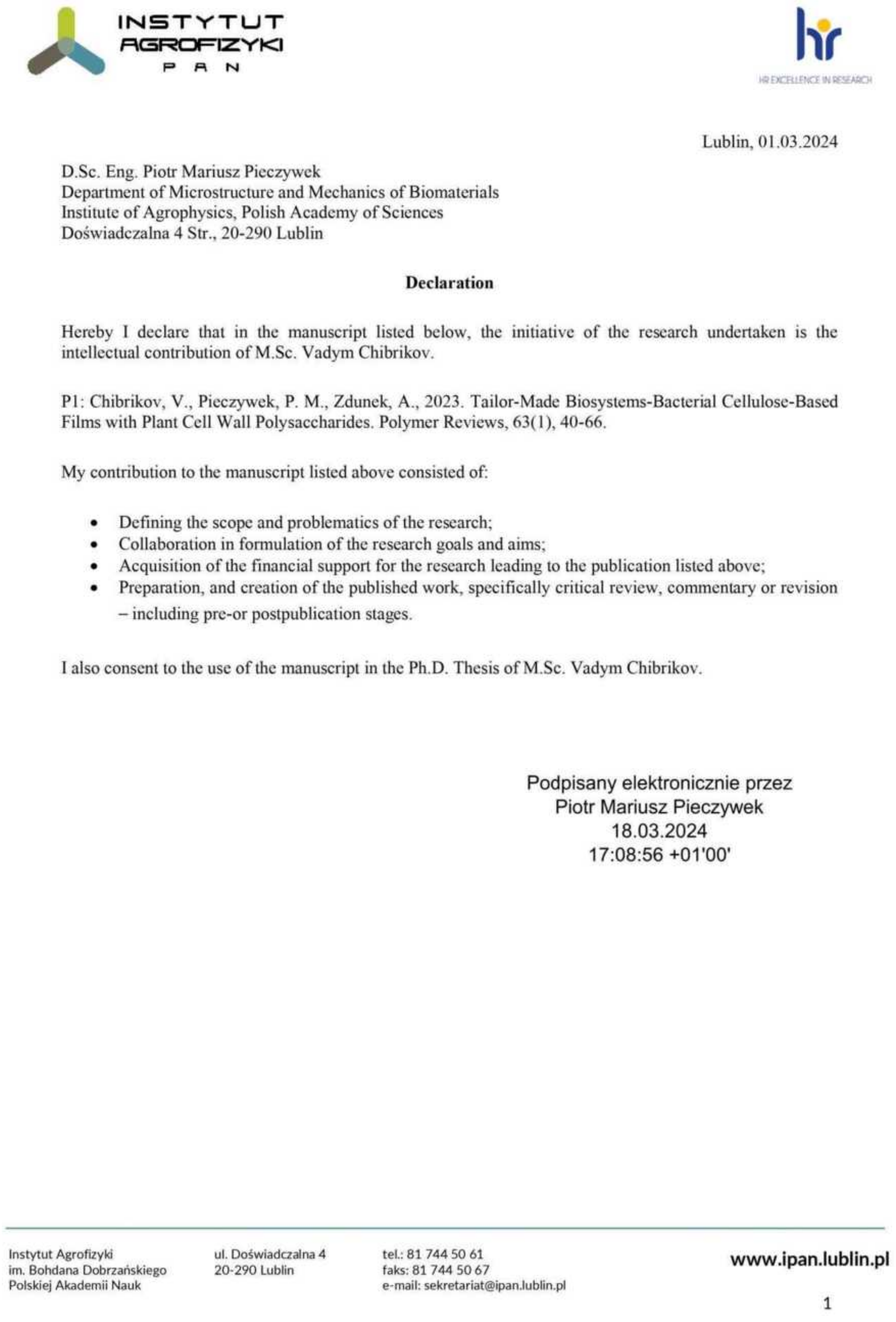

INSTYTUT AGROFIZYKI PAN

HR EXCELLENCE IN RESEARCH

Lublin, 01.03.2024

D.Sc. Eng. Piotr Mariusz Pieczywek
Department of Microstructure and Mechanics of Biomaterials
Institute of Agrophysics, Polish Academy of Sciences
Doświadczalna 4 Str., 20-290 Lublin

Declaration

Hereby I declare that in the manuscript listed below, the initiative of the research undertaken is the intellectual contribution of M.Sc. Vadym Chibrikov.

P1: Chibrikov, V., Pieczywek, P. M., Zdunek, A., 2023. Tailor-Made Biosystems-Bacterial Cellulose-Based Films with Plant Cell Wall Polysaccharides. Polymer Reviews, 63(1), 40-66.

My contribution to the manuscript listed above consisted of:

- Defining the scope and problematics of the research;
- Collaboration in formulation of the research goals and aims;
- Acquisition of the financial support for the research leading to the publication listed above;
- Preparation, and creation of the published work, specifically critical review, commentary or revision – including pre-or postpublication stages.

I also consent to the use of the manuscript in the Ph.D. Thesis of M.Sc. Vadym Chibrikov.

Podpisany elektronicznie przez
Piotr Mariusz Pieczywek
18.03.2024
17:08:56 +01'00'

Instytut Agrofizyki
im. Bohdana Dobrzańskiego
Polskiej Akademii Nauk

ul. Doświadczalna 4
20-290 Lublin

tel.: 81 744 50 61
faks: 81 744 50 67
e-mail: sekretariat@ipan.lublin.pl

www.ipan.lublin.pl

1

INSTYTUT
AGROFIZYKI
PAN

HR EXCELLENCE IN RESEARCH

Lublin, 01.03.2024

D.Sc. Eng. Piotr Mariusz Pieczywek
Department of Microstructure and Mechanics of Biomaterials
Institute of Agrophysics, Polish Academy of Sciences
Doświadczalna 4 Str., 20-290 Lublin

Declaration

Hereby I declare that in the manuscript listed below, the initiative of the research undertaken is the intellectual contribution of M.Sc. Vadym Chibrikov.

P2: Pieczywek, P. M., Chibrikov, V., Zdunek, A., 2023. *In silico* studies of plant primary cell walls–structure and mechanics. Biological Reviews, 98(3), 887-899.

My contribution to the manuscript listed above consisted of:

- Defining the scope and problematics of the research;
- Collaboration in formulation of the research goals and aims;
- Acquisition of the financial support for the research leading to the publication listed above;
- Preparation, creation and presentation of the published work, specifically visualization/data presentation;
- Preparation, creation and presentation of the published work, specifically writing the initial draft.

I also consent to the use of the manuscript in the Ph.D. Thesis of M.Sc. Vadym Chibrikov.

Podpisany elektronicznie przez
Piotr Mariusz Pieczywek
18.03.2024
17:08:58 +01'00'

INSTYTUT
AGROFIZYKI
PAN

HR EXCELLENCE IN RESEARCH

Lublin, 01.03.2024

D.Sc. Eng. Piotr Mariusz Pieczywek
Department of Microstructure and Mechanics of Biomaterials
Institute of Agrophysics, Polish Academy of Sciences
Doświadczalna 4 Str., 20-290 Lublin

Declaration

Hereby I declare that in the manuscript listed below, the initiative of the research undertaken is the intellectual contribution of M.Sc. Vadym Chibrikov.

P3: Chibrikov, V., Pieczywek, P. M., Cybulska, J., Zdunek, A., 2023. Evaluation of elasto-plastic properties of bacterial cellulose-hemicellulose composite films. Industrial Crops and Products, 205, 117578.

My contribution to the manuscript listed above consisted of:

- Defining the scope and problematics of the research;
- Collaboration in formulation of the research goals and aims;
- Providing materials and equipment necessary for conducting the research;
- Management and coordination responsibility for the research activity planning and execution;
- Oversight and leadership responsibility for the research activity planning and execution, including mentorship external to the core team;
- Acquisition of the financial support for the research leading to the publication listed above;
- Programming; implementation of the computer code and supporting algorithms; testing of existing code components;
- Application of statistical, mathematical, and other formal techniques to analyze or synthesize study data;
- Management activities to annotate (produce metadata), scrub data and maintain research data (including software code, necessary for interpreting the data itself) for initial use and later reuse;
- Preparation, and creation of the manuscript, specifically critical review, commentary or revision – including pre-or postpublication stages;
- Preparation, and creation of the published work, specifically visualization/data presentation.

I also consent to the use of the manuscript in the Ph.D. Thesis of M.Sc. Vadym Chibrikov.

Podpisany elektronicznie przez
Piotr Mariusz Pieczywek
18.03.2024
17:09:00 +01'00'

INSTYTUT
AGROFIZYKI
PAN

HR EXCELLENCE IN RESEARCH

Lublin, 01.03.2024

D.Sc. Eng. Piotr Mariusz Pieczywek
Department of Microstructure and Mechanics of Biomaterials
Institute of Agrophysics, Polish Academy of Sciences
Doświadczalna 4 Str., 20-290 Lublin

Declaration

Hereby I declare that in the manuscript listed below, the initiative of the research undertaken is the intellectual contribution of M.Sc. Vadym Chibrikov.

P4: Chibrikov, V., Pieczywek, P. M., Cybulska, J., Zdunek, A., 2024. Coarse-grained molecular dynamics model to evaluate the mechanical properties of bacterial cellulose–hemicellulose composites. Carbohydrate Polymers, 121827.

My contribution to the manuscript listed above consisted of:

- Defining the scope and problematics of the research;
- Collaboration in formulation of the research goals and aims;
- Providing materials and equipment necessary for conducting the research;
- Management and coordination responsibility for the research activity planning and execution;
- Oversight and leadership responsibility for the research activity planning and execution, including mentorship external to the core team;
- Acquisition of the financial support for the research leading to the publication listed above;
- Programming; implementation of the computer code and supporting algorithms; testing of existing code components;
- Application of statistical, mathematical, and other formal techniques to analyze or synthesize study data;
- Management activities to annotate (produce metadata), scrub data and maintain research data (including software code, where it is necessary for interpreting the data itself) for initial use and later reuse;
- Preparation, and creation of the manuscript, specifically critical review, commentary and revision – including pre- and postpublication stages;
- Preparation, and creation of the published work, specifically visualization/data presentation.

I also consent to the use of the manuscript in the Ph.D. Thesis of M.Sc. Vadym Chibrikov.

Podpisany elektronicznie przez
Piotr Mariusz Pieczywek
18.03.2024
17:09:04 +01'00'

INSTYTUT
AGROFIZYKI
PAN

HR EXCELLENCE IN RESEARCH

Lublin, 01.03.2024

D.Sc. Eng. Piotr Mariusz Pieczywek
Department of Microstructure and Mechanics of Biomaterials
Institute of Agrophysics, Polish Academy of Sciences
Doświadczalna 4 Str., 20-290 Lublin

Declaration

Hereby I declare that in the manuscript draft listed below, the initiative of the research undertaken is the intellectual contribution of M.Sc. Vadym Chibrikov.

P5: Chibrikov, V., Pieczywek, P. M., Cybulska, J., Zdunek, A. The effect of hemicellulose-specific enzymes on the structure and mechanical performance of cellulose-hemicelllose hydrogels.

My contribution to the manuscript listed above consisted of:

- Defining the scope and problematics of the research;
- Collaboration in formulation of the research goals and aims;
- Providing materials and equipment necessary for conducting the research;
- Management and coordination responsibility for the research activity planning and execution;
- Oversight and leadership responsibility for the research activity planning and execution, including mentorship external to the core team;
- Acquisition of the financial support for the research leading to the publication listed above;
- Programming; implementation of the computer code and supporting algorithms; testing of existing code components;
- Application of statistical, mathematical, and other formal techniques to analyze or synthesize study data;
- Management activities to annotate (produce metadata), scrub data and maintain research data (including software code necessary for interpreting the data itself) for initial use and later reuse;
- Preparation, and creation of the work, specifically critical review, commentary and revision – including pre- and postpublication stages;
- Preparation, and creation of the work, specifically visualization data presentation.

I also consent to the use of the manuscript in the Ph.D. Thesis of M.Sc. Vadym Chibrikov.

Podpisany elektronicznie przez
Piotr Mariusz Pieczywek
18.03.2024
17:09:06 +01'00'

8.3. Justyna Cybulska

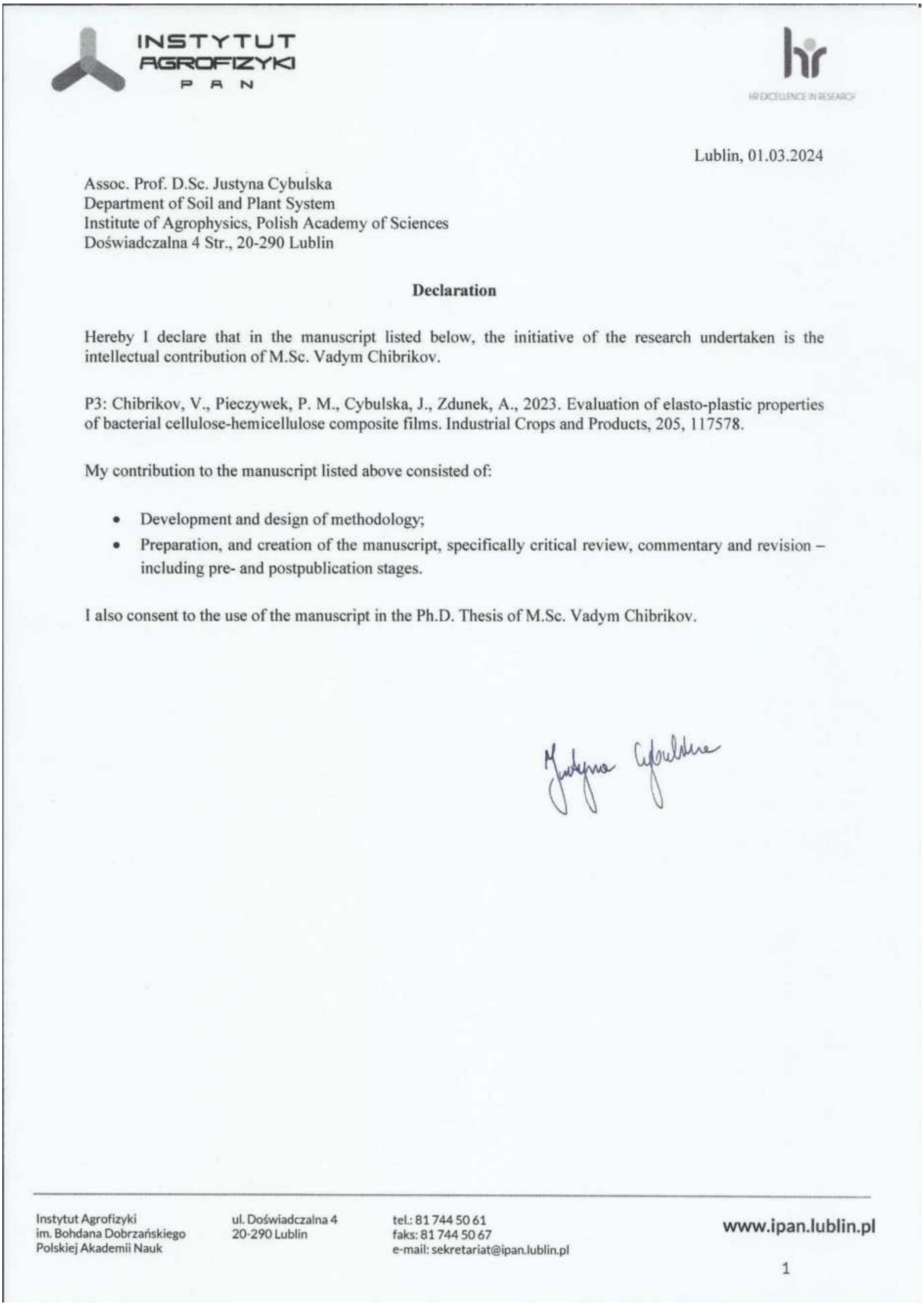

INSTYTUT
AGROFIZYKI
PAN

HR EXCELLENCE IN RESEARCH

Lublin, 01.03.2024

Assoc. Prof. D.Sc. Justyna Cybulska
Department of Soil and Plant System
Institute of Agrophysics, Polish Academy of Sciences
Doświadczalna 4 Str., 20-290 Lublin

Declaration

Hereby I declare that in the manuscript listed below, the initiative of the research undertaken is the intellectual contribution of M.Sc. Vadym Chibrikov.

P3: Chibrikov, V., Pieczywek, P. M., Cybulska, J., Zdunek, A., 2023. Evaluation of elasto-plastic properties of bacterial cellulose-hemicellulose composite films. Industrial Crops and Products, 205, 117578.

My contribution to the manuscript listed above consisted of:

- Development and design of methodology;
- Preparation, and creation of the manuscript, specifically critical review, commentary and revision – including pre- and postpublication stages.

I also consent to the use of the manuscript in the Ph.D. Thesis of M.Sc. Vadym Chibrikov.

Justyna Cybulska

Instytut Agrofizyki
im. Bohdana Dobrzańskiego
Polskiej Akademii Nauk

ul. Doświadczalna 4
20-290 Lublin

tel.: 81 744 50 61
faks: 81 744 50 67
e-mail: sekretariat@ipan.lublin.pl

www.ipan.lublin.pl

1

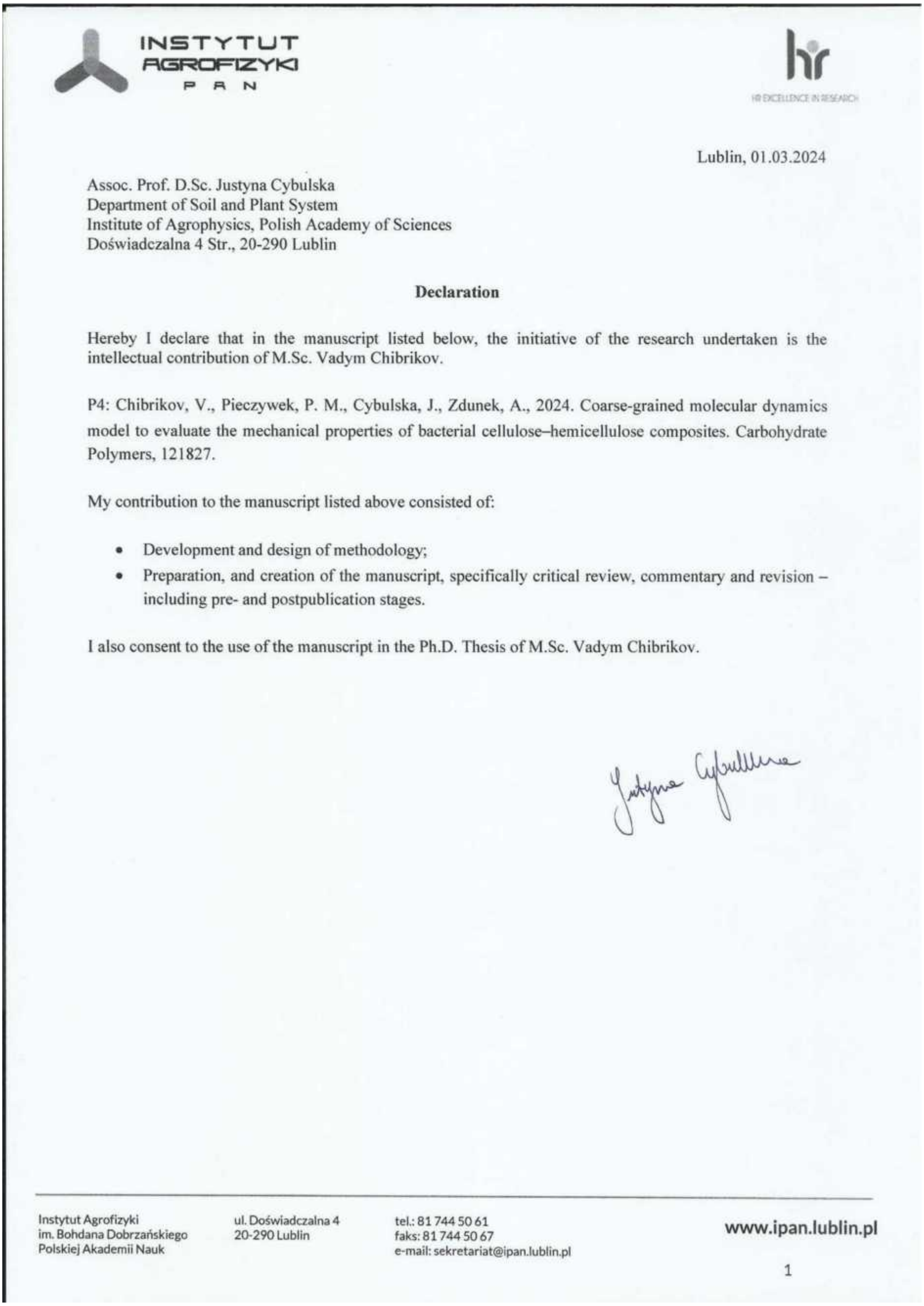

INSTYTUT
AGROFIZYKI
PAN

HR EXCELLENCE IN RESEARCH

Lublin, 01.03.2024

Assoc. Prof. D.Sc. Justyna Cybulska
Department of Soil and Plant System
Institute of Agrophysics, Polish Academy of Sciences
Doświadczalna 4 Str., 20-290 Lublin

Declaration

Hereby I declare that in the manuscript listed below, the initiative of the research undertaken is the intellectual contribution of M.Sc. Vadym Chibrikov.

P4: Chibrikov, V., Pieczywek, P. M., Cybulska, J., Zdunek, A., 2024. Coarse-grained molecular dynamics model to evaluate the mechanical properties of bacterial cellulose–hemicellulose composites. Carbohydrate Polymers, 121827.

My contribution to the manuscript listed above consisted of:

- Development and design of methodology;
- Preparation, and creation of the manuscript, specifically critical review, commentary and revision – including pre- and postpublication stages.

I also consent to the use of the manuscript in the Ph.D. Thesis of M.Sc. Vadym Chibrikov.

Justyna Cybulska

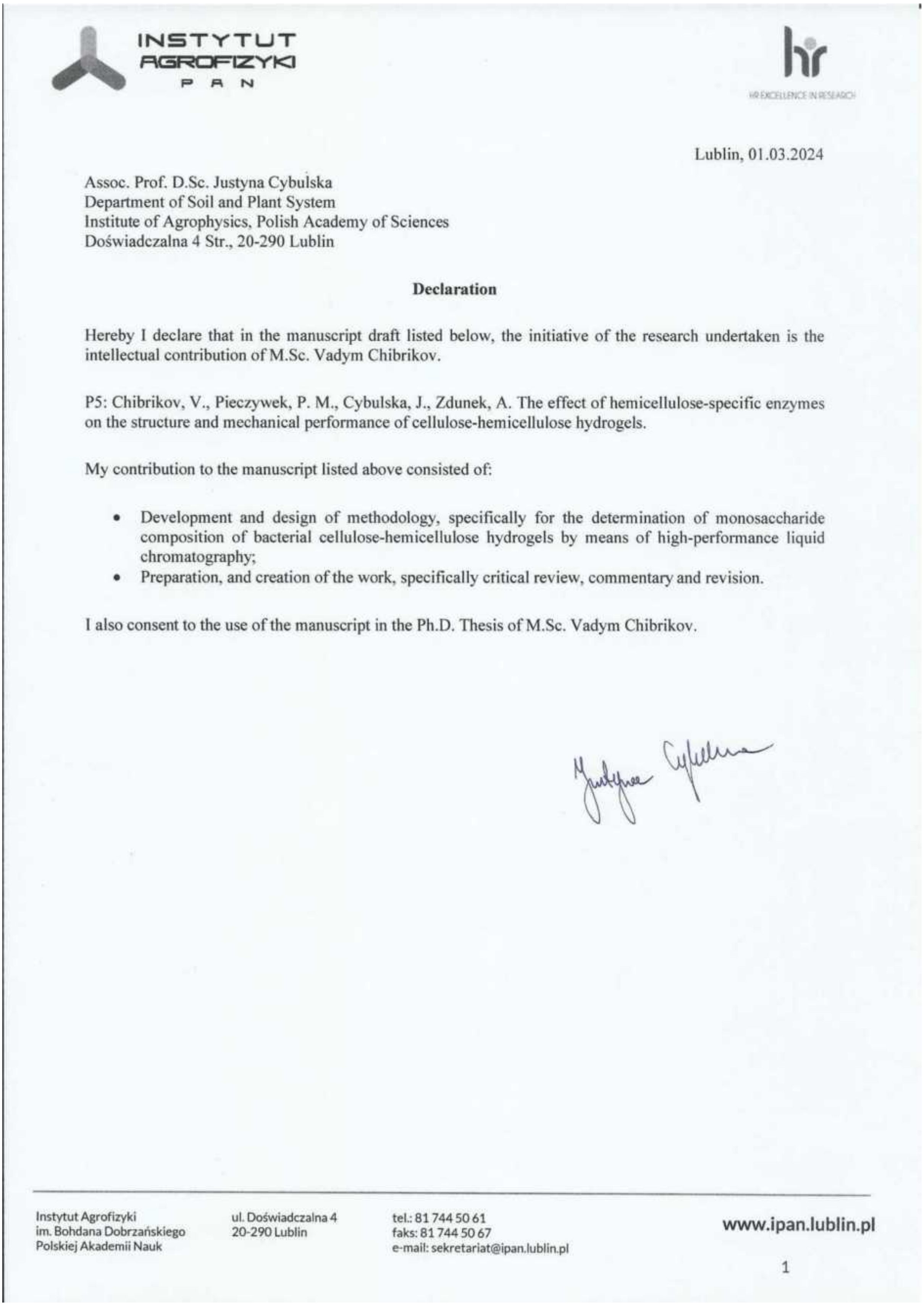

INSTYTUT
AGROFIZYKI
PAN

HR EXCELLENCE IN RESEARCH

Lublin, 01.03.2024

Assoc. Prof. D.Sc. Justyna Cybulska
Department of Soil and Plant System
Institute of Agrophysics, Polish Academy of Sciences
Doświadczalna 4 Str., 20-290 Lublin

Declaration

Hereby I declare that in the manuscript draft listed below, the initiative of the research undertaken is the intellectual contribution of M.Sc. Vadym Chibrikov.

P5: Chibrikov, V., Pieczywek, P. M., Cybulska, J., Zdunek, A. The effect of hemicellulose-specific enzymes on the structure and mechanical performance of cellulose-hemicellulose hydrogels.

My contribution to the manuscript listed above consisted of:

- Development and design of methodology, specifically for the determination of monosaccharide composition of bacterial cellulose-hemicellulose hydrogels by means of high-performance liquid chromatography;
- Preparation, and creation of the work, specifically critical review, commentary and revision.

I also consent to the use of the manuscript in the Ph.D. Thesis of M.Sc. Vadym Chibrikov.

Justyna Cybulska

8.4. Artur Zdunek

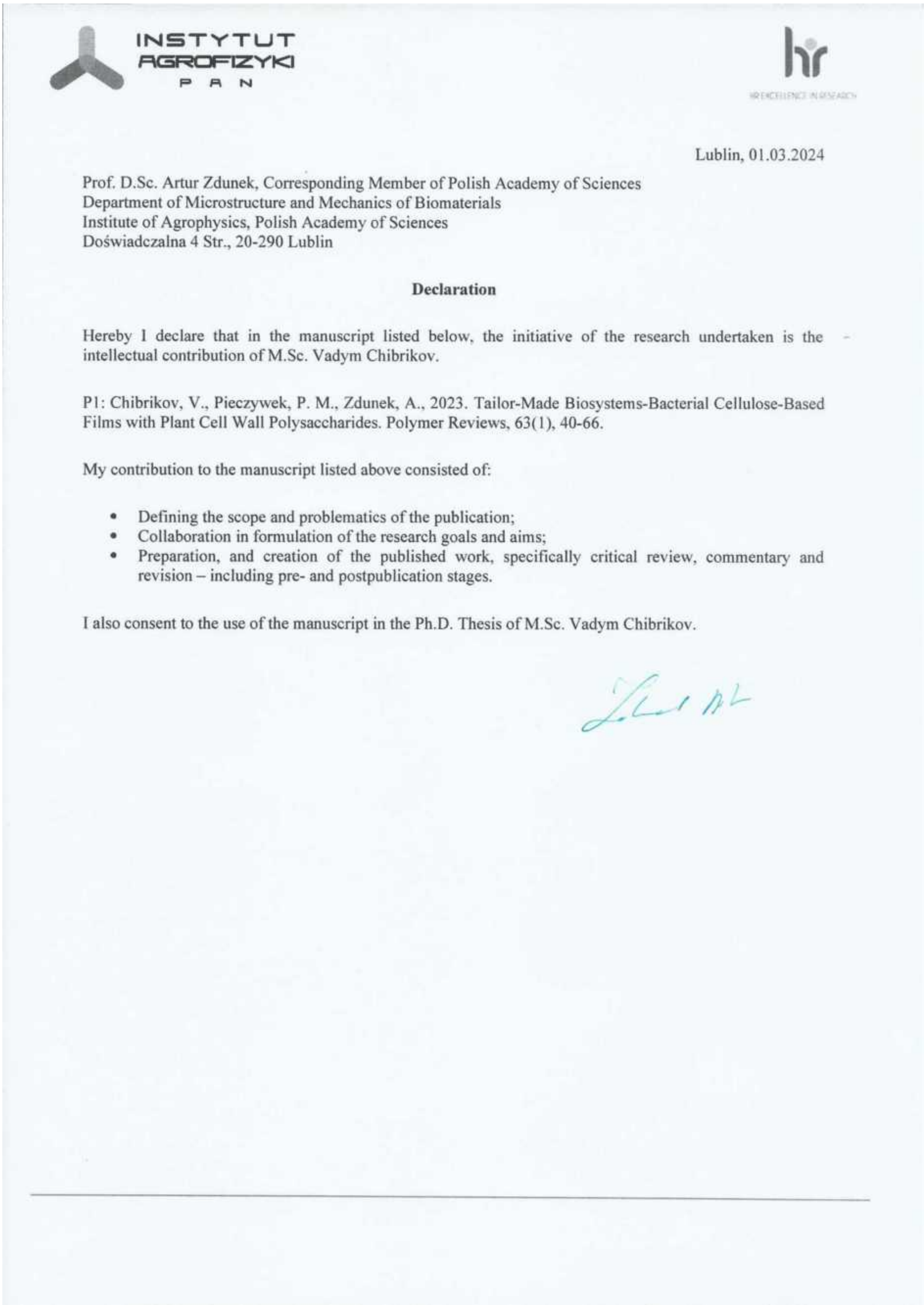

INSTYTUT
AGROFIZYKI
PAN

HR EXCELLENCE IN RESEARCH

Lublin, 01.03.2024

Prof. D.Sc. Artur Zdunek, Corresponding Member of Polish Academy of Sciences
Department of Microstructure and Mechanics of Biomaterials
Institute of Agrophysics, Polish Academy of Sciences
Doświadczalna 4 Str., 20-290 Lublin

Declaration

Hereby I declare that in the manuscript listed below, the initiative of the research undertaken is the intellectual contribution of M.Sc. Vadym Chibrikov.

P1: Chibrikov, V., Pieczywek, P. M., Zdunek, A., 2023. Tailor-Made Biosystems-Bacterial Cellulose-Based Films with Plant Cell Wall Polysaccharides. Polymer Reviews, 63(1), 40-66.

My contribution to the manuscript listed above consisted of:

- Defining the scope and problematics of the publication;
- Collaboration in formulation of the research goals and aims;
- Preparation, and creation of the published work, specifically critical review, commentary and revision – including pre- and postpublication stages.

I also consent to the use of the manuscript in the Ph.D. Thesis of M.Sc. Vadym Chibrikov.

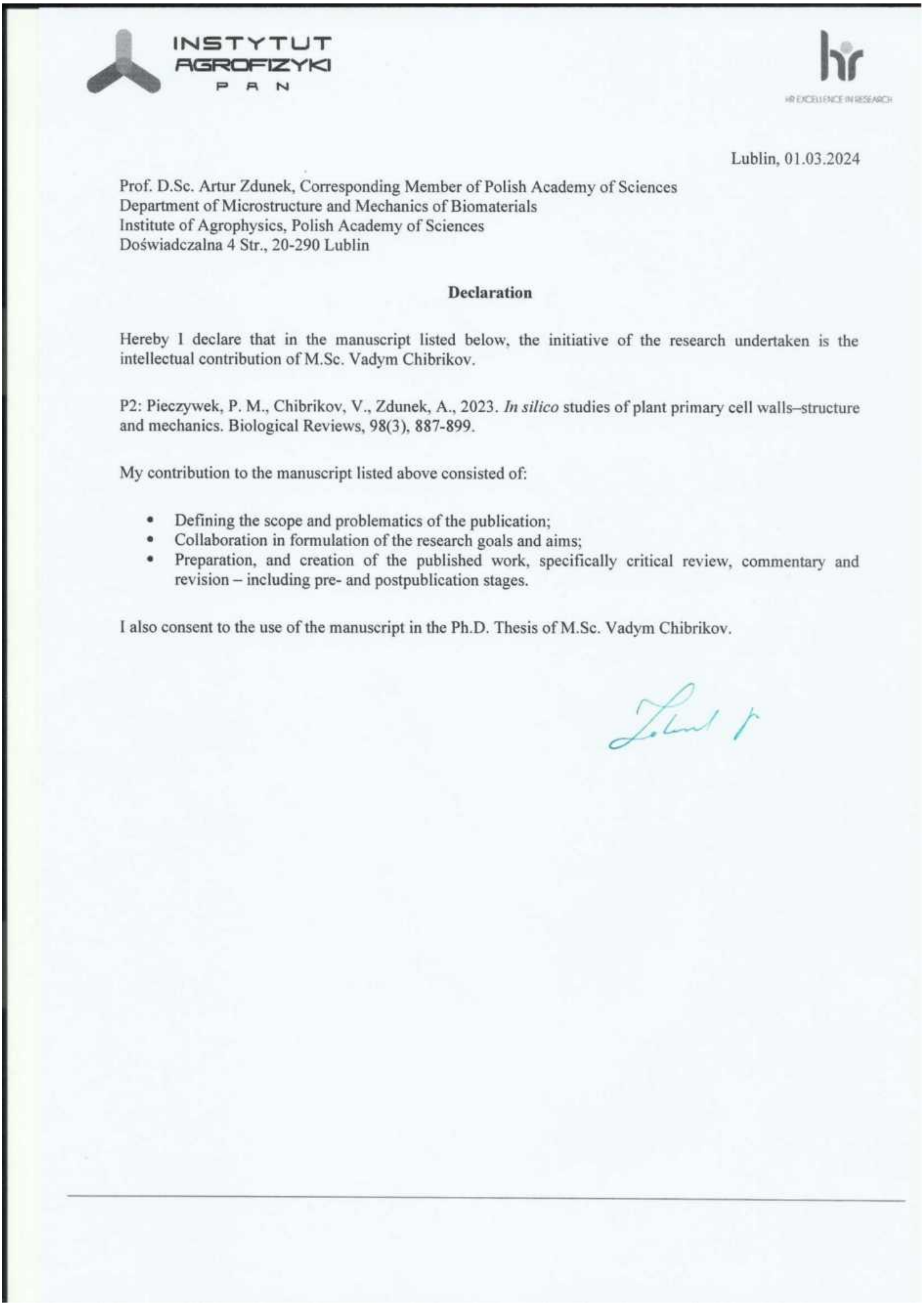

INSTYTUT
AGROFIZYKI
PAN

HR EXCELLENCE IN RESEARCH

Lublin, 01.03.2024

Prof. D.Sc. Artur Zdunek, Corresponding Member of Polish Academy of Sciences
Department of Microstructure and Mechanics of Biomaterials
Institute of Agrophysics, Polish Academy of Sciences
Doświadczalna 4 Str., 20-290 Lublin

Declaration

Hereby I declare that in the manuscript listed below, the initiative of the research undertaken is the intellectual contribution of M.Sc. Vadym Chibrikov.

P2: Pieczywek, P. M., Chibrikov, V., Zdunek, A., 2023. *In silico* studies of plant primary cell walls–structure and mechanics. Biological Reviews, 98(3), 887-899.

My contribution to the manuscript listed above consisted of:

- Defining the scope and problematics of the publication;
- Collaboration in formulation of the research goals and aims;
- Preparation, and creation of the published work, specifically critical review, commentary and revision – including pre- and postpublication stages.

I also consent to the use of the manuscript in the Ph.D. Thesis of M.Sc. Vadym Chibrikov.

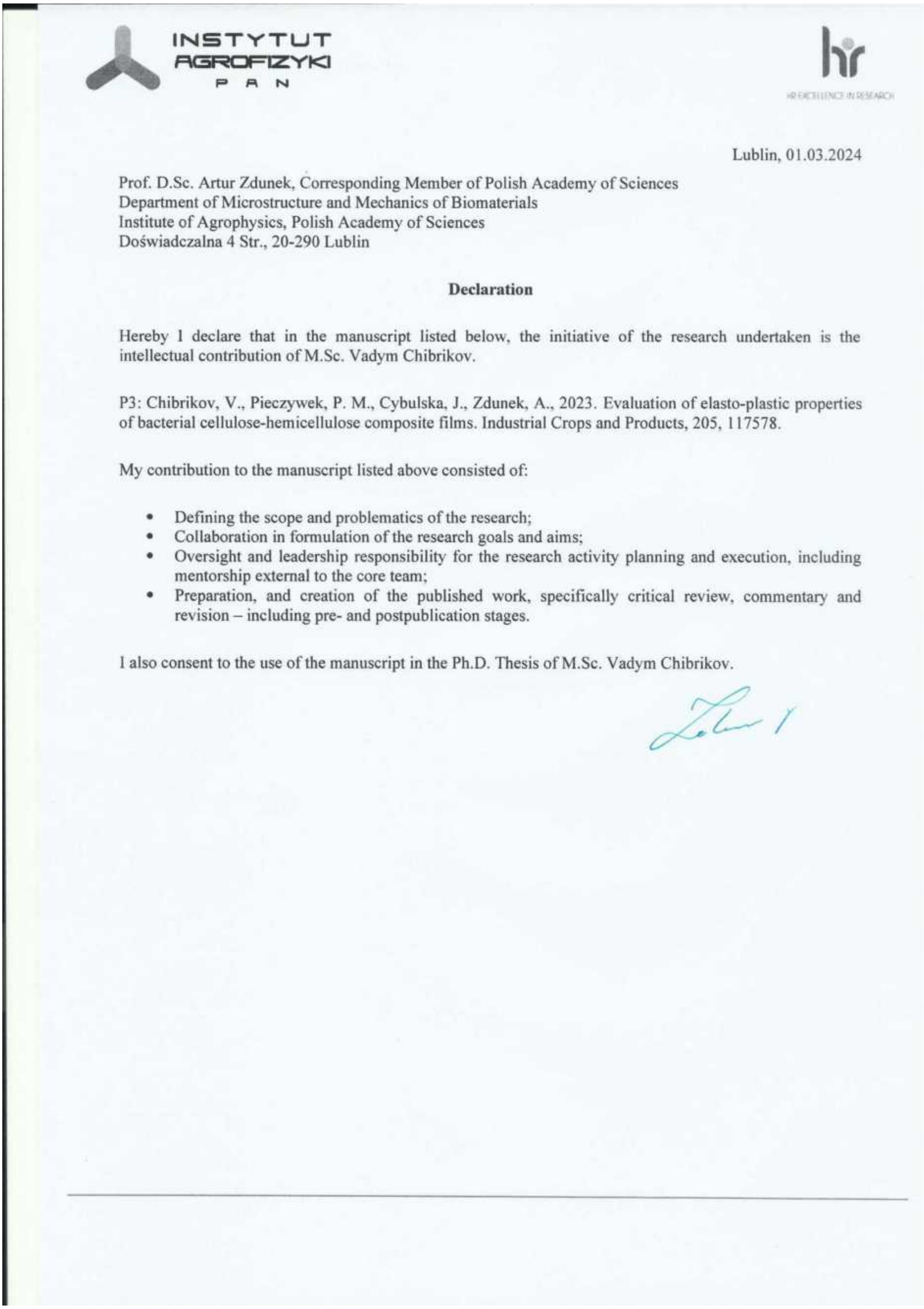

INSTYTUT
AGROFIZYKI
PAN

HR EXCELLENCE IN RESEARCH

Lublin, 01.03.2024

Prof. D.Sc. Artur Zdunek, Corresponding Member of Polish Academy of Sciences
Department of Microstructure and Mechanics of Biomaterials
Institute of Agrophysics, Polish Academy of Sciences
Doświadczalna 4 Str., 20-290 Lublin

Declaration

Hereby I declare that in the manuscript listed below, the initiative of the research undertaken is the intellectual contribution of M.Sc. Vadym Chibrikov.

P3: Chibrikov, V., Pieczywek, P. M., Cybulska, J., Zdunek, A., 2023. Evaluation of elasto-plastic properties of bacterial cellulose-hemicellulose composite films. Industrial Crops and Products, 205, 117578.

My contribution to the manuscript listed above consisted of:

- Defining the scope and problematics of the research;
- Collaboration in formulation of the research goals and aims;
- Oversight and leadership responsibility for the research activity planning and execution, including mentorship external to the core team;
- Preparation, and creation of the published work, specifically critical review, commentary and revision – including pre- and postpublication stages.

I also consent to the use of the manuscript in the Ph.D. Thesis of M.Sc. Vadym Chibrikov.

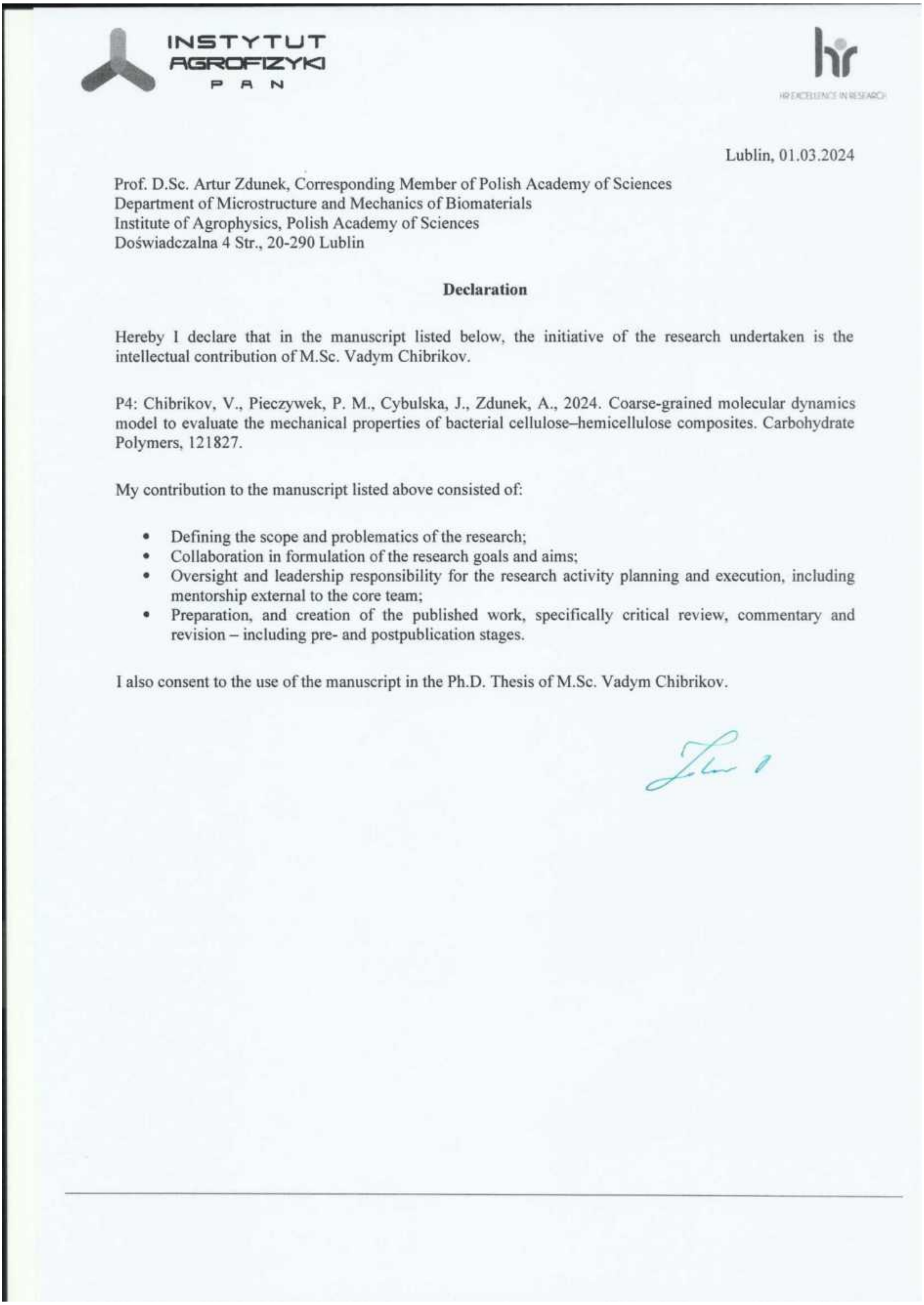

INSTYTUT
AGROFIZYKI
PAN

HR EXCELLENCE IN RESEARCH

Lublin, 01.03.2024

Prof. D.Sc. Artur Zdunek, Corresponding Member of Polish Academy of Sciences
Department of Microstructure and Mechanics of Biomaterials
Institute of Agrophysics, Polish Academy of Sciences
Doświadczalna 4 Str., 20-290 Lublin

Declaration

Hereby I declare that in the manuscript listed below, the initiative of the research undertaken is the intellectual contribution of M.Sc. Vadym Chibrikov.

P4: Chibrikov, V., Pieczywek, P. M., Cybulska, J., Zdunek, A., 2024. Coarse-grained molecular dynamics model to evaluate the mechanical properties of bacterial cellulose–hemicellulose composites. Carbohydrate Polymers, 121827.

My contribution to the manuscript listed above consisted of:

- Defining the scope and problematics of the research;
- Collaboration in formulation of the research goals and aims;
- Oversight and leadership responsibility for the research activity planning and execution, including mentorship external to the core team;
- Preparation, and creation of the published work, specifically critical review, commentary and revision – including pre- and postpublication stages.

I also consent to the use of the manuscript in the Ph.D. Thesis of M.Sc. Vadym Chibrikov.

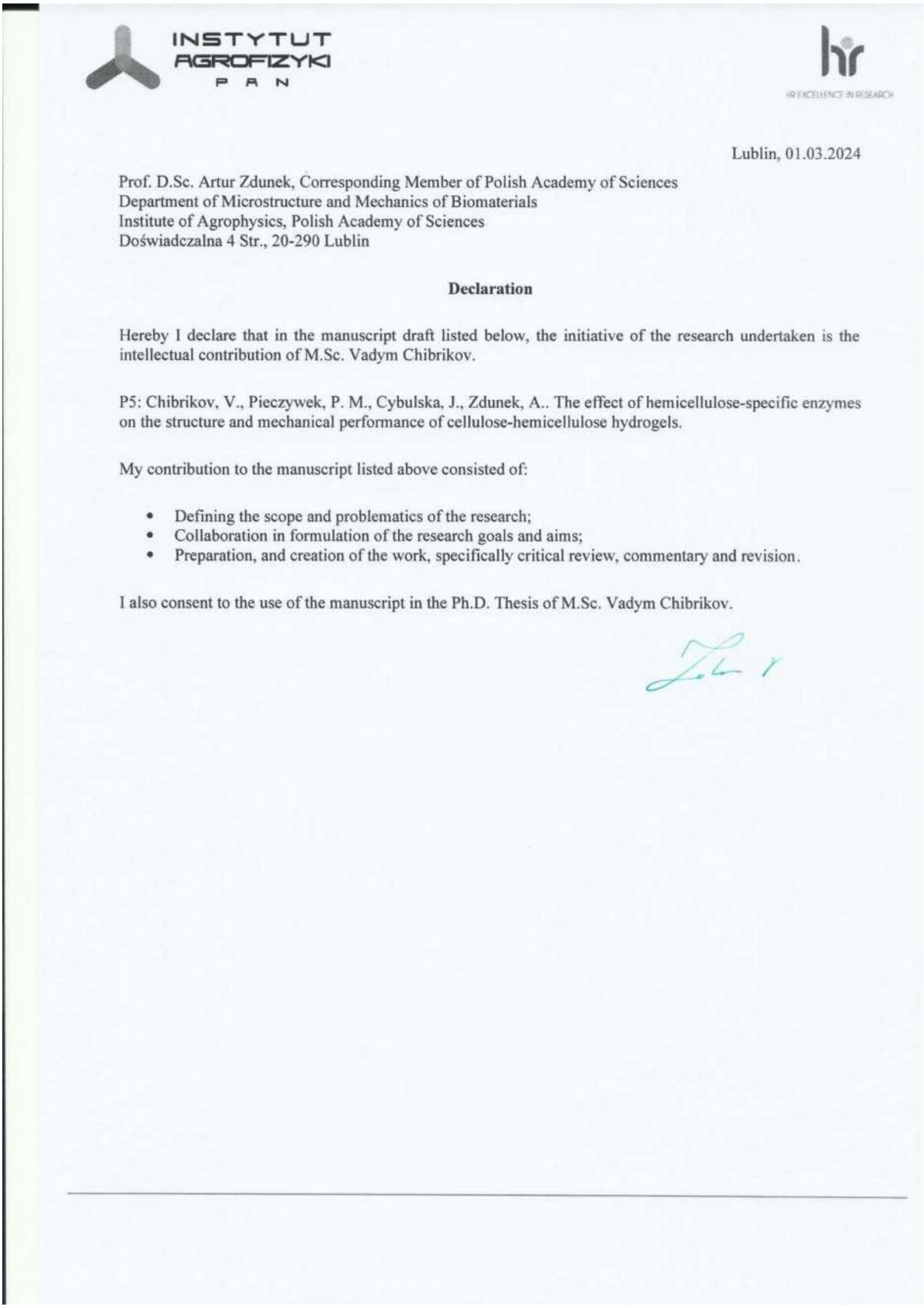

INSTYTUT AGROFIZYKI PAN

HR EXCELLENCE IN RESEARCH

Lublin, 01.03.2024

Prof. D.Sc. Artur Zdunek, Corresponding Member of Polish Academy of Sciences
Department of Microstructure and Mechanics of Biomaterials
Institute of Agrophysics, Polish Academy of Sciences
Doświadczalna 4 Str., 20-290 Lublin

Declaration

Hereby I declare that in the manuscript draft listed below, the initiative of the research undertaken is the intellectual contribution of M.Sc. Vadym Chibrikov.

P5: Chibrikov, V., Pieczywek, P. M., Cybulska, J., Zdunek, A.. The effect of hemicellulose-specific enzymes on the structure and mechanical performance of cellulose-hemicellulose hydrogels.

My contribution to the manuscript listed above consisted of:

- Defining the scope and problematics of the research;
- Collaboration in formulation of the research goals and aims;
- Preparation, and creation of the work, specifically critical review, commentary and revision.

I also consent to the use of the manuscript in the Ph.D. Thesis of M.Sc. Vadym Chibrikov.

9. Academic Resume

Personal info: Vadym Chibrikov

Education

2014-2018
National University of Kyiv-Mohyla Academy, Faculty of Natural Sciences, Department of Chemistry, Bachelor in Chemistry

2018
Bachelor's degree in Chemistry;
Bachelor Thesis: *Clarification and concentration of Sorghum saccharatum juice by membrane methods* (in Ukrainian);
Conducted at: National University of Kyiv-Mohyla Academy, Faculty of Natural Sciences, Department of Chemistry
Supervised by: D.Sc. Eng. Polina Vakuliuk

2018-2020
National University of Kyiv-Mohyla Academy, Faculty of Natural Sciences, Department of Chemistry, Master in Chemistry

2020
Master's degree in Chemistry;
Master Thesis: *Obtaining of glucose-fructose Sorghum saccharatum syrup by membrane distillation* (in Ukrainian);
Conducted at: National University of Kyiv-Mohyla Academy, Faculty of Natural Sciences, Department of Chemistry
Supervised by: D.Sc. Eng. Prof. Polina Vakuliuk

2020 - ongoing
Institute of Agrophysics, Polish Academy of Sciences, Department of Microstructure and Mechanics of Biomaterials, Ph.D. in Agriculture and Horticulture

Activities related to Ph.D. Thesis

Oral presentations on an international conferences:

1. Chibrikov, V., Pieczywek P.M., Zdunek, A., Visualization and structural characterization of plant cell wall hemicelluloses, 20th International Workshop for Young Scientists “BioPhys Spring 2021”, 18-19.05.2021, Lublin, Poland.
2. Chibrikov, V., Pieczywek P.M., Cybulska, J., Zdunek, A., Effect of plant cell wall polysaccharides on mechanical properties of bacterial cellulose-based composites, 21st Internatonal Workshop for Young Scientists “BioPhys Spring 2022”, 30-31.05.2022, Nitra, Slovakia.
3. Chibrikov, V., Pieczywek P.M., Cybulska, J., Zdunek, A., Effect of hemicelluloses on structure and mechanical properties of bacterial cellulose-based composites, 15th Bratislava Symposium on Saccharides, 20-24.06.2022, Smolenice, Slovakia.
4. Chibrikov, V., Pieczywek, P.M., Cybulska, J., Zdunek, A. Mechanical properties of bacterial cellulose-hemicellulose plant cell wall analogues - a numerical simulation study, 14th International Conference on Agrophysics, 11-13.09.2023, Lublin, Poland.

Oral presentations on Polish conferences:

1. Chibrikov, V., Pieczywek P.M., Zdunek, A., Modeling of mechanical properties of hemicellulose-cellulose networks in plant cell wall analogues, III Konferencja Doktorantów pt. „Cztery żywioły - współczesne problemy w naukach o życiu”, 18.12.2020, Warszaw, Poland.
2. Chibrikov, V., Pieczywek P.M., Zdunek, A., Structural property analysis of bacterial cellulose-hemicellulose composites, Warsztaty Dla Młodych Badaczy, 25.10.2021, Lublin, Poland.
3. Chibrikov, V., Pieczywek P.M., Cybulska, J., Zdunek, A., Effect of plant cell wall polysaccharides on mechanical properties of bacterial cellulose-based composites, XXVII Warsztaty Biofizyczne, 26-27.05.2022, Kazimierz Dolny, Poland.
4. Chibrikov, V., Pieczywek P.M., Cybulska, J., Zdunek, A. Bacterial cellulose-hemicellulose composites: structure, molecular and mechanical properties, VI Konferencja Naukowa “Szkoła Inżynerii Systemów BioTechnicznych”, 14-17.09.2022, Gietrzwałd, Poland.
5. Chibrikov, V., Pieczywek, P.M., Cybulska, J., Zdunek, A. Elasto-plastic properties of bacterial cellulose composites reinforced with hemicelluloses, XXVIII Lubelskie Warsztaty Biofizyczne, 25-26.05.2023, Kazimierz Dolny, Poland.
6. Chibrikov, V., Pieczywek, P.M., Cybulska, J., Zdunek, A. Badania symulacyjne właściwości mechanicznych analogów ściany komórkowej roślin, Warsztaty dla Młodych Badaczy, 30.11-01.12.2023, Lublin, Poland.

Poster presentations on an international conferences:

1. Chibrikov, V., Pieczywek P.M., Zdunek, A., Structural property analysis of bacterial cellulose-hemicellulose composites, 13th International Conference on Agrophysics: Agriculture in changing climate, 15-16.11.2021, Lublin, Poland.

2. Chibrikov, V., Pieczywek, P.M., Cybulska, J., Zdunek, A. Modeling of mechanical properties of hemicellulose-cellulose networks in plant cell wall analogues, XVI Plant Cell Wall Meeting, 18-22.06.2023, Malaga, Spain.

Other activities

Manuscript authorships:

1. Chibrikov, V., Vakuliuk, P., Hryhorenko, N., Gunko, S., Sobczuk, H., 2022. Technological improvement of the *Sorghum saccharatum* syrup production by membrane technologies. *Journal of Water and Land Development*, 54, 131-137. DOI: 10.24425/jwld.2022.141564
2. Chibrikov, V., Vakuliuk, P., Sobczuk, H., 2023. Sweet sorghum juice clarification and concentration: a review. *Critical Reviews in Food Science and Nutrition*. DOI: 10.1080/10408398.2023.2245033
3. Drobek, M., Cybulska, J., Frąc, M., Pieczywek, P., Pertile, G., Chibrikov, V., Nosalewicz, A., Feledyn-Szewczyk, B., Sas-Paszt, L., Zdunek, A., 2024. Microbial biostimulants affect the development of pathogenic microorganisms and the quality of fresh strawberries *(Fragaria ananassa Duch.*). *Scientia Horticulturae*, 327, 112793. DOI: 10.1016/j.scienta.2023.112793

Oral presentations on an international conferences:

1. Chibrikov, V., Vakuliuk, P., Sobczuk, H. Sweet sorghum juice clarification and concentration by membrane methods: a review, 2nd Conference "Membrane Materials - Modification and Separation", 26-28.09.2023, Toruń, Poland.

Poster presentations on an international conferences:

1. Chibrikov, V., Vakuliuk, P., Hryhorenko, N. Technological improvement of *Sorghum saccharatum* syrup production by membrane technologies. Membrane processes and installations in food technologies and engineering, 03-04.11.2020, Kyiv, Ukraine.

Participances in scientific projects:

1. Cellulose-pectin hydrogels cross-linked with divalent metal ions for immobilization of antagonistic microorganisms (*OPUS19* program; project number - 2020/37/B/NZ9/03159), 01.10.2023-30.09.2024.
2. Research and dissemination of knowledge on pectin, cellulose and fiber content in fruits and vegetables (*Science for Society II* program, project number - NdS-II/SP/0258/2023/01), 01.03.2024-ongoing.

Internships:

1. Primary Cell Wall Team, Department of Development, Signaling and Modeling, Institut Jean-Pierre Bourgin (Versailles, France). Theme of research stay: Investigation of the patterns of cellulose-pectin interactions by visualization with 3D direct stochastic optical reconstruction microscopy (3D dSTORM), 15.04.2024-13.07.2024.

Applications:

1. Project application - Formation of permeable bacterial cellulose fiber networks from apple pomace. *PRELUDIUM22* program.
2. Project application - Extracellular polysaccharides of *Komagataeibacter xylinus* cultivated in byproduct media and its application in tunable fiber networks. *PRELUDIUM23* program.
3. Scholarship application - Scholarship for Young Scientists, *SMN19* program.
4. Award application - Award of the President of the Polish Academy of Sciences Branch in Lublin for young researchers for the best scientific work in 2023.

Certificates and workshop participations:

1. Polish B1/B2, ONpolish, 15.07.2022.
2. R Essential Training: Wrangling and Visualizing Data, LinkedIn Learning, 20.07.2022.
3. Introduction to Data Science, LinkedIn learning, 30.07.2022.
4. Become a Data Analytics Specialist, LinkedIn Learning, 21.08.2022.
5. Writing in the Sciences, Stanford University, 01.04.2023.
6. Nanotechnology: A Maker's Course, Duke University, 10.04.2023.
7. Materials Data Sciences and Informatics, Georgia Institute of Technology, 16.04.2023.
8. Fundamentals of Material Science, Shanghai Jiao Tong University, 30.04.2023.
9. English C2, EFSET, 28.02.2024.
10. Understanding Research Methods, University of London, 24.03.2024.
11. Simulation and Modeling of Natural Processes, University of Geneva, 10.04.2024.
12. Good Manufacturing Practices for Food Safety and ISO 22000, GxP Training, 31.07.2024.
13. French A1, SuperMemo, 28.08.2024.

Duties fulfilled:

1. Member of an Organizing Committee, IV Conference of Doctorate Students "The Four Elements - Contemporary Issue in the Life Sciences", 14.12.2021, Lublin-Warsaw, Poland.
2. Social media moderator, 14th International Conference on Agrophysics, 11-13.09.2023, Lublin, Poland.
3. Vice Chair, Ph.D. Council, Institute of Agrophysics, Polish Academy of Sciences, 01.10.2022-30.09.2023.
4. Manuscript Reviewer, Food Science & Nutrition, 18.10.2023.
5. Member of an Organizing Committee, VI Conference of Doctorate Students "The Four Elements - Contemporary Issue in the Life Sciences", 14.12.2023, Lublin-Warsaw, Poland.
6. Secretary, Ph.D. Council, Institute of Agrophysics, Polish Academy of Sciences, 01.10.2023-30.09.2024.
7. Technician, Department of Microstructure and Mechanics of Biomaterials, Institute of Agrophysics, Polish Academy of Sciences, 01.10.2023-30.09.2024.

Activities in support of science:

1. Participance in XVII Lublin Science Festival with a presentations entitled Wet experiments, 20-24.09.2021, Lublin, Poland.
2. Participance in a podcast on the dissemination of knowledge in the field of agrophysics, “Agrophysics 101”, Sharing is Caring FarmNetz Podcast, 25.08.2023.
3. Participance in XIX Lublin Science Festival with a presentations entitled Bacteria in the service of humanity, 18-22.09.2023, Lublin, Poland.
4. Interview on science communication with graphics, BioRender blog, 16.05.2024.